UNIVERSITÀ
degli STUDI
di CATANIA

INTERNATIONAL DOCTORATE IN CHEMICAL SCIENCES
XXVIII CYCLE
CURRICULUM: ORGANIC CHEMISTRY

Nunzio Cardullo

SYNTHESIS OF NATURAL-DERIVED POLYPHENOLS AS POTENTIAL ANTICANCER AGENTS

PhD thesis

Tutor: Prof. C. Tringali
Coordinator: Prof. S. Sortino

A.A. 2013-3015

'Natural Products have served as an important source of drugs since ancient times and about half of the useful drugs today are derived from natural sources.'

C. Tringali[1]

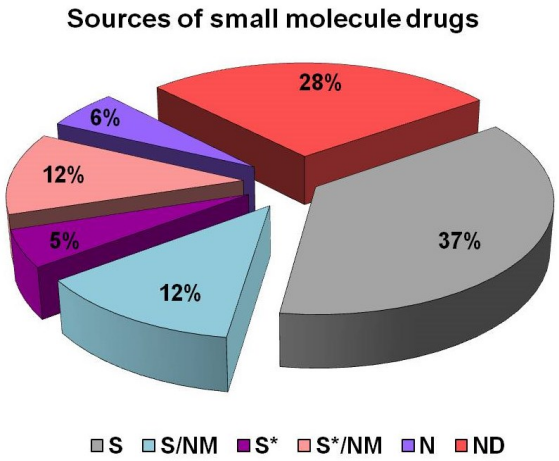

Figure1. Sources of small molecule drugs, 1981–2006: Codes are as follows: "N", natural product; "ND", derived from a natural product and usually a semisynthetic modification; "S", totally synthetic drug often found by random screening/modification of an existing agent; "S*", made by total synthesis, but the pharmacophore is/was from a natural product. The subcategory is as follows: "NM", natural product mimic. [2]

'…the use of information from nature and from compounds that though formally "synthetic" are derived from natural products, or mimic natural product topographies, can be used in a variety of ways to lead to novel structures with (hopefully) therapeutic potential.'

D. J. Newman[2]

LIST OF ABBREVIATIONS

AbL	*Agaricus bisphorus* Laccase
BOP	Benzotriazole-1-yl-oxy-tris-(dimethylamino)-phosphonium hexafluorophosphate
CD_3COCD_3	Acetone-d_6
C_5D_5N	Pyridine-d_5
CD_3OD	Methanol-d_4
$CDCl_3$	Chloroform-d_1
CH_2Cl_2	Methylene Chloride
$CHCl_3$	Chloroform
C NMR	Carbon Nuclear Magnetic Resonance
g-COSY	Gradient COrrelation SpectroscopY
CD	*Circular Dichroism*
DMF	*N*,*N*-dimethylformamide
DMSO	Dimethylsulfoxide
EI MS	Electron Impact Mass Spectrometry
Et_2O	Diethyl ether
EtOAc	Ethyl acetate
EtOH	Ethanol
ESI MS	ElectrSpray Mass Spectrometry
g-HSQCAD	Gradient Heteronuclear Single Quantum Coherence Adiabatic
g-HMBCAD	Gradient Heteronuclear Multiple-Bond Correlation Adiabatic
GI_{50}	Concentration Inhibiting 50% of cell Growth
H NMR	Proton Nuclear Magnetic Resonance
HPLC	High Performance Liquid Chromatography
HRP	Horseradish Peroxidase
IC_{50}	Concentration Inhibiting 50% of activity
***m*CPBA**	*meta*-chloroperbenzoic acid
IPA	Isopropyl alcohol
MeOH	Methanol
LDA	Lithium Diisopropyl amide
PE	Petroleum ether

PoL	*Pleurotus ostreatus* Laccase
R_f	Retention Factor
RP-18	Reverse Phase C-18
rt	Room Temperature
TEA	Triethylammine
THF	Tetrahydrofuran
TLC	Thin Layer Chromatography
TvL	*Trametes versicolor* Laccase
t_R	*Retention Time*
UV	Ultraviolet

TABLE OF CONTENTS

1. INTRODUCTION

Extracts from plants or other organisms have been used for thousands of years as medicines and today a multitude of researchers continue to be inspired by the astonishing structural variety of natural products to identify potential lead compounds for drug discovery. In the simplest of terms, a natural product is a small molecule (generally with a molecular weight below 3000 Da) that is produced by a biological source; often the term is considered as synonymous for secondary metabolite and natural products research focuses on the biosynthesis and the study of chemical properties and biological functions of secondary metabolites. These are organic compounds not ubiquitous in all organisms, and represent an expression of the individuality of the species; secondary metabolites do not exert primary biological functions directly involved in the normal growth, development or reproduction of an organism but they may serve as chemical defense, intra- or interspecies communication, sexual attraction and to other purposes conferring an advantage to the organism producing them. The main families of secondary metabolites include isoprenoids, polyketides, alkaloids, non ribosomial peptides and polyphenols, these latter directly derived from shikimate pathway, as phenylpropanoids and lignans, or from a mixed biosynthetic pathway (shikimate/ acetate and/or malonate pathways), as stilbenoids or flavonoids.

My thesis is devoted to the family of polyphenols with the specific goal of synthesize new natural-derived polyphenols compounds and study their chemical and biological properties.

1.1. POLYPHENOLS

The term ‘polyphenols’, was originally used as synonym for ‘vegetable tannins’ to indicate the vegetable substances able to convert animal skin into leather, that is the ‘tanning action’. Later, Haslam [3] proposed a definition of plant polyphenols including specific structural characteristics common to all phenolics having a tanning property; however, this definition has subsequently been broadened in the common use and low-molecular weight phenolic compounds (not soluble in water and without tanning action) were also included. More recently, the term ‘polyphenols’ has been further extended to include phenolic metabolites biosynthetically derived through the shikimate and/or the acetate/malonate pathways. Indeed, metabolic modification of some shikimate/acetate intermediates can lead to ‘polyphenols’ paradoxically lacking of the phenolic functions, such as some lignans originated by dimerization of a phenylpropanoid unit (C6C3)[4] or without ‘free’ hydroxyl groups (such as some polymethoxyflavones)[5] although their carbon framework is strictly related, or identical to that of the phenolic analogue. In addition, many naturally occurring derivatives such as polyphenolic glycosides, esters and ethers are normally included in research studies on polyphenols. This large group of chemical products, mainly found in higher plants, include more than 8000 compounds, many of whom display important biological properties. These secondary metabolites of plants frequently have an important ecological role for the plant, ex. as defense agents against ultraviolet radiation or aggression by pathogens and predators. Many of them are also found in edible plants and have become popular for their chemopreventive properties against degenerative pathologies.

The polyphenols are generally subdivided in main families, namely flavonoids, stilbenoids, phenylpropanoids and lignans. Actually, lignans, the related neolignans and other oligomeric compounds are strictly related to phenylpropanoids being biosynthetically derived from them through oxidative coupling.

Over the past 15 years, researchers and food manufacturers have become increasingly interested in polyphenols, the main reason probably being the growing evidence of antioxidant properties of this class of natural products;[6] their great abundance in our diet (edible fruits, herbs, vegetables are source of polyphenols) and their role in the prevention of various diseases associated with oxidative stress, such as cancer, cardiovascular and

neurodegenerative diseases.[7,8] Furthermore, polyphenols, which frequently constitute the active principles of many medicinal plants, modulate the activity of a wide range of enzymes and cell receptors. The hypothesis that regular assumption of dietary polyphenols may help to prevent cancer is supported by many epidemiological, *in vitro* and *in vivo* studies[9, 10, 11] corroborated by some clinical trials.[12,13] Consequently, a considerable number of researches has recently been developed on biological properties of a growing number of low molecular weight dietary polyphenols, such as the stilbenoid resveratrol (**1**) found in grape and red wine, the green tea catechins, and in particular epigallocatechin-3-gallate (EGCG, **2**), the soya isoflavone genistein (**3**), the yellow pigment curcumin (**4**) found in turmeric (curry), ellagic acid (**5**), a component of pomegranate, the widespread caffeic acid (**6**) and its phenylethyl ester CAPE (**7**), found in honeybee propolis.

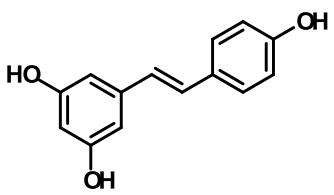

1

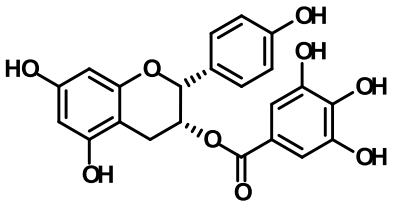

2

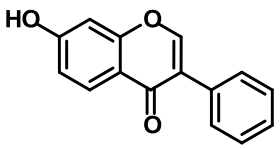

3

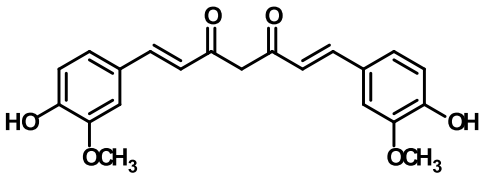

4

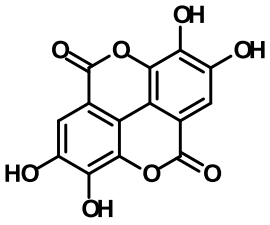

5

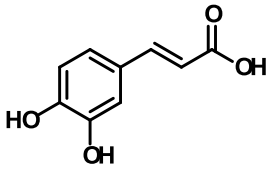

6

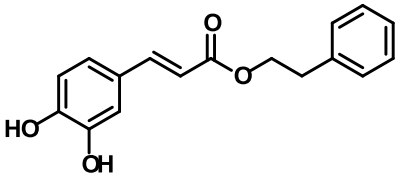

7

Resveratrol (*E*-3,5,4'-trihydroxystilbene, **1**) is considered one of the most extensively studied polyphenols with cancer chemopreventive activity; a recent review by J. Pezzuto[14] lists 512 references solely on the carcinogenesis inhibitory properties of resveratrol. The

popularity of this stilbenoid dates back to the observed inverse correlation between a high-fat diet and low mortality risk of heart disease, attributed to red wine consumption in some southern regions of France, the so-called 'French paradox'.[15] Another popular beverage, green tea, has been the subject of a lot of epidemiological studies suggesting that its regular consumption can be associated with reduced incidence of some cancer diseases.[16] Recently, ECGC (**2**), one of the main component of green tea, was reported to inhibit tumor invasion and angiogenesis, processes that are essential for tumor growth and metastasis; in addition, various potential mechanisms involved in antitumor activity of **2** have been described, including inhibition of matrix metalloproteinase and proteasome.[17] Curcumin (**4**) has been shown to possess a wide range of biological activities including anti-inflammatory, antioxidant, antimicrobial and anticancer effects.[18] Finally caffeic acid (**6**) and in particular its naturally occurring ester CAPE (**7**) were reported for antioxidant, anti-inflammatory and antibacterial activity.[19]

Notwithstanding the importance attributed to dietary polyphenols in cancer prevention, a problem arises about their poor bioavailability and fast metabolic conversion, frequently observed for natural polyphenols:[20,21] this has prompted many research groups to synthesize analogues of these molecules, with improved metabolic stability and bioavailability, and possibly with more potent biological activity.[22] These optimized analogues may be useful as 'lead compounds' for the discovery of new chemotherapeutics/adjuvant agents. In some cases optimized analogues have shown improved activity even through a different, more effective, mechanism of action with respect to the natural model.

1.2. STILBENOIDS AND RELATED COMPOUNDS

A chapter in a book and a review recently published by Spatafora and Tringali confirm the importance of natural-derived polyphenols as potential anticancer agents.[23, 24] Among the compounds cited therein, many synthetic stilbenoids have been prepared as derivatives of the above cited resveratrol (**1**), as well as of the combretastatin A-4 (**8**), a cytotoxic stilbenoid, originally isolated by Pettit *et al*. from the root bark of *Combretum caffrum*,[25] known as a potent inhibitor of tubulin polymerization[26, 27] and a tumor vascular targeting agent.[28] Notwithstanding the clear structural analogy, the majority of studies on resveratrol or combretastatin A-4 analogues have been carried out separately, probably because **8** is highly cytotoxic and has attracted the attention of researchers mainly as a potential anticancer

therapeutic agent, whereas **1**, found in edible plants like grapes or peanuts, is considered a 'safe molecule' and has been studied mainly for its cancer chemopreventive or other beneficial properties. Among the synthetic analogues of combretastatin A-4, it is worth of citation the (*Z*)-3,4′,5-trimethoxylstilbene-3′-*O*-phosphate (**9**), very recently reported as a novel vascular disrupting agent with potent microtubule inhibitory activity, cytotoxic activity towards seven tumor cell lines in the nM range, and antiangiogenic properties.[24] Moreover, molecular docking simulations have showed that some *Z*-polymethoxystilbenes are able to bind effectively to the colchicine binding site of tubulin, similarly to the binding mode of **8**. In a recent study, the (*Z*)-3,5,4′-trimethoxystilbene (**10**), able to bind to the colchicine site of tubulin, showed the highest antiproliferative activity towards SW480 human colorectal cell (IC_{50} = 0.3 μM); nevertheless, a strictly related compound, (*Z*)-2-hydroxy-3,5,3′,5′-tetramethoxystilbene (**11**) proved to have the best calculated binding affinity to the colchicine site of tubulin, although resulting less potent than **10**, with IC_{50} = 7 μM.[29, 30] This observation suggests that some potentially good candidates as tubulin inhibitors probably do not reach the tubulin pocket because other factors such as absorption, distribution and metabolism have a critical role.

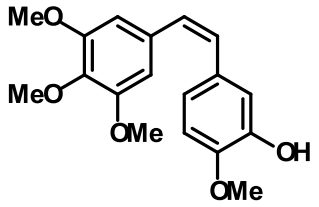

8

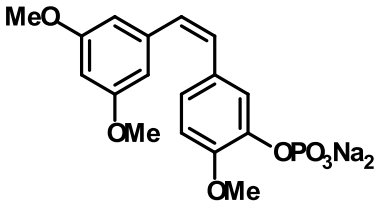

9

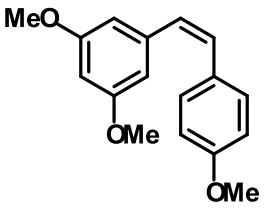

10

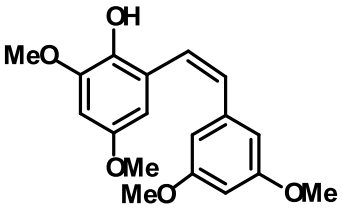

11

The search for antiangiogenic agents has recently became of great importance in cancer chemotherapy, given that new vessel growth accompanies several pathologies and in particular solid tumor growth.[31,32](*E*)-polymethoxystilbenes have recently showed promising properties as potential antitumor agents: the 2-hydroxy-3,5,4′-trimethoxystilbene **12** has

proved to be a potent antiangiogenic agent, able to inhibit, in the range 1 – 100 μM after 96h exposure, up to the 80% of neovascularisation in a porcine aortic endothelial cell *in vitro* model;[33] **12** was also evaluated for its effects on swine granulosa cells where it decreased progesterone levels and inhibited VEGF output.[34] An isomer of **12**, the 2-hydroxy-4,3′,5′-trimethoxystilbene (**13**), proved to be an effective apoptotic agent for breast cancer cells;[35] as well as the aldehyde 2-formyl-3,5,4′-trimethoxystilbene (**14**) resulted more active than the anticancer drug 5-fluorouracil against the nasopharyngeal epidermoid tumor cell line KB (IC_{50} = 9.2 μM).[36]

In a collaborative study carried out by the laboratories of Prof. C. Tringali (University of Catania) and that of Dr. A. Di Pietro (CNRS, France), a series of polymethoxystilbenes were synthesized and evaluated as inhibitors of ABCG2, an efflux pump protein involved in multi-drug resistance (MDR); among them, the 3,5,3′,4′-tetramethoxystilbene (**15**), previously reported as antiproliferative and tubulin inhibitor[23, 37, 38] resulted the most potent inhibitor of mitoxantrone efflux, with IC_{50} = 0.16 μM.[39] The above cited data suggest that (*E*)-polymethoxystilbenes are a subgroup of resveratrol-related polyphenols with promising antiproliferative properties. Some of these bioactive compounds have been the subject of recent pharmacokinetic studies because of their presumed longer half-life and reduced metabolic conversion with respect to their hydroxylated analogues. For instance, compound **15** showed better oral bioavailability, longer terminal elimination half-life, greater plasma exposure and lower clearance than lead **1**. Similar pharmacokinetic results have been obtained also for 3,5,4′-trimethoxystilbene (**16**, GI_{50} = 2.92 μM against androgen non-responsive human prostate tumor cells DU-145),[40] and for the 3,5,3′,4′,5′-pentamethoxystilbene (**17**),[41] known for interesting antitumor properties.[42, 43] Its isomer, 2,4,3′,4′,5′-pentamethoxystilbene (**18**) is reported in two recent papers indicating this compound as a potent pro-apoptotic factor in colon cancer cells (Caco-2, HT-29 and SW1116), targeting microtubules[44] and inhibiting colitis-associates colorectal carcinogenesis in mice.[45]

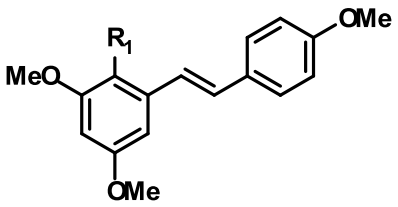

12 $R_1 = OH$
14 $R_1 = COOH$

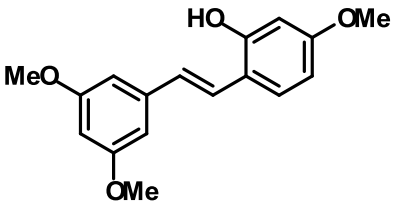

13

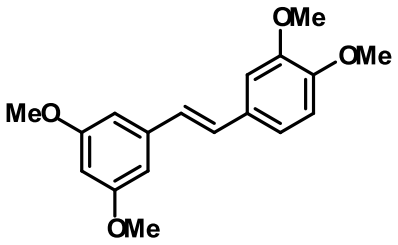

15

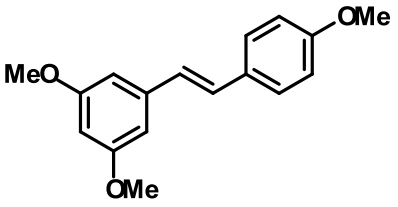

16

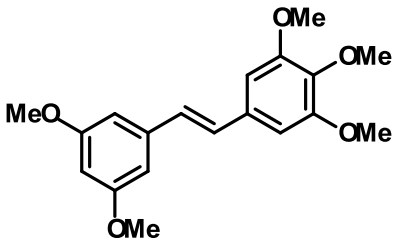

17

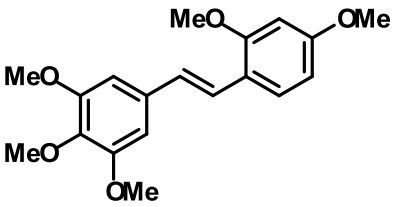

18

These data, in addition to those previously reported on anti-tumor stilbene-based resveratrol analogues[22] indicate that polymethoxystilbenes are a subgroup of resveratrol analogues worth of further study and chemical optimization. Although the combretastatin-related *Z*-stilbenoids in many cases resulted more potent antiproliferative agents than the *E*-substituted isomers, it has been showed that the formers are prone to isomerization during storage and administration and in the course of metabolism in liver microsomes.[46]

Many examples of chemical modification of bioactive polyphenols are reported as a strategy for selectively direct an active compound towards target-specific receptors or other factors expressed in tumor cells, sparing the not cancerous ones.[47, 48] Among them, glycoconjugates incorporating a sugar moiety, should act as target specific saccharide transporters, and might accumulate selectively in some tumor cells where primarily glucose transporters (GLUTs) are over-expressed,[49, 50] due to the altered glucose metabolism (the so-

called 'Warburg effect'). [51] Moreover, they should also be hydrolyzed by specific β-glucosidases and β-galactosidases, thereby allowing the release of the active aglycone. [52]

Some examples of such anti-tumor glycoconnjugates are below reported; the 4-β-D -glucoside of curcumin (**19**), the well-known yellow pigment found in turmeric (*Curcuma longa*),[53] proved to be the most potent in a series of glycoconjugates tested on a panel of colon cancer cells: Caco-2, HT29 and T84 cells;[54] after 96h, **19** showed an IC_{50} = 10.3 μM on Caco-2 cells. In the same study, the β-D-galactoside of the synthetic anticancer drug diethylstilbestrol (**20**) was also evaluated, although resulting significantly less potent than compound **19** (IC_{50} = 75 μM on Caco-2 cells). A recent review about biologically active glycosides reports some natural glyco-stilbenes found in many families of higher plants (Vitaceae, Gnetaceae, Polygonaceae, Liliaceae, Moraceae, and Cyperaceae).[55] Among these, resveratroloside (**21**), found in grape and wine, showed cytotoxic activity against human oral squamous cell carcinoma and salivary gland tumor cell lines, but none important cytotoxity towards normal human gingival fibroblasts. Kimura *et al*. have studied the effects of piceid (**22**) and 3,5,4'-trihydroxystilbene-2- *O*-β-D-glucoside (**23**) on tumor growth and lung metastasis in mice bearing highly metastatic Lewis lung carcinoma tumor, revealing that **23** has inhibitory effect in the DNA synthesis (IG_{50} = 81 μM).[56] In addition, stilbene glucosides **22** and **23** have shown antiangiogenic activity, by inhibition of the capillary-like tube networks formation of Human Umbilical Vein Endothelial Cell (HUVEC).

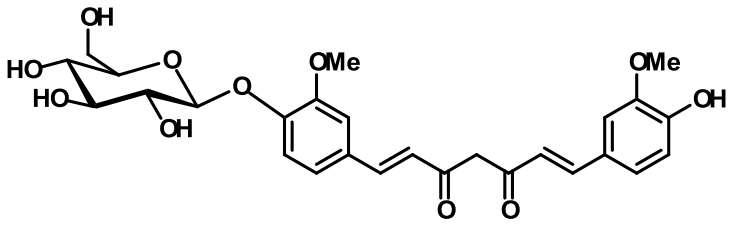

19

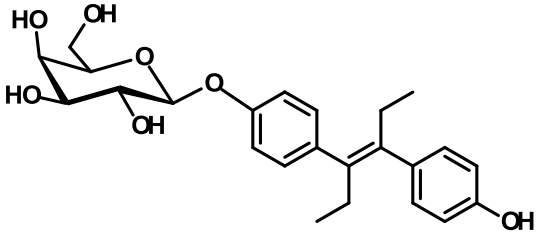

20

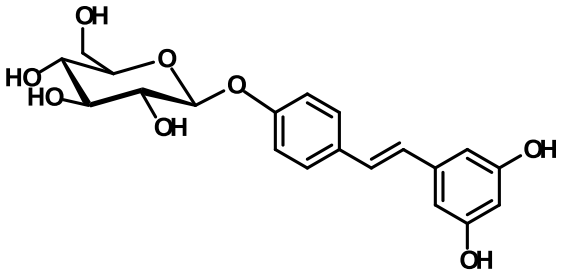

21

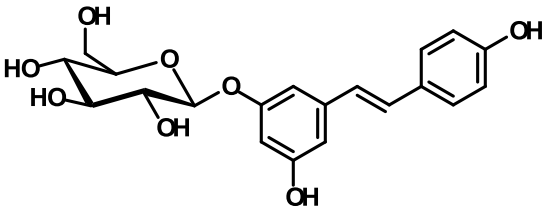

22

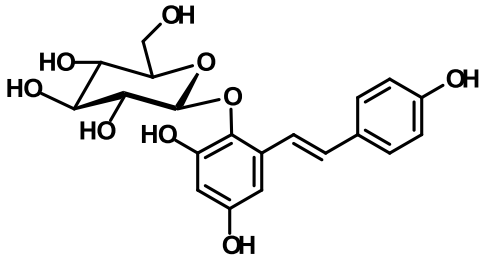

23

1.3. DERIVATIVES OF PHENOLIC CINNAMIC ACIDS

Phenolic cinnamic acids are key intermediates in shikimate biosynthetic pathway as precursors of a variety of natural products with an aromatic moiety, including stilbenoids and flavonoids. The most common members of this group are the *p*-coumaric (**24**), caffeic (**6**) ferulic (**25**) and sinapic (**26**) acids. These compounds are widespread in nature and have been found in many fruits, vegetables and cereals in the form of free acids or esters. They are able to produce beneficial effects on human body and consequently considered nutraceuticals. Most of them find application in perfumery (as fragrance materials), cosmetic industries and in pharmaceutics for their wide range of biological properties: among others, antioxidant, anti-inflammatory, antimicrobial, antifungal, antidiabetic, anticholesterolemic, anti-hyperglycemic and UV-protective activity.[57] Some examples are worth of citation here: methyl caffeate (**27**), found in many plants and in turkey berries (from *Solanum torvum*) is reported to posses antitumor activity against Sarcoma 180 as well as antimicrobial activity.[58] Chlorogenic acid (**28**), a naturally occurring ester of caffeic acid with (-)-quinic acid, is found in coffee beans (*Coffea* spp.) and in artichokes (*Cynara scolymus*), it is reported to be antioxidant, anti-inflammatory and cancer chemopreventive agent.[59] Recently, Jin *et al*. showed a strong activity of compound **28** as inhibitor of matrix metalloproteinase-9 (MMP-9), involved also in tumor cell invasion and metastasis.[60]

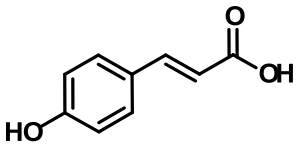

24

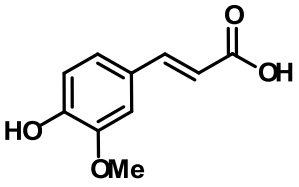

25

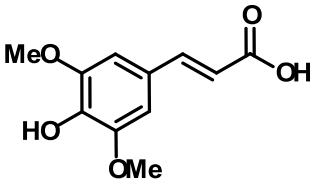

26

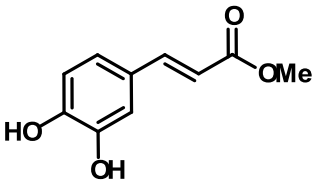

27

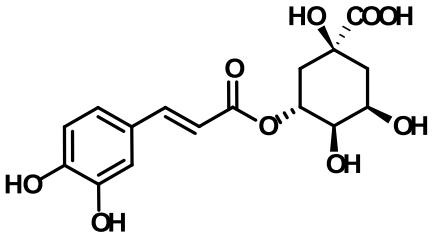

28

CAPE (**7**), already cited above, is a bioactive constituent of honey bee propolis, probably one of the most studied caffeic acid derivatives for its interesting biological properties including antiproliferative activity.[61] A study on development and validation of a spectrometric method for the determination of **7** in rat plasma and urine showed that it is rapidly absorbed and excreted both as unmodified molecule and as glucuronide conjugate.[62] In addition, the chemotherapeutic effectiveness of esters may be reduced by their possible hydrolysis by intracellular esterases; conversely, amide isosteric analogues are generally associated with higher metabolic stability than esters.

In the last decade, a large number of phenolic amides have been studied as antioxidant or anti-inflammatory agents, as 5-lipoxygenase,[63] tyrosinase [64] or α-glucosidase inhibitors.[65] Among the many promising cinnamic amides reported in the recent literature, I wish cite here some examples. Compounds **29** and **30** showed a pronounced antioxidant activity in the microsomal lipid peroxydation (IC_{50} = 0.29 and 0.59 μM), higher than vitamin E and quercetin (2.8 e 0.95 μM respectively.[66] The naturally occurring *N*-(*p*-coumaroyl)serotonin (**31**)[67] and the synthetic amide **32**[68] have been reported as tyrosinase inhibitors (IC_{50} = 74 μM and 2.2 μM respectively), of potential use in the food and cosmetic industries and in medicine in prevention and treatment of hyperpigmentation and in melanoma characterized by melanin accumulation.[69]

In a study on inhibitors of the viral surface proteins neuraminidases (NAs), involved in the diffusion of influenza virus, the compound **33**, a caffeic acid amide, proved to be a potent NAs inhibitor with anti-influenza virus activity of 31.2 μM.[70]

A library of synthetic cinnamic acyl 1,3,4-thiadiazole amides has been evaluated for antiproliferative activity and tubulin polymerization inhibition on cancer cells.[71] Compound **34** resulted a potent antiproliferative agent (IC_{50} = 0.28 μg/mL for MCF-7 and IC_{50} = 0.52 μg/mL for A549), comparable to tubulin inhibitor colchicine.

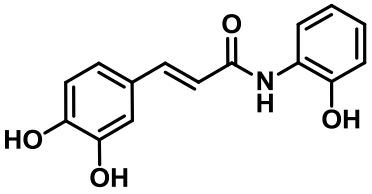

29

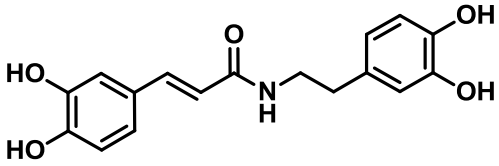

30

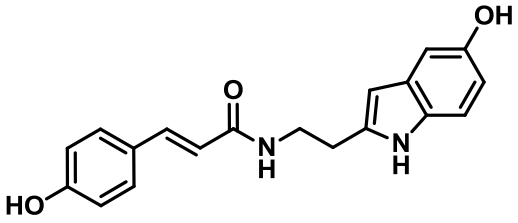

31

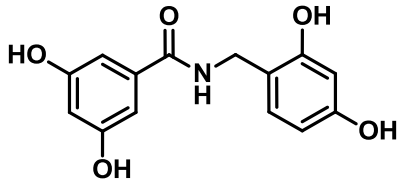

32

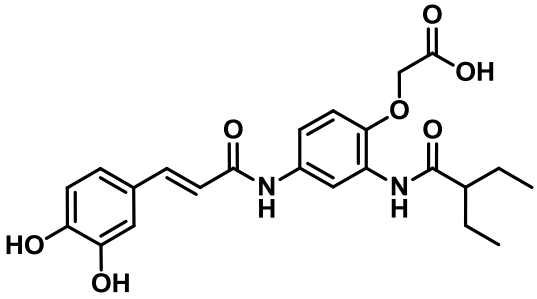

33

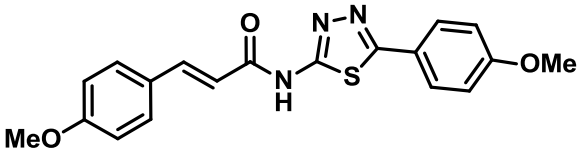

34

The strategy to block cell division is just one of successful area of research for the development and progress of cancer drugs. Matrix Metalloproteinases (MMPs) are zinc-dependent proteolytic enzymes (endopeptidases) which play a pivotal role in the degradation of all extracellular matrix proteins and are also involved in pathological events such as tumor growth, invasion and metastasis. In a recent work a number of cinnamoyl amides has been synthesized and evaluated for selective MMPs inhibition;[72] among these, caffeoyl amides **35** – **37** showed IC_{50} values around 3.6 and 2.3 nM on MMP-2 and MMP-9.

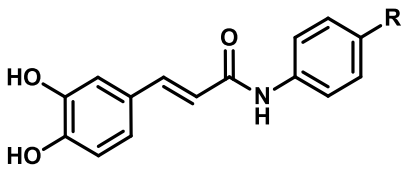

35 R = OH
36 R = OMe
37 R = Me

1.3.1. *m*PGES-1 inhibitors as a new generation of anti-inflammatory agents

Inflammation is a biochemical response of body tissues to harmful physiological and pathological stimuli, such as irritants, pathogens or damaged cells; NSADs are the most used anti-inflammatory drugs and they reduce the inflammation by inhibiting the activity of Cyclooxygenanses (COX) and consequently the biosynthesis of prostaglandins (chemical mediators in inflammation). Inflammation can also play a pathogenic role in a variety of acute or chronic (neuro)degenerative diseases such as cancer, rheumatoid arthritis, epilepsy, amyotrophic lateral sclerosis, Alzheimer's and Parkinson's diseases. Moreover, the inducible isoform COX-2 is the major contributor to the inflammation and disease progression than constitutively expressed COX-1. For this reason, a new generation of anti-inflammatory drugs such as rofecoxib and valdecoxib, selective COX-2 inhibitors, have been employed for suppression of pain and inflammation; unfortunately they also caused adverse cardiovascular effects and were withdrawn from the U.S. market.

In a recent article it is suggested that future anti-inflammatory therapy should be targeted through a specific proinflammatory prostanoid synthase or receptor rather than to block the entire COX-2 signaling.[73] In this contest, prostaglandin E synthases (PGES) which are involved in the conversion of PGH_2 in PGE_2, are a new biological target in treatment of chronic inflammatory diseases. More precisely, among the three PGES isoforms, the *m*PGES-1 (microsomal Prostaglandin E Synthase, type-1) is responsible for the pro-inflammatory stimuli-dependent production of PGE_2 and it is up-regulate under inflammatory events in various tissues.[74] A selective inhibitor of *m*PGES-1 would be able to inhibit PGE_2 production induced by inflammation, sparing constitutive PGE_2 and the other prostanoids production (PGD_2, PGI_2, TXA_2 see Figure 8).

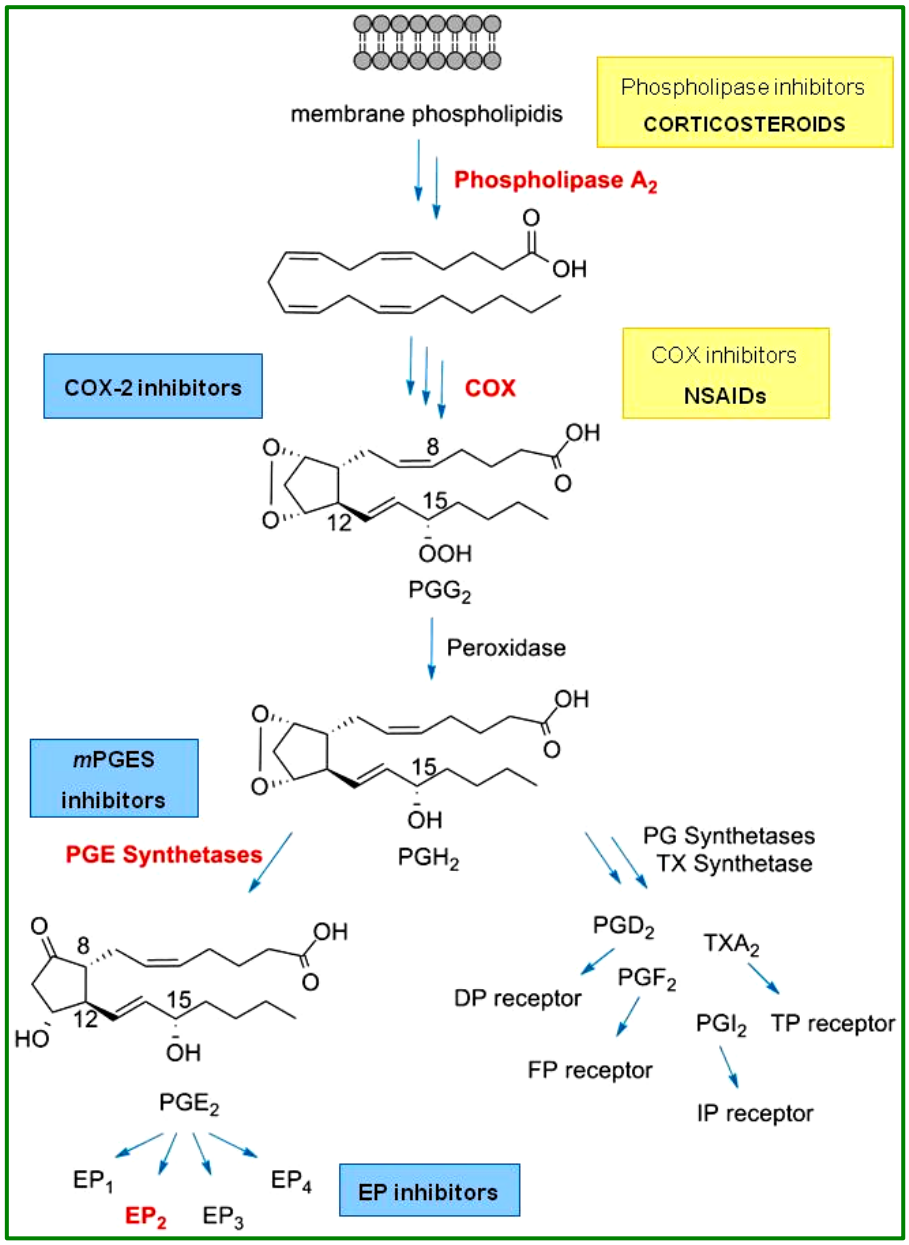

Figure 2. Representation of biosynthesis of prostaglandins and possible unspecific (with yellow) and specific (with blue) inhibitors of the process.

Among *m*PGES-1 inhibitors, a series of benzoxazole piperidinecarboxamides has been described, in particular the hit **38** proved to be a promising inhibitor by *in vitro* assay, but it lacked potency in cell-based assay. Structure–activity optimization of **38** lead to synthesize compounds **39** and **40** which showed enhanced inhibitory activity by both *in vitro* (IC_{50} of 3 and 2 nM respectively) and *in vivo* (IC_{50} of 109 and 53 nM respectively) assays. The optimization occurred also under the pharmacokinetic profile and compound **40** was selected as clinical candidate.[75]

Imidazoquinolines are another structural class of *m*PGES-1 inhibitors;[76] compound **41** was the most potent (IC_{50} = 9.1 nM) with a high selectivity (>1000 fold) over both COX-1 and COX-2. A virtual screening method employing a structural model of *m*PGES-1 on 200000 compounds deposited in the Korean Chemical Bank (http://www.chembank.org) identified 9 hits inhibiting more than 80% of enzyme at 25 μM and, after optimization of the lead **42**, compound **43** was obtained resulting a promising *m*PGES-1 inhibitor with an IC_{50} value of 1.7 μM.[77]

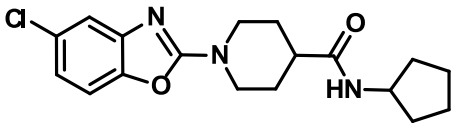

38

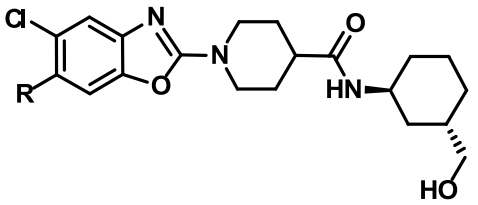

39 R=4-chlorophenyl
40 R=4-(trifluoromethoxy)phenyl

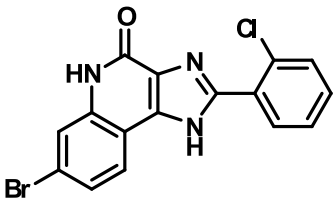

41

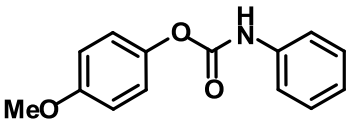

42

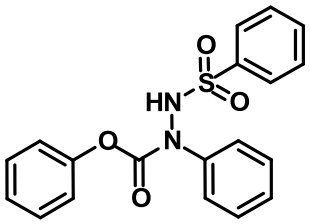

43

1.4. LIGNANS AND NEOLIGNANS

1.4.1. Occurrence, bioactivity and biosynthesis of lignans and neolignans

A further group of promising compounds in the search for natural-derived antitumor agents is that of lignans, distributed in many higher plants (in wooden parts, roots, leaves, flowers, fruits and seeds) and including several examples of compounds with antitumor activity. Lignans and other related compounds (neolignans, oxyneolignans and others) are accumulated in vascular plants probably as chemical defense agents and this may explain the wide variety in their reported biological activities, including cytotoxic, antimitotic,

antiangiogenic,[78] cardiovascular[79] and antiviral (including HIV),[80] but also antileishmanial[81] and antifeedant activity. [82] The most cited example of bioactive natural lignan is podophyllotoxin (**19**), whose optimization has afforded the anticancer drug etoposide (**20**).

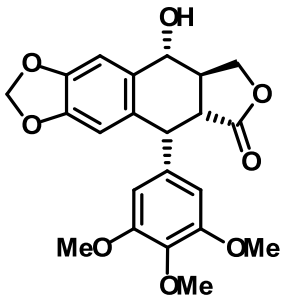

44

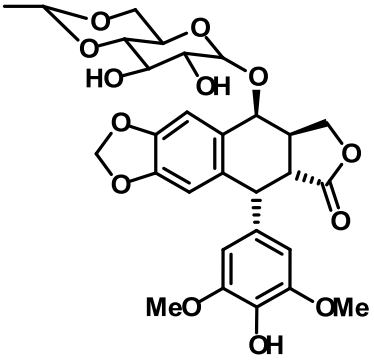

45

Lignans share with other phenolic compounds a common biosynthetic origin from shikimic acid. Their carbon skeleton is normally constituted by two phenylpropanoid units (C6C3, monolignols), whose 8-8′ radical coupling originates the natural dimeric lignans.[83] Their biosynthesis has been widely studied and is exemplified in Scheme 1 where the formation of (+)-pinoresinol **48** from the monolignol coniferyl alcohol (**46**) is reported. In the first step an oxidase gives rise to the coniferyl alcohol radical, whose mesomeric forms are illustrated; subsequently, a coupling reaction affords a reactive quinone-methide intermediate **47** whose intramolecular cyclization gives the product **48**.[84]

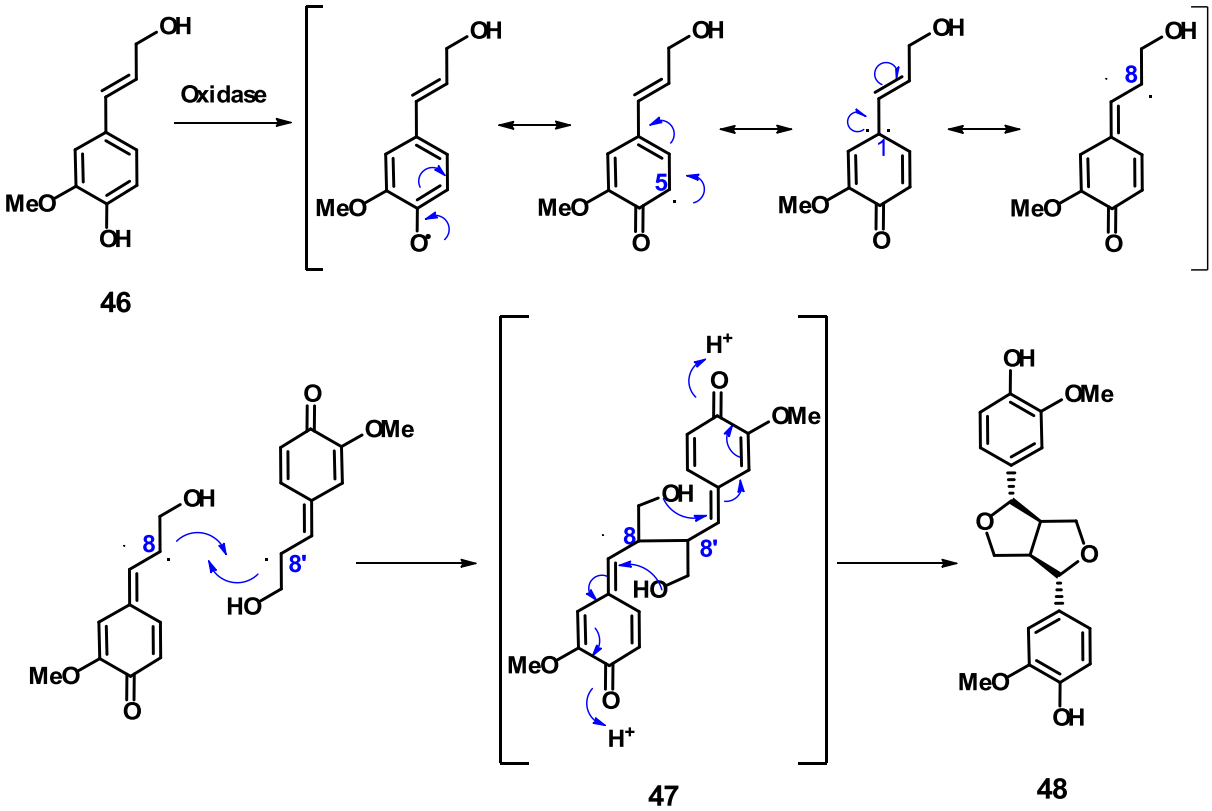

Scheme 1

In principle it is possible to mimic the biosynthesis of natural lignans in laboratory where the relevant precursors are subjected to oxidative coupling reactions mediated by enzymes or oxidative reagents (see paragraph 1.4.2. for details). Even if natural lignans are found as pure enantiomers, that is lignan biosynthesis is under stereochemical control, *in vitro* oxidative coupling (including enzyme-mediated reactions) normally affords racemic mixtures.[85] This point has been adequately studied: in an authoritative study by Davin *et al.*,[86] and more recently in a mini-review,[87] it is reported that the stereospecificity in 8-8'-radical coupling in plants is due to so-called 'Dirigent Proteins (DPs). The role of DPs is to host a couple of coniferyl radicals in binding site, in order to determine the stereochemical asset of the quinone-methide intermediate and consequently, the stereogenic centres of final product, for example in (+)-pinoresinol biosynthesis the two radicals are oriented '*si*-face to *si*-face' (Figure 3).

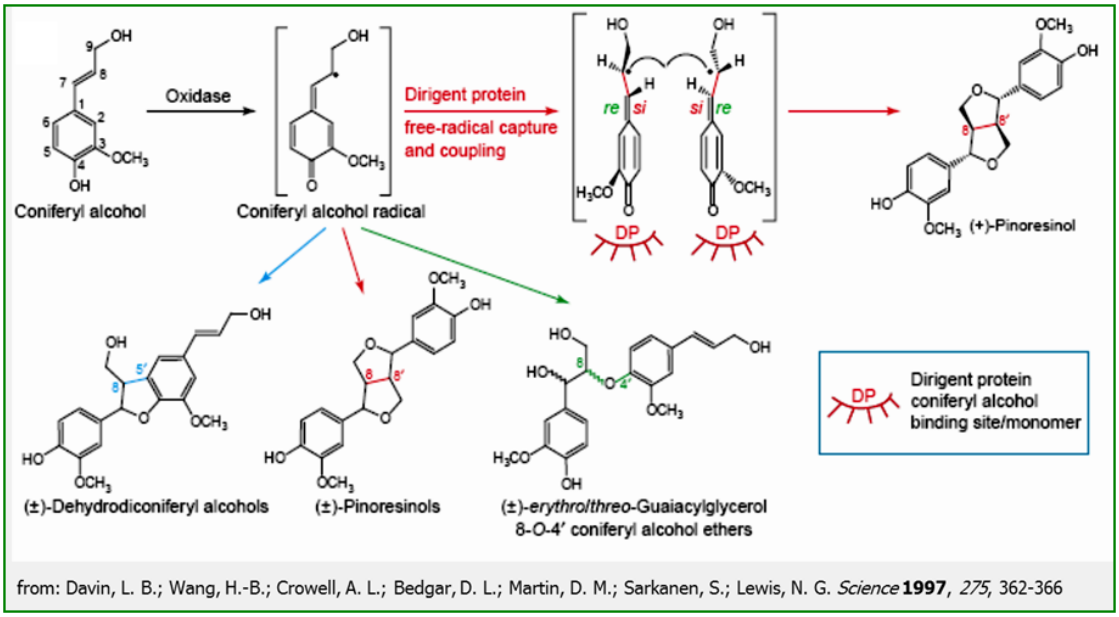

Figure 3. Bimolecular phenoxy radical coupling from *E*-coniferyl alcohol; random" coupling products and stereoselective coupling product (+)-pinoresinol.

According to the IUPAC recommendations,[88, 89] 'neolignans' are distinguished in referring to dimers with a carbon linkage between two C6C3 units different from 8-8', as for example in (+)-dehydrodiconiferyl alcohol **50**, whose biosynthesis, outlined in Scheme 2, proceeds via the quinone-methide intermediate **49**, which is formed through an 8-5′ oxidative coupling; also in this case a specific Dirigent Protein carries the reaction out under stereochemical control.[84]

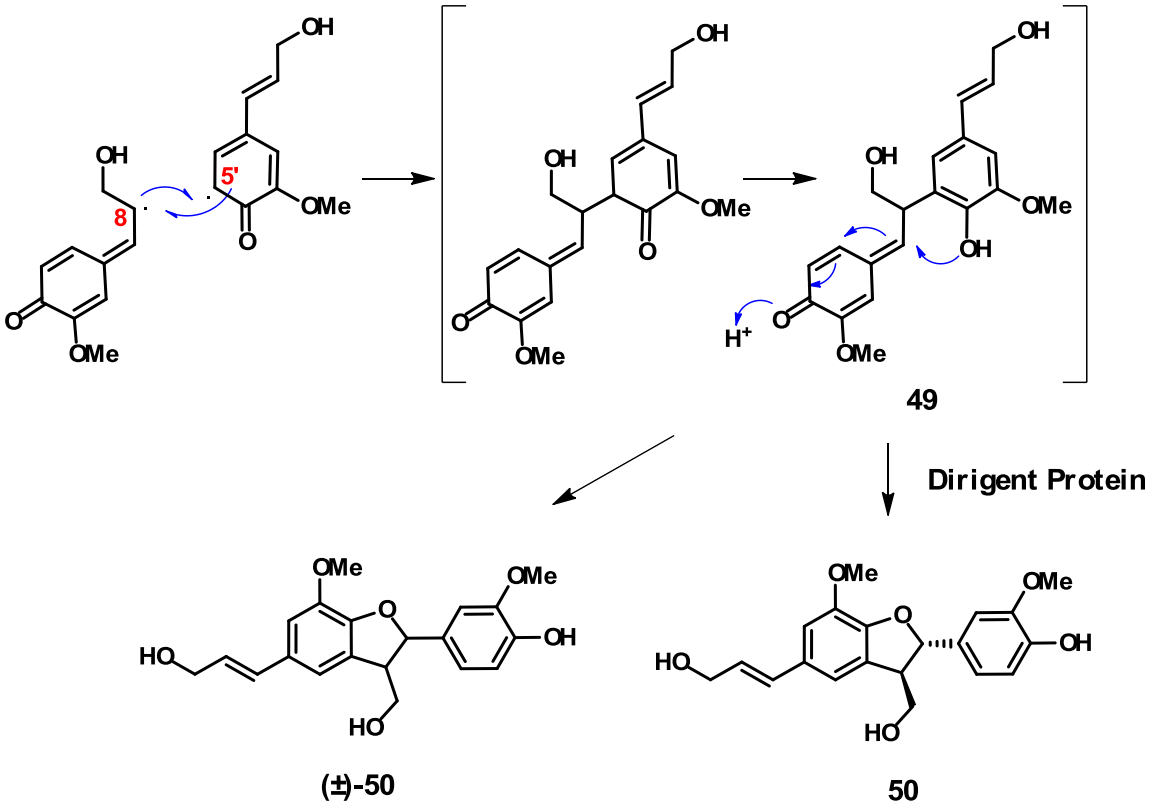

Scheme 2

Lignans, neolignans and related compounds are an attractive target for chemical synthesis/modification in view of their biological properties as well as of their structural variety. Some synthetic studies were inspired by natural neolignan 3',4-di-*O*-methylcedrusin (**51**), the active principle of Dragon's blood, a red viscous latex extracted from the cortex and by slashing the bark of various *Croton* spp. (Euphorbiaceae), used in South American popular medicine for several purposes, including wound healing and for its antiproliferative activity.[90]

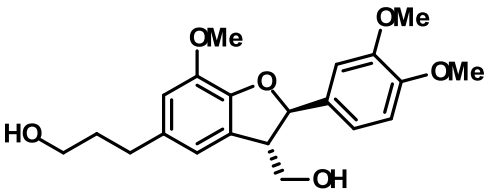

51

In 1999, Pieters and co-workers synthesized a series of 19 dihydrobenzofuran neolignans through a biomimetic reaction involving oxidative dimerization of *p*-coumaric, caffeic, or ferulic acid methyl esters, included compound **51**. These compounds were

submitted to the screening of the 60 human tumor cell lines panel developed on the National Cancer Institute (NCI) for potential anticancer activity.[91] From this study the racemic neolignan **52** (methyl caffeate dimer) proved to be the most promising antitumor compound with an average GI_{50} value of 0.3 μM. After chiral preparative-scale HPLC, the pure enantiomers were submitted to NCI protocol for anticancer activity and the 2*R*,3*R*-enantiomer of **52** was twice active than the racemic mixture as tubulin polymerization inhibitor, while the 2*S*,3*S*-enantiomer had minimal activity. Among the wide number of cell lines of NCI library compound **52** has turned out to be more active against some breast cancer cell lines (MDA-MB-435, MDA-N, and BT-549) with GI_{50} values ≈ 10 nM. Moreover, submicromolar IC_{50} value (0.2 μM) was proved for growth inhibition in HL 60 human leukemia cells; here again texting the two enantiomers separately was observed an increase of activity for 2*R*,3*R* enantiomer (IC_{50} = 0.08 μM). *In vivo* experiments on chorioallantoic membrane (CAM assay) have pointed out a pronounced antiangiogenic activity for the **52** 2*R*,3*R* enantiomer.[78] More recently, flow cytometric analysis in Jurkat T cell line has proved that compound **52** causes G2/M phase arrest and subsequent apoptosis through specific activation of caspase 3 and of some pro-apoptotic proteins.[92] Also the methyl ferulate dimer **53**, tested according to NCI protocol showed cytostatic activity, as mitotic inhibitor, with an average GI_{50} of 3.3 μM;[91] indeed, the synthetic dihydrobenzofuran neolignan **54** tested on Jurkat T lymphocytes ($p53^{+}/^{+}$) has revealed an induction of apoptosis with arrest in the G2/M phase of the cell cycle and inhibition of cell growth with GI_{50} of 0.1 μM.[93, 94]

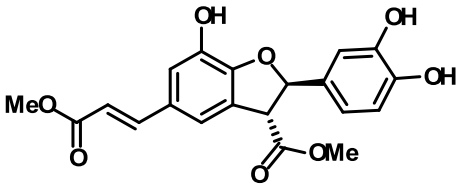

(±)-52

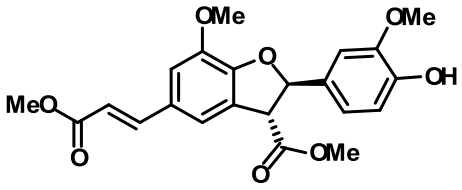

(±)-53

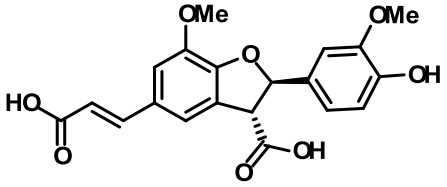

(±)-54

Further bioactive dihydrobenzofuran neolignans have been reported; among them, bohemenan H (**55**) and bohemenan K (**56**) showed strong cytotoxic activity against HeLa, Hep-2 and A-549 cell lines.[95] Dihydrobenzofuran neolignans originated by coupling of phenylpropanoid amides (neolignanamides) have been reported less frequently in the literature: *trans*-grossamide (**57**), showing moderate cytotoxic activity in LNCaP cells;[96] tribulusamides A (**58**) and B (**59**), isolated from *Tribulus terrestris* fruits, are reported for hepatoprotective activity.[97] Neolignanamides are then sub-group of the lignan family worth of deeper investigation, in view of their relative rarity in nature and the consequent limited number of biological studies concerning them. Generally amides show an higher metabolic stability than the isosteric esters; thus, neolignanamides should result more effective as potential chemotherapeutic agents than neolignans generated by coupling of phenylpropanoid esters.

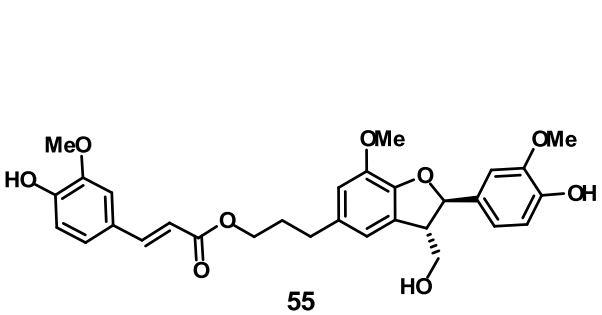

55

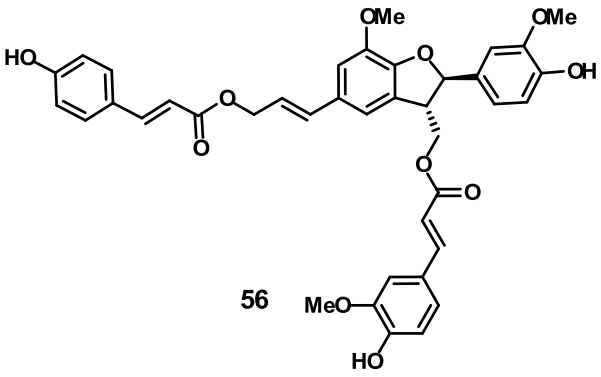

56

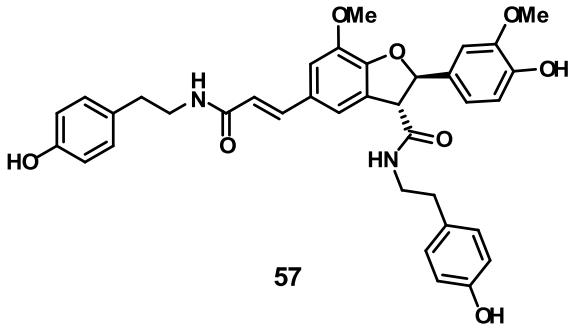

57

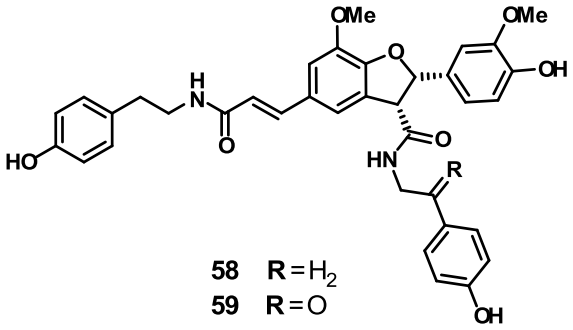

58 R = H_2
59 R = O

In the first part of this paragraph, I introduced the structural and biosynthetic difference between lignans and neolignans (see Schemes 1 and 2 and Figure 3). (+)-Pinoresinol (**48**), biosynthesized by 8-8' oxidative coupling reaction in presence of the proper DP, as above reported, is a lignan with a furofuran skeleton. Generally, plants give rise to a large diversity of dimeric products (lignans and/or neolignans) with various carbon skeleton types. Other examples of lignans are: podofillotoxin (**44**) with the typical aryl

tetrahydronaphtalene structure; the dienolignan cannabisin G (**60**) with a 2,3-bis(arylmethylene)succinic acid type skeleton; the aryldihydronaphtalene thomasidioic acid (**61**),the benzo[*k,l*]xanthene mongolicumin A (**62**), and the dibenzylbutyrolactone enterolactone (**63**) which will be discussed in the following.

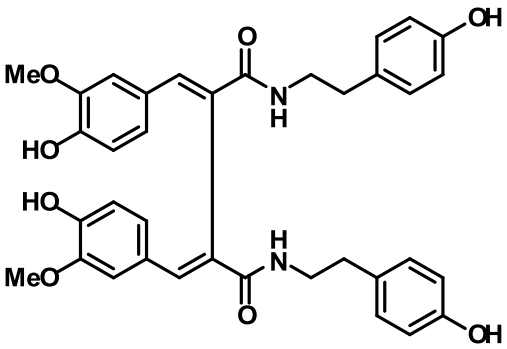

60

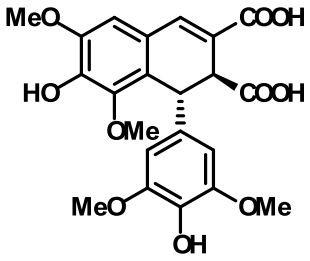

61

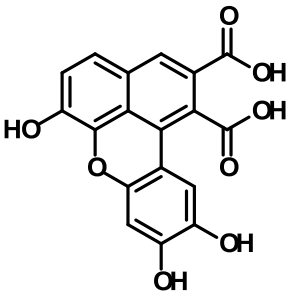

62

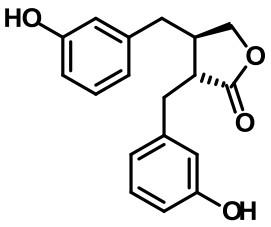

63

1.4.1.1. Benzo[k,l]xanthene lignans

Benzo[*k,l*]xanthene lignans are very rarely reported both among natural products and synthetic analogues. Nowadays only six naturally occurring benzaxanthenes are known, and the most representatives are rufrescide (**64**) isolated from *Cordia rufescens*, mongolicumin A (**62**) from *Taraxacum mongolicum*, its methyl ester **65** recently isolated from *Orobanche cernua* Loefling[98] and yunnaneic acid H (**66**) from *Salvia yunnanensis*. Due to their rarity in nature and the low yield of previous synthetic reactions to obtain analogues,[99] until recent times these compounds were almost unexplored with regard to their biological properties and possible pharmacological applications. In 2009, C. Daquino in collaboration with C. Tringali published a simple synthetic methodology to obtain benzo[*k,l*]xanthene lignans with high yields.[100] With this new method, based on a biomimethic approach, natural and unnatural benzoxanthenes have been synthesized and their biological properties have been evaluated.

Among them, the benzoxanthene obtained by oxidative coupling reaction of CAPE (**67**) showed DNA binding properties as intercalating agent, [101] antiangiogenic [102] and antiproliferative activity.[103]

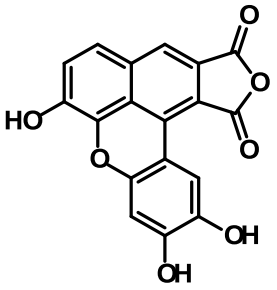

64

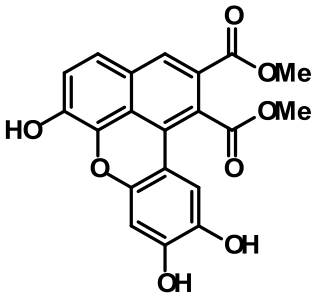

65

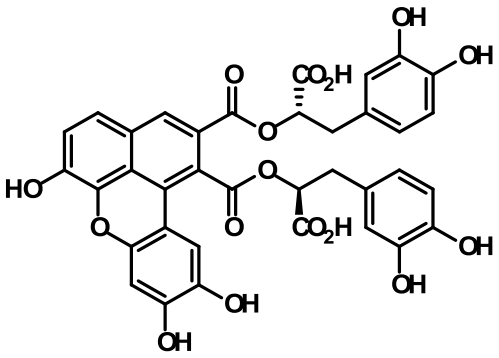

66

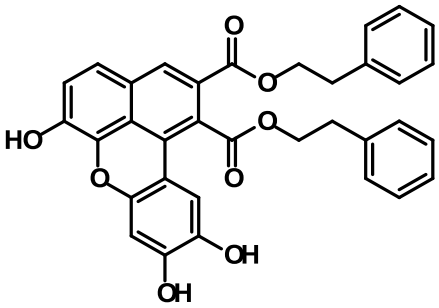

67

1.4.1.2. Mammalian lignans

In the early 80s, new dimeric compounds, enterolactone (**63**) and enterodiol (**68**) were found in mammalian fluids; [104 , 105] these two lignans became the most representative compounds of the rare 'mammalian lignans' subclass, also called enterolignans. Actually these lignans are obtained by intestinal bacteria conversion of plant lignans [106] including mataresinol (**69**), secolariciresinol (**70**) and pinoresinol (**48**) which are normally present in cereals (sesame and flax seeds), in beverages (coffee, tea) and in some fruits (berries). A growing number of *in vitro* and *in vivo* studies reported compounds **63** and **68** for their effect against health disorders such as cardiovascular diseases, brain function disorders, menopausal symptoms, and osteoporosis. [107] Moreover these two endogenous metabolites act against prostatic hyperplasia, [108] breast, [109] bowel, and other cancers. In recent years additional enterolignans related to **63** and **68** were detected in biological samples, but most of them remain unidentified. Thus, the structure and biological properties of these minor metabolites are still unknown.

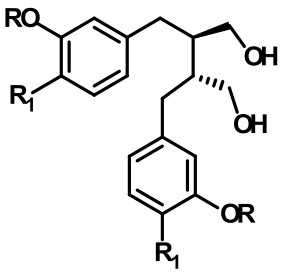

68 R = R$_1$ = H
70 R = Me, R$_1$ = OH

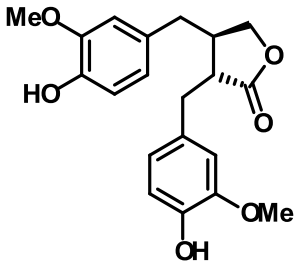

69 R = Me, R$_1$ = OH

Many research groups reported the total synthesis of the most representative mammalian lignans, while other articles described the synthesis of deuterium-labelled enterolignans.[110] In this contest, enterolignans labelled with stable isotopes have been employed for many purposes, such as quantitative analysis (by HPLC- or GC-MS) also in biological samples; evaluation of biological activities or study of their biogenetic pathways. In addition, labelled enterolignans may be useful to study their bioavailability, distribution, metabolism and interaction with possible biological targets.

1.4.2. Biomimetic synthesis of lignans and neolignans

The synthesis of dimeric compounds from monomeric phenols may be carried out by coupling of radical species through metal- or enzyme-mediated reactions. Both the methods try to mimic the lignan biosynthesis, based on oxidative coupling reactions, and for this reason these methods are frequently named 'biomimetic reactions'.

Oxidant agents as Ag_2O, $FeCl_3$, MnO_2, $Mn(OAc)_3$ and others, were reported to give dimers following the mechanism reported in Scheme 1 for lignans or in Scheme 2 for neolignans synthesis (mainly 8-5' coupling). In most cases the radical coupling reaction in presence of a metal occurs without any control on regio- and stereo-specifity and leads to a mixture of different dimer products.[111] A recent work on the biomimetic synthesis of natural and unnatural lignans of caffeic esters reported that the manganese-mediated reactions afforded in good yields the 8-8' dimers, namely lignans with benzoxanthene and aryl dihydronaphtalene skeleton. Conversely, in the presence of Ag_2O the main product was the 8-5' dihydrobenzofuran neolignan. A mechanism for the formation of these dimers has been proposed (in Scheme 3 the proposed mechanism for the benzoxanthene formation is reported) and experimental data and calculations corroborated the "orientation" effect towards 8-8′ coupling in presence of Manganese ions.[99]

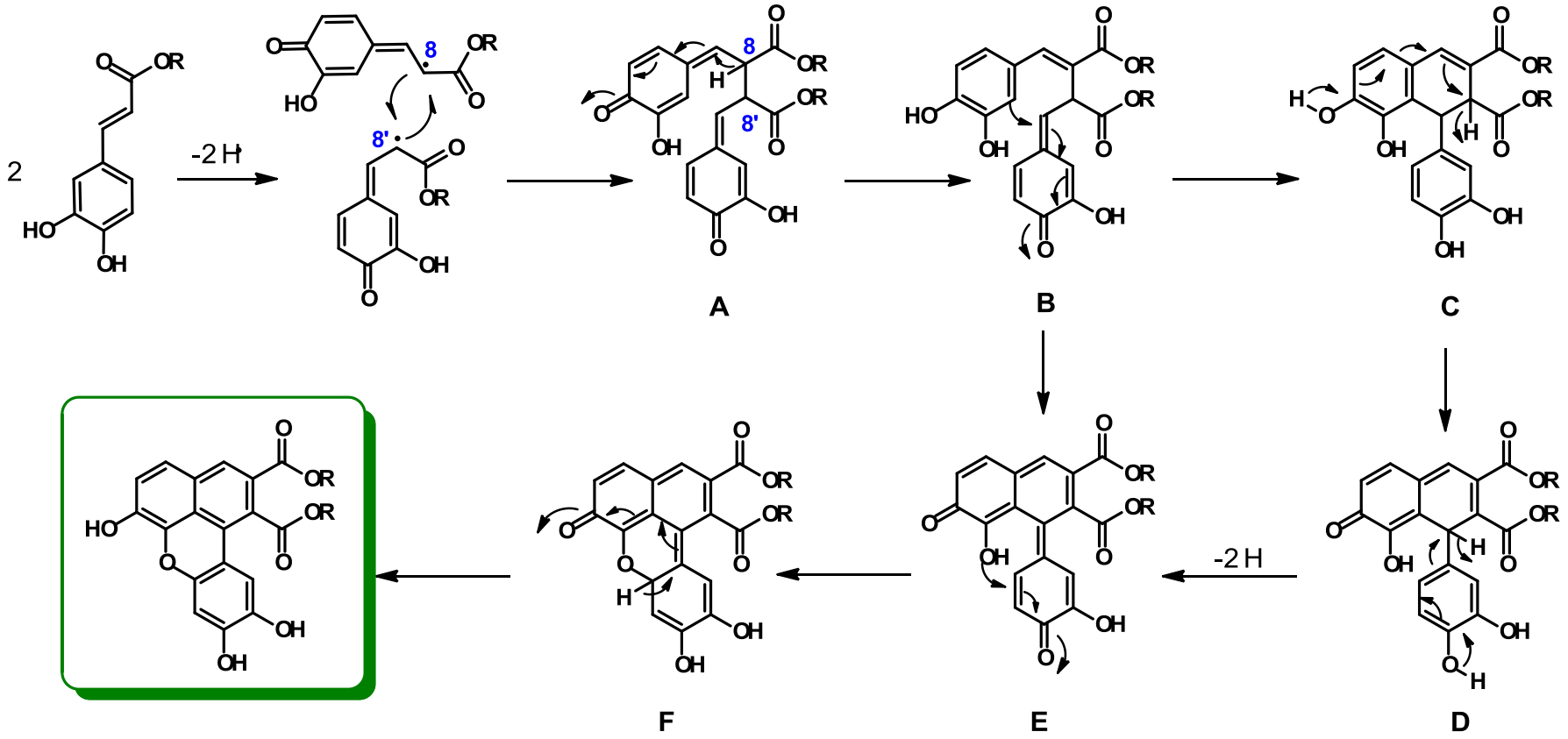

Scheme 3

The other biomimetic methodology is based on the use of enzyme-mediated reactions turning to be a sustainable process due to the use of environmentally friendly oxidases which convert O_2 or H_2O_2 into water. Laccases (polyphenol oxidases) belong to the family of blue multicopper oxidases. These enzymes oxidize a broad range of substrates, preferably phenolic compounds and natural and natural-derived neolignans can be obtained.[112] The structure of the enzymatic site and the mechanism of reaction today is well known and reported below in Figure 3 and in Figure 4. Precisely, laccase catalyzes the one-electron oxidation of four reducing-substrate molecules with the concomitant four-electron reduction of molecular oxygen to water (Figure 4), resulting in a green cycle.[113, 114]

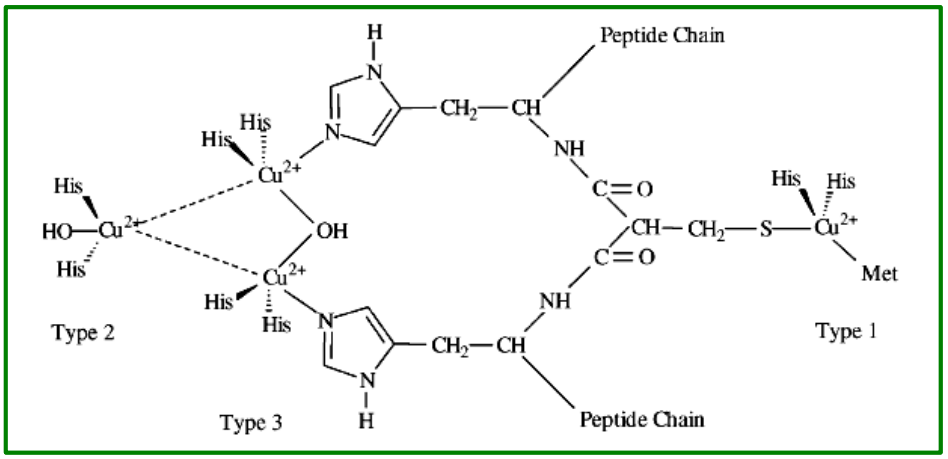

Figure 3. Model of the active-site structure of a laccase made of four copper atoms. Type 1 (T1) copper confers the typical blue colour to the protein and is the site where substrate oxidation takes place. Type 2 (T2) and Type 3 (T3)copper form a trinuclear cluster, where reduction of molecular oxygen and release of water takes place.[115]

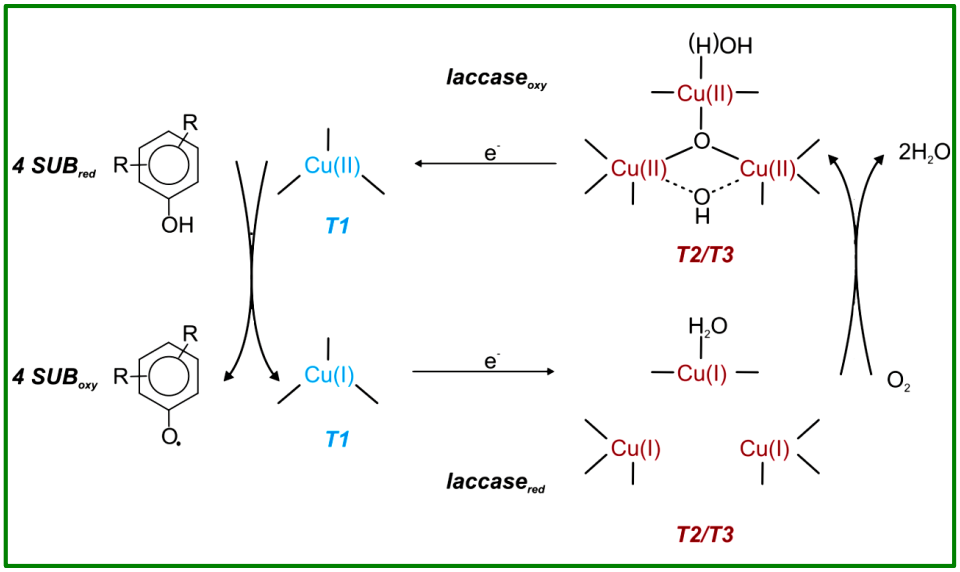

Figure 4. Schematic representation of a fungal laccase catalytic cycle. Two molecules of water result from the reduction of molecular oxygen (at T2/T3) and the concomitant oxidation (at the T1 copper site) of four substrate molecules to the corresponding radicals.[112]

Peroxydases are eme-protein working through the formation of a phenoxy radical and concomitant reduction of hydrogen peroxide (H_2O_2) to water, [116] as depicted in Figure 5. Also these enzymes have been used for biomimetic synthesis of dihydrobenzofurans. [117]

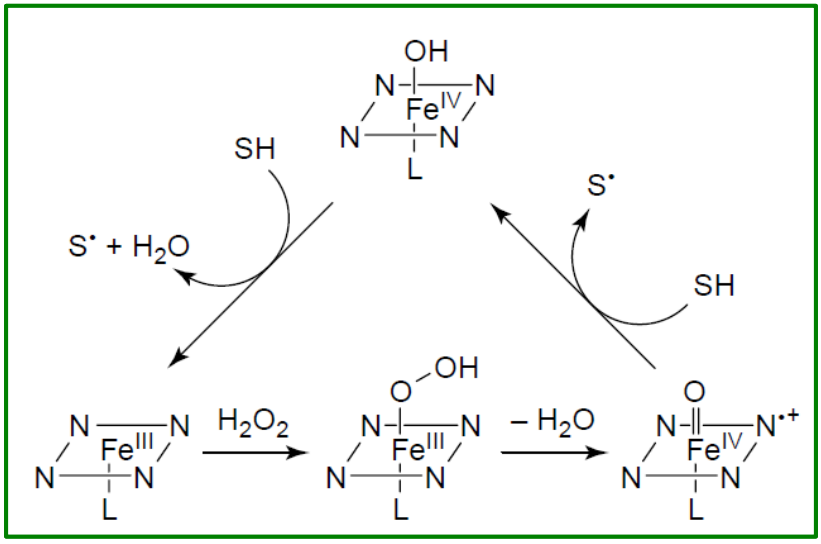

Figure 5. Schematic representation of Horseradish Peroxidase (HRP) catalytic cycle. Abbreviations: SH = substrate, S$^\bullet$ = radical substrate .

The application of enzyme-mediated reactions is common to various fields, including synthetic and analytical purposes,[114,118] environmental purpose for the wastewater treatment,[119] and biotechnology purpose for must and wine stabilization.[120]

1.5. NATURAL-DERIVED PROTEASOME INHIBITORS

The ubiquitin-proteasome system is involved in selective protein degradation and regulates almost all cellular events such as cell cycle progression, signal transduction, cell death, and others.[121] Therefore, proteasome inhibition is a promising therapeutic target, in particular for cancer therapy.[122] The synthetic dipeptidyl boronate, bortezomib (**70**), a drug for the treatment of multiple myeloma, many years ago become the first-in-class proteasome inhibitor at nanomolar concentration; but it gave cytotoxic effects at the same concentration.[123] Actually many molecules are in clinical trials; and many have showed higher cytotoxic activity than bortezomib. Because of systemic toxicity and side effects of them, research is oriented to developed less invasive drugs and many natural products and synthetic analogues have been studied as proteasome inhibitors. For instance, the marine bacterial metabolite salinosporamide A (**71**), interacting with the 20S proteasome subunit, proved to be a cytotoxic proteasome inhibitor[124] and is currently under evaluation (in clinical trials) against refractory lymphomas and myelomas, as well as various solid tumors.[125] The neolignan honokiol (**72**) has been reported as an apoptosis-inducer compound acting through an ubiquitin/proteasome mediated mechanism.[126] Many known proteasome inhibitors include an amide function; among them, sirbactins (general structure **73**) are natural macrocyclic β-lactames with an α,β-unsaturated amide function and recently have been reported as a class of promising proteasome inhibitors with IC_{50} in namomolar range.[127]

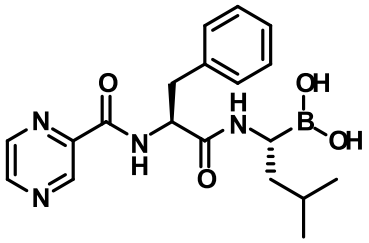

70

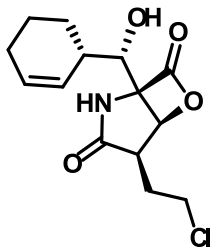

71

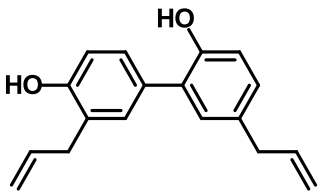

72

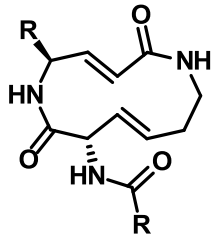

73

Some natural polyphenols, in particular those found in food and beverages, haverecently received growing attention as potential proteasome inhibitors; among them, the already cited epigallocatechin 3-gallate (**2**) resulted a potent covalent inhibitor of the 20S proteasome (IC_{50} <1 μM *in vitro*; in tumor cells IC_{50} = 1 – 10 μM).[128, 129] Moreover, because of the low metabolic stability of this polyphenol, some synthetic efforts have been made to obtain more stable analogues. For instance, the EGCG peracetate resulted more potent than the natural molecule as proteasome inhibitor, apoptosis inducer, and growth inhibitor in MDA-MB-231 breast cancer cells, resulting highly active also *in vivo*.[130] Resveratrol (**1**) was suggested to act as moderate proteasome inhibitor[131] as well as the natural 1,3-diarylpropanoid broussonin B (**74**), [132] isolated from *Anemarrhena asphodeloides*, which shows structural analogies with resveratrol and with dihydrostilbenes. An attractive example of natural proteasome inhibibitor including phenolic moieties and α,β-unsaturated amide function is avenanthramide C (**75**), a bioactive polyphenol found mainly in oats which possess anti-inflammatory properties through inhibition of NF-κB activation and suppress proteasome activity.[133]

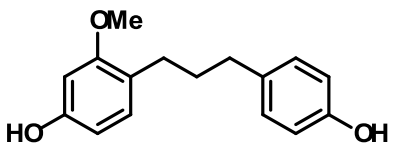

74

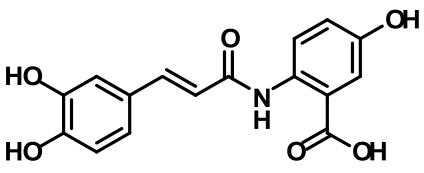

75

1.6. OBJECTIVES

The main goal of this PhD project is the synthesis of natural-derived polyphenols with potential antitumor activity. In the next section I will discuss about my research activity focused on different topics; most of them have been developed in the frame of collaborative studies.

- The recent growing attention to glycoconjugates as target-specific antiproliferative agents or effective pro-drugs lead the synthesis of new polymethoxystilbene derivatives conjugated with glucosyl and galctosyl moieties. Some biological properties of the new glycosides will be evaluated.
- The synthesis of two bioactive dimethoxystilbenes and a pre-clinical pharmacokinetic study by HPLC, in collaboration with Prof. H. Lin (University of Singapore), will be reported.
- A library of cinnamoyl amides will be evaluated as *m*PGES-1 inhibitors by a virtual screening in collaboration with Prof. G. Bifulco (University of Salerno). The best candidates will be synthesized and submitted to a cell-free bioassay in the laboratory of Prof. O. Werz (University of Jena).
- The promising biological properties and the structural variety of natural neolignans lead the synthesis of a library of dihydrobenzofuran dimers with amidic functions. An environmentally-friendly biomimetic methodology will be applied and the new compounds will be evaluated for their antiproliferative activity.
- In the frame of a collaboration with Prof. A. Casapullo (University of Salerno) an inverse virtual screening employing the approach of Compound-centric chemical proteomics (CCCP) will be employed to find new biological targets for the bioactive subclass of benzo[*k,l*]xanthene lignans.
- A preliminary study on new strategies for the synthesis of fully deuterated enterolactone, performed during a stage at the University of Helsinki, will be described .
- Some natural-derived polyphenols will be synthesized and evaluated as potential proteasome inhibitors in collaboration with Prof. R. Purrello (University of Catania) and Dr. A. M. Santoro (IBB-CNR of Catania).

The antiproliferative activity (with MTT assay) of polymethoxystilbene glycoconjugates and neolignanamides will be carried out by Prof. D. Condorelli (University of Catania).

2. RESULTS AND DISCUSSION

2.1. POLYMETHOXYSTILBENE GLYCOSIDES

Polymetoxystilbenes are a group of natural and natural-derived polyphenols which have proved better biological stability and activity than related phenolic stilbenoids such as resveratrol (**1**, see Introduction for specific examples). Although *Z*-polymethoxystilbenes have frequently showed an higher activity with respect to their *E*-stereoisomers, their intrinsic low stability, due to their easy conversion to the *E* form, prompted us to explore the possibility to enhance the anti-tumor properties of the more stable *E*-polymethoxystilbenes by selected chemical modification.

Among the target-specific receptors studied for anticancer drugs, glucose transporters (GLUTs), overexpressed in tumor cells, have recently been considered as a possible target for saccharide conjugated with antitumor compounds. These may selectively direct (and eventually release) the active aglycon towards tumor cells, sparing other noncancerous ones (drug/pro-drug strategy).

2.1.1. Synthesis and characterization

On this basis I planned the synthesis of gluco- and galactoconjugates of three polymethoxystilbenes as reported in the following.

The new stilbene glycosides were obtained with simple but effective reactions and the employed synthetic approach is reported in Scheme 4.[134]

The Wittig-type chemistry probably is one of the best approach for the synthesis of the stilbene nucleus based on non-metal-catalyzed reactions. Indeed the Horner-Emmons-Wadsworth olefination allows to obtain *E*-stilbenes with high selectivity over the *Z*-isomer. With this procedure three previously reported polymethoxystilbenes, studied for their biological properties, namely the 3,5,3′,4′-tetramethoxystilbene (**15**), the 3,5,4′-trimethoxystilbene (**16**) and the 3,5,3′,5′-tetramethoxystilbene (**82**) were synthesized; in a previous step, 3,5-dimethoxybenzyl bromide (**76**) and 4-methoxybenzyl chloride (**77**) were converted into the proper benzyl phosponates (**78** and **79** respectively) according to the Arbuzov rearrangement (Scheme 4a). These intermediates, in the presence of the suitable aldehydes gave the expected *E*-stilbenes with high yields.[35]

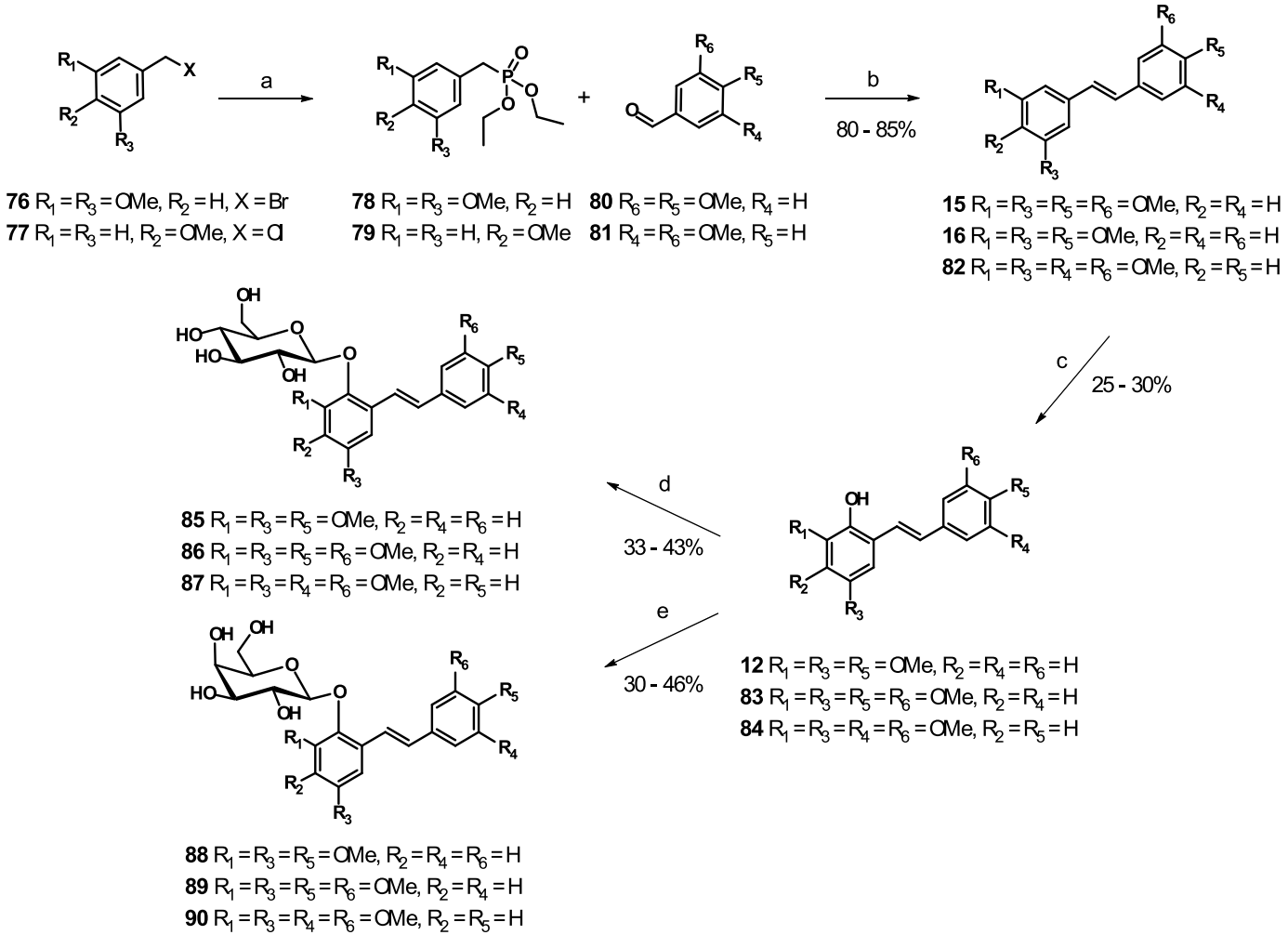

Scheme 4: **(a)** $P(OCH_2CH_3)_3$, 130 °C, 5 h; **(b)** CH_3ONa, DMF, 0 °C, 30 min, rt, 1 h, 100 °C, 1 h, rt, 24 h; **(c)** *m*-CPBA, CH_2Cl_2, rt, 35 min; **(d)** K_2CO_3, TBACl, MeOH:H_2O/ $CHCl_3$, tetra-*O*-acetyl-α-D-glucopyranosyl bromide, 24 h; **(e)** K_2CO_3, TBACl, MeOH:H_2O/ $CHCl_3$, tetra-*O*-acetyl-α-D-galactopyranosyl bromide.

The stilbenoids **15**, **16** and **82** were then subjected to mild hydroxylation at C-2 by *m*-CPBA (Scheme 1c) affording the corresponding 2-hydroxy-polymethoxystilbenes **12**, **83** and **84**. Their synthesis has previously been reported and in that article, atomic charge calculations (with PM3 semi-empirical optimizations) suggested that the hydroxylation probably occurs via regioselective aromatic electrophilic substitution of the activated *ortho* and *para* positions (respect to methoxy groups).[35] Compounds **12**, **83** and **84** are reported to inhibit the proliferation of SW480 colorectal tumor cells.[30]

The final step in this synthetic project was the conjugation of the 2-hydroxyderivatives to the anomeric carbon of an activated sugar via a nucleophilic substitution (S_N). Glycosydic bonds can be formed either through an S_N2 type mechanism, usually under basic conditions with glycosyl halides, or through an S_N1 type mechanism under acidic conditions. The choice of the reaction conditions depends on both the nature of glycosydic donor that the electron-donor or withdrawing properties of glycosydic acceptor.

Actually, there are several specific problems associated with glycosylation of phenols due to the electron-withdrawing properties of aromatic ring. From a general analysis results that:

- under acid conditions, phenols are weaker nucleophiles than alcohols; acceptable yields of *O*-glycoside derivative can be obtained using phenols carrying electron-donating groups, but this can also get a considerable amounts of *C*-glycoside product.
- under basic conditions, phenols are more acidic than alcohols, they are easily deprotonated and phenolate anions (especially those bearing electron-withdrawing substituents), as strong nucleophiles, give good yields.

A recent review summarizes the main procedures for glycosylation of different aromatic residues using the most common carbohydrates as donor of the glycosidic linkage.[135] Glycosyl halides result the most frequently used carbohydrate donors for aromatic *O*-glycosylation. Differently to the other types of donors, for example glycosyl acetates give low yields and the anomerization both of the starting material and of the product; glycosyl halides selectively give the *O*-glycosylation product with satisfactory yields (Scheme 5). Another advantage is that bromides are obtained as the thermodynamically favored α-anomer and since glycosylation generally results with the inversion of stereochemistry (S_N2 mechanism), the final product is a β-glycoside.

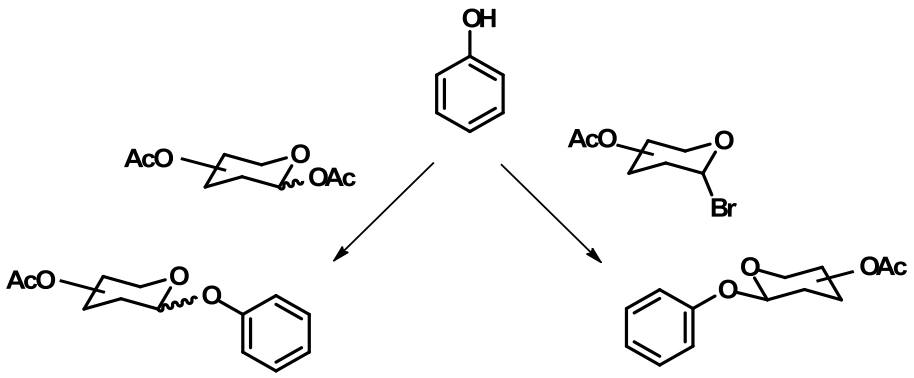

Scheme 5

Furthermore, this simple procedure has the character of a biomimetic synthesis because also in biological systems natural glycosides are formed through the reaction of an activated saccharide with the proper aglycone precursor.

The glycosylation protocol was of course optimized through several attempts (by changing temperature, solvent and reagents), to find the more suitable reaction conditions to obtain the desired *E*-polymethoxystilbene-2-*O*-β-D-gluco- and galactosides employing the tetra-*O*-acetyl-α-D-glucopyranosyl bromide and tetra-*O*-acetyl-α-D-galactopyranosyl bromide respectively. In a first attempt, reaction was carried out in basic condition and in dry ethanol at room temperature. In this conditions the reaction was slow and afforded a complex mixture of products. Better results were obtained in a biphasic system made up of H_2O:MeOH/$CHCl_3$ (keeping basic condition) and in presence of a phase transfer catalyst (tetrabutyl ammonium chloride, TBACl); the procedure was further optimized by temperature modulation (see Experimental section for details). The final reaction conditions are reported in Scheme 4d-e; as shown the applied strategy has the advantage gives in one step both the expected conjugation and acetyl function hydrolysis (but not glycoside bond hydrolysis) with 30-46% yield. No by-product was obtained from glycosilation and the recovered unreacted substrate eventually could be recycled for further reaction. With this procedure three polymethoxystilbene-2-*O*-β-D-glucosides (**85** - **87**) and the corresponding galactosides (**88** – **90)** were obtained after purification on Reverse Phase C-18. The new compounds were subjected to full structural characterization through spectral analysis including 2D NMR methods (COSY, HSQC, HMBC) which allowed unambiguous assignment of all ^{1}H and ^{13}C NMR signals. Some details of this characterization are reported in the following; in Table 1 and Table 2 respectively the ^{1}H and ^{13}C NMR data assignments for the glucosides **85** – **87** and **88** – **90** are collected.

Table 1: ^{1}H and ^{13}C NMR spectroscopic data of compounds **85** – **87**[a]

position	85		86		87	
	δ_C	δ_H (mult, *J* Hz)	δ_C	δ_H mult (*J* Hz)	δ_C	δ_H mult (*J* Hz)
1	134.1		133.9		141.1	
2	139.1		139.1		139.2	
3	154.5		154.7		154.7	
4	100.5	6.53 (d, 2.5)	100.7	6.53 (d, 3.0)	101.11	6.55 (d, 2.7)
5	158.4		158.4		158.4	
6	101.5	6.82 (d, 2.5)	101.5	6.82 (d, 3.0)	101.66	6.83 (d, 2.7)
7	123.1	7.67 (d, 16.5)	123.4	7.68 (d, 16.5)	125.8	7.77 (d, 16.2)
8	130.1	7.04 (d, 16.5)	130.3	7.03 (d, 16.5)	130.5	7.02 (d, 16.2)
1′	131.9		132.6		133.5	
2′	129.1	7.54 (d, 8.7)	110.8	7.27 (d, 1.5)	105.7	6.77 (d, 2.0)
3′	115.1	6.92 (d, 8.7)	150.68		162.5	
4′	160.9		150.46		101.08	6.40 (t, 2.0)
5′	115.1	6.92 (d, 8.7)	112.9	6.94 (d, 8.0)	162.5	
6′	129.1	7.54 (d, 8.7)	121.5	7.13 (dd, 1.5, 8.0)	105.7	6.77 (d, 2.0)
1″	106.4	4.72 (d, 8.0)	106.4	4.72 (d, 8.5)	106.2	4.74 (d, 8.0)
2″	75.9	3.56 (dd, 8.0, 9.0)	75.9	3.57 (dd, 8.5, 7.0)	75.9	3.56 (dd, 8.0, 8.5)
3″	77.9	3.48-3.42* (m)	77.98	3.43*(dd, 7.0, 7.5)	77.92	3.46-3.42* (m)
4″	71.5	3.48-3.42* (m)	71.6	3.45* (dd, 7.5, 4.0)	68.7	3.46-3.42* (m)
5″	78.1	3.20(ddd, 3.0, 5.0, 6.5)	78.01	3.18 (m)	78.02	3.18 (m)
6″	62.7	3.77 (dd, 3.0, 12.0) 3.67 (dd, 5.0, 12.0)	62.7	3.76 (dd, 3.5, 12.0) 3.66 (dd, 5.0, 12.0)	63.2	3.77 (dd, 2.5, 11.0) 3.65 (dd, 5.5, 11.0)
3-OCH$_3$	56.7	3.86 (s)	56.63	3.86 (s)	56.7	3.86 (s)
5-OCH$_3$	56.1	3.84 (s)	56.07	3.84 (s)	56.1	3.84 (s)
3′-OCH$_3$			56.49	3.91 (s)	55.9	3.83 (s)
4′-OCH$_3$	55.7	3.82 (s)	56.72	3.85 (s)		
5′-OCH$_3$					55.9	3.83 (s)

[a] Recorded in CD_3OD (500 MHz for ^{1}H NMR and 125 MHz for ^{13}C NMR). Signals with identical superscript (*) are partially overlapped.

Table 2: ^{1}H and ^{13}C NMR spectroscopic data of compounds **88** – **90**[a]

position	88		89		90	
	δ_C	δ_H (mult, *J* Hz)	δ_C	δ_H mult (*J* Hz)	δ_C	δ_H mult (*J* Hz)
1	133.6		133.4		140.6	
2	139.5		139.2		139.4	
3	154.6		154.5		154.6	
4	100.7	6.76 (d, 3.0)	100.6	6.77 (d, 3.0)	101.13	6.78 (d, 2.5)
5	157.4		157.2		157.3	
6	101.5	7.23 (d, 3.0)	100.9	7.26 (d, 3.0)	101.06	7.25 (d, 2.5)
7	123.2	8.60 (d, 16.5)	123.8	8.64 (d, 16.5)	123.0	8.75 (d, 16.4)
8	129.3	7.49 (d, 16.5)	129.4	7.52 (d, 16.5)	129.6	7.54 (d, 16.4)
1′	131.4		131.7		133.0	
2′	128.7	7.86 (d, 8.5)	110.0	7.72 (d, 2.0)	105.1	7.27 (d, 2.3)
3′	114.7	6.99 (d, 8.5)	150.1		161.6	
4′	159.9		149.6		101.13	6.71 (t, 2.3)
5′	114.7	6.99 (d, 8.5)	112.3	6.94 (d, 8.5)	161.6	
6′	128.7	7.86 (d, 8.5)	120.8	7.40 (dd, 2.0, 8.5)	105.1	7.27 (d, 2.3)
1″	107.2	5.46 (d, 8.0)	107.2	5.49 (d, 7.5)	107.2	5.48 (d, 8.0)
2″	73.6	4.93(dd, 8.0, 9.0)	73.3	4.92 (bdd, 7.5)	73.2	4.91 (dd, 8.0, 8.3)
3″	75.4	4.32 (dd, 3.5, 9.0)	75.2	4.32*(dd, 5.5, 9.3)	75.1	4.32 (dd, 3.3, 8.3)
4″	69.9	4.75 (bd, 3.5)	69.6	4.72 (bs)	69.5	4.70 (bd, 3.3)
5″	77.0	4.08(bt, 6.5)	76.7	4.09 (bdd, 5.5, 7.0)	76.7	4.08 (bdd, 5.5, 7.0)
6″	61.9	4.63 (dd, 6.5, 10.5) 4.36 (dd, 6.5, 10.5)	61.7	4.59 (dd, 7.0, 10.5) 4.36*(dd, 5.5, 10.5)	61.5	4.59 (dd, 7.0, 10.5) 4.35 (dd, 5.5, 10.5)
3-OCH$_3$	56.4	3.83 (s)	56.2	3.84 (s)	56.2	3.84 (s)
5-OCH$_3$	55.6	3.84 (s)	55.4	3.84 (s)	55.4	3.83 (s)
3′-OCH$_3$			55.8	3.94 (s)	55.3	3.82 (s)
4′-OCH$_3$	55.3	3.70 (s)	55.7	3.79 (s)		
5′-OCH$_3$					55.3	3.82 (s)

[a] Recorded in C_5D_5N (500 MHz for ^{1}H NMR and 125 MHz for ^{13}C NMR). Signals with identical superscript (*) are partially overlapped

However, ESI-MS and NMR spectra (^{1}H, ^{13}C, gCOSY, gHSQCAD, gHMBCAD) of glycosides **85** – **90** are reported in Supporting Material section (Appendix A), while the UV data and $[\alpha]_D^{25}$ values are reported in the Experimental section, where their synthesis is described in detail.

As an example of spectral analysis, the ^{1}H NMR spectrum of glucoside **86** is reported in Figure 6. The typical spin systems of stilbenoid moiety are clearly seen at lower fields: three signals at 7.27, 7.13 and 6.94 ppm imputable to an AMX system of ring B protons (H-2′, H-6′ and H-5′ respectively), two doublets at 6.82 and 6.53 ppm due to protons H-6 and H-4 respectively relative to ring A and the AB system due to the olefinic proton signals (7-H and 8-H protons) showing a *trans*-coupling constant (16.5 Hz). The four singlets in the 3.91 - 3.84 ppm region were assigned to the methoxy groups of the stilbenoid moiety.

Signals due to the glucosyl moiety are observed in the approximate range 3 – 5 ppm typical of saccharidic proton signals; the anomeric proton signal was easily recognized at 4.72 ppm as a doublet with axial/axial coupling constant ($J_{a,a}$ = 8.5 Hz) confirming that the reaction occurred with the inversion of configuration at C-1 and the desired β-glucoside was obtained. The other saccharide proton signals were unambiguously assigned thanks to COSY correlations highlighted in Figure 7 with red arrows.

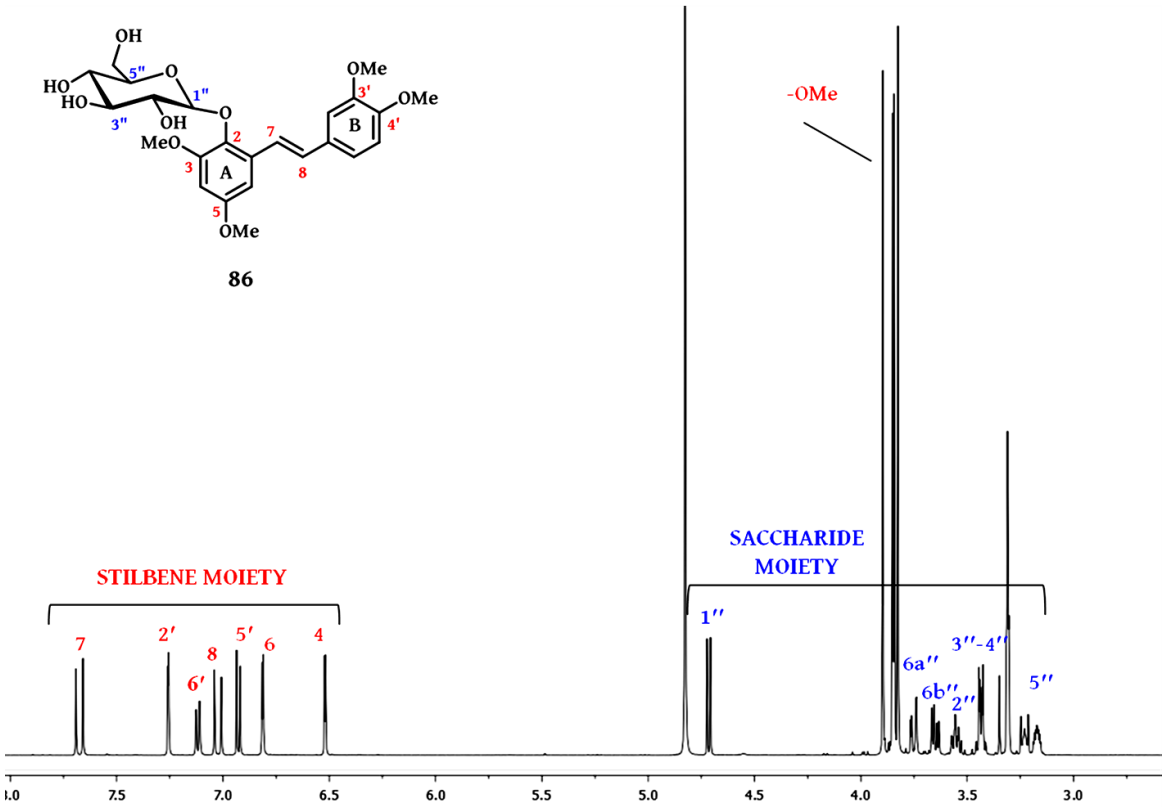

Figure 6: ^{1}H NMR spectrum (CD_3OD, 500 MHz) of **86**.

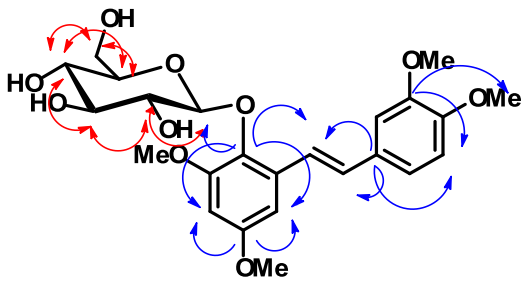

Figure 7: Selected COSY (red arrows) and HMBC (blue arrows) correlations for **86**

The ^{13}C-NMR spectrum of **86** is reporte in Figure 8, and shows 24 signals as expected; the signal at 106.4 ppm immediately confirms the glycosidic bond formation. HSQC and HMBC experiments allowed the unambiguous assignment of all carbon resonances. Among the deshielded quaternary sp^2 carbons (reasonably bound to oxygen atoms), the signal at 139.1 ppm was easily attributed to C-2 on the basis of its HMBC correlation with the H-4, H-6, H-7 signals of stilbene moiety and H-1" signal of glucose: this was an indisputable evidence that an *O*-glycosidic bond has been formed. Moreover, the other quaternary carbon signals were discriminated on the basis of their long range correlations. Thus, the signal at 158.4 which correlated with aromatic proton signals at 6.82 and 6.53 ppm

(H-6 and H-4) clearly was the C-5; the signal at 132.6 which correlated with olefinic proton signal H-7 at 7.68 ppm and with aromatic proton signal H-5' at 6,94 ppm, obviously was assigned as C-1'. The same observations were done for the carbon signals at 154.7, 150.68, 150.46 and 133.9 ppm (C-3, C-3', C-4' and C-1). In turn, the long range coupling (^{3}J) between the carbon C-3, C-5, C-3' and C-4' and methoxy groups protons signals (3.86, 3.84 3.91 and 3.85 ppm) allowed the unambiguous assignment for methyl ether groups supporting the correlations observed in HSQC. In Figure 8 the key HMBC correlations are highlighted with blue arrows.

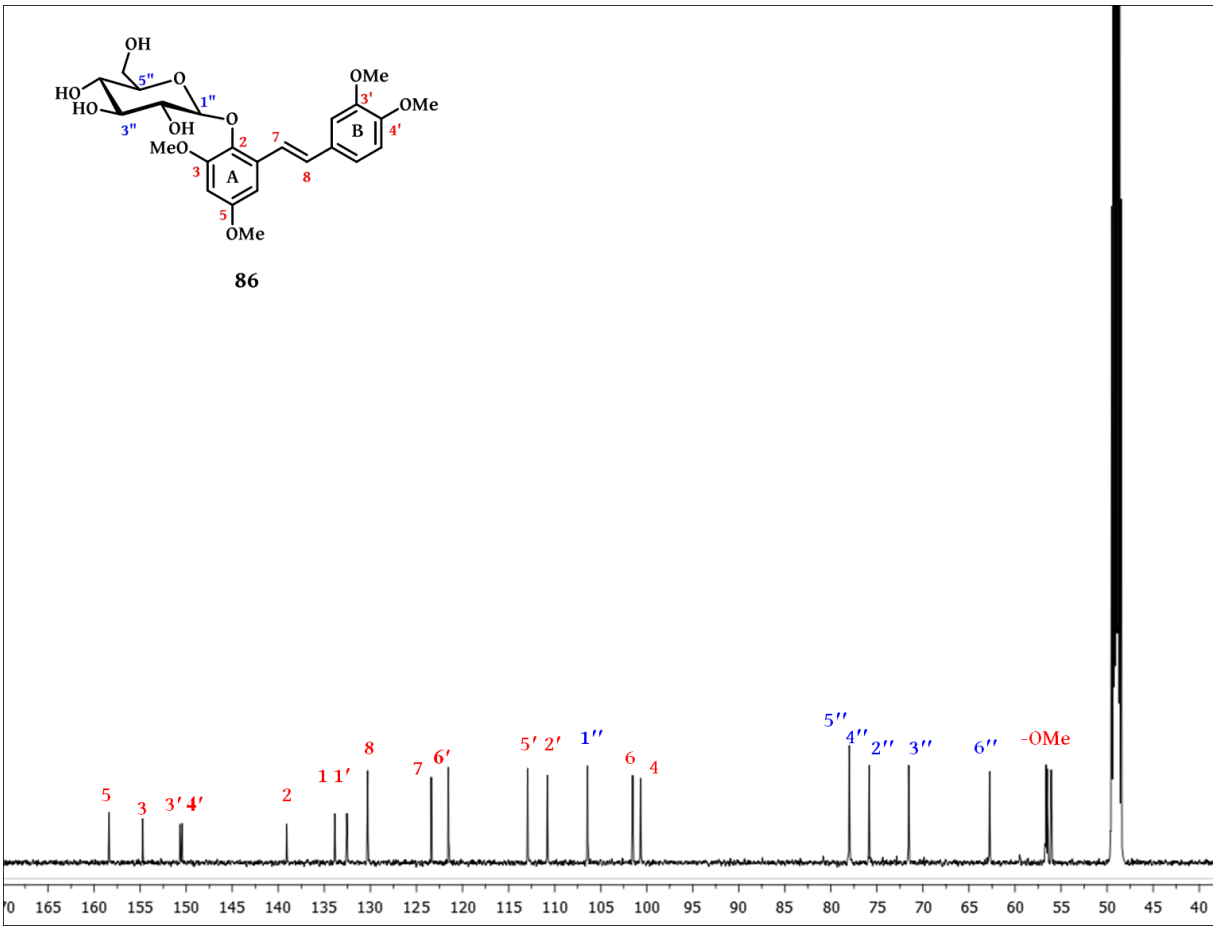

Figure 8: ^{13}C NMR spectrum (CD_3OD, 125 MHz) of **86**.

The same procedure led to the correct characterization of the remaining compounds as reported in Tables 1 and 2.

2.1.2. Antiproliferative activity

The glycoconjugates **85** – **90** were evaluated for antiproliferative activity towards two human cancer cells, the colon Caco-2 and the neuroblastoma SH-SY5Y cell lines with the Mosmann bioassay (MTT), in the laboratory of Prof. D. Condorelli (University of Catania). The 2-hydroxypolymethoxystilbenes **12**, **83** and **84** – **19** were included in the panel, both for comparison with the related conjugates and for a further evaluation of their previously observed antiproliferative activity on SW480 colon carcinoma cells.[35] In Table 3 the results are reported as the concentration inhibiting the 50% cell growth (GI_{50}); in this bioassay the anticancer dug 5-fluorouracil (**5-FU**) was used as positive control.

Table 3: Antiproliferative activity of compounds **12**, **83 - 90**[a]

Compounds	GI_{50} (μM) ± SD[b]	
	Caco-2[c]	**SH-SY5Y**[d]
12	5.8 ± 0.9	4.5 ± 0.5
83	3.0 ± 0.4	14.3 ± 3.5
84	> 100	> 100
85	> 100	21.9 ± 4.3
86	> 100	> 100
87	44.2 ± 5.8	> 100
88	> 100	48.4 ± 6.1
89	> 100	> 100
90	16.0 ± 2.8	22.5 ± 4.1
5-FU	2.2 ± 0.8	1.5 ± 0.1

[a] GI_{50} were calculated after 72 h of continuous exposure relative to untreated controls. [b] Values are the mean (± SD) of four experiments; [c] Caco-2: human colon carcinoma; [d] SH-SY5Y: neuroblastoma

Six of the tested compounds exhibited growth inhibition against at least one cell line, although the biological response shows significant variations for the different cell lines. In particular, compounds **83**, **87** and **90** proved more active towards Caco-2 (GI_{50} = 3.0, 44.2 and 16.0 μM respectively), whereas **85** and **88** were more active towards SH-SY5Y cells (GI_{50} = 21.9 and 48.4 μM respectively); compound **12** proved highly active both on Caco-2 and SH-

SY5Y cells. It is worth noting that compound **83** is potently active against Caco-2 cells with a GI_{50} value comparable to that of the anticancer drug 5-FU.

These results indicate that the 2-hydroxypolymethoxystilbenes **12** and **83** are able to interact with the cells; the substantial inactivity of compound **84** is rather surprising if one takes account of its close structural similarity with **83**. Interestingly, a reduction of the cantiproliferative activity was observed as an effect of conjugation of **12** and **41** both with glucose (**85** and **86** respectively) and galactose (**88** and **89** respectively): their conjugates are inactive towards Caco-2 cells, whereas a moderate activity is observed only for **86** and **88** towards SH-SY5Y cells. This suggests that, at least in Caco-2 cells, these compounds may not effectively uptake or may not adequately hydrolyze and do not interact with the biological target as conjugates. The reverse is observed for the inactive aglicone **84**: both its conjugates (**87** and **90**) are active towards Caco-2 cells, and the galactoside **90** also on SH-SY5Y cells.

In order to have further data to explain the biological results, we submitted the six stilbenoid glycosides to hydrolytic reactions in the presence of β-glucosidase or β-galactosidase, as an *in vitro* experimental model for a possible hydrolysis by intracellular enzymes.

2.1.3. Enzymatic cleavage assay

In order to evaluate the possible cleavage activity of endo-glycosidases (β-glucosidases and β-galactosidases), I developed an HPLC method to study the release of aglycone from compounds **85** – **90**, in presence of β-glucosidase from almonds or of β-galactosidase from *Aspergillus oryzae*.

The method was previously tested on the standards *p*-nitrophenyl β-D-glucopyranoside (*p*NP β-Glc) and *o*-nitrophenyl β-D-galactopyranoside (*o*NP β-Gal) in order to evaluate also the activity of the two enzymes on both gluco- and galacto-derivatives. Compounds **85** – **90** were dissolved in DMSO and diluted in phosphate buffer to a final concentration of around 5.0×10^{-5} M (the final concentration of DMSO did not exceed 1.0 %); the enzymatic reactions were incubated at 37 °C and the course of hydrolysis was monitored by HPLC on RP-18 at 305 nm up to 96 h. As an example, in Figures 9 and 10 the HPLC profiles respectively for compound **87** (in presence of β-glucosidase from almonds) and **90** (in presence of β-galactosidase from *Aspergillus oryzae*) are reported; it is evident that the former undergoes enzymatic hydrolysis and the second shows no hydrolysis.

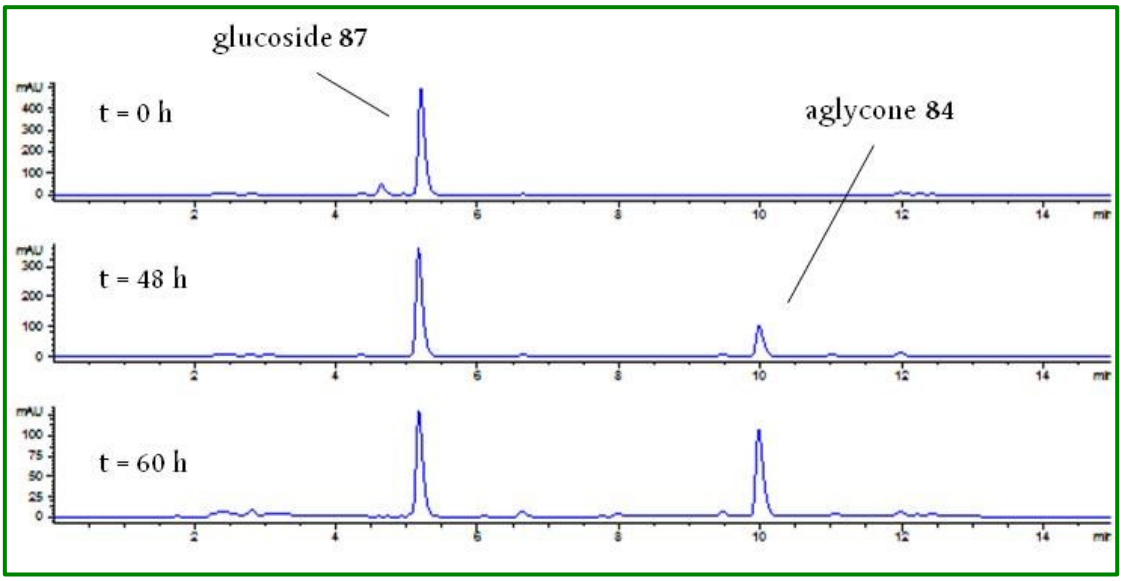

Figure 9: HPLC profiles of **87** at selected time intervals, λ: 305 nm

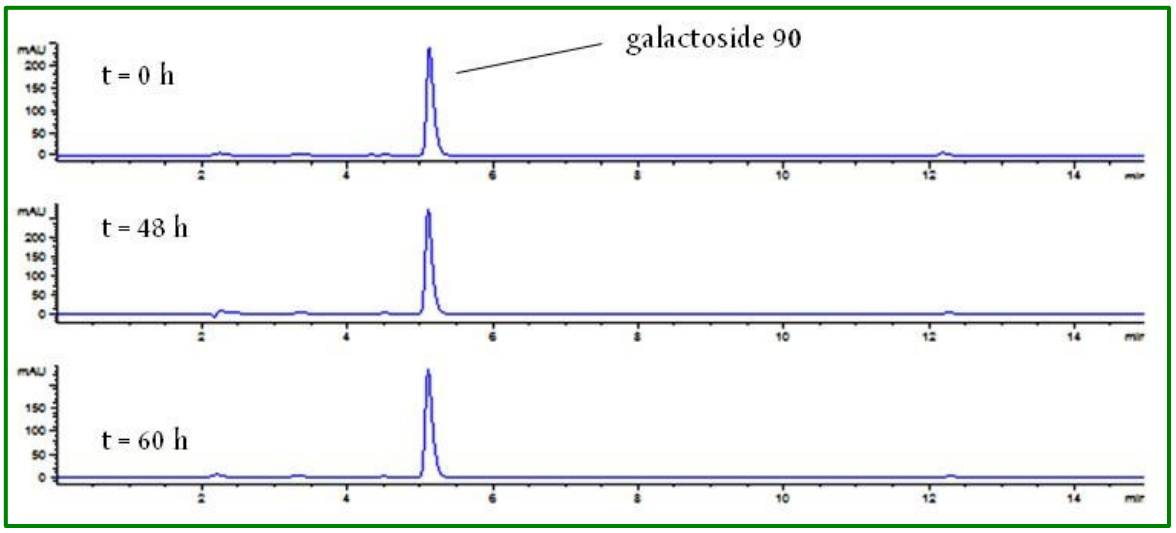

Figure 10: HPLC profiles of **90** at selected time intervals, λ: 305 nm

In order to quantify the aglycone released by the cleavage assay, calibration curves were carried out for aglycones **12**, **83** and **84**; the residual concentration of glycosides, was indirectly determined, through the quantification of aglycon released in time. The residual concentration of each substrate (**S** in graphics) at different times, up to 96 h was plotted and the kinetic hydrolysis profiles for the six glycoconjugates in presence of β-glucosidase from almonds and of β-galactosidase from *Aspergillus oryzae* are reported in Figure 11. With the green marker I depicted the kinetics for compounds which undergo to hydrolytic reaction, while with the blue marker I depicted the slow hydrolytic kinetic profiles.

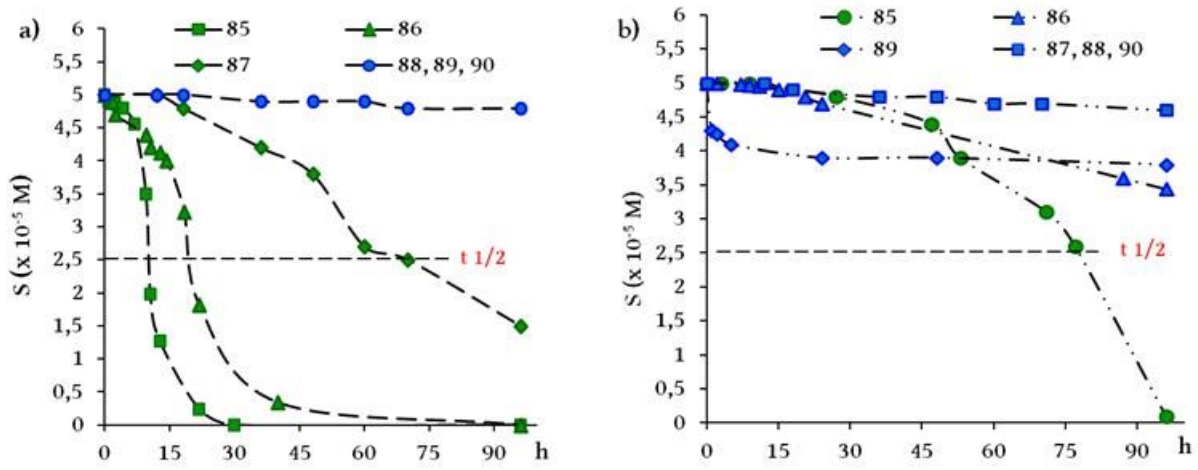

Figure 11: Kinetic hydrolysis profiles of **85 – 90** at 37 °C (pH = 7.2) in the presence of: **a**) β-glucosidase from almond, **b**) β-galactosidase from *A. oryzae*. S = Substrate.

More than 50% of the glucosides **85** – **8**7 were hydrolyzed until 96 h by β-glucosidase from almonds, showing an half-life time ($t_{1/2}$) of 11, 20 and 70 h respectively; conversely no significant hydrolysis was observed for galactosides **88** – **90**. Whereas, all the glycosides were not hydrolyzed by β-galactosidase up to 96 h except compound **85** which underwent a very slow hydrolysis, with half-life of 77 h. In summary, only **85** and **86** were significantly hydrolyzed by β-glucosidase, with a half-life much shorter than the 72 h duration of the biological assays (**87** showed half-life paragonable to duration of biological assay).

These results suggested that, although glucoside **85** are not adequately taken up in tumor cells, the high hydrolytic rate by intracellular β-glucosidases, (and slower by intracellular β-galactosidases) affording the active aglycone **12**, might justify the observed activity. The observed growth inhibition by **87**, **88** and **90** (Table 3) indicate that these conjugates are adequately taken up, at least by one of the two cell lines; their activity, that seems not attributable to the hydrolytic release of the aglycone, should be due to their specific structural features.

The lack of hydrolytic effect by β-glucosidase and especially by β-galactosidase for most of the glycosides prompted us to investigate if these compounds might act as β-glucosidase or β-galactosidase inhibitors.

2.1.4. Glycosidases inhibition assay

A slight modification of the method of Tsujii *et al.* [136] was used to evaluate the inhibition of β-glucosidase from almonds, β-galactosidase from *A. oryzae* by compounds **85** – **90**. Finally also the α-glucosidase from *Saccharomyces cerevisiae* was employed into the assay given the growing interest towards α-glucosidase inhibitors as potential anti-diabetic agents.

Firstly, the activity of the three enzymes was spectrophotometrically determined at 405 nm by monitoring the release of *p*-nitrophenol and *o*-nitrophenol from the substrates (standards) *p*NP-β-Glc or *p*NP-α-Glc for glucosidases) and *o*NP-β-Gal (for galactosidase), respectively at 25 °C. Preliminary kinetic studies of the three enzymes in the presence of pertinent substrate have provided the incubation times after that there is no change in the intensity of absorption spectrum of substrate (30 min for β-glucosidase and β-galactosidase and 1.5 h for α-glucosidase). In this way, the absorbance variation observed in the subsequent experiments with the six compounds **85** – **90** was only ascribed to the inhibitor effect of glycosides.

In Figure 12 I reported the UV spectra of *p*NP α-Glc after 1.5 h of incubation with the α-glucosidase (with the black line) and in presence of increasing amounts of **89** (from blue to orange) which was one of the three glycosides with best inhibition activity against the α-glucosidase from *S. cerevisiae* (IC_{50} = 70 μM). Conversely, in Figure 13 I reported the UV spectra of *p*NP α-Glc after 1.5 h of incubation with the same enzyme (with the black line) and in presence of increasing amounts of **88** (from blue to orange) as an example of no significant inhibitory activity. The percentage of inhibition was determined for each compound from the residual activity by comparing the enzyme activity with and without compounds and the concentration required for 50% inhibition of enzyme activity under the assay conditions was defined as the IC_{50} value. In Table 4 the IC_{50} values for the inhibition of the three enzymes are summarised; acarbose was used as positive control.

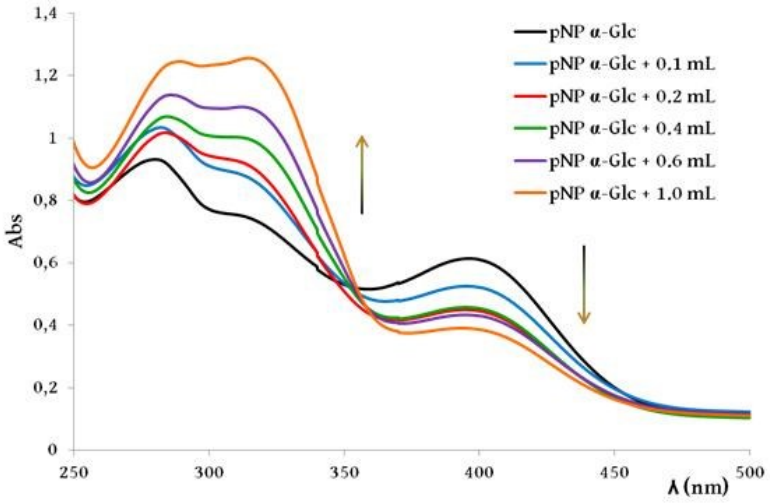

Figure 12: UV spectra of *p*NP α-Glc in presence of α-glucosidase and increasing amounts of **89** after 1.5 h incubation.

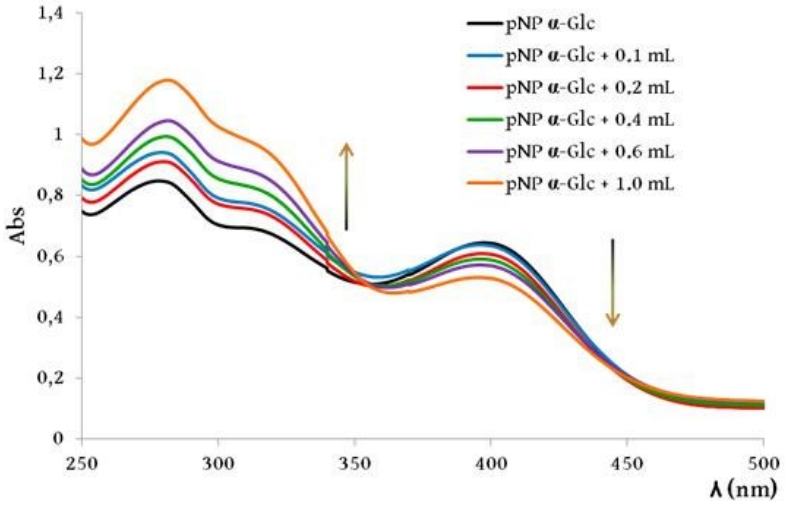

Figure 13: UV spectra of *p*NP α-Glc in presence of α-glucosidase and increasing amounts of **90** after 1.5 h incubation.

Table 4: β-glucosidase, β-galactosidase and α-glucosidase inhibitory activity of **85 – 90**

Compounds	IC_{50} (µM) ± SD[a]		
	β-glucosidase from almonds	**β-galattosidase from *A. oryzae***	**α-glucosidase from *S. cerevisiae***
85	208 ± 47	n.d.	91 ± 17
86	192 ± 50	258 ± 42	78 ± 21
87	272 ± 16	297± 68	133 ± 19
88	350 ± 6	298 ± 68	201 ± 29
89	170 ± 60	299 ± 53	70 ± 3
90	n.i.	296 ± 12	332 ± 70
Acarbose			65 ± 9

[a] Values are the mean (± SD) of three experiments; n.i.: no inhibition; n.d: not determined

Most of the compounds showed moderate inhibitory activity towards the three enzymes with IC_{50} values in the approximate range 170 – 350 μM. These data are noteworthy, if compared with previously reported IC_{50} values of other glycosidase inhibitors.[137] All the determined IC_{50} values are substantially similar and no significant difference was observed between glucosides and galactosides. Noteworthy, compounds **85**, **86** and **89** (IC_{50} = 91, 78, 70 μM respectively) showed a promising inhibitory activity towards α-glucosidase, in particular if compared with the anti-diabetic drug acarbose (IC_{50} = 65 μM),[138] or with many previously reported α-glucosidase inhibitors, whose IC_{50} values are higher than 100 μM.[139] In this regard we would also mention here that resveratrol (**1**) and other related stilbenoids have previously been reported for α-glucosidase inhibition,[140, 141] antidiabetic or antiobesity activity.[142] In addition, the stilbenoid glucoside desoxyrhaponticin (5-hydroxy-4'-methoxystilbene-3-*O*-β-d-glucopyranoside) isolated from *Rheum emodi*[143] and closely related to compounds **85** – **90**, was reported as yeast α-glucosidase inhibitor.

Finally, it is also noteworthy that the most effective α-glucosidase inhibitors **86** and **89** showed a negligible antiproliferative activity.

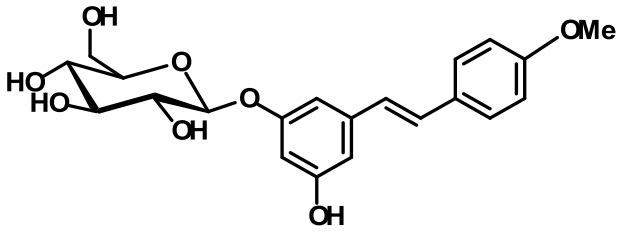

desoxyrhaponticin

2.2. DIMETHOXYSTILBENES

As reported in the Introduction, some bioactive polymethoxystilbenes have been studied recently for their bioavailability because of their presumed longer half-life and reduced metabolic conversion with respect to their hydroxylated analogues. In this context, I synthesized two previously reported dimethoxystilbenes, namely compounds **95** and **96**. These dimethoxystilbenes were obtained according to the Arbuzov rearrangement followed by the Horner-Emmons-Wadsworth reaction (See Scheme 6). Very briefly, after the activation of benzyl bromide (**91**) into the pertinent phosponate (**92**), by reaction with the appropriate aldehyde the two *E*-dimethoxystilbenes were obtained. The analysis of ^{1}H and ^{13}C NMR spectra and the comparison of spectral data (reported in Experimental, section 5.3.2.) with those previously reported confirmed the formation of expected compounds.

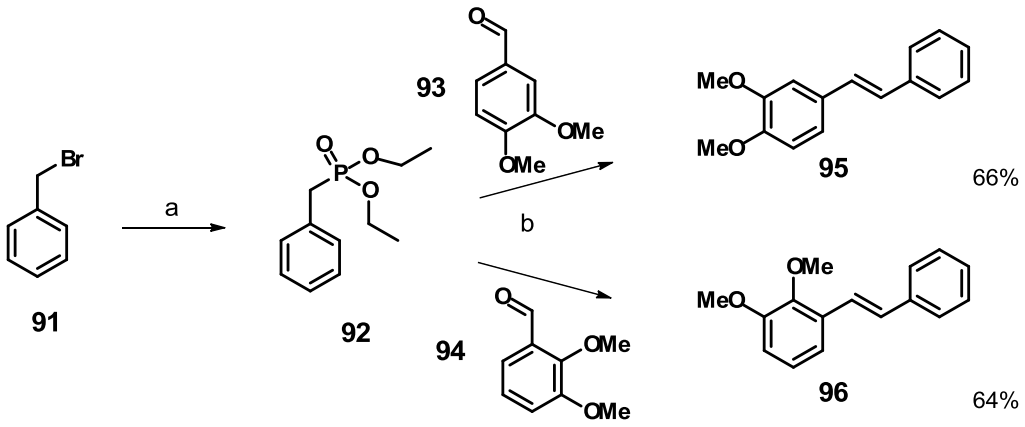

Scheme 6: (a) $P(OCH_2CH_3)_3$, 130 °C, 5 h; **(b)** CH_3ONa, DMF, 0 °C, 30 min, rt, 1h, 100 °C, 1h, rt, 24h.

The 3,4-dimethoxystilbene (**95**) has preiously been reported for the promising anti-angiogenic activity in various pre-clinical models;[144] the 2,3-dimethoxystilbene (**96**) has been reported as inhibitor of NF-kB activation induced by human tumor necrosis factor alpha (TNF-α).

These two compounds were delivered to the laboratory of Prof. Lin and submitted to the pharmacokinetic study: the results have been recently published.[145] In this study a simple HPLC method was developed and validated to determine **95** and **96** in rat plasma and showed

that these stilbenoids have low and erratic plasma exposure, fast clearance and poor oral bioavailability.

2.3. DERIVATIVES OF PHENOLIC CINNAMIC ACIDS

2.3.1. Synthesis of cinnamic amides as *m*PGES-1 inhibitors

In the Introduction I have reported that simple amide derivatives of natural cinnamic acids may be worth of investigation as possible lead compounds for various chemotherapeutic applications including *m*PGES-1 inhibitors; this latter is a new target for the development of a new class of selective anti-inflammatory drugs.

In this context, I devoted part of my PhD research activity to the synthesis of natural-derived polyphenolic amides. In the frame of a collaboration with the group of Prof. G. Bifulco (University of Salerno) in search for a new generation of anti-inflammatory agents, a library of 22 cinnamic acid amides (**97 - 118**) have been evaluated in a virtual screening aimed to discovery new *m*PGES-1 inhibitors.

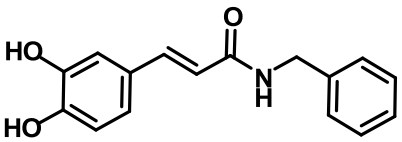

97

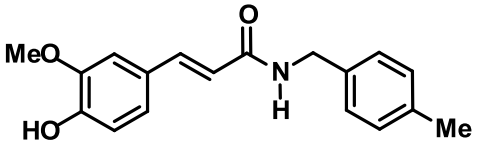

101

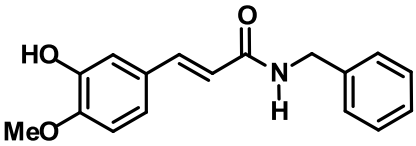

98

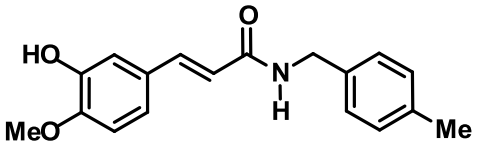

102

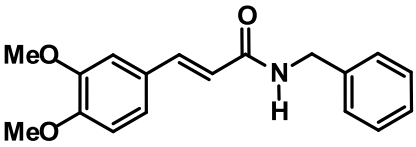

99

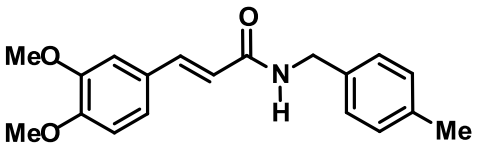

103

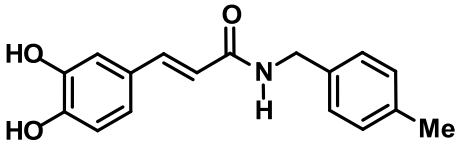

100

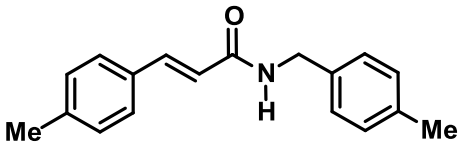

104

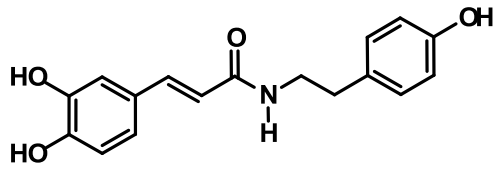

105

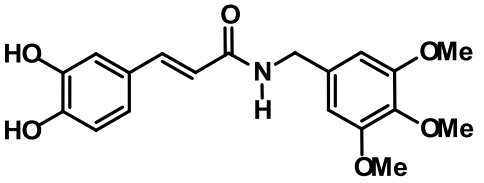

112

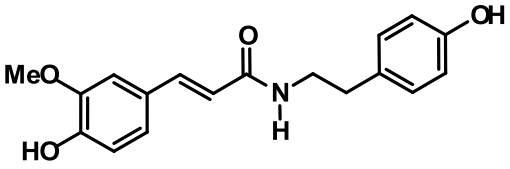

106

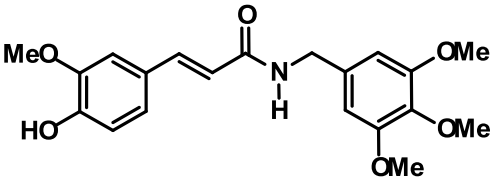

113

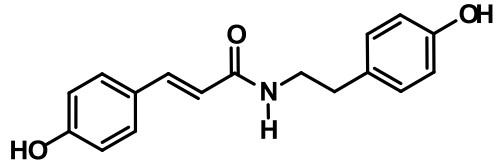

107

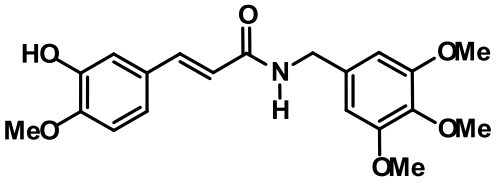

114

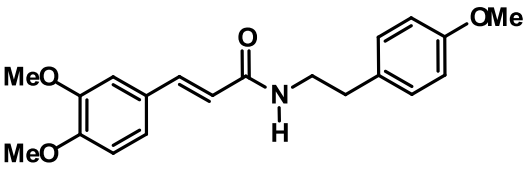

108

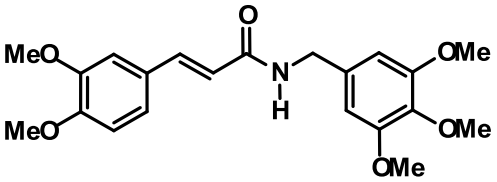

115

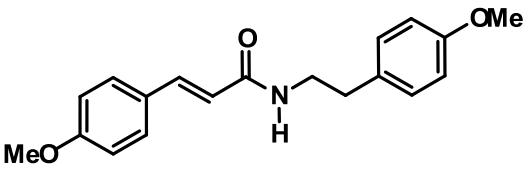

109

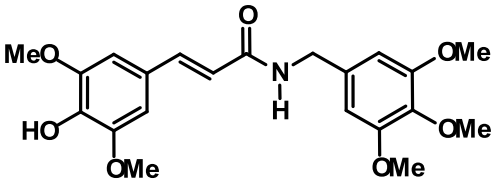

116

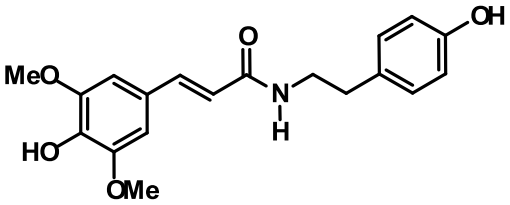

110

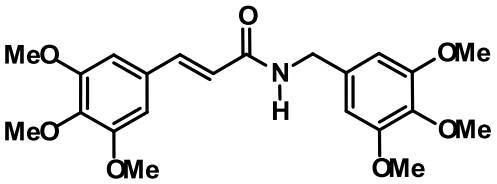

117

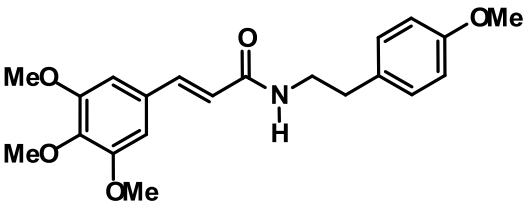

111

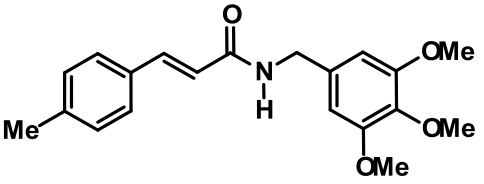

118

The library has been designed on the basis of structural features found in previously reported biologically active amides: namely a) the structural portion of acryl and cinnamic amides; b) the presence of a phenolic moiety derived from natural phenolic acids (*p*-coumaric, caffeic, ferulic, and synapic); c) the presence of a portion derived from amines with aromatic pendants with different steric hindrance and lipophilicity.

The binding energy values of the complex enzyme-substrate (ES) for the 22 cinnamoyl amides are reported in Table 5.

Table 5. Binding Energy values (using the software Autodock 4.2) of **97 - 118** with *m*-PGES-1.

Compound	Binding energy (kcal/mol)
97	-6.18
98	-6.12
99	-5.89
100	-6.32
101	-5.91
102	-5.99
103	-5.07
104	-6.19
105	-6.24
106	-6.07
107	-6.02
108	-6.30
109	-6.35
110	-6.05
111	-6.21
112	-5.87
113	-5.61
114	-6.43
115	-6.07
116	-5.92
117	-6.02
118	-6.18

The docking showed very similar binding energy values for the 22 cinnamic acid amides, in the range -5.61 and -6.43 kcal/mol suggesting that these compounds show comparable affinity for the binding site of *m*PGES-1. A careful analysis of the ES complex interactions revealed more information: the presence of the phenolic –OH in *para* position of cinnamic moiety, when present, is involved in the hydrogen bonds formation (as donor and/or acceptor); the aromatic ring partially sits in the pocket of catalytic site (stabilized by vand der Waals and π-π interactions). Moreover, caffeic acid derivatives bearing a further OH group on the aromatic ring are able to form (as donors) a hydrogen bond with the glutamate residue of glutathione (*m*PGSE-1 is a GSH dependent enzyme).

In the Figure 14 the binding site model of *m*PGES-1 and the key interactions with compound **100** are reported: the OH group in *para* position is involved as donor in a hydrogen bond with the carboxyl group of the side chain of Asp49 and as acceptor with the NH group of Ala45; the aromatic portion of caffeic acid established a 'cation-π' interaction with Arg126. The 4-methylbenzyl residue partially sits in the pocket of the catalytic site stabilized by π-π interaction with aromatic ring of Tyr130 and by van der Waals interactions with Ile32, Ala31, Tyr28, Thr131.

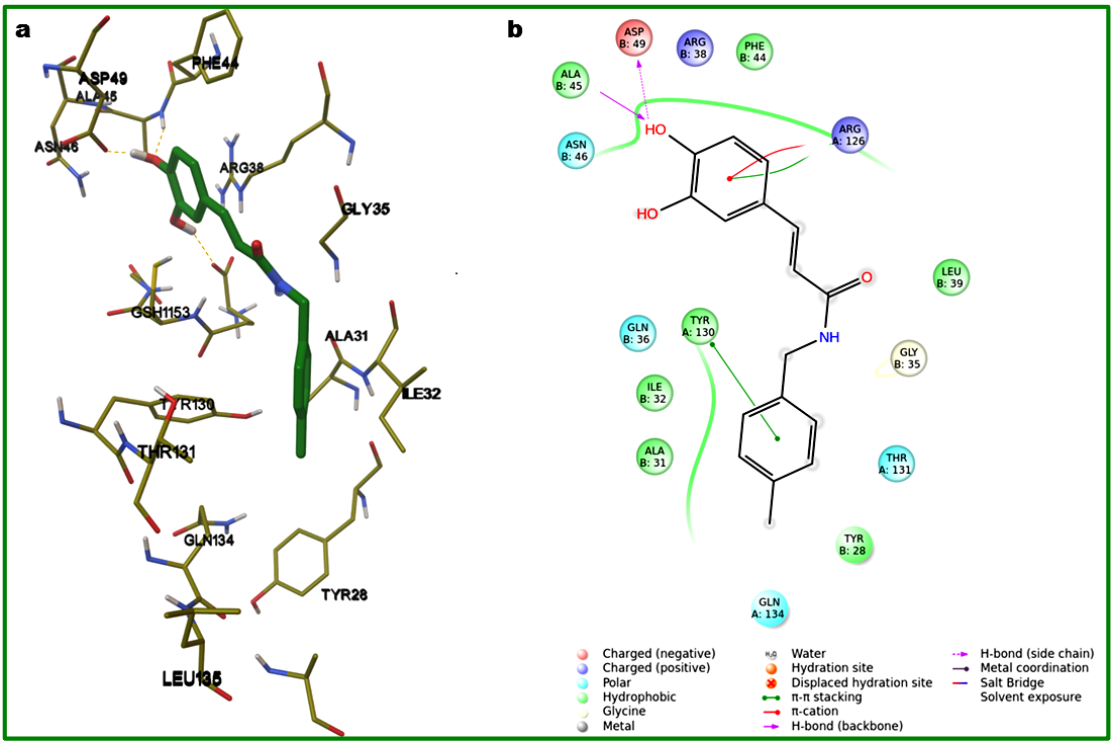

Figura 14: Binding site model of *m*PGES-1 with compound **100**. a) 3D model of interaction of **100** with *m*PGES-1; the enzyme and the amide are depicted by sticks (by atom type: red for O, white for H, blue for N, yellow for carbon backbone of enzyme and green for carbon skeleton of **100)**. b) 2D representation of *m*PGES-1 interactions with **100**.

On the basis of the above reported data, six of the 22 cinnamoyl amides were selected for the synthesis, namely compounds **100**, **102**, **113** and **114**; compounds without free fenolic groups, **108** and **117**, were chosen as negative controls.

The synthesis of the selected cinnamoyl amides was carried out according to the general procedure summarised in Scheme 7: the reaction involves the amidation of caffeic (**6**), ferulic (**25**) and sinapic acids (**26**) by reaction with the appropriate amine (4-methylbenzylamine, **119**; 3,4,5-trimethoxybenzylamine, **120** and tyramine, **121**) in basic conditions (triethylamine, TEA) and in the presence of benzotriazol-1-yloxy)tris(dimethylamino)phosphonium hexafluorophosphate (BOP) as carboxyl activating agent. Previously efforts by employing other activating agents (DCC, EDC…) and in different conditions did not work or gave lower yields.

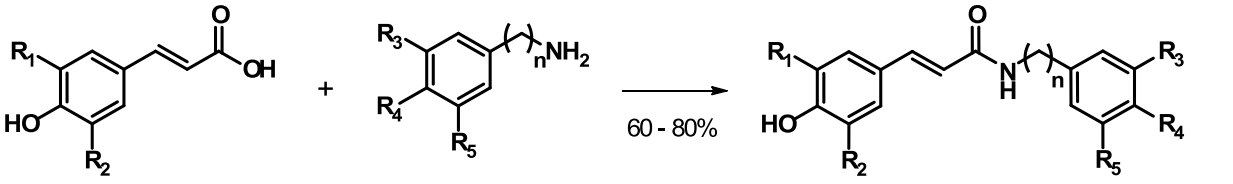

6 $R_1 = OH, R_2 = H$
25 $R_1 = OMe, R_2 = H$
26 $R_1 = R_2 = OMe$

119 $R_2 = R_4 = H, R_3 = Me, n = 1$
120 $R_2 = R_3 = R_4 = OMe, n = 1$
121 $R_2 = R_4 = H, R_3 = OH, n = 2$

100 $R_1 = OH, R_2 = R_3 = R_5 = H, R_4 = Me, n = 1$
105 $R_1 = R_4 = OH, R_2 = R_3 = R_5 = H, n = 2$
112 $R_1 = OH, R_2 = H, R_3 = R_4 = R_5 = OMe, n = 1$
113 $R_1 = R_3 = R_4 = R_5 = OMe, R_2 = H, n = 1$
116 $R_1 = R_2 = R_3 = R_4 = R_5 = OMe, n = 1$

Scheme 7: DMF, TEA, 0 °C, 15 min, BOP solution (CH_2Cl_2) 0 °C, 30 min, rt, 24 h.

With this reaction the amides **100** and **113** were obtained in good yield after purification. Whereas amides **105**, **112** and **116**, and also **100** were employed in a further step, in order to obtain the pertinent methyl derivatives **108**, **114**, **117** and **102** respectively. As reported in Scheme 8 the reaction occurred employing methyl iodide (MeI) as alkylating agent in dry acetone and in basic condition.

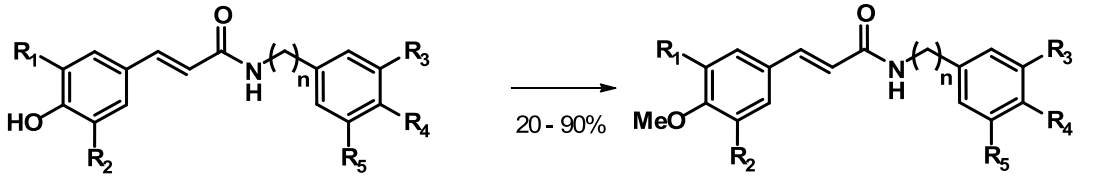

100 $R_1 = OH, R_2 = R_3 = R_5 = H, R_4 = Me, n = 1$
105 $R_1 = R_4 = OH, R_2 = R_3 = R_5 = H, n = 2$
112 $R_1 = OH, R_2 = H, R_3 = R_4 = R_5 = OMe, n = 1$
116 $R_1 = R_2 = R_3 = R_4 = R_5 = OMe, n = 1$

102 $R_1 = OH, R_2 = R_3 = R_5 = H, R_4 = Me, n = 1$
108 $R_1 = R_4 = OMe, R_2 = R_3 = R_5 = H, n = 2$
114 $R_1 = OH, R_2 = H, R_3 = R_4 = R_5 = OMe, n = 1$
117 $R_1 = R_2 = R_3 = R_4 = R_5 = OMe, n = 1$

Scheme 8: dry K_2CO_3, dry acetone, MeI, 56 °C.

The new compounds were subjected to full spectral analysis for structural characterization and their ESI MS and ^1H and ^{13}C NMR spectra are reported in Supporting Material section (Appendix B); where necessary 2D experiments were run in order to achieve an unambiguous assignment of all the detected resonances. In Tables 6 and 7 I reported respectively the ^1H and ^{13}C NMR data for compounds **100**, **102**, **112** (run in CD_3OD), and for **108**, **113**, **114**, **116** and **117** (run in $CDCl_3$). The caffeoyl tyramine **105** is a naturally occurring phenolic amide and the spectroscopic data obtained were in agreement with those previously reported.[146]

Globally the ^1H NMR spectrum of a cinnamoyl amide presents the majority of signals at lower fields due to the cinnamic moiety protons but also to the amine aromatic portion; often the analysis of COSY correlations and of multiplicity (*J* values) allow to discriminate between the former and the latter. The most significant signal in ^1H NMR spectrum as well as in ^{13}C spectrum is the signal related to CH_2 in α position respect to amide function which usually is detected around 4.4 ppm as proton signal and around 45 ppm as carbon resonance.

In ^{13}C spectrum also the resonance around 165 – 167 ppm for amide quaternary carbon is indicative of the amide linkage formation. The NMR spectra of methyl derivatives are very similar to those of the pertinent amide employed as starting material and usually the presence of a new signal around 3.8 ppm in the ^1H spectrum and at around 56 ppm in the ^{13}C spectrum (typical for methoxyls) is diagnostic. Indeed the (de)shielded signals related to adjacent protons and carbons respect to methoxy group could give information about the methyl position.

Table 6: ^{1}H and ^{13}C NMR spectroscopic data of compounds **100**, **102**, **112**[a]

position	100		102		112	
	δ_C	δ_H (mult, *J* Hz)	δ_C	δ_H mult (*J* Hz)	δ_C	δ_H mult (*J* Hz)
1	127.2		128.0		128.2	
2	113.7	7.01 (d, 2.0)	120.7		115.1	7.01 (d, 2.0)
3	145.3		146.5		148.9	
4	147.4		149.4	7.03 (d, 2.0)	146.7	
5	115.0	6.76 (d, 9.0)	113.1	6.92 (d, 8.0)	116.5	6.76 (d, 8.5)
6	126.9	6.91 (dd, 2.0, 9.0)	111.1	7.01 (dd, 2.0, 8.0)	122.2	6.91 (dd, 2.0, 8.5)
7	141.0	7.43 (d, 15.5)	140.7	7.45 (d, 16.0)	142.7	7.44 (d, 15.0)
8	120.7	6.40 (d, 15.5)	117.8	6.50 (d, 16.0)	118.2	6.42 (d, 15.0)
9	167.7		167.5		169.2	
1′	135.5		135.4		136.2	
2′	127.2	7.19 (d, 8.0)	127.2	7.19 (d, 8.0)	106.0	6.64 (s)
3′	128.7	7.14 (d, 8.0)	128.7	7.14 (d, 8.0)	154.6	
4′	136.5		136.5		138.2	
5′	128.7	7.14 (d, 8.0)	128.7	7.14 (d, 8.0)	154.6	
6′	127.2	7.19 (d, 8.0)	127.2	7.19 (d, 8.0)	106.0	6.64 (s)
7′	42.6	4.42 (s)	42.6	4.43 (s)	44.5	4.42 (s)
4′-Me	19.7	2.31 (s)	19.7	2.31 (s)		
4-OMe			54.9	3.88 (s)		
3′/5′-OMe					56.6	3.82 (s)
4′-OMe					61.1	3.74 (s)

[a] Recorded in CD_3OD (500 MHz for ^{1}H NMR and 125 MHz for ^{13}C NMR)

Table 7: ^{1}H and ^{13}C NMR spectroscopic data of compounds **108**, **113**, **114**, **116**, **117**[a]

position	108		113		114		116 [117][b]	
	δ_C	δ_H (mult, *J* Hz)	δ_C	δ_H mult (*J* Hz)	δ_C	δ_H mult (*J* Hz)	δ_C	δ_H mult (*J* Hz)
1	127.8		127.3		128.0		127.3 [137.1]	
2	109.6	7.01 (d, 2.0)	109.6	7.01 (d, 1.5)	113.1	7.11 (d, 2.0)	104.8 [104.9]	6.73 [6.60] (s)
3	149.1		147.5		146.5		147.2 [153.3]	
4	150.5		146.7		149.5		127.3[130.3]	
5	111.0	7.14 (d, 8.0)	114.7	6.91 (d, 8.5)	111.1	6.83 (d, 8.5)	147.2 [153.3]	
6	121.9	7.06 (dd, 2.0, 8.0)	122.2	7.08 (dd, 1.5, 8.5)	117.1	7.00 (dd, 2.0, 8.5)	104.8 [104.9]	6.73 [6.60] (s)
7	140.8	7.54 (d, 15.0)	141.5	7.69 (d, 16.0)	140.8	7.58 (d, 15.5)	141.6 [141.1]	7.55 [7.56] (d, 15.5)
8	118.5	6.19 (d, 15.0)	117.9	6.28 (d, 16.0)	120.7	6.25 (d, 15.5)	118.2 [119.9]	6.30 [6.40] (15.5)
9	166.0		165.9		167.5		165.9 [165.7]	
1′	130.8		134.0		134.7		134.0 [139.6]	
2′	130.8	6.86 (d, 8.5)	105.1	6.56 (s)	104.6	6.54 (s)	105.0 [105.0]	6.52[6.49] (s)
3′	114.1	6.83 (d, 8.5)	153.3		153.2		153.5 [153.4]	
4′	158.3		141.5		142.6		141.6[134.0]	
5′	114.1	6.83 (d, 8.5)	153.3		153.2		153.5 [153.4]	
6′	130.8	6.86 (d, 8.5)	105.1	6.56 (s)	104.6	6.54 (s)	105.0 [105.0]	6.52 [6.49] (s)
7′	40.9	3.62 (m)	44.2	4.51 (d, 6.5)	43.0	4.49 (d, 5.5)	44.2 [43.96]	4.46 [4.45] (d, 5.5)
8′	34.7	2.82 (t, 6.0)						
3-OMe	55.2	3.79 (s)	55.9	3.86 (s)			56.1 [56.06]	3.87 [3.79] (s)
4-OMe	55.8	3.89 (s)			54.9	3.83 (s)	[60.9]	[3.79] (s)
5-OMe							56.1 [56.06]	3.87 [3.79] (s)
3′/5′-OMe			56.2	3.92 (s)	55.1	3.85 (s)	56.2 [56.08]	3.82 [3.82] (s)
4′-OMe	55.9	3.88 (s)	60.9	3.84 (s)	59.6	3.91 (s)	60.9 [60.7]	3.80 [3.83] (s)
NH		5.60 (bs)		5.84 (bt, 6.5)		5.84 (bt, 5.5)		6.13 [6.36] (bs)

[a] Recorded in $CDCl_3$ (500 MHz for ^{1}H NMR and 125 MHz for ^{13}C NMR). [b] Spectroscopic data of **116** methylated are reported in square brackets.

As an example, I report below the ^{1}H and ^{13}C NMR spectra of compound **100** (Figures 15 and 16, respectively) with the pertinent assignments.

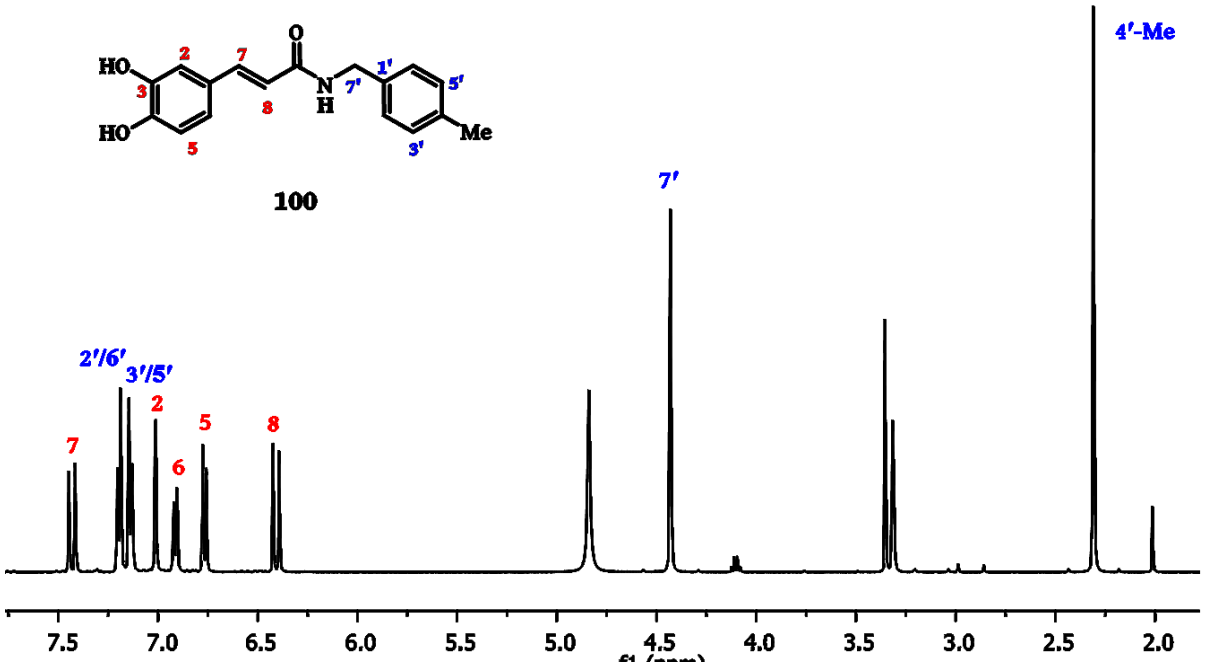

Figure 15: ^{1}H NMR spectrum (CD_3OD, 500 MHz) of **100**

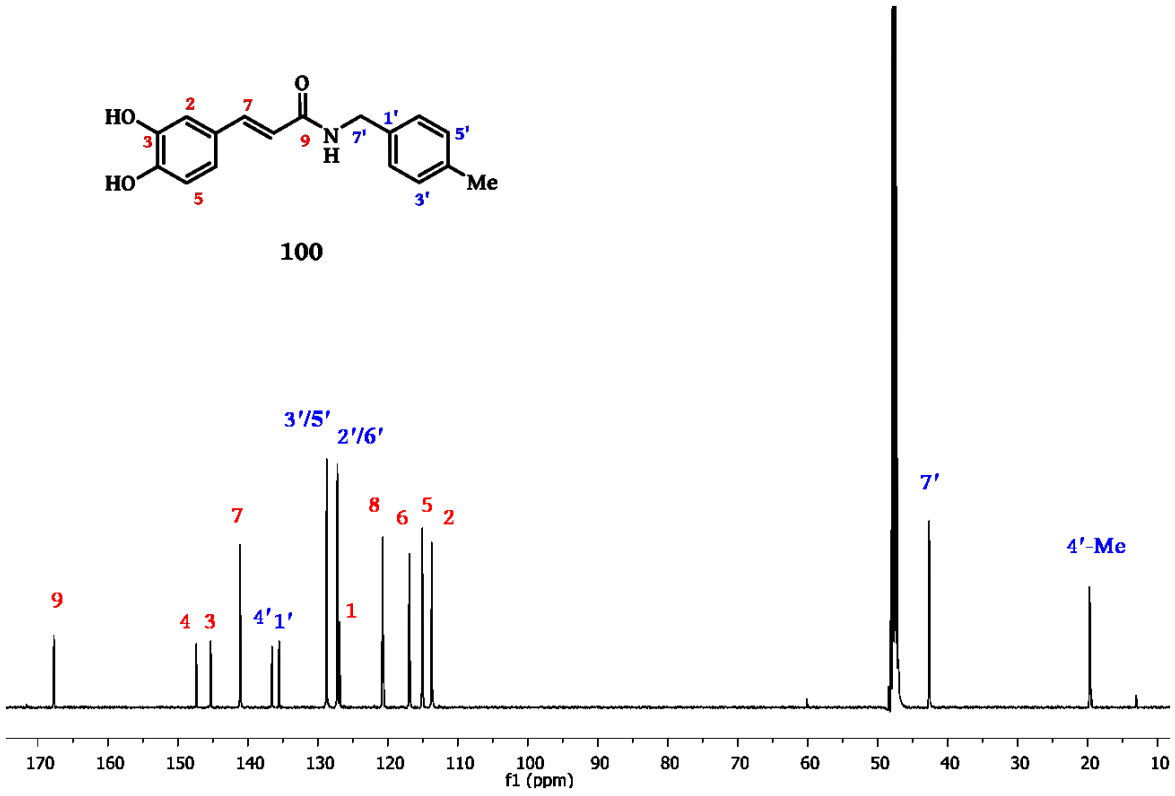

Figure 16: ^{13}C NMR spectrum (CD_3OD, 125 MHz) of **100**

2.3.2. *In vitro m*PGES-1 inhibition assay

The six cinnamic amides **100**, **102**, **108**, **113**, **114** and **117** were evaluated for the *m*PGES-1 inhibition with a well-established cell-free assay, [147] in collaboration with the research team of Prof. O. Werz (University of Jena). The assay was performed using the microsomal fractions of interleukin-1β (IL-1β)-stimulated A549 cells (as source for *m*PGES-1); PGE2 formed by enzymatic conversion of PGH2 (20 μM as exogenous substrate for *m*PGES-1) was analyzed by RP-HPLC.

The results of the test are reported in Figure 17. These data show that the majority of the amides under study resulted inactive or very scarcely active, whereas compound **100** showed a moderate inhibitory activity (30% of inhibition at 10 μM); these data supported previsions based on interactions observed with docking study. In addition, these preliminary results show that although amides **100**, **102**, **108**, **113**, **114** and **117** have close structural analogies and their calculated energy binding values with *m*PGES-1 are very similar, only **100** show inhibitory activity, indicating caffeic acid as a promising scaffold in the design of *m*PGES-1 inhibitors.

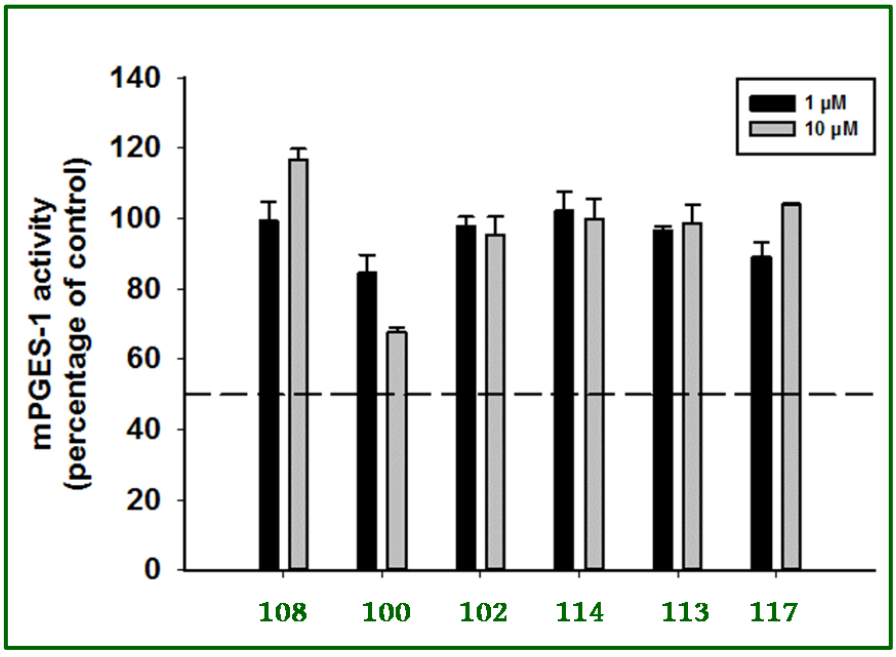

Figure 17: Inhibition of *m*PGES-1 activity by the tested compounds. Microsomal preparations of IL-1β-stimulated A549 cells were pre-incubated with compounds at concentration of 1 (black histogrmas) and 10 μM (grey histograms).

2.3.3. Optimization study of *m*PGES-1 inhibitors

The virtual screening and the *in vitro* assay allowed the identification of caffeic acid as a promising scaffold in the design of *m*PGES-1 inhibitors. Thus, an optimization study of the lead amide **100** was carried out and docking study allowed to select new caffeic acid amides as potential *m*PGES-1 inhibitors, namely compounds **122** – **125**. The four caffeoyl amides were submitted to a molecular docking study and the proper binding energy values calculated in the same condition of the previous experiment, are reported in Table 8 together with structures. Compounds **122** – **125** showed binding energy values in the range -8.10 and -8.32 kcal/mol, approximately 2 units lower than the energy values obtained for the other compounds (reported in Table 5); the lowest binding energy value was observed for **123** which is the only one with a longer alkyl arm (ethyl instead of methyl) between caffeoyl amide scaffold and the other aromatic moiety.

Table 8: Chemical structures of **122** – **125** and binding energy values[a]

Compounds	Chemical structures	Binding energy (kcal/mol)
122	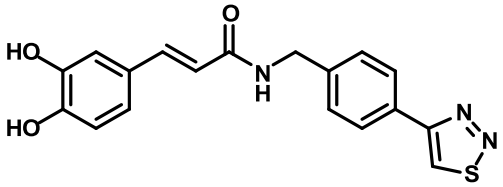	-8.20
123	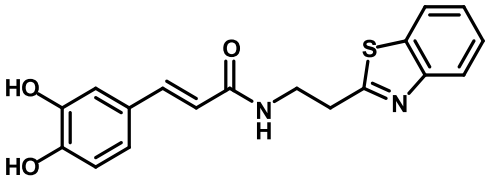	-8.10
124	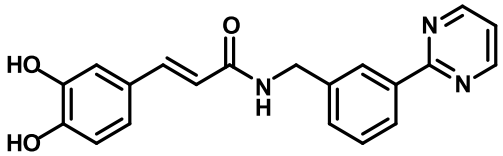	-8.18
125	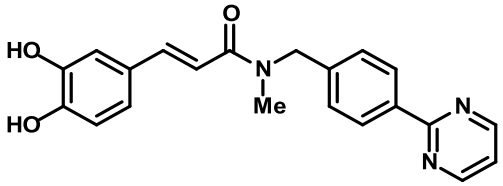	-8.32

[a] Binding energy are calculated with software Autodock 4.2.

In Figure 18 a binding site model of *m*PGES-1 with compound **122** is reported as an example of the docking study. A glance to enzyme-substrate sites involved in the interaction

revealed that the catechol moiety is involved in hydrogen bond formation both with the catalytic site and with the closer GSH co-factor (with glutamate residue chain). The aromatic moiety of caffeic acid was also involved in interactions with closer aminoacids side chain of *m*PGES-1 active site, as well as the benzyl amide residue and the thiadiazolyl ring are involved in π-π staking interactions with aromatic nucleus of Tyr130 and Tyr28 respectively. In the Figure 18 all the above mentioned interactions are reported both in 3D and 2D model of ES complex.

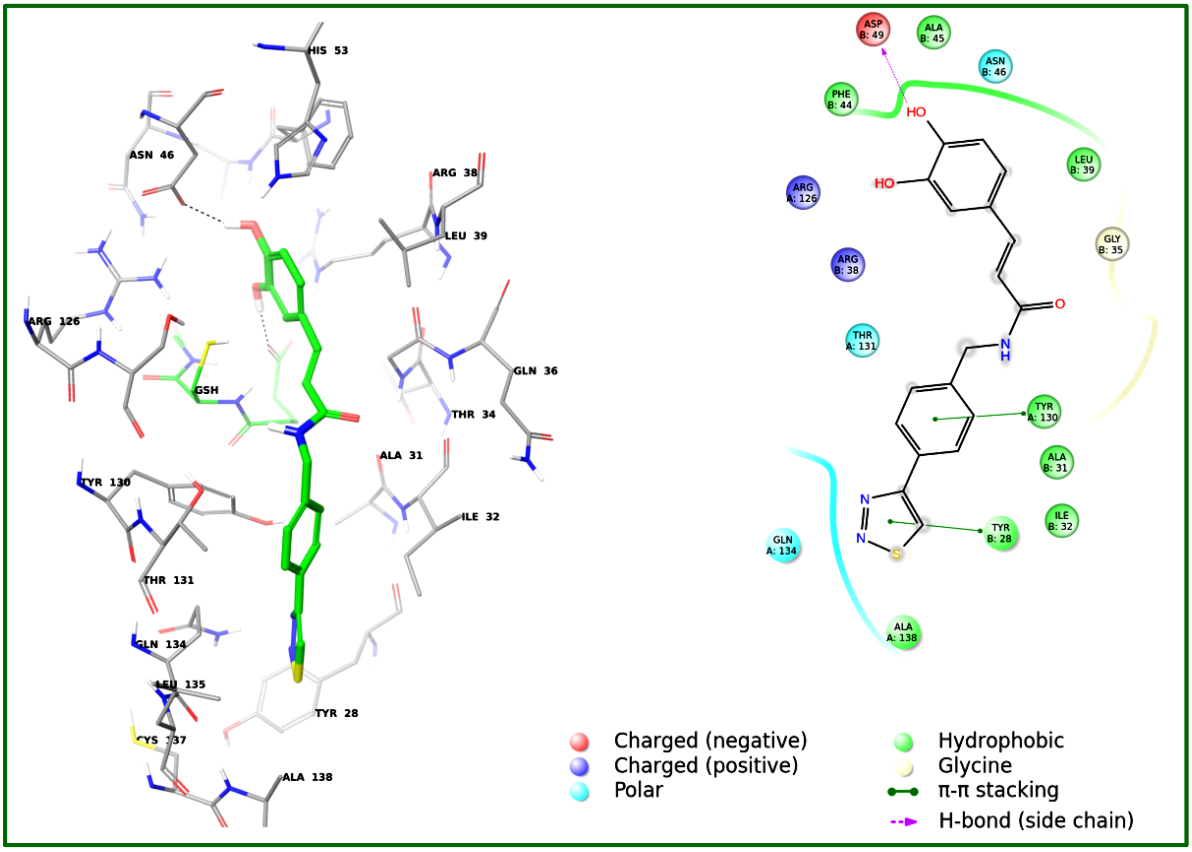

Figure 18: Binding site model of *m*PGES-1 with compound **122**. a) 3D model of interaction of **122** with *m*PGES-1; the enzyme and the amide are depicted by sticks (by atom type: red for O, white for H, blue for N, yellow for S, grey for carbon backbone of enzyme and green for carbon skeleton of **122**). 2D representation of *m*PGES-1 interactions with **122**.

On the basis of this study, we proceed with the synthesis of the amides **122** – **125**; they were obtained according to the procedure reported in Scheme 9 and described in detail in Experimental section.

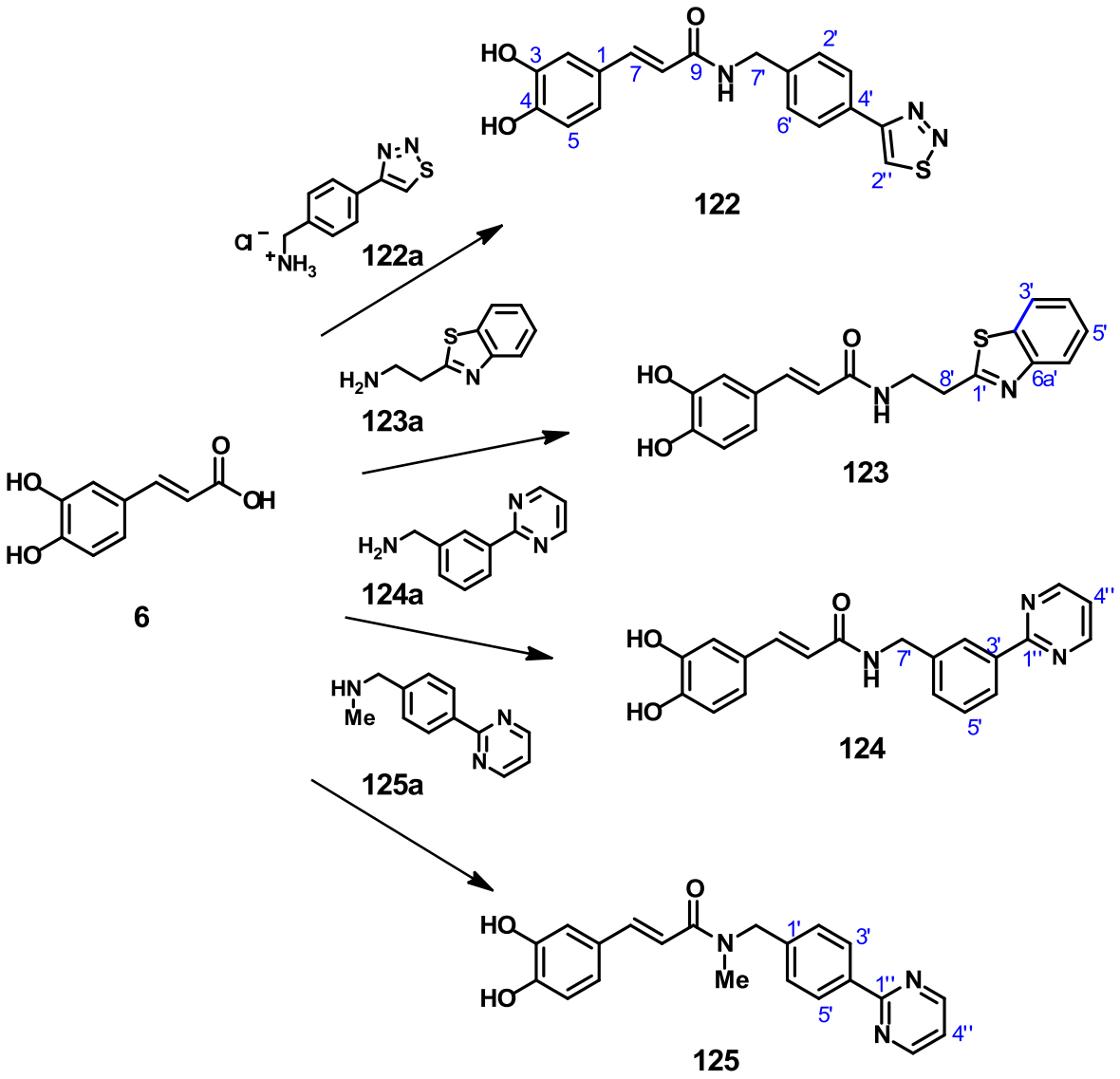

Scheme 9: DMF, TEA, 0 °C, 15 min, BOP solution (CH_2Cl_2) 0 °C, 30 min, rt, 24 h.

The previously unreported amides were characterized by ESI MS spectrometry and NMR spectroscopy. The MS, ^{1}H, ^{13}C and gCOSY spectra are reported in Supporting Material section (Appendix B); the NMR data are listed in Table 9 and the assignments were aided by the study of COSY and HMBC correlations. The amide **125** was obtained in micro scale; its ^{1}H NMR spectrum showed broad signals, mostly split. The splitting could be the result of the steric hindrance around disubstituted amide function. This evidences may be in agreement with the presence of *cis*- and *trans*-amide mixture and in Table 9 the proton assignments for both isomers are reported.

Caffeoyl amides **122** – **125** have been delivered to Prof. O. Wertz and their evaluation as *m*PGES-1 inhibitors is currently in progress.

Table 9: ^{1}H and ^{13}C NMR spectroscopic data of compounds **122 - 125**[a]

position	122[b]		123[c]		124[c]		125[c]
	δ_C	δ_H (mult, *J* Hz)	δ_C	δ_H mult (*J* Hz)	δ_C	δ_H mult (*J* Hz)	δ_H mult (*J* Hz)[d]
1	128.2		136.4		128.32		
2	115.8	7.02 (d, 1.8)	115.1	7.02 (d, 1.5)	115.1	6.98 (d, 1.5)	7.09 [6.97] (d, 1.5)
3	142.2		145.7		146.7		
4	148.1		148.8		148.8		
5	117.2	6.76 (d, 8.1)	116.5	6.79 (d, 8.2)	116.5	6.73 (d, 8.5)	6.79 [6.74] (d, 8.5)
6	121.6	6.92 (dd, 1.8, 8.1)	122.3	6.93 (dd, 1.5, 8.2)	122.2	6.88 (dd, 1.5, 8.5)	7.01 [6.92] (dd, 1.5, 8.5)
7	141.7	8.25 (d, 16.0)	142.5	7.42 (d, 15.5)	142.6	7.41 (d, 15.5)	7.55 [7.54] (d, 15.5)
8	119.4	7.01 (d, 16.0)	118.1	6.38(d, 15.5)	118.3	6.41 (d, 15.5)	6.93 [6.86] (d, 15.5)
9	167.3		169.5		169.3		
1′	136.2		171.2		140-7		
2′	129.2	7.69 (d, 8.5)			128.34	8.34 (bt)	7.41 (bt)
2a′			144.4				
3′	128.3	8.28 (d, 8.5)	122.8	7.97 (dd, 2.0, 8.0)	139.1		8.39 [8.42] (d, 8.5)
4′	132.2		127.3	7.52 (bt)	129.9	7.44 (d, 5.5)	
5′	128.3	8.28 (d, 8.5)	126.2	7.43 (, 8.0)	128.1	8.26 (bt)	
6′	129.2	7.69 (d, 8.5)	123.1	7.97 (dd, 2.0, 8.0)	129.9	7.44 (d, 5.5)	7.41 (bt)
6a′			154.1				
7′	43.8	4.94 (d, 5.0)			44.2	4.55 (s)	4.79 (s)
8′			34.7	3.42 (t, 6.7)			
9′			40.0	3.82 (t, 6.7)			

1″	163.3		165.7		
2″	130.8	9.34 (s)			
3″/5″			158.7	8.79 (d, 5.0)	8.84 (d, 4.5)
4″			120.8	7.30 (t, 5.0)	7.35 (bdd)
N-Me					3.19 [3.09] (s)
NH		9.31 (bt)			

[a] 500 MHz for ^{1}H NMR and 125 MHz for ^{13}C NMR. [b] Recorded in C_5D_5N. [c] Recorded in CD_3OD. [d] In the square brackets the δ values of minor isomer are reported .

2.4. DIHYDROBENZOFURAN NEOLIGNANS

Lignans and neolignans are two classes of natural compounds synthesized by many higher plants. As showed in the Introduction, their various structures are normally originated by oxidative coupling of two phenylpropanoid radicals (C6C3); according to IUPAC nomenclature, 8-8' coupling gives lignans, while dimers obtained from linkage different to 8-8' (such as 5-8'; 5-5'; O-8; O-5) are indicated as neolignans.

Since the discovery of many biological activities exhibited by some lignans and neolignans, new natural-derived analogues were synthesized. Some neolignans derived from caffeic or ferulic acids derivatives have shown interesting biological properties including enhanced antioxidant activity[112] (with respect to that of the monomer) or noticeable anti-tumor activity.[78, 91-94] Some neolignans bearing amide functions (neolignanamides) have been reported for antitumor and other properties (see also Introduction), but these dimeric amides are less frequently cited in the literature and monomeric amides have rarely been employed for biomimetic synthesis of new dimers. The study of dimeric amides could be of some interest also because it is known that amides generally show an higher metabolic stability than their isosteric esters; this may be of crucial importance if the compounds under study could be degraded by intracellular esterase enzymes before reaching the biological target. Moreover, amidic linkage could be involved in additional interaction (as donor and acceptor of H-bonds in a specific enzyme task for example) to enhance the activity of the pharmacophore portion; consequently amide could represent by itself a pivotal function towards a target.

Thus, part of my doctorate work was dedicated to obtain new neolignans based on 8-5′ coupling of cinnamic acid related amides; more specifically, I tried to get these compounds with mild and environmentally friendly conditions.

In the construction of a library of phenolic cinnamoyl amides as substrates for dimerization reactions, I selected derivatives of different cinnamic acids, namely caffeic (**6**), *p*-coumaric (**24**) and ferulic (**25**), and amines of different lipophilicity and steric hindrance, namely the amines **119** – **121**, in order to obtain some structure/activity relationship data.,

This work consisted of several phases: the synthesis of cinnamoyl amides; the oxidative coupling reaction of the former; the purification and characterization of the obtained dimers; the evaluation of their biological properties.

2.4.1. Synthesis of cinnamic acid amides

The cinnamic acid amides **100**, **101**, **105** – **107**, **112**, **113**, **126** and **127** were prepared by amidation reaction of naturally occurring phenolic acids (caffeic, *p*-coumaric and ferulic) with three amines as globally reported in Scheme 10a. Briefly, the reaction was carried out in the presence of a weak nucleophile base (TEA) and of the carboxyl activating agent BOP. Among the phenolic amides obtained, the cinnamoyl derivatives with tyramine (**121**), namely compounds **105** – **107**, are known and the spectroscopic data acquired were in agreement with the previously reported.[146,148] The other amides were submitted to full spectral analysis for the structural characterization and their ESI MS, ^{1}H and ^{13}C NMR spectra are reported in Supporting Material section (Appendix B). The NMR data for **100**, **105**, **112** and **113** has been reported in the previous paragraph, in Tables 6 and 7, while the spectroscopic data of remaining amides **101**, **126** and **127** are listed in Table 10.

Table 10: ^{1}H and ^{13}C NMR spectroscopic data of compounds **101**, **126**, **127**[a]

position	101		126		127	
	δ_C	δ_H (mult, *J* Hz)	δ_C	δ_H mult (*J* Hz)	δ_C	δ_H mult (*J* Hz)
1	128.2		127.7		127.7	
2	111.6	7.10* (d, 2.0)	130.6	7.41 (d, 8.5)	130.6	7.41 (d, 8.5)
3	149.2		116.7	6.79 (d, 8.5)	116.7	6.79 (d, 8.5)
4	149.8		160.5		160.6	
5	116.5	6.80 (d, 8.5)	116.7	6.79 (d, 8.5)	116.7	6.79 (d, 8.5)
6	123.2	7.02 (dd, 2.0, 8.5)	130.6	7.41 (d, 8.5)	130.6	7.41 (d, 8.5)
7	142.3	7.49 (d, 16.0)	142.1	7.49 (d, 15.7)	142.3	7.55 (d, 15.7)
8	118.7	6.48 (d, 16.0)	118.3	6.45 (d, 15.7)	118.2	6.46 (d, 15.7)
9	168.9		169.1		169.1	
1′	136.8		136.9		136.2	
2′	128.6	7.11* (d, 8.5)	128.6	7.14 (d, 8.0)	106.0	6.64 (s)
3′	130.1	7.18 (d, 8.5)	130.1	7.20 (d, 8.0)	154.6	
4′	137.9		138.0		138.3	
5′	130.1	7.18 (d, 8.5)	130.1	7.20 (d, 8.0)	154.6	
6′	128.6	7.11* (d, 8.5)	128.6	7.14 (d, 8.0)	106.0	6.64 (s)
7′	44.0	4.42 (s)	44.1	4.43 (s)	44.5	4.42 (s)
4′-Me	21.1	2.26 (s)	21.1	2.31 (s)		
3-OMe	56.3	3.82 (s)	55.9	3.86 (s)		
3′/5′-OMe					56.6	3.82 (s)
4′-OMe					61.1	3.74 (s)

[a] Recorded in CD_3OD (500 MHz for ^1H NMR and 125 MHz for ^{13}C NMR). *Signals partially overlapped

2.4.2. Biomimetic synthesis of dihydrobenzofuran neolignanamides

Compounds **100**, **101**, **105** – **107**, **112**, **113**, **126** and **127** were submitted to a preliminary screening of enzyme-mediated oxidative coupling reactions. In order to verify the possible role of different factors in the formation of the coupling products, the cinnamic amides previously synthesized were submitted to different experiments employing four different enzymes, namely *Agaricus bisphorus* Laccase (AbL), *Pleurotus ostreatus* Laccase (PoL), *Trametes versicolor* Laccase (TvL) and Horseradish peroxidase (HRP). Moreover, the reactions were carried out in a biphasic system made up of two organic solvents (where the substrate was solubilised) namely ethyl acetate (EtOAc) or methylene chloride (CH_2Cl_2) and acetate buffer (pH = 4.7), containing the enzyme. Further experiments were carried out in monophasic system of acetate buffer with 1% of dimethylsulphoxide (DMSO; see Experimental section for details). The reactions were monitored by HPLC on RP C-18 at regular time intervals. Based on the HPLC profiles of the reactions at different times, the best conditions for coupling reaction were found both in terms of substrate conversion and in terms of formation of a main product.

As an example, I reported five HPLC profiles obtained for substrates **100**, **101**, **126** and **127** with the four enzymes as representative of the 96 preliminary experiments carried out. In Figure 19 the chromatographic profiles of **127** in the presence of AbL and of the three different co-solvents is reported. No products were obtained by AbL-mediated reaction even after 24 hours neither for compound **127** nor for the other substrates evaluated.

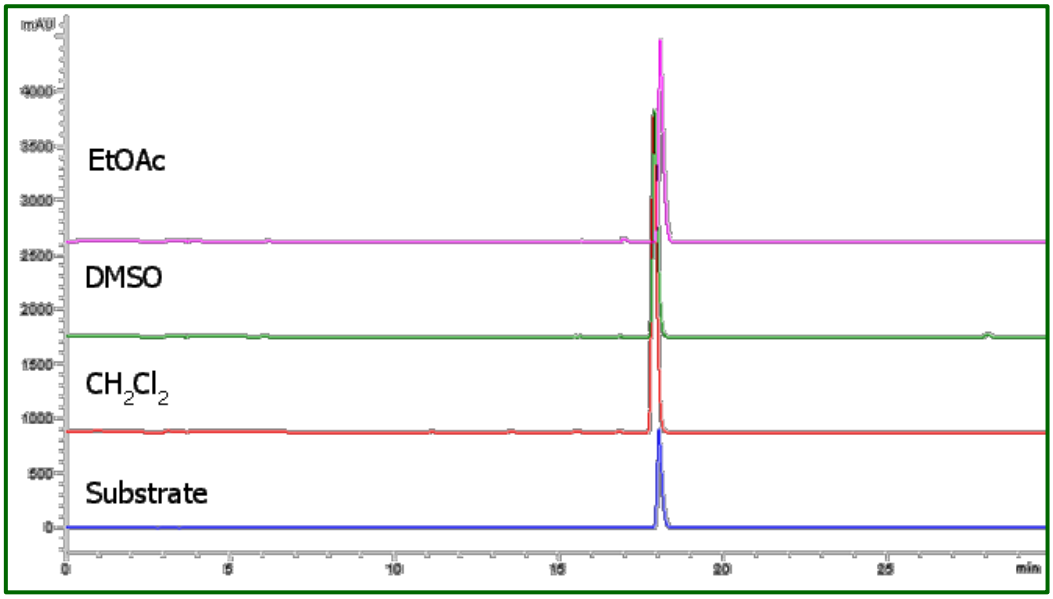

Figure 19: HPLC profiles of **127** with AbL; λ: 325 nm.

In PoL-mediated reactions a partial conversion of the monomer into less polar products (at least 3) was observed when EtOAc or DMSO were used as co-solvent; no products were obtained in CH_2Cl_2 as evident from the HPLC profiles for compound **126** (Figure 20).

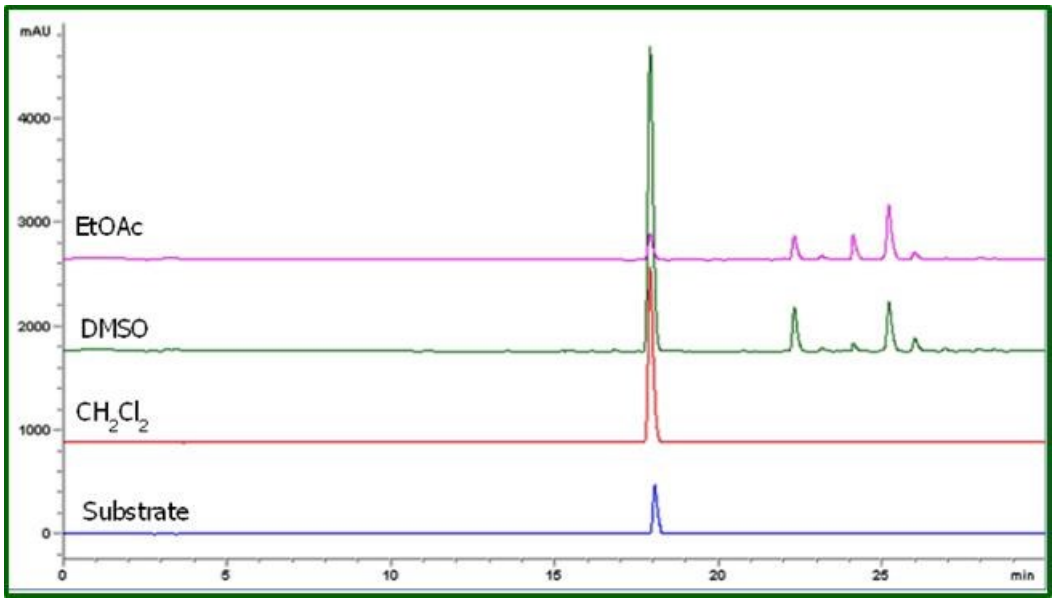

Figure 20: HPLC profiles of **64** with PoL; λ: 325 nm.

Preliminary screenings on **100** in the presence of TvL revealed a partially conversion of the substrate in less polar products in DMSO and in EtOAc as reported in Figure 21. For all the caffeoyl amides, only a major reaction product was observed in CH_2Cl_2, with complete conversion of substrate (almost total) within 2 h. The same was observed for the other monomers in EtOAc as reported in Figure 22 for the *N-trans*-feruloyl-4-methylbenzylamide **101**.

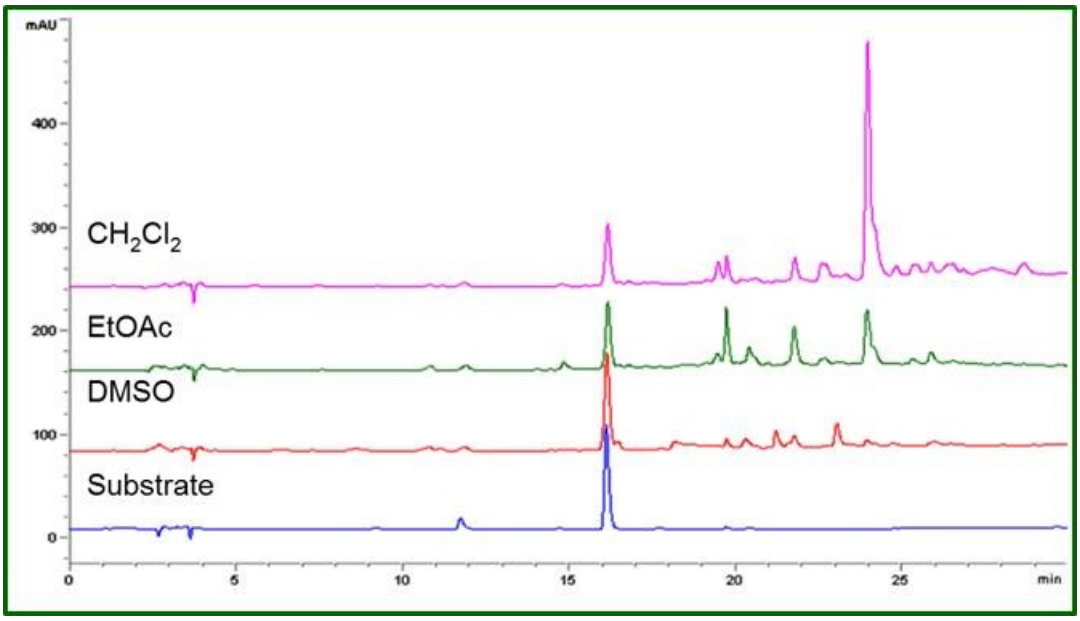

Figure 21: HPLC profiles of **100** with TvL; λ: 325 nm.

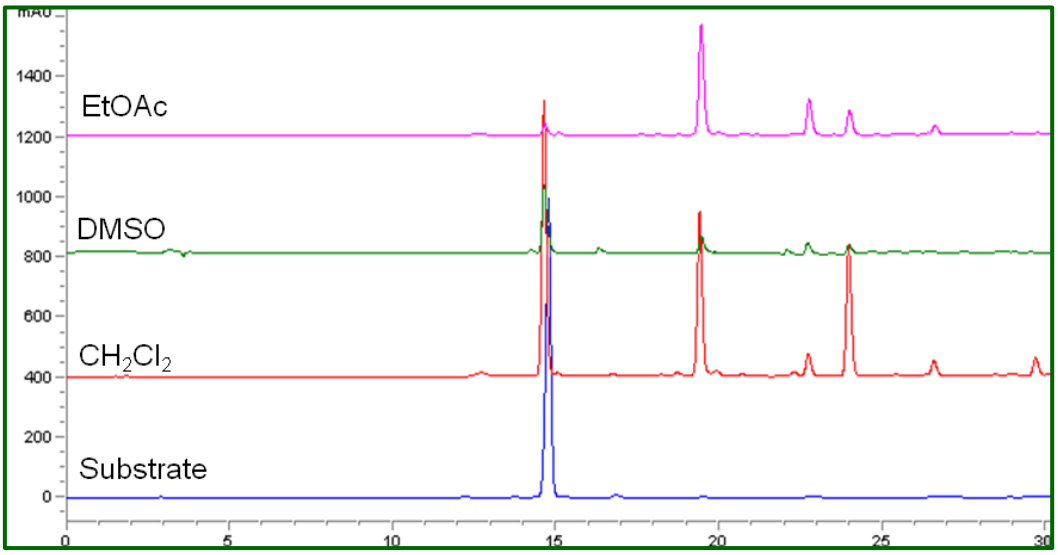

Figure 22: HPLC profiles of **101** with TvL; λ: 325 nm.

The screening with HRP did not show a significant conversion of the substrate, mostly for coumaric amides **107 126**, **127**. Other amides such as in the case of **101**, whose HPLC profiles are reported in Figure 23, in EtOAc gave a main product less polar than substrate; anyway, only a partial consumption of substrate was observed differently from the TvL-mediated reactions.

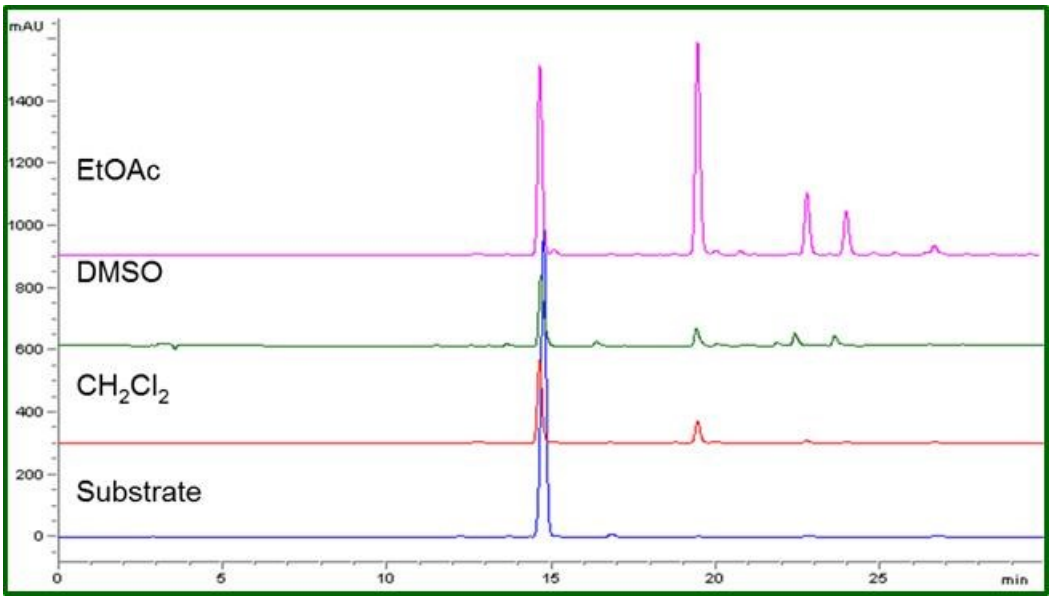

Figure 23: HPLC profiles of **101** with HRP; λ: 325 nm.

On the basis of preliminary results the TvL-mediated oxidative reaction resulted selective towards the formation of a major possible dimeric product. This enzyme was used for the *in macro* synthesis of the new dimers by suitably varying the co-solvent according the evidences upon reported (and on the basis of the solubility of the substrate; see Experimental section for details) as described in Scheme 10b-d.

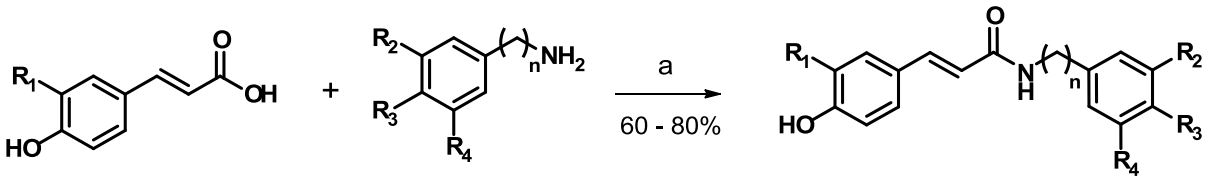

6 R_1 = OH
24 R_1 = H
25 R_1 = OMe

119 R_2 = R_4 = H, R_3 = Me, n = 1
120 R_2 = R_3 = R_4 = OMe, n = 1
121 R_2 = R_4 = H, R_3 = OH, n = 2

100 R_1 = OH, R_2 = R_4 = H, R_3 = Me, n = 1
101 R_1 = OMe, R_2 = R_4 = H, R_3 = Me, n = 1
105 R_1 = R_3 = OH, R_2 = R_4 = H, n = 2
106 R_1 = OMe, R_2 = R_4 = H, R_3 = OH, n = 2
107 R_1 = R_2 = R_4 = H, R_3 = OH, n = 2
112 R_1 = OH, R_2 = R_3 = R_4 = OMe, n = 1
113 R_1 = R_2 = R_3 = R_4 = OMe, n = 1
126 R_1 = R_2 = R_4 = H, R_3 = Me, n = 1
127 R_1 = H, R_2 = R_3 = R_4 = OMe, n = 1

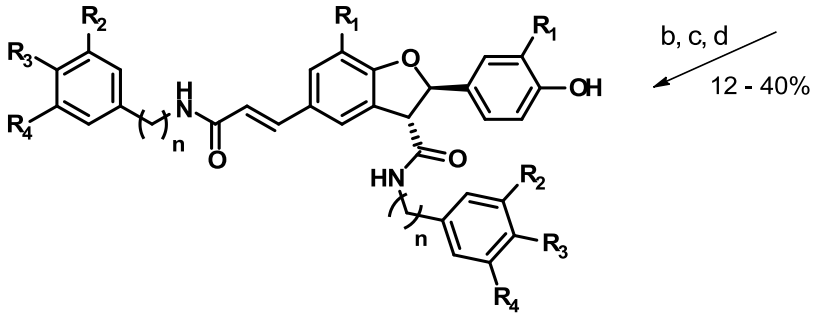

(±)-**57** R_1 = OMe, R_2 = R_4 = H, R_3 = OH, n = 2
(±)-**128** R_1 = H, R_2 = R_3 = R_4 = OMe, n = 1
(±)-**129** R_1 = R_2 = R_4 = H, R_3 = OH, n = 2
(±)-**130** R_1 = R_2 = R_4 = H, R_3 = Me, n = 1
(±)-**131** R_1 = OH, R_2 = R_3 = R_4 = OMe, n = 1

(±)-**132** R_1 = R_3 = OH, R_2 = R_4 = H, n = 2
(±)-**133** R_1 = OH, R_2 = R_4 = H, R_3 = Me, n = 1
(±)-**134** R_1 = R_2 = R_3 = R_4 = OMe, n = 1
(±)-**135** R_1 = OMe, R_2 = R_4 = H, R_3 = Me, n = 1

Scheme 10: (**a**) DMF, TEA, 0 °C, 15 min, BOP solution (CH_2Cl_2) 0 °C, 30 min, rt, 24 h ; (**b**) TvL solution (acetate buffer, 0.1 M, pH = 4.7), EtOAc-DMSO, 24 h; (**c**) TvL solution (acetate buffer, 0.1 M, pH = 4.7), CH_2Cl_2, 2 h; (**d**) TvL solution (acetate buffer, 0.1 M, pH = 4.7), EtOAc, 4 h.

Although this reaction is mediated by enzyme, it occurs with regio- and diastereoselectivity, but not enantioselectivity and consequently gave racemic mixtures of the *trans* diasteromers; in Scheme 10 only one enantiomer is showed.

Each main product, after purification, was submitted to full spectroscopic characterization. The MS spectrometry with a peak at *m*/*z* value twice the molecular weight of the substrate (less 2 u.m.a.) suggested the formation of a dimeric product. Moreover, the analysis of 1D NMR spectra, aided by the careful interpretation of 2D NMR experiments (COSY, HSQC, HMBC) allowed the identification of the dimeric product as a neolignan with a dihydrobenzofuran skeleton (namely an 8-5′ dimer) and an unambiguous assignment of all

^{1}H and ^{13}C NMR signals and the identification of the structure. corroborating the formation of the.

A typical ^{1}H NMR spectrum of a dihydrobenzofuran dimer, presents in the lower field region the resonances for an unmodified cinnamic moiety protons as well as for the aromatic protons of amide pendants; generally the presence of a pairs of resonances for the pendants is indicative of the formation of a dimer. Moreover, the two mutually coupled doublets around 6.0 and 4.0 ppm are diagnostics for two methine protons differently shielded, namely for the two proton of dihydrofuran ring; the *J* value of these signals gives information about the geometry of the C-2 – C-3 linkage of dihydrofuran ring. In the same way in a typical ^{13}C NMR spectrum of an 8-5′ dimer the presence of two typical resonances for methine sp^3 carbons around 85 and 55 ppm is diagnostic for the the formation of a dimer with a dihydrobenzofuran skeleton.

As a representative example, I report below the ^{1}H and ^{13}C NMR spectra of racemate (±)-**128** (Figures 24 and 25 respectively) with the pertinent assignments.

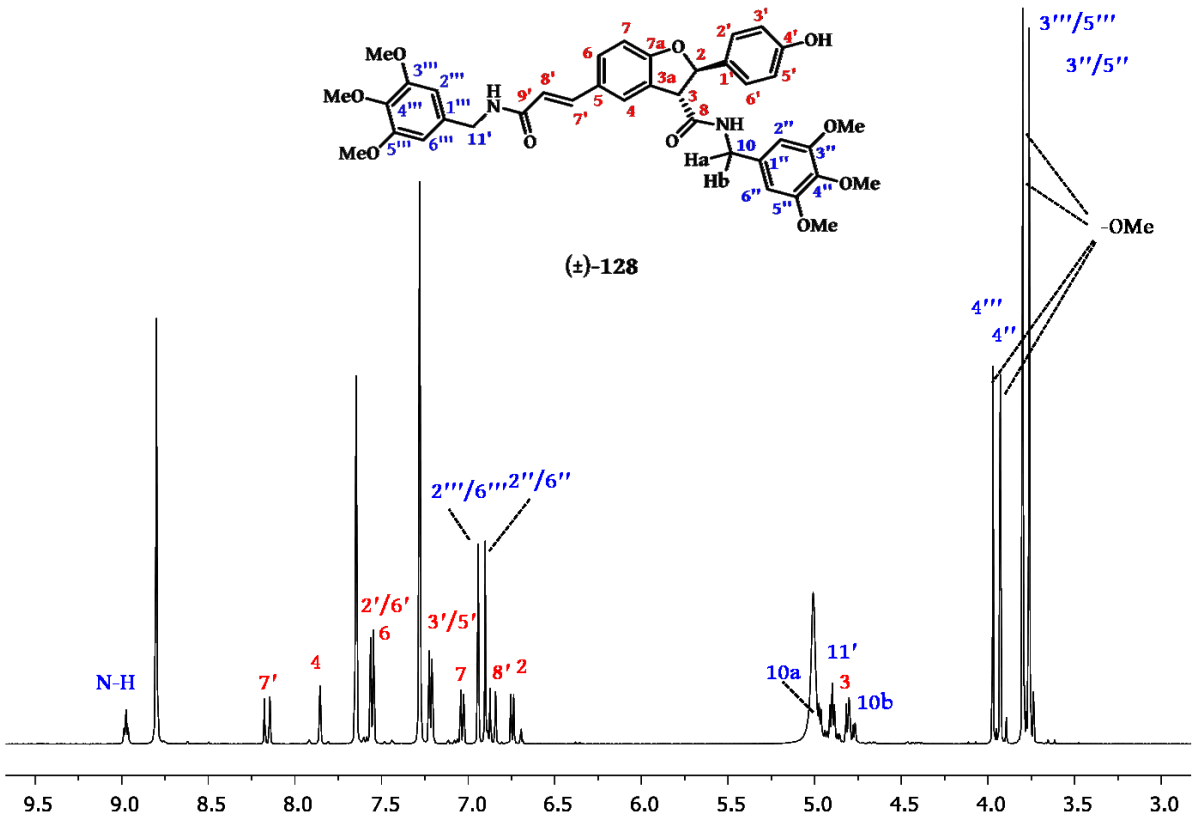

Figure 24: ^{1}H NMR spectrum (C_5D_5N, 500 MHz) of (±)-**128**.

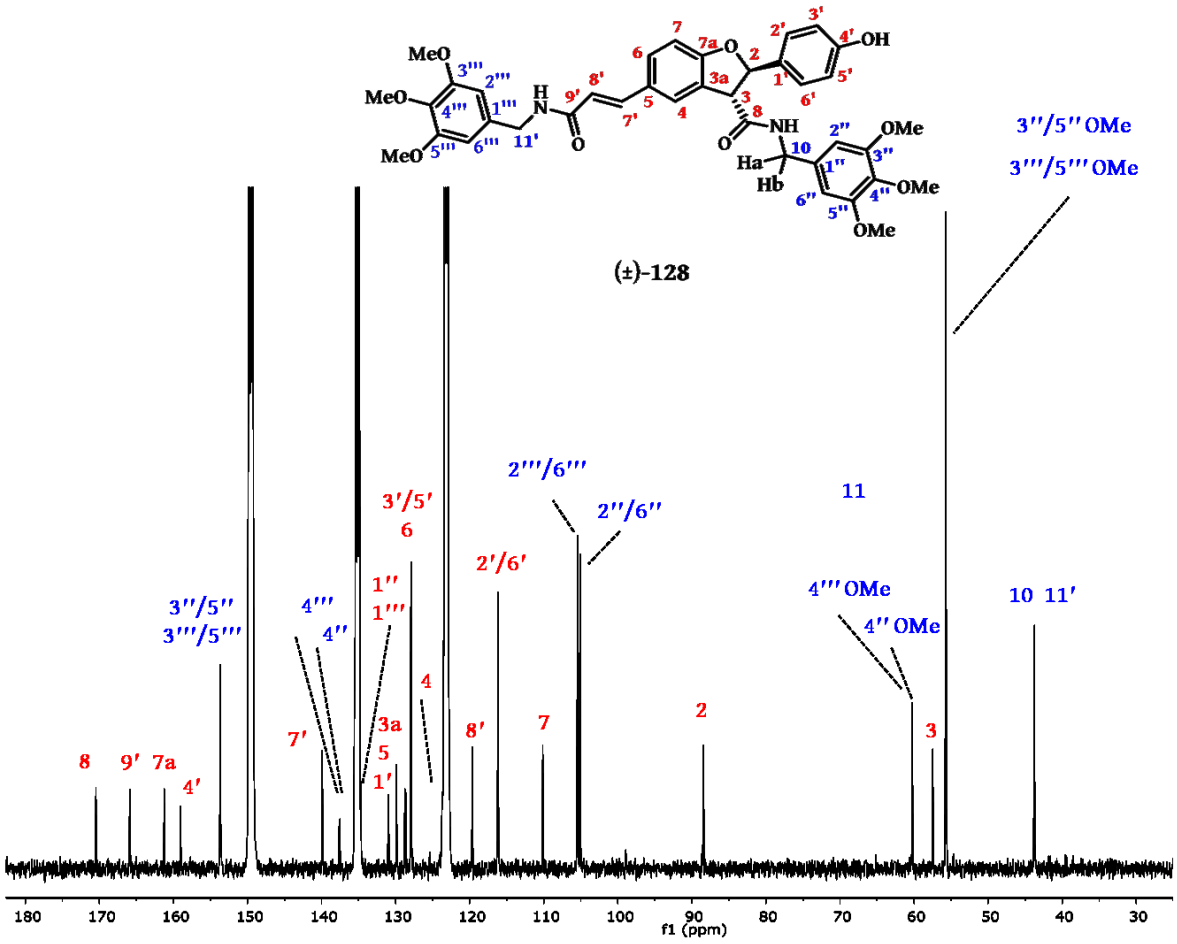

Figure 25: ^{13}C NMR spectrum (C_5D_5N, 125 MHz) of (±)-**128**.

At lower fields region of ^{1}H spectrum of (±)-**128**, the two singlets at 6.94 and 6.90 ppm are clearly assigned to the aromatic protons H-2″/6″ and H-2‴/6‴ of two 3,4,5-trimethoxybenzyl moieties, as well as the two mutually coupled doublets at 8.16 and 6.86 ppm with a J = 15.5 Hz were clearly detected for the AB system of *trans* olefinic protons namely H-7′ and H-8′. The two doublets at 7.56 and 7.22 ppm which mutually coupled (J = 8.5 Hz) were assigned to the four aromatic protons of *para*-disubstituted aromatic ring (AA′-BB′ system) of coumaric moiety indicated as H-2′-/6′ and H-3′/5′ respectively. At upper fields, the presence of four singlets for methyl ether protons of two 3,4,5-trimethoxybenzyl residue (3.97 ppm for 3″-/5″-OCH_3, 3.93 for 4″-OCH_3 and 3.80 and 3.76 for 3‴-/5‴-OCH_3 and 4‴-OCH_3 respectively) together with the above mentioned resonances suggested the formation of a dimer of amide **127** through a coupling involving one of the two *trans*-double bonds and leaving unchanged the other one. Moreover, the triplet at 4.90 ppm which in COSY spectrum showed a correlation with the triplet at 8.97 ppm of amide proton (J = 6.0 Hz) was

clearly identified as the α-CH_2 of amide function, after the interpretation of carbon resonance and of the HMBC correlations this signal was unambiguously assigned as H-11′. With the same approach the two double doublets at 4.98 and 4.81 ppm which mutually coupled with a geminal constant (J = 15 Hz) were assigned to C-10 methylene carbon (40.4 ppm) as enantiotopic Ha-10 and Hb-10 protons. Undoubtedly, the most important signals for the structure determination of compound were the two mutually coupled signals at 6.75 and 4.81 ppm of two different deshielded methine protons, typically for a furan ring. These two key signals for the H-2 and H-3 respectively suggested the formation of a dihydrobenzofuran neolignan. Moreover the J value of 8.3 Hz for these proton signals, according to literature data for similar compounds, suggested that compound (±)-**128** was a racemic mixture of the two *trans* enantiomers. Most of the carbon resonance of ^{13}C spectrum were assigned with the support of HSQCAD spectrum, in addition the study of the HMBC experiment correlations allowed to built approximated sub-structure and finally the expected structure (±)-**128** reported in Scheme 10. In Figure 26 some key HMBC correlations are indicated.

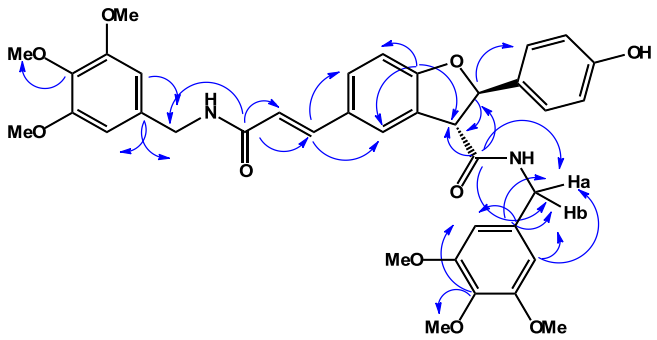

Figure 26: selected HMBC correlations for (±)-**128**.

The typical sp^2 quaternary carbons of amide functions at 170. 5 and 165.9 ppm were discriminated on the basis of HMBC correlation: the 170.5 ppm carbon signal correlates with the methine proton H-2 (at 6.75 ppm) of dihydrofuran ring, and with the two double doublets at 4.98 and 4.81 ppm, it was unambiguously assigned to C-8; similarly, the 165.9 ppm signal was assigned to C-9′ of α-β unsatured amide for its correlations with 8.16 6.86 and 4.90 ppm signals (H-7′, H-8′ and H-11′ respectively). In the same way, the resonances at 129.9 and 110.1 ppm were unambiguously assigned to C-6 and C-7 of dihydrobenzofuran nucleus; analogously the 105.1 ppm (correlates with 6.90, 4.98 and 4.81 ppm) was assigned to the two isochronous carbons C-2″ and C-6″ and for the same reasons the 105.4 ppm resonance was assigned to C-2‴ and C-6‴ (see Figure 26 for details).

An analogous methodology was employed for the unambiguous characterization of the other compounds (±)-**57**, (±)-**129** – (±)-**135**. The ESI MS and NMR spectra (^{1}H, ^{13}C, gCOSY, gHSQCAD, gHMBCAD) of the nine dihydrobenzofuran neolignanamides (±)-**57**, (±)-**128** – (±)-**135** are reported in Supporting Material section (Appendix C).

The spectral data of (±)-**57**, namely of the naturally occurring *trans*-grossamide were in agreement with those previously published;[146b] the ^{1}H and ^{13}C NMR data assignments for the remaining racemic neolignanamides (±)-**128** – (±)-**131** and (±)-**132** – (±)-**135** are listed in Tables 11 and 12 respectively.

Table 11: ^{1}H and ^{13}C NMR spectroscopic data of compounds (±)-**128** - (±)-**131**[a]

position	(±)-128[b]		(±)-129[c]		(±)-130[b]		(±)-131[c]	
	δ_C	δ_H (mult, *J* Hz)	δ_C	δ_H (mult, *J* Hz)	δ_C	δ_H mult (*J* Hz)	δ_C	δ_H mult (*J* Hz)
2	88.4	6.75 (d, 8.3)	87.2	6.04 (d, 8.0)	88.9	6.69 (d, 8.0)	75.1	5.34 (d, 5.5)
3	57.5	4.81# (d, 8.3)	56.3	4.14 (d, 8.0)	58.0	4.77 (d, 8.0)	77.4	4.87 (d, 5.5)
3a	127.9		127.7		128.4		127.7	
4	123.7	7.86 (s)	125.1	6.84# (bs)	124.6	7.86 (bs)	119.1	
5	128.7		127.6		130.0		129.3	
6	129.9	7.56* (d, 8.5)	127.5	7.46 (dd, 2.0, 8.5)	129.9	7.56# (bd, 8.0)	114.4	6.97 (s)
7	110.1	7.04 (d, 8.5)	109.4	6.81 (d, 8.5)	110.5	7.01 (d, 8.0)	144.8	
7a	161.3		160.6		161.7		145.3	
8	170.5		169.2		170.9		166.3	
10	43.8	4.98 (m) 4.81# (m)	40.4	3.72 (m) 3.44 (m)	43.8	4.83 (d, 6.0)	42.6	4.37 (dd, 5.7, 15.0) 4.22 (dd. 5.7, 15.0)
11			33.5	2.91-2.73# (m)				
1′	128.6		131.2		131.5		143.4	
2′	116.2	7.56* (d, 8.5)	115.2	7.21 (d, 8.5)	116.6	7.53# (d, 8.5)	115.8	7.14 (d, 2.0)
3′	128.7	7.22 (d, 8.5)	127.2	6.86 (d, 8.5)	128.3	7.22 (d, 8.5)	143.2	
4′	159.1		157.4	OH 8.48 (bs)	159.4		143.2	
5′	128.7	7.22 (d, 8.5)	127.2	6.86 (d, 8.5)	128.3	7.22 (d, 8.5)	117.1	6.95 (d, 8.5)
6′	116.2	7.56* (d, 8.5)	115.2	7.21 (d, 8.5)	116.6	7.53* (d, 8.5)	121.4	7.09 (dd, 2.0, 8.5)
7′	139.9	8.16 (d, 15.5)	139.9	7.45 (d, 16.0)	140.2	8.13 (d, 15.5)	138.8	7.47 (d, 16.0)
8′	119.7	6.86 (d, 15.5)	118.0	6.48 (d, 16.0)	120.3	6.92 (d, 15.5)	120.3	6.60 (d, 16.0)

9′	165.9		166.4		166.5		164.9	
11′	43.8	4.90 (t, 6.0)	41.0	3.56 (bt, 6.5)	43.6	4.87 (dd, 6.5, 13.5)	42.9	4.43 (d, 5.5)
12′			34.5	2.91-2.73# (m)				
1″	134.7		129.58		136.09		134.9	
2″/6″	105.1	6.90 (s)	129.54	7.10 (d, 8.5)	128.1	7.44* (d, 7.5)	104.5	6.46 (s)
3″/5″	153.7		115.8	6.83 (d, 8.5)	129.6	7.17° (d, 7.5)	153.2	
4″	137.5		155.8	OH 8.79 (bs)	137.4		137.1	
1‴	134.7		129.9		136.8		134.9	
2‴/6‴	105.4	6.94 (s)	129.4	7.10 (d, 8.5)	128.2	7.47* (d, 7.5)	105.0	6.66 (s)
3‴/5‴	153.7		115.0	6.78 (d, 8.5)	129.7	7.20° (d, 7.5)	153.3	
4‴	137.7		155.6	8.15 (bs)	137.4		137.2	
4″-Me					21.06	2.29 (s)		
4‴-Me					21.05	2.26 (s)		
3″/5″-OMe	55.7	3.76 (s)					55.27	3.72 (s)
4″-OMe	60.25	3.93 (s)					59.3	3.67 (s)
3‴/5‴-OMe	55.7	3.80 (s)					55.30	3.79 (s)
4‴-OMe	60.28	3.97 (s)					59.4	3.69 (s)
9-NH						9.72 (t, 6.0)		7.89 (t, 5.7)
10′-NH		8.97 (bt, 6.0)		7.49 (bt, 6.5)		9.11 (t, 6.5)		7.59 (t, 5.5)

[a] 500 MHz for ^{1}H NMR and 125 MHz for ^{13}C NMR. [b] Recorded in C_5D_5N. [c] Recordend in CD_3COCD_3. °, *, # Signals with the same superscript are partially overlapped.

Table 12: ^{1}H and ^{13}C NMR spectroscopic data of compounds (±)-**132** - (±)-**135**[a]

position	(±)-132[b]		(±)-133[c]		(±)-134[c]		(±)-135[c]	
	δ_C	δ_H (mult, *J* Hz)	δ_C	δ_H (mult, *J* Hz)	δ_C	δ_H mult (*J* Hz)	δ_C	δ_H mult (*J* Hz)
2	77.9	5.00 (d, 6.9)	76.9	5.18 (d, 6.5)	88.0	6.10 (d, 8.3)	88.0	5.34 (d, 8.3)
3	79.6	4.40 (d, 6.9)	78.7	4.78 (d, 6.5)	56.8	4.35 (d, 8.3)	57.0	4.34 (d, 8.3)
3a	123.6		127.7		128.7		128.4	
4	120.5	6.73# (s)	119.9	6.95# (s)	112.8	7.13 (s)	111.9	7.16 (s)
5	130.6		130.1		139.6		139.4	
6	115.7	6.83* (s)	115.9	6.97# (s)	115.3	7.06 (s)	116.3	7.11 (s)
7	145.0		146.1		144.5		144.5	
7a	145.2		146.8		149.4		149.5	
8	168.8		166.7		169.4		169.5	
10	42.3	3.33 (m) 4.19 (m)	42.7	4.37 (dd, 6.0, 15.0) 4.21 (dd, 6.0, 15.0)	42.98	4.59 (dd, 7.0, 15.0) 4.31 (dd, 6.0, 15.0)	42.7	4.46 (t, 5.0)
11	35.5	2.53 (m) 2.43 (m)						
1′	141.2		144.5		131.4		131.6	
2′	115.6	7.16 (d, 2.0)	116.2	6.97# (d, 2.0)	109.6	7.04 (d, 2.0)	109.5	7.02 (d, 2.0)
3′	146.6		144.4		147.5		147.4	
4′	147.3		144.4		146.7		146.6	OH 7.69 (bs)
5′	117.3	7.10 (dd, 2.0, 8.4)	121.2	6.83 (d, 8.0)	114.8	6.84 (d, 8.0)	114.8	6.84 (d, 8.0)
6′	130.9	6.97 (d, 8.4)	115.2	6.76 (dd, 2.0, 8.0)	118.9	6.89 (dd, 2.0, 8.0)	118.7	7.88 (dd, 2.0, 8.0)
7′	141.1	7.43 (d, 15.7)	139.8	7.48 (d, 15.5)	129.0	7.47 (d, 16.0)	129.0	7.49 (d, 15.5)

8′	120.4	6.44 (d, 15.7)	122.1	6.66 (d, 15.5)	119.1	6.38 (d, 16.0)	119.3	6.57 (d, 15.5)
9′	169.0		165.9		164.9		165.1	
11′	42.6	3.46 (t, 7.4)	43.1	4.45 (d, 5.5)	42.93	4.46 (d, 4.5)	42.3	4.47 (d, 5.5)
12′	35.8	2.75 (t, 7.4)						
1″	134.7		136.3		135.26		136.6	
2″/6″	130.7	7.05 (d, 8.4)	127.8	7.04 (d, 8.0)	104.8	6.67 (s)	127.4	7.22 (d, 8.0)
3″/5″	116.3	6.72# (d, 8.4)	129.45	6.87 (d, 8.0)	153.23		128.8	7.13 (d, 8.0)
4″	156.9		136.9		137.01		136.15	
1‴	131.3		136.7		135.05		136.3	
2‴/6‴	130.7	6.84* (d, 8.5)	128.3	7.22 (d, 8.0)	105.0	6.70 (s)	127.3	7.24 (d, 8.0)
3‴/5‴	116.3	6.66 (d, 8.5)	129.53	7.12 (d, 8.0)	153.33		128.7	7.15 (d, 8.0)
4‴	156.8		137.4		137.26		136.06	
4″-Me			20.82	2.62 (s)			19.9	2.30 (s)
4‴-Me			20.83	2.61 (s)			19.9	2.28 (s)
7-OMe					55.34	3.90 (s)	55.3	3.90 (s)
3′-OMe					55.34	3.829 (s)	55.2	3.81 (s)
3″/5″-OMe					55.34	3.833 (s)		
4″-OMe					59.51	3.72 (s)		
3‴/5‴-OMe					55.34	3.76 (s)		
4‴-OMe					59.40	3.68 (s)		
9-NH				8.07 (t, 6.0)				7.95 (bt, 5.0)
10′-NH				7.88 (t, 5.5)		8.05 (bt)		7.53 (bt, 5.5)

[a] 500 MHz for ^{1}H NMR and 125 MHz for ^{13}C NMR. [b] Recorded in C_3OD. [c] Recordend in CD_3COCD_3. *, # Signals with the same superscript are partially overlapped

2.4.3. Antiproliferative activity of dihydrobenzofuran neolignanamides

In collaboration with the research team of Prof. D. Condorelli (University of Catania) the nine neolignanamides (±)-**57**, (±)-**128** – (±)-**135** were evaluated for their antiproliferative activity (MTT assay)[149] against three human cancer cell lines, namely Caco-2 (human colon carcinoma), MCF-7 (human mammary adenocarcinoma) and PC-3 (human prostate cancer) cells. The results are summarized in Table 13; for each neolignanamide (tested as racemic mixture) the concentration inhibiting the 50% cell growth (GI_{50}) is reported; 5-Fluorouracil (**5-FU**) was included in the bioassay and used as positive control.

Table 13: Antiproliferative activity of racemates (±)-**57**, (±)-**128** – (±)-**135**

Compounds	GI_{50} (μM) ± SD[a]		
	Caco-2[b]	MCF-7[c]	PC-3[d]
(±)-57	> 100	24.0 ± 2.3	21.0 ± 1.9
(±)-128	42.3 ± 4.1	44.6 ± 4.9	52.0 ± 4.1
(±)-129	28.9 ± 1.6	33.2 ± 3.8	26.0 ± 2.1
(±)-130	3.5 ± 0.3	6.9 ± 0.1	3.7 ± 0.2
(±)-131	>100	>100	>100
(±)-132	>100	39.7 ± 4.2	66.2 ± 7.1
(±)-133	16.4 ± 1.4	42.0 ± 3.6	13.0 ± 1.1
(±)-134	59.1 ± 3.9	23.0 ± 2.6	38.0 ± 2.5
(±)-135	0.70 ± 0.01	2.0 ± 0.1	1.9 ± 0.1
5-FU	5.5 ± 0.4	4.4 ± 0.1	4.9 ± 1.1

[a]GI_{50} calculated after 72 h of continuous exposure relative to untreated controls. Values are the mean (± SD) of four experiments; [b] Caco-2: human colon carcinoma; [c] MCF-7: human mammary carcinoma; [d] PC-3: human prostate cancer.

Notwithstanding the close structural analogy of these compounds, the GI_{50} values show significant variation and suggested some structure-biological activity relationship. Neolignans bearing 3,4,5-trimethoxyl groups (**128**, **131**, **134**) or the tyramine pendant (**57**, 1**29**, **132**) were inactive or scarcely active, with **57** showing the lower GI_{50} value (21 μM) towards PC-3 cells. The observed moderate antiproliferative activity of *trans*-grossamide **57** is in agreement with the moderate cytotoxic activity previously reported on LNCaP cells (IC_{50} = 33 μM).[96] A different profile is observed for compounds bearing the 4-methylbenzyl

residues (**130**, **133**, **135**) showing from moderate to high antiproliferative activity and GI_{50} values in the range 42 – 0.7 μM. In particular, in this subgroup the activity grows in the order feruloyl > *p*-coumaroyl > caffeoyl: namely the neolignanamide **135** (obtained by coupling of a feruloyl amide) is the most potent antiproliferative agent, with GI_{50} values (0.7, 2.0 and 1.9 μM towards Caco-2, MCF-7 and PC-3 cells, respectively) significantly lower than those of the reference drug 5-FU; compound **130** (derived from a *p*-coumaroyl amide) resulted slightly less potent, although showing GI_{50} values (3.5, 6.9 and 3.7 μM towards Caco-2, MCF-7 and PC-3 cells, respectively) comparable or lower than that of 5-FU; finally the caffeoyl neolignanamide **133** resulted only moderately active towards all the three cell lines (16,4, 42,0 and 13,0 μM towards Caco-2, MCF-7 and PC-3 cells, respectively). By the way, the caffeoyl dimer **131** showed no activity towards all cell lines.

Of course in cell bioassays a number of different factors may affect the results, among others cell membrane permeation, diffusion and metabolic stability. Lipophilicity of compounds under biological study usually is a critical parameter in particular with regard to cell uptake. Thus, to highlight a possible connection between lipophilicity and antiproliferative assay, we employed an HPLC method which correlates the capacity factor (*K*) of a given compound with its lipophilicity (namely, with its log P).[150, 151] This method is particularly useful when the direct measurement of log P may be difficult for some or all compounds under study. The HPLC profiles of neolignanamides (±)-**57**, (±)-**128** – (±)-**135** are reported in Figure 27; the HPLC profile of ascorbic acid (**AA**), used as high polar reference standard, is also reported. On the basis of this experimental work, the *K* values for the above cited compounds were determined and are reported in Table 14. For the sake of completeness, we added in Table 14 the calculated log P values.

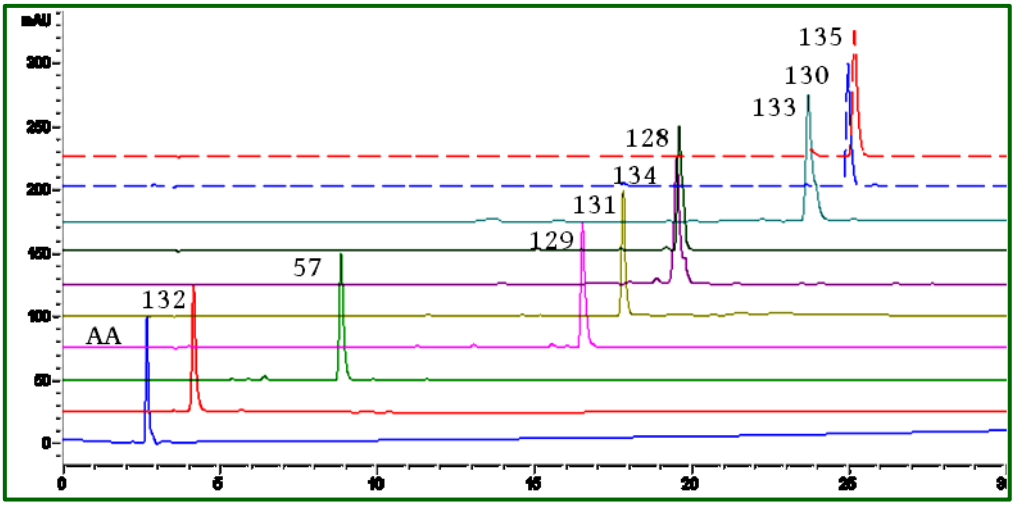

Figure 27: Stacked plot of RP18-HPLC-UV for racemates (±)-**57**, (±)-**128**- (±)-**135**. With blue line the HPLC profile of **ascorbic acid** (**AA**, as standard) is reported.

Table 14: calculated log P and experimental *K* values for compounds (±)-**57**, (±)-**128**- (±)-**135**

Compounds	log P[a]	*K*[b]
(±)-57	2.25 ± 0.58	2.32
(±)-128	1.40 ± 0.64	6.35
(±)-129	3.15 ± 0.49	5.20
(±)-130	5.11 ± 0.55	8.36
(±)-131	-0.55 ± 0.71	5.69
(±)-132	1.20 ± 0.58	0.56
(±)-133	3.16 ± 0.63	7.89
(±)-134	0.50 ± 0.71	6.32
(±)-135	4.21 ± 0.63	8.45

[a] calculated log P values were obtained with ACD/labs log P program version 11;[b] capacity factors were calculated by the expression $K = (t_R - t_0)/ t_0$.

As it is evident from both Figure 27 and Table 14, the neolignanamides **130**, **133** and **135** with the highest *K* values (highlighted in red) also show the highest calculated log P values, that is, are the most lipophilic in this series, presumably due to the lipophilic character of the 4-methyl benzyl pendants. It is also worth noting that the most potent antiprolifertive compound **135** (feruloyl dimer) results the most lipophilic, followed by the highly active compound **130** (*p*-coumaroyl dimer) showing very similar K values; **133** (caffeoyl dimer), the

third compound in order of lipophilicity, is also the third in order of antiproliferative activity. These data strongly suggest a possible relationship between lipophilic character (which is in turn correlated with membrane cell permeation) and antiproliferative activity. Of course, further structural details may have a role in the interaction with the biological target.

2.4.4. Chiral resolution and determination of absolute configuration

The two racemic mixtures (±)-**130** and (±)-**135**, with the most promising antiproliferative activity values, were subjected to chiral resolution. A preliminary screening to optimize the resolution conditions (see Figure 28) was carried out: three different chiral columns, namely Chiralpak-IA, Lux-1 Cellulose and Lux-2 Cellulose were used, coupled with a number of eluting systems (*n*-hexane/IPA-EtOH and CH_3CN/IPA-EtOH with different ratios). Details are reported in the Experimental Section.

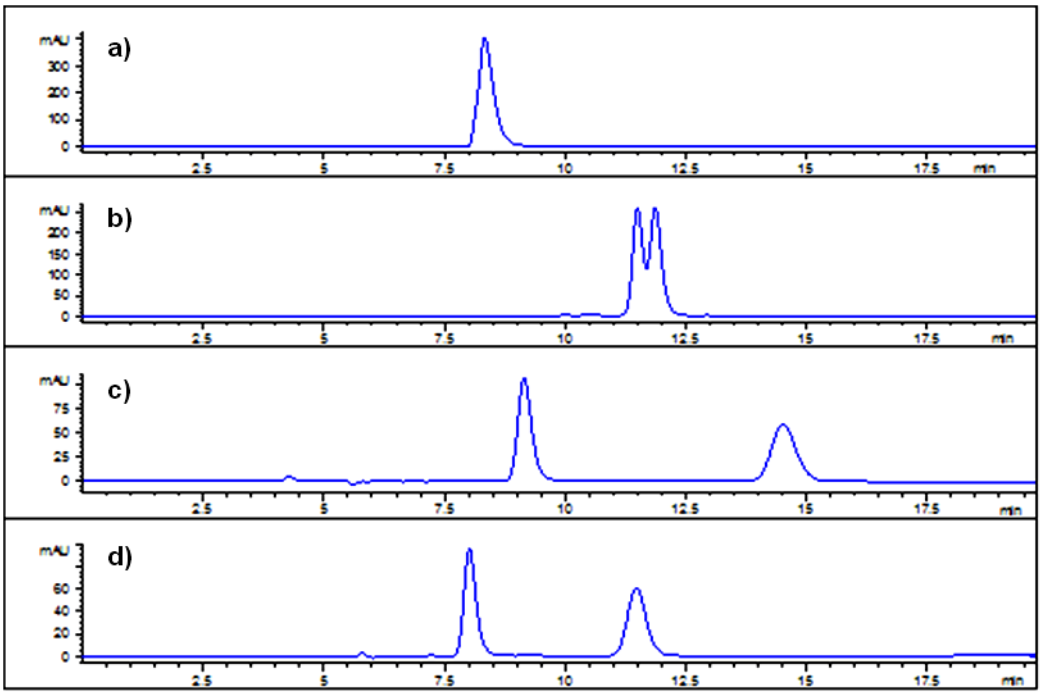

Figure 28: HPLC profiles of racemate (±)-**130** in different conditions: **a**) Chiralpack IA, *n*-hexane: IPA 75:25; **b**) Lux Cellulose-2, CH_3CN:EtOH 80:20; **c**) Lux Cellulose-2, *n*-hexane: EtOH 45:55; **d**) Lux Cellulose-2, *n*-hexane: EtOH 35:65.

Finally, the chiral resolution of racemate (±)-**130** has been carried on Lux-2 Cellulose employing *n*-hexane:EtOH 35:65 as eluent. The HPLC profiles of the racemic mixture and of the two enantiomers run in the above reported conditions are reported in

Figure 29; in these conditions the enantiomers **130-A** and **130-B** showed retention times of 8.09 and 11.42 minutes respectively.

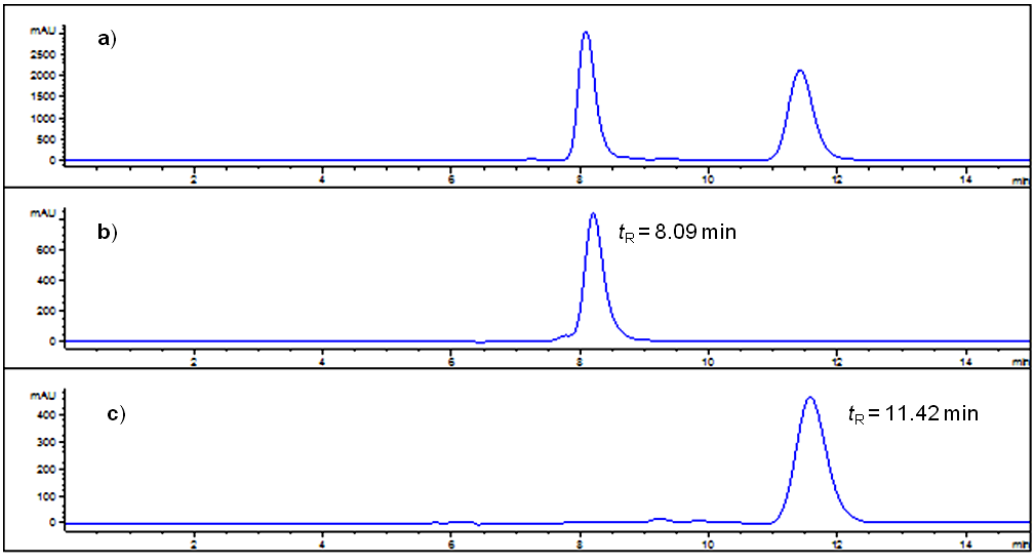

Figure 29: Chiral HPLC profiles of **a**) (±)-**130**; **b**) enantiomer **130-A**; **c**) enantiomer **130-B**.

Also the chiral resolution of racemate (±)-**135** has been carried on Lux-2 Cellulose employing *n*-hexane:EtOH 30:70 as the eluent. In this conditions, the enantiomers **135-A** and **135-B** eluted with retention times of 11.59 and 13.63 minutes respectively. The HPLC profiles of the racemic mixture and of the pure enantiomers are reported in Figure 30.

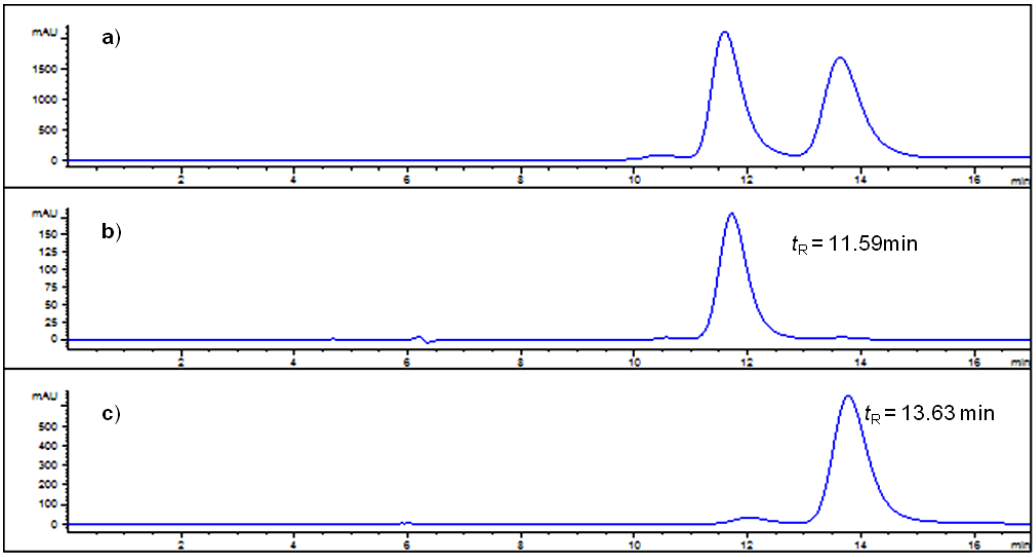

Figure 30: Chiral HPLC profiles of **a**) (±)-**135**; **b**) enantiomer **135-A**; **c**) enantiomer **135-B**.

The pure enantiomers were characterized by Circular Dichroism spectroscopy (CD) and by optical rotation polarimetric measurements. The CD spectrum of **130-A** (reported in Figure 31a with blue line) showed a positive Cotton effect in the range 250 – 325 nm in agreement with the experimental $[\alpha]_D^{20}$ = + 108.3; conversely, the CD spectrum of enantiomer **130-B** (reported in Figure 31a with red line) gave a negative Cotton effect in the range 250 – 325 nm, in agreement with the value of $[\alpha]_D^{20}$ = - 105.0. The same was observed for the other pair of enantiomers, namely the CD spectrum of **135-A** (reported in Figure 31b with blue line) showed a positive Cotton effect in the range 250 – 325 nm for in agreement with the experimental $[\alpha]_D^{20}$ = + 117.8; while the enantiomer **135-B** (reported in Figure 31b with red line) gave a negative Cotton effect in the range 250 – 325 nm, in agreement with the value of $[\alpha]_D^{20}$ = - 114.6.

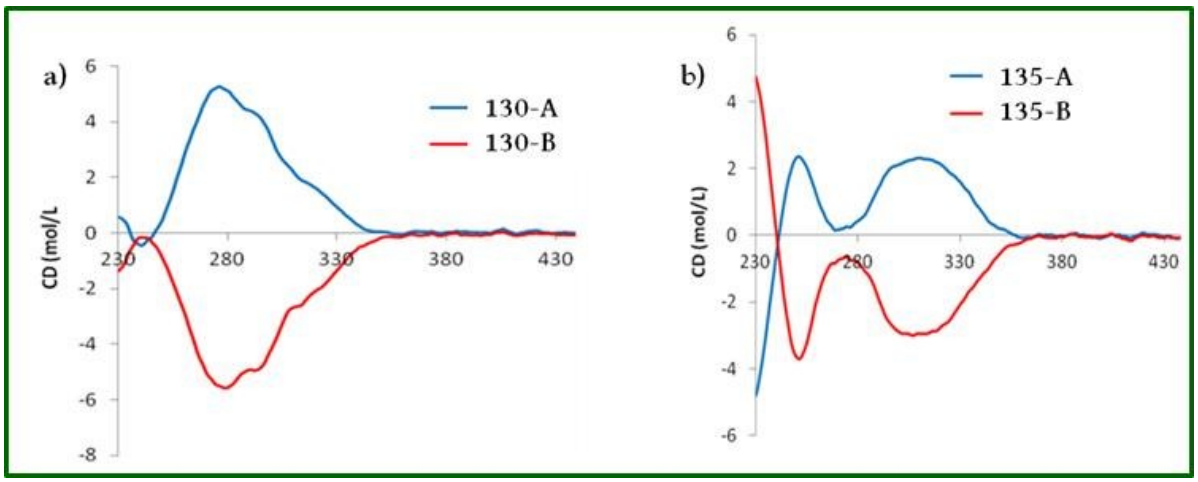

Figure 31: **a**) CD spectra of **130-A** and **130-B**; **b**) CD spectra of **135-A** and **135-B**.

One of the most useful methods for the determination of absolute configuration is the comparison of CD spectra and [α] values with that of closely related compounds of known absolute configuration.[152] Thus, the comparison of the chiro-optical data acquired for **130-A**, **130-B**, **135-A** and **135-B** with literature values of closely related compounds such as 3′,4-di-*O*-methylcedrusin **51** [153] methylcaffeate lignan **52**,[91] (-)-ephedradine A, [154] and Hordatine A,[155]was used to determine the absolute stereochemistry of the new reported enantiomers. By the way, in Figure 32 the CD spectra of methylcaffeate lignan enantiomers are reported, showing a positive Cotton effect for the enantiomer (**2*S*,3*S*)-52** and a negative Cotton effect for (**2*R*,3*R*)-52**.

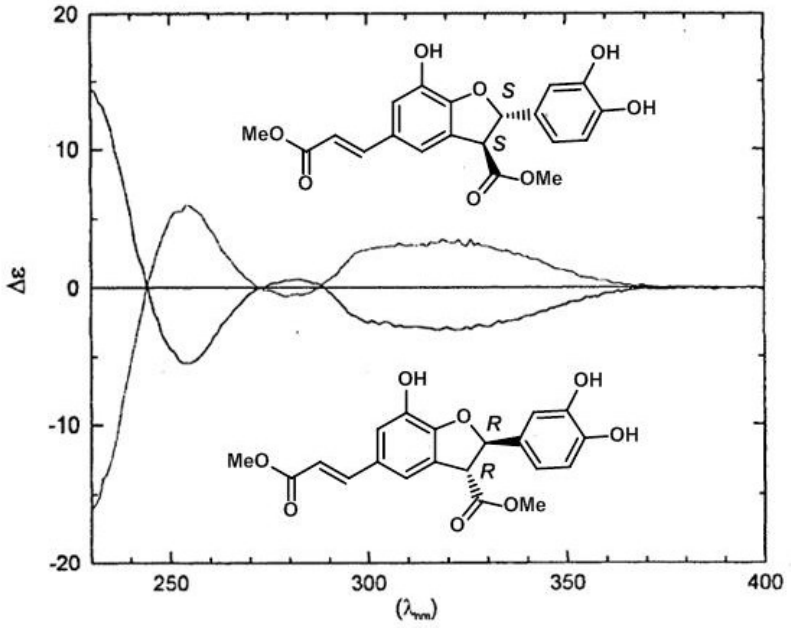

Figure 32: CD spectra of (**2*S*,3*S*)-52** (**2*R*,3*R*)-52**.[91]

These and other literature data allowed to establish the absolute configuration of the enantiomer **130-A** and **135-A** as **2*S*,3*S*** and that of enantiomers **130-B** and **135-B** as the **2*R*,3*R***.

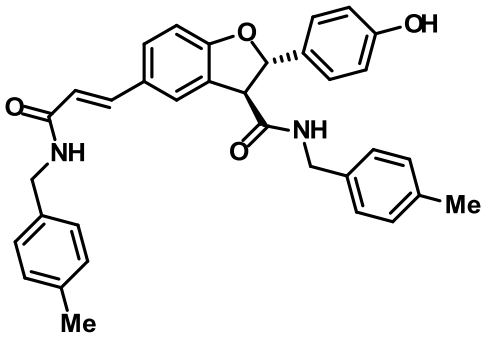

(2*S*,3*S*)-130

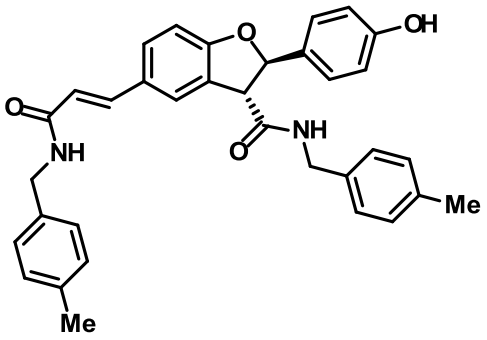

(2*R*,3*R*)-130

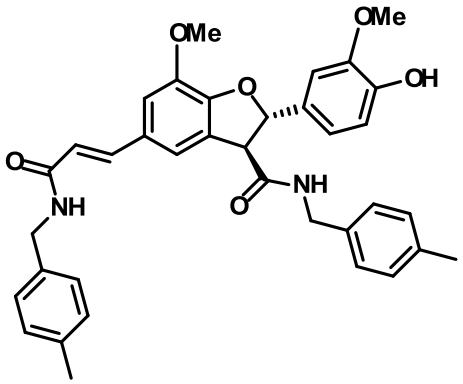

(2*S*,3*S*)-135

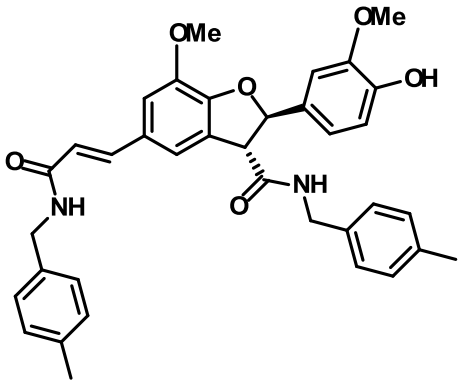

(2*R*,3*R*)-135

2.4.5. Antiproliferative activity of pure enantiomers

The two pairs of enantiomers (**2*S*,3*S*)-130**, (**2*R*,3*R*)-130** and (**2*S*,3*S*)-135**, (**2*R*,3*R*)-135** were assayed for their antiproliferative activity; **5-FU** was used as positive reference also in this experiment. The results are reported in Table 15 as GI_{50} values; for an immediate comparison also the GI_{50} values of the racemates (±)-**130** and (±)-**135** are reported. The interpretation of these data is not straightforward: in the case of (±)-**130**, the most active enantiomer towards all three cell lines is 2*R*,3*R*, resulting also more active than the racemate with GI_{50} values of 2.1 (Caco-2 cells), 1.7 (MCF-7 cells) and 2.4 μM (PC-3 cells), whereas the less potent enantiomer 2*S*,3*S* resulted a slightly more active than the racemic mixture. It is worth of nothing that in previous works on cytotoxic and antiangiogenic activities of neolignan (±)-**52**, the (2*R*,3*R*) enantiomer proved to be the most active of the couple.[78, 91] Conversely, in the case of (±)-**135** both enantiomers resulted less active than the racemate on all cell lines, and the 2*S*,3*S* enantiomer proved to be more potent than 2*R*,3*R* enantiomer. This results contrast with the previous and suggest that for neolignanamide **130** the activity was related with the stereochemistry of dihydrofuran ring and the higher activity of the enantiomer with 2*R*,3*R* configuration could be related with a better affinity with a specific target. The other experiment is rather surprising and we are planning to repeat the test; if confirmed, this

result suggest a possible synergic effect of the two enantiomers, for instance through interaction with different targets.

Table 15: Antiproliferative activity of (**2*S*,3*S*)-130**, (**2*R*,3*R*)-130**, (**2*S*,3*S*)-135**, (**2*R*,3*R*)-135** and racemates (±)-**130** and (±)-**135**

Compounds	GI_{50} (μM) ± SD[a]		
	Caco-2[b]	MCF-7[c]	PC-3[d]
(±)-130[e]	3.5 ± 0.3	6.9 ± 0.1	3.7 ± 0.2
(2*S*,3*S*)-130	3.3 ± 0.3	5.3 ± 0.1	2.5 ± 0.2
(2*R*,3*R*)-130	2.1 ± 0.2	1.7 ± 0.1	2.4 ± 0.1
(±)-135[e]	0.70 ± 0.01	2.0 ± 0.1	1.9 ± 0.1
(2*S*,3*S*)-135	4.8 ± 0.5	2.6 ± 0.1	2.9 ± 0.2
(2*R*,3*R*)-135	18.0 ± 1.9	4.4 ± 0.2	6.5 ± 0.4
5-FU	6.0 ± 0.5	3.7 ± 0.3	5.4 ± 1.8

[a]GI_{50} calculated after 72 h of continuous exposure relative to untreated controls. Values are the mean (± SD) of three experiments; [b]Caco-2: human colon carcinoma; [c]MCF-7: human mammary carcinoma; [d]PC-3: human prostate cancer. [e] Values added for comparison.

2.5. BENZO[*k,l*]XANTHENE LIGNANS: A CHEMICAL PROTEOMIC STUDY

Benzo[*k,l*]xanthene lignans are a rare subclass of natural and unnatural lignans; as showed in the Introduction, recently the research group of Prof. C. Tringali (University of Catania) has been published a simple synthetic methodology to obtain benzoxanthene lignans by a biomimetic approach.[100] Although some biological activities of these dimers have been studied,[101-103] globally the properties of these unusual lignans remain largely unexplored.

In the frame of a collaboration with Prof. A. Casapullo (University of Salerno), the Compound-Centric Chemical Proteomic approach (CCCP)[156,157]or "*fishing for partners*" has been employed for the identification of new target proteins for benzoxanthene lignans.

CCCP is a multidisciplinary method which utilizes small molecule probes to selectively capture target proteins from complex biological matrices, basing on the classical drug affinity chromatography in combination with high-resolution mass spectrometry (HR-MS) and bioinformatic tools for the identification of binding proteins. A typical CCCP experiment flowchart is reported in Figure 33; as shown many fields are involved (synthetic organic chemistry, cell biology, mass spectrometry and biochemistry); it starts with the immobilizing of bioactive compound on a matrix and to follow it is incubated with the cell

extract lysate. The affinity chromatography will remove the non-specifically bound proteins and finally the captured targeted proteins are recovered and separated by gel-electrophoresis. After protein(s) digestion the HR-RS peptides analysis allows the identification of the targeted protein(s).

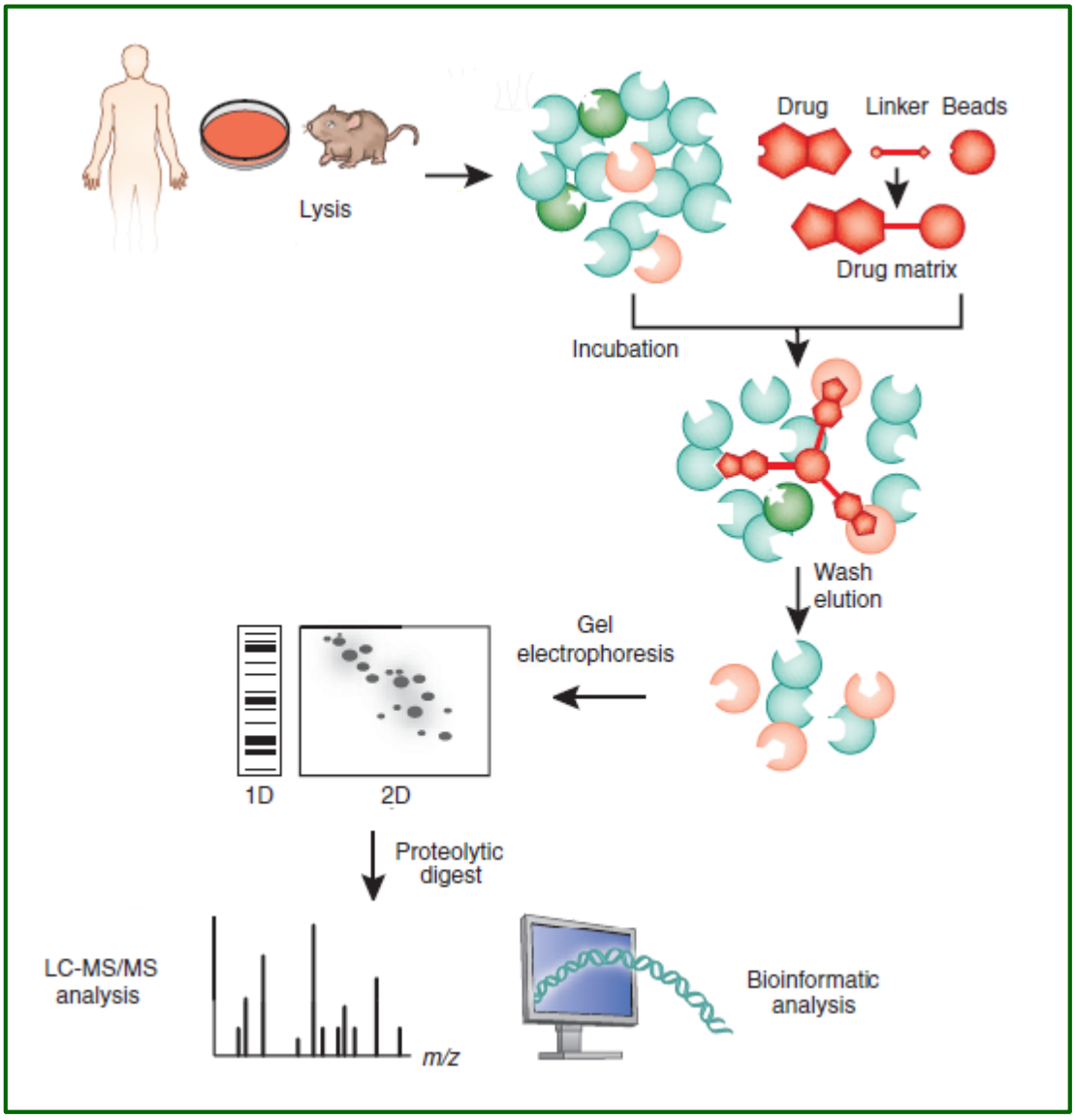

Figure 33: General experiment flowchart of Chemical proteomic approach Compound Centric Chemical Proteomic CCCP.

2.5.1. Synthesis of benzo[*k*,*l*]xanthene lignan 137

In order to apply the CCCP strategy, the design and synthesis of a new benzoxanthene core lignan suitable for orthogonal functionalization and immobilization on sepharose beads matrix via epoxidic linker has been realized. A benzoxanthene core bearing hydroxyl alkyl chains of suitable length was selected for this goal. The synthesis of compound **137** was carried out employing the Mn-mediated biomimetic methodology, summarized in Scheme 11.

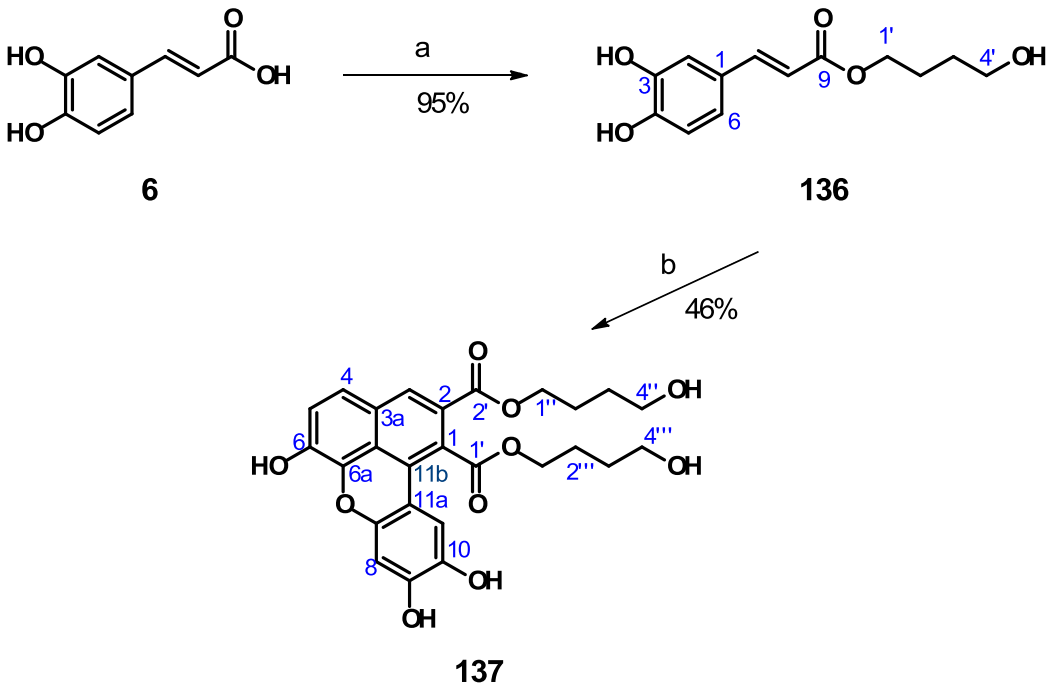

Scheme 11: (**a**) 1,4-butanediol, H_2SO_4, 50 °C, 24 h; (**b**) $Mn(OAc)_3$ CH_2Cl_2, 40 °C, 3 h.

As first step the synthesis of a suitable caffeic ester was carried out; 1,4-butanediol was reacted with caffeic acid (**6**) through the Fisher esterification and the intermediate **136** was obtained with 95% yield. The new compound was fully characterized and the ESI MS and NMR spectra are reported in Supporting Material Section (Appendix B). The NMR data, listed in Table16, were in agreement with the formation of expected ester **136**.

The signals expected for caffeic moiety were clearly recognized in the upper fileds region of ^{1}H (7.6 -6.0 ppm) and ^{13}C (170 – 110 ppm) NMR spectra, whereas, the resonances for butanediol chain in ^{1}H NMR spectrum were assigned to the two triplets at 4.17 and 3.60 ppm (CH_2-1′ and CH_2-4′ respectively) and the multiplets at 1.76 and 1.62 ppm (CH_2-2′ and

CH_2-3′ respectively as confirmed by COSY correlations). Analogously the resonances at 64.7, 62.1 and 26.2 ppm (C-1′, C-4′ and C-2′/C-3′) in ^{13}C spectrum were assigned to ester chain.

The dimerization of **136** was carried out by oxidative coupling, employing $Mn(OAc)_3$ as oxidative agent. In these conditions, the benzoxanthene **137** was recovered with 46% yield (after PLC purification).

The new benzoxanthene was fully characterized by MS spectrometry 1D and 2D NMR spectroscopy; in Figures 34 and 35 the ^1H and ^{13}C NMR spectra of **137** are reported, (for the other spectra see Appendix C in Supporting Material section). The ESI MS spectrum suggested the formation of a dimer with the presence of a main peak at 497.3 *m/z* for the pseudo molecular ion $[M-H]^-$, corresponding to expected 498, equal to twice the molecular weight of the substrate **136** (less than 6 uma).

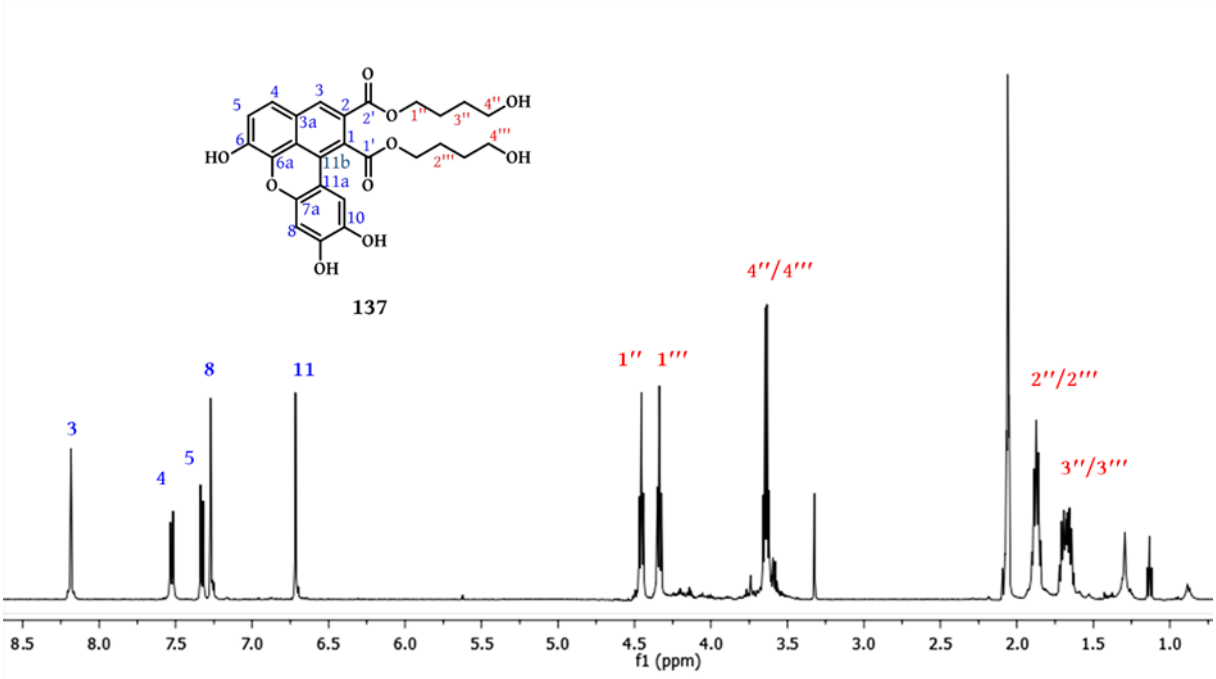

Figure 34: ^1H NMR spectrum (CD_3COCD_3, 500 MHz) of **137**.

The ^1H NMR spectrum of **137** showed the typical signals for the benzoxanthene core, namely three singlets at 8.18, 7.27 and 6.72 ppm for H-3, H-8 and H-11 respectively and two doublets at 7.53 and 7.33 mutually coupled (J = 8.5 Hz; see COSY spectrum) for H-4 and H-5 respectively. These resonances are unambiguously assigned studying HMBC correlations. In the upper fields region (4.6 – 1.6 ppm) of ^1H NMR spectrum the resonances for alkyl chains were detected: two differently shielded triplets for the α- methylene protons (respect to ester functions) at 4.46 and 4.34; two partially overlapped triplets, integrating for four protons,

namely for the two methylenes 4″-/4‴-CH_2 3.65 and 3.63 ppm and two multiplets at 1.86 and 1.68 ppm integrating for eight protons the remaining methylenes 2″-/2‴-CH_2 and 3″-/3‴-CH_2 respectively as suggested by COSY correlations.

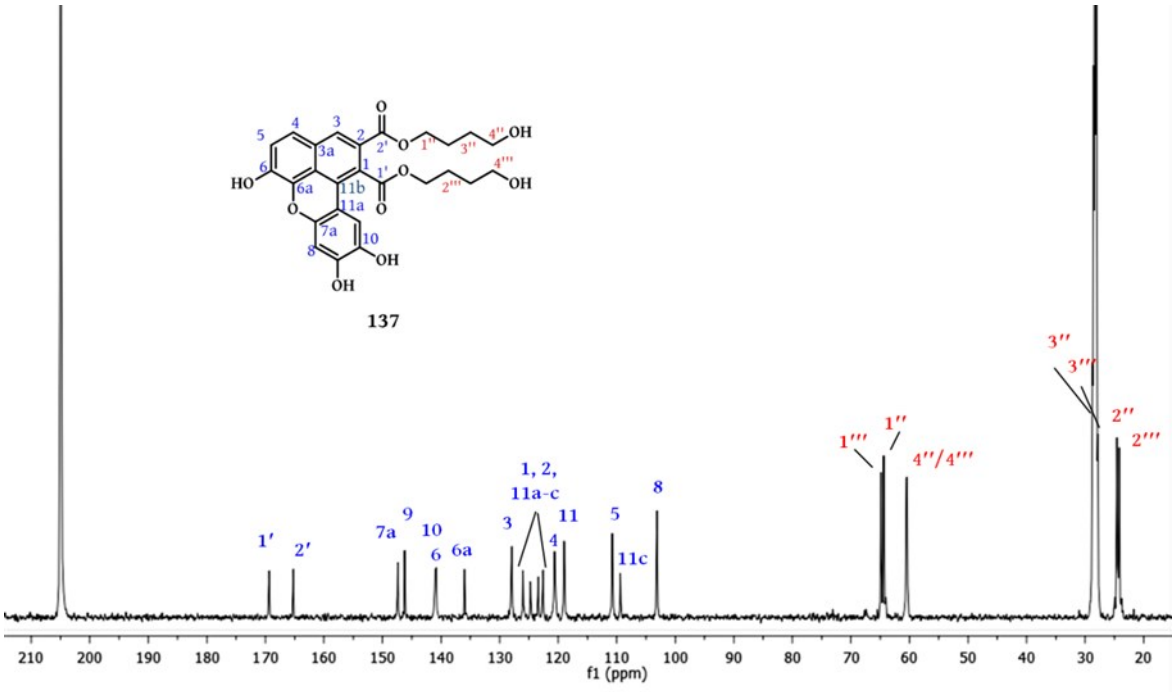

Figure 35: ^{13}C NMR spectrum (CD_3COCD_3, 125 MHz) of **137**.

The upper fields region of carbon spectrum (65 – 24 ppm) showed seven resonances for the eight sp^3 methylene carbons which were assigned through the study of HSQC correlations, but it was not possible to discriminate between the two chains signals. However, the HMBC spectrum revealed a series of crucial correlations for the unambiguously assignments of the two side chains signals as well as for quaternary carbon and for the two methylene carbon C-3″/3‴ assignments whose signals were overlapped with solvent methyl residual signal at 29.8 ppm. The signal for carboxylic ester C-2′ at 165.3 ppm, which was assigned thanks to the key HMBC correlation with 3-H proton signal at 8.18 ppm, showed also a correlation with the triplet at 4.34 ppm allowing in turn, the assignment for that triplet as H-4″. Analogously, the HMBC correlation between the signals 169.4 and 4.46 ppm allowed to assign this latter as H-4‴. In the same way all the resonances observed for the two butanediol chains were properly assigned as well as the other resonances. The spectroscopic data are collected in Table 16 together with those of the monomer **136**.

Table 16: ^{1}H and ^{13}C NMR spectroscopic data of compounds **136** and **137**[a]

position	136		137	
	δ_C	δ_H (mult, *J* Hz)	δ_C	δ_H mult (*J* Hz)
1	127.6		127.3	
2	115.1	7.15 (d, 2.0)	126.0	
3	146.3		129.2	8.18 (s)
3a			127.4	
4	148.7		126.0	7.53 (d, 8.5)
5	116.3	6.86 (d, 8.3)	112.5	7.33 (d, 8.5)
6	122.5	7.03 (dd, 2.0, 8.3)	142.3	
7	145.6	7.54 (d, 15.9)		
7a			148.8	
8	115.7	6.28 (d, 15.9)	104.4	7.27 (s)
9	167.5		147.6	
10			142.1	
11			121.9	6.72 (s)
11a			123.9	
11b			131,1	
11c			130.05	
1′	64.7	4.17 (t, 6.7)	170.6	
2′	26.2	1.76 (m)	165.3	
3′	26.2	1.62 (m)		
4′	62.1	3.60 (t, 6.4)		
1″			65.1	4.46 (t, 6.5)
2″			25.9	1.86 (m)
3″			29.8#	1.68 (m)
4″			61.8	3.65* (t, 6.3)
1‴			65.7	4.43 (t, 6.7)
2‴			25.5	1.86 (m)
3‴			29.8#	1.68 (m)
4‴			61.7	3.63* (t, 6.3)

[a] Recorded in CD_3COCD_3 (500 MHz for ^{1}H NMR and 125 MHz for ^{13}C NMR). #Signals partially overlapped with the residual solvent signal. *Signals partially overlapped

2.5.2. Chemical proteomics: discovery of new targets

The benzoxanthene **137** was submitted to CCCP chemical proteomic approach in the laboratory of Prof. A. Casapullo. Compound **137** was immobilized on sepharose beads with epoxidic functionalities. The immobilization was quantified by HPLC and the benzoxanthene-bearing beads was incubated with HeLa cells (Human hepitheloid cervix carcinoma) lysate for 16 h at 4 °C. The mixture was then submitted to separation by chromatography affinity removing the non-specifically bound proteins with several washing steps and finally the captured targeted proteins were recovered and separated by gel-electrophoresis on SDS-PAGE. In Figure 36 the electrophoretic profile is reported and by comparison with the control it was evident that the benzoxanthene **137** showed selectivity towards a protein. The gel band was subjected to an *in situ* digestion protocol and the peptides were analyzed through LC-MS/MS followed by a Mascot database search that identified the target protein as the proteasome sub-unit β5. Two independent experiments were carried out giving the same bioinformatic result with a score higher than 100.

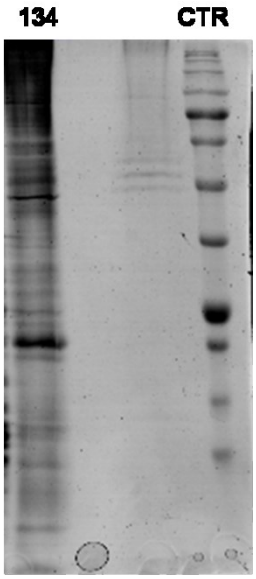

Figure 36: SDS-PAGE of **137**.

2.5.3. Benzoxanthene lignans as potential proteasome inhibitors

The data obtained with the CCCP approach for benzoxanthene **137** prompted to extend this work by testing the potential proteasome inhibitory activity of some previously reported benzoxanthenes, selected on the basis of their previously reported properties[101-103] and in

particular those with higher lipophilicity, which proved to be effectively taken up into the cells. Thus, three previously reported benzoxanthenes **67**, **138** and **139**, bearing respectively phenethyl, ethyl and butyl side chains were re-synthesized according to the above cited procedure (Scheme 12) and described with details in the Experimental section (5.5.2.)

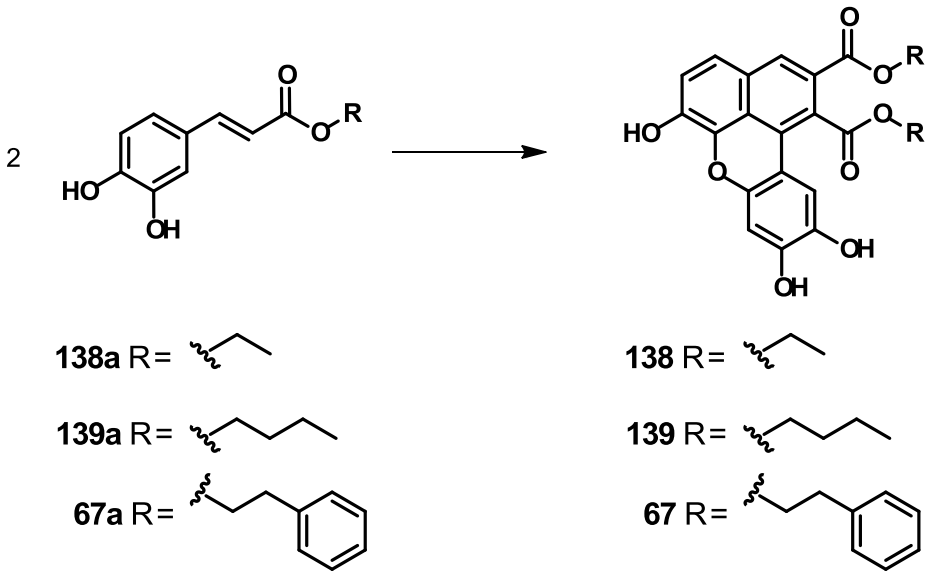

Scheme 12: $Mn(OAc)_3$, CH_2Cl_2, rt, 24 h.

Through a collaboration with the laboratory of Prof. A. Casapullo, the four benzoxanthenes were evaluated as proteasome inhibitors on HeLa cells (cell lysate was used for the *in vitro* assay) towards the chymotrypsin-like, trypsin and caspase activities of Proteasome 20S. The inhibition was carried out employing a spectrofluorimetric method and in Table 16 the concentration inhibiting the 50 % (IC_{50}) of chymotrypsin-like, trypsin and caspase activities is ported for the *in vitro* bioassays.

Table 17: Proteasome inhibition assay on HeLa cell lysate of **67**, **137** – **139** [a]

Compounds	***In vitro* IC_{50} (μM)**		
	caspase activity	**trypsin activity**	**chymotrypsin-like activity**
67	7.9	48.8	37.6
137	35.8	76.2	16.8
138	14.9	3.9	32.4
139	18.2	52.6	20.3

[a] caspase, trypsin and chymotrypsin-like residual activities were measured with a spectrofluorimeter (excitation, 380 nm; emission, 460 nm).

According to the preliminary data summarised in Table 17, compound **67** showed a promising inhibition against caspase activity (7.9 µM), whereas the benzoxanthenes **138** and **139** resulted with a moderate inhibition activity. On the other hand the benzoxanthene **138** resulted a selective inhibitor of trypsin activity of proteasome showing a IC_{50} value of 3.9 µM; all the other three compounds were scarcely active, with IC_{50} values in the range 76.2 – 48.8 µM. All the tested benzoxanthenes showed a comparable inhibitory activity towards the chymotrypsin-like activity. Compound **137** with the more hydrophilic side chains proved to be the less promising proteasome inhibitor, followed by the benzoxanthene **139**.

The preliminary data about the *in vivo* bioassay of the lignans **137**– **139** are reported as % inhibiting the trypsin, caspase and chymotrypsin-like activity in Figure 37a, b and c respectively; on the basis of the *in vitro* assay results, benzoxanthene lignans **67**, **137** – **139** were the tested at concentration of 25 µM.

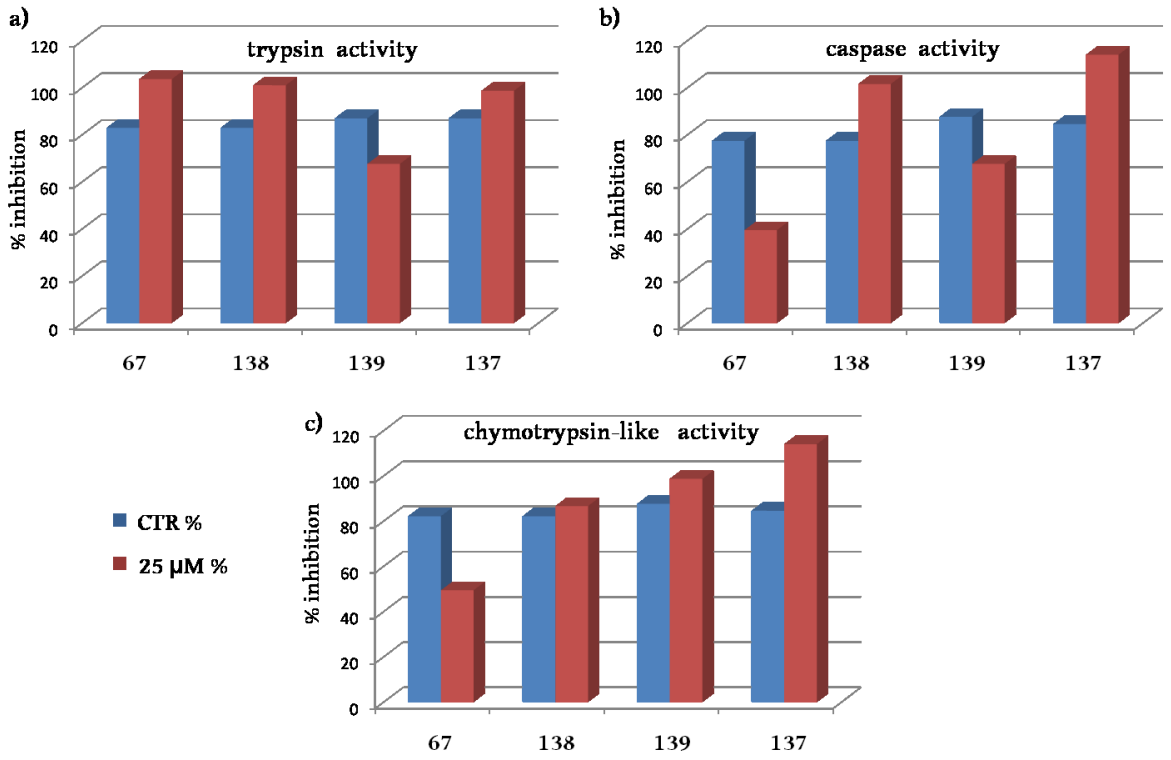

Figure 37: Activity of **67**, **137** -**139** on: **a**) trypsin site, **b**) caspase site, **c**) chymotrypsin-like site of proteasome .

As shown in Figure 37a, only the benzoxanthene **139** showed a moderate inhibitory activity toward the trypsin activity of proteasome. The Figure 37b activity shows the highest inhibitory activity of compound **67** towards caspase site with an inhibition of about the 50%

at 25 μM; confirming the data observed in the *in vitro* assay. Compound **139** showed a moderate inhibition also for the caspase activity. The hystograms reported in Figure 37c show an inhibition of about the 50% of chymotrypsin-like activity for benzoxanthene **67** and no activity for the other three compounds.

These preliminary data (obtained by *in vitro* and *in vivo* assays) suggest that benzoxanthenes **67** and **139** are worthy of further studies.

2.6. SYNTHESIS OF DEUTERATED ENTEROLACTONE, A MAMMALIAN LIGNAN

In the Introduction (1.4.1.2 paragraph), I dealed with enterolignans, a group of modified lignans found in mammalian fluids,[104, 105] the most representative members of which are enterolactone (**63**) and enterodiol (**68**). These enterolignans and their synthetic analogues have been the subject of an increasing number of *in vitro* and *in vivo* studies for their action against many health disorders and for their antiproliferative activity on many cancer cells.[107]

In this contest, enterolignans labelled with stable isotopes are often employed in qualitative and quantitative analysis of biological samples, in biological assays or to study the biogenetic pathway of mammalian lignans. The preparation of deuterated enterolignans is consequently an interesting synthetic target. One reported method regards the deuteration of lignanolactones and it is based on H/D exchange by electrophilic aromatic substitution reaction; to this purpose the reagent D_3PO_4 x BF_3/D_2O is formed *in situ* (Scheme 13).[158]

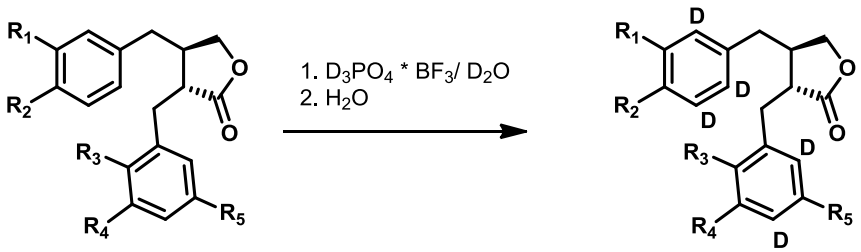

$R_1 = R_4 = OH, R_2 = R_3 = R_5 = H$
$R_1 = R_4 = R_5 = OH, R_2 = R_3 = H$
$R_1 = R_2 = OMe, R_3 = H, R_4 = R_5 = OH$
$R_1 = OH, R_2 = R_3 = H, R_4 = R_5 = OMe$
$R_1 = R_2 = R_4 = R_5 = OMe, R_3 = H$
$R_1 = OH, R_2 = R_5 = H, R_3 = R_4 = OMe$
$R_1 = OH, R_2 = R_4 = R_5 = H, R_3 = OMe$
$R_1 = OH, R_2 = R_3 = R_4 = R_5 = H$

$R_1 = R_4 = OH, R_2 = R_3 = R_5 = D$
$R_1 = R_4 = R_5 = OH, R_2 = R_3 = D$
$R_1 = R_2 = OMe, R_3 = D, R_4 = R_5 = OH$
$R_1 = OH, R_2 = R_3 = D, R_4 = R_5 = OMe$
$R_1 = R_2 = R_4 = R_5 = OMe, R_3 = D$
$R_1 = OH, R_2 = R_5 = D, R_3 = R_4 = OMe$
$R_1 = OH, R_2 = R_4 = R_5 = D, R_3 = OMe$
$R_1 = OH, R_2 = R_3 = R_4 = R_5 = D$

Scheme 13: adapted from a work of E. Leppälä *et al*.[158]

More recently, in a new method for the synthesis of polydeuterated lignans, DCl has been used as deuteration reagent in D_2O and in presence of the ionic liquid 1-butyl-3-methylimidazolium chloride ([bmim]Cl) as cosolvent (Scheme 14).[159] In this condition the proton exchange only occurs at the activated (*ortho-para*) positions of the aromatic ring.

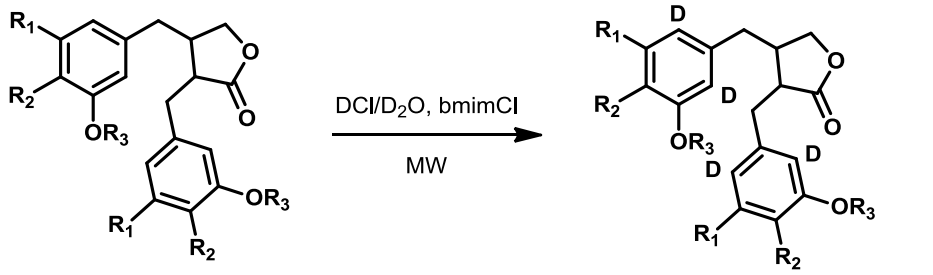

35 $R_1 = R_2 = R_3 = H$
37 R_1 =H, R_2 = OH, R_3 = Me

$R_1 = R_3 = H$, $R_2 = D$
R_1 =D, R_2 = OH, R_3 = Me

Scheme 14: adapted from a work of M. Pohjoispää *et al*.[159]

The above cited methods are useful to exchange the aromatic protons with deuterium, but the protons of the aliphatic moiety are not involved in the reaction. Thus, obtaining an enterolactone derivative with an higher level in deuteration is still a research goal, and for this reason, during a stage in the laboratory of Prof. K. Wähälä at the University of Helsinki, I carried out some experiments with this aim.

In a first step of the work I planned a possible route to reach this goal through the synthesis of the intermediate **146** (see Scheme 15), as versatile synthon to be employed in further deuteration reactions. The, simple, commercially available and low-cost reagents 3-hydroxy benzaldehyde (**140**) and succinic acid dimethyl ester (**142**) were employed in a Stobbe condensation reaction, followed by alkylation with mono-deuterated benzyl bromide (**145**) to afford the desired product **146**.

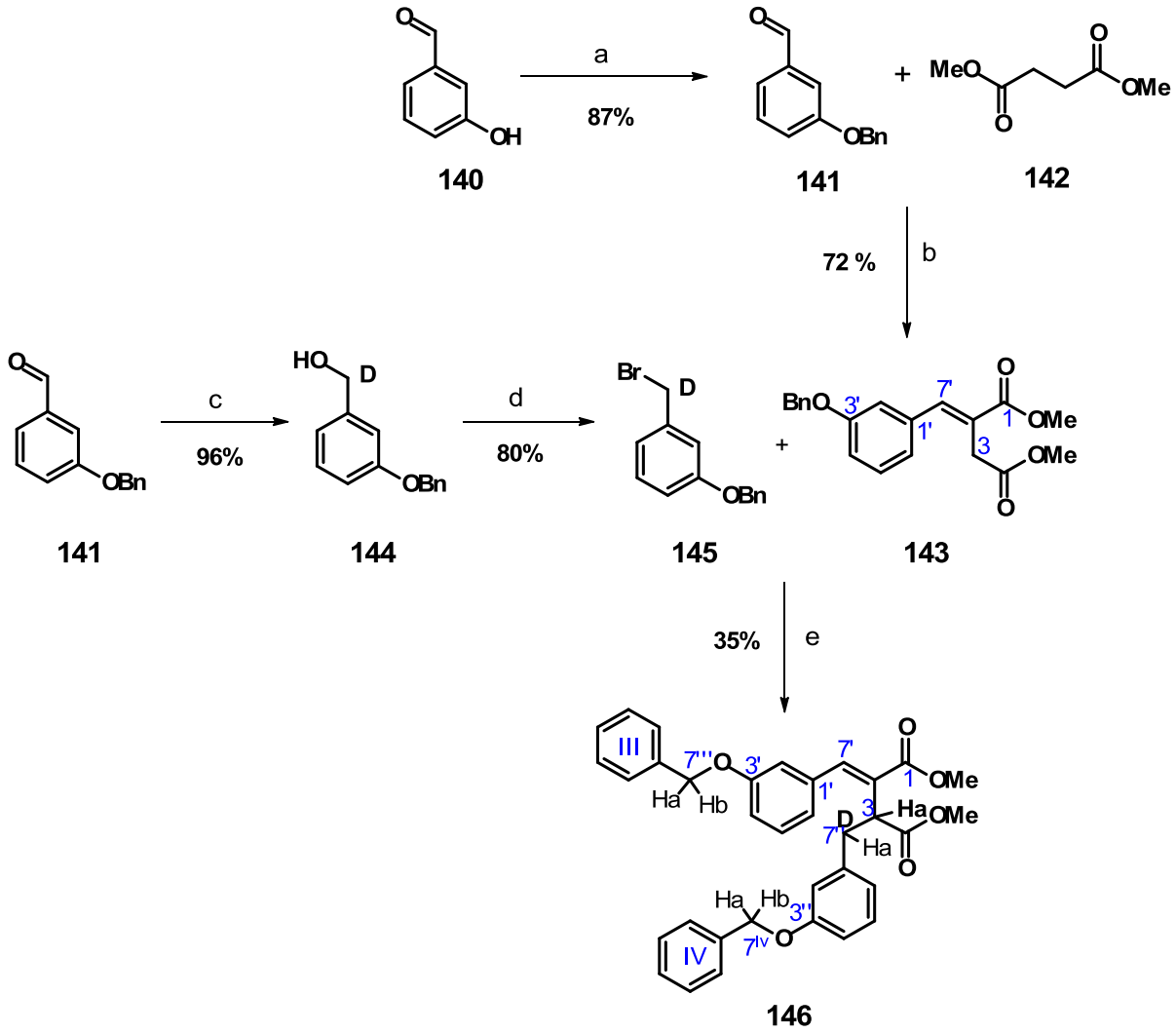

Scheme 15: (**a**) K_2CO_3, KI, BnCl, EtOH, 78 °C, 4 h; (**b**) 1. EtONa, EtOH, 78 °C 4 h, 2. H_2SO_4, MeOH, 65 °C, 12 h; (**c**)$LiAlD_4$, dry Et_2O, rt, 20 min; (**d**) PBr_3, dry benzene, rt, 2 h; (**e**) LDA, THF, -78 °C, 24 h.

Firstly the protection of 3-hydroxy benzaldehyde phenolic group was carried out by benzylation reaction; actually Stobbe condensation has been previously employed on phenolic compounds without protection, but the reaction occurred with low yield or failed.[160] A portion of the intermediate **141** was employed in the subsequent step for the condensation with **142** in presence of a strong base, and after work-up the recovered crude mixture was refluxed in methanol and in acid condition in order to re-esterify the carboxylic function(s). Purification afforded the intermediate **143** with 72% and the main peak at 340 *m*/*z* in the MS spectrum (reported in Supporting Material, Appenix D) as well as the analysis of resonance in ^{1}H and ^{13}C NMR spectra (Figures 38 and 39) suggested the stereo-selective formation of 2-*trans*-benzylidenesuccinate **143**.

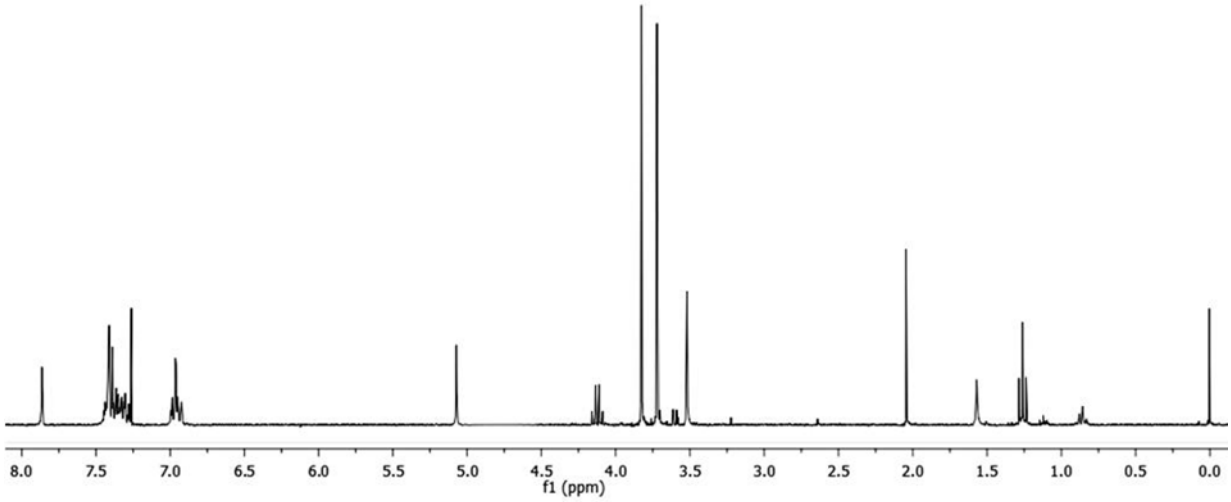

Figure 38: ^{1}H NMR spectrum ($CDCl_3$, 300 MHz) of **143**.

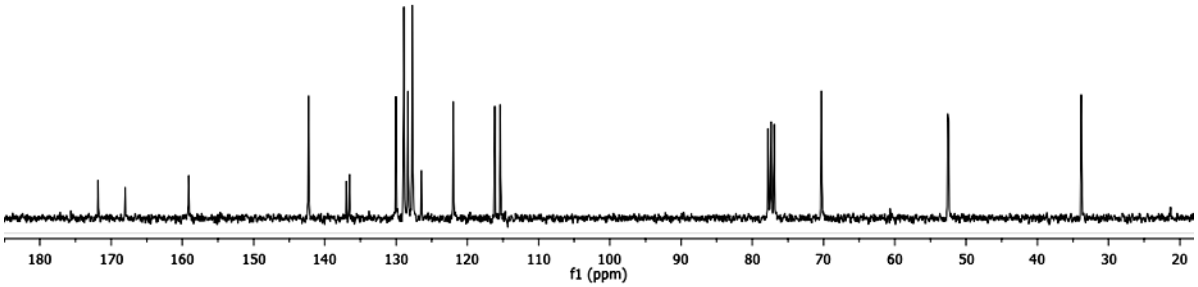

Figure 39: ^{13}C NMR sperctrum ($CDCl_3$, 75 MHz) of **143**.

A number of resonances in the ^{1}H NMR spectrum were diagnostics for the identification of **143**: namely, the presence of a singlet, integrating for two protons, at 3.54 ppm for methylene protons at C-3 position of succinic moiety; two singlets at 3.84 and 3.74 ppm each integrating for three protons, attributable to the two methoxyl groups, and the shielded singlet at 7.88 ppm for the olefinic proton H-7′, typical for *E*-isomers.[161] Also the 17 resonances detected in the ^{13}C NMR spectrum were in agreement with the formation of **143**. The presence of two signals at 171.8 and168.0 ppm for two different shielded carboxylic ester groups, for C-4 and C-1 respectively, the signal at 142.3 ppm for a sp^2 methine carbon (C-7′), the signal at 126.3 ppm for the quaternary sp^2 carbon C-2 and the resonance for methylene carbon C-3 at 33.8 ppm were the most significant data. In Table 18 all the resonance assigned for **143** are listed.

A part of intermediate **141** was converted in the proper [D_1]-benzyl bromide **145**. Precisely the reduction of **141** in the presence of lithium alluminium deuteride ($LiAlD_4$) afforded almost in quantitative yield the mono-deuterated benzyl alcohol **144** as confirmed by MS spectrum with a main peak at 215 *m/z*. In addition, the ^{1}H NMR spectrum of intermediate **144** showed a singlet at 4.62 ppm for the proton H-7′, which integrate only for one proton instead of two as expected after deuteration. The mono-deuteration was corroborated by the presence of a triplet at 64.6 ppm in the proton-decoupled ^{13}C NMR spectrum attributable to C-7 methylene carbon. All the assigned resonances are reported in Experimental section (5.5.3.3.); while the MS and NMR spectra are reported as Supporting Material in Appendix D.

A classical bromination reaction, carried out with PBr_3 gave the desired [D_1]-benzylbromide **145** starting from **144**. The EI-MS spectrum showed the expected isotopic peaks at 277 and 279 *m/z* for $^{12}C_{14}{}^{1}H_{12}{}^{2}H^{79}Br^{16}O$ and $^{12}C_{14}{}^{1}H_{12}{}^{2}H^{81}Br^{16}O$ respectively. The ^{1}H and ^{13}C NMR spectra (Appendix D) of **145** were similar to that of compound **144** except for the shielding of the δ values related to H-7 (4.45 ppm) C-7 and C-1 (33.4 and 139.3 ppm) at higher fields. The spectral data are reported in Experimental section (5.5.3.4.).

In the final step, the intermediates **143** and **145** were involved in an alkylation reaction by treating with LDA (*in situ* generated) at - 78 °C under Ar atmosphere and in dry conditions. This reaction afforded compound **146** with 35% yield after purification and it was submitted to spectral analysis. In the EI-MS spectrum, the peak at 537 *m/z*, as expected, suggested the 2,3-dibenzyl succinic acid derivative formation with retention of deuterium atom. In the same spectrum a series of fragments related to **146** were also detected, namely the peak at 506 *m/z* due to the loss of a methoxy group $[M\text{-}OMe]^{+}$, as well as the peaks at 446 and 354 *m/z* caused by loss of a benzyl group and of a phenyl benzyloxy group respectively. The ^{1}H and ^{13}C NMR spectra of **146** (Figures 40 and 41) show an increased number of signals in the aromatic region, respectively between 7.5 – 6.4 ppm and 160 – 110 ppm (see Table 18 for the assignments), respect to that detected for compound **143**, confirming the occurred alkylation with protected mono-deuterated benzyl bromide (**145**). In addition, the presence in the ^{1}H spectrum of three signals for the methine protons H-7″ and H-3 suggested that **146** has been obtained as a mixture of diasteroisomers (in Scheme 15 only one of the possible diasteromeres is drawn). Precisely, the signal at 4.01 ppm, integrating for 1 H may be assigned to Ha-7″/Hb-7″; and the two differently shielded doublets at 3.33 and 2.92 ppm (J = 5.7 Hz and J = 10.0 Hz respectively), integrating each for 0.5, may be assigned to Ha-3 and

Hb-3. Further diagnostic resonances for the formation of **146** were two pair of mutually coupled signals in ^{1}H NMR spectrum (4.96 and 4.91ppm, J = 11.8 Hz; 4.83 and 4.75 ppm, J = 11.7 Hz), assignable to two AB systems for methylene protons of the benzyl protecting groups. Other diagnostic resonances in the ^{13}C spectrum were the signals at 70.1, 69.8 ppm (C-7‴ and C-7^{IV} respectively), the deshielded signal at 45.5 ppm for the methyne carbon in α-position to ester function (C-3) and the triplet at 36.1 ppm (CHD signal for the C-7″).

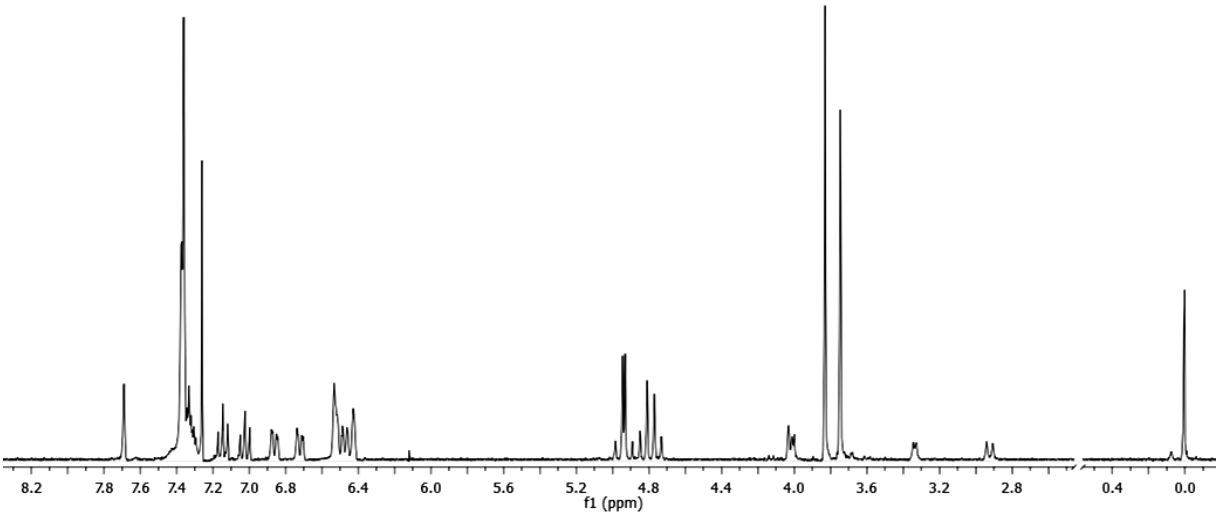

Figure 40: ^{1}H NMR spectrum ($CDCl_3$, 300 MHz) of **146**.

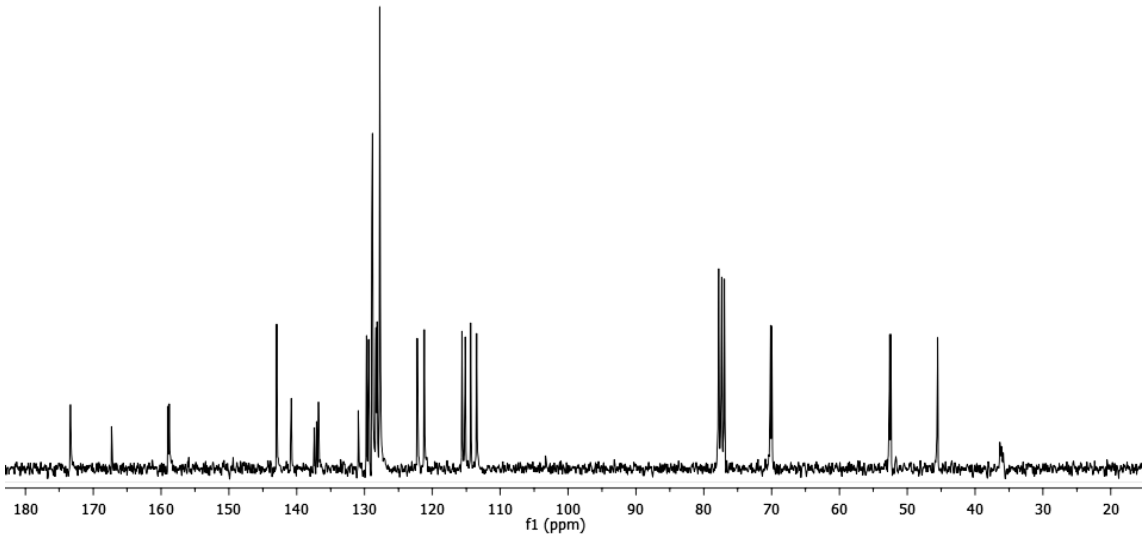

Figure 41: ^{13}C NMR spectrum ($CDCl_3$, 75 MHz) of **146**.

Table 18: ^{1}H and ^{13}C NMR spectroscopic data of compounds **143** and **146**[a]

position	136		137	
	δ_C	δ_H (mult, *J* Hz)	δ_C	δ_H mult (*J* Hz)
1	168.0		167.3	
2	126.4		130.9	
3	33.8	3.54 (s)	45.5	3.35 (d, 5.0) 2.93 (d, 10.0)
4	171.8		173.4	
1′	136.5		136.9	
2′	115.4	6.98* (d, 1.8)	115.6	6.49 (m)
3′	159.1		159.0	
4′	116.1	6.95 (bd, 8.0)	114.4	6.49 (m)
5′	130.0	7.42# (m)	129.7	7.16 (t, 8.1)
6′	121.9	6.99* (dd, 1.8, 7.7)	122.9	6.83 (dd, 2.1, 8.1)
7′	142.3	7.88 (s)	143.0	7.70 (s)
1″	136.9		140.9	
2″	127.7	7.42# (m)	115.2	6.49 (m)
3″	128.9	7.37# (m)	158.8	
4″	128.3	7.31 (dd, 2.0, 7.6)	113.5	6.49 (m)
5″	128.9	7.37# (m)	129.4	7.03 (t, 7.08)
6″	127.7	7.42# (m)	121.2	6.73 (dd, 2.0, 7.8)
7″	70.3	5.09 (s)	36.1	4.03 (m)
1‴			137.4	
2‴/6‴			127.7	7.35 (m)
3‴/5‴			128.8	7.35 (m)
4‴			128.3	7.35 (m)
7‴			70.1	4.97 (d, 11.8) 4.92 (d, 11.8)
1^{IV}			137.1	
$2^{IV}/6^{IV}$			127.1	7.35 (m)
$3^{IV}/5^{IV}$			128.8	7.35 (m)
4^{IV}			128.2	7.35 (m)
7^{IV}			69.8	4.84 (d, 11.7) 4.76 (d, 11.7)
1-OMe	52.6	3.84 (s)	52.6	3,84 (s)
4-OMe	52.4	3.74 (s)	52.4	3,76 (s)

[a] Recorded in $CDCl_3$ (300 MHz for ^{1}H NMR and 75 MHz for ^{13}C NMR). #, *Signals are partially overlapped.

Compound **146** is a versatile synthon which can be employed in the synthesis of [D_7]-enterodiol (**147**) and [D_5]-enterolactone (**148**) by highly yield steps involving deuteration followed by reduction reactions and eventually lactonization (Scheme 16).

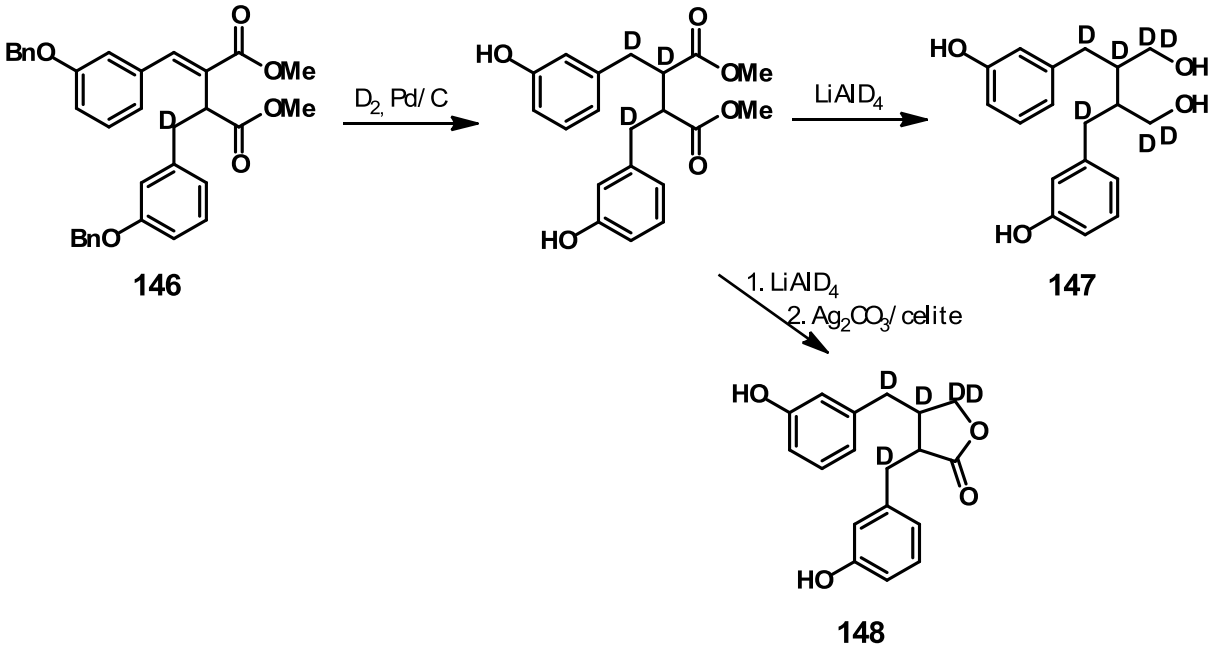

Scheme 16

Indeed, this successful synthesis, applied to [D_2]-succinate as reported in Scheme 17 will give fully deuterad [D_{12}]-enterolactone **149** or other related deuterated lignans starting from the proper substituted benzaldehyde.

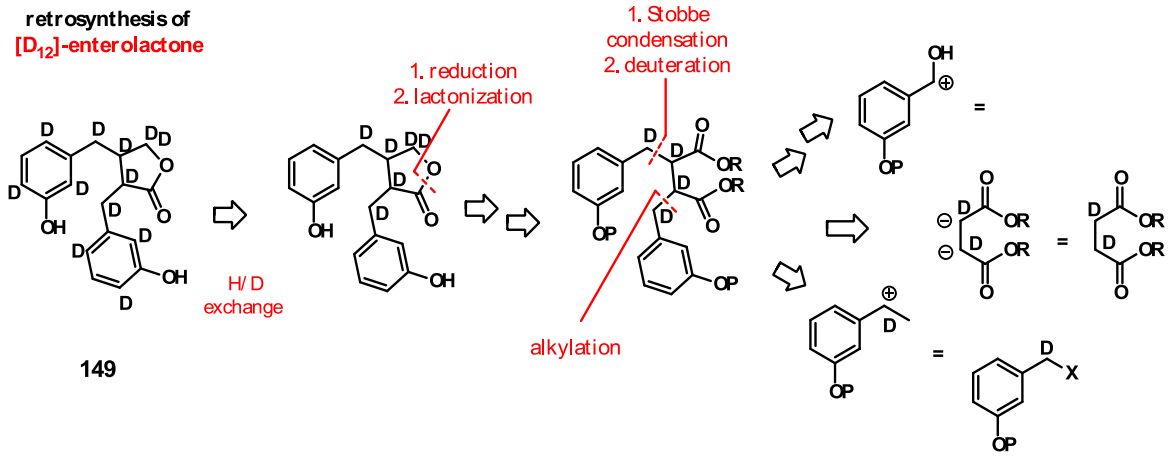

Scheme 17

2.7. NATURAL-DERIVED PROTEASOME INHIBITORS

In recent years proteasome become a pivotal target for the developing of new anticancer drugs. It was demonstrated that generally cancer cells have higher levels of proteasome activity than noncancerous ones, maybe because of their increased metabolism and higher levels of oxidative stress and growth factors. It's clear that molecules which can interact with proteasome modifying its activity are potential anticancer agents. A number of molecules have been synthesized with this aim and to date many are in clinical trials and some of them have showed systemic toxicity and side effects. For this reason, research is oriented to developed less invasive drugs with selective action on tumor cells.

According to literature data, as reported in the Introduction, natural products and their analogues or derivatives have been widely texted with interesting results. Two examples are the diaryl propanoid broussonin B (**74**)[132] and the phenolic cinnamic amide avenanthramide C (**75**).[133]

In this background, two dihydropolymethoxystilbenes (as diarylpropanoids analogues) and a small library of cinnamoyl amides (as avenanthramides C analogues) have been synthesized and evaluated as potential proteasome inhibitors.

2.7.1. Synthesis of dihydropolymethoxystilbenes as proteasome inhibitors

Compounds **150** and **151** have been obtained in quantitative yield by catalytic hydrogenation of the pertinent tetramethoxystilbenes **15** and **82** respectively (Scheme 18). These latter were synthesized according to the Horner-Emmons-Wadsworth olefination as previously described (Scheme 4).

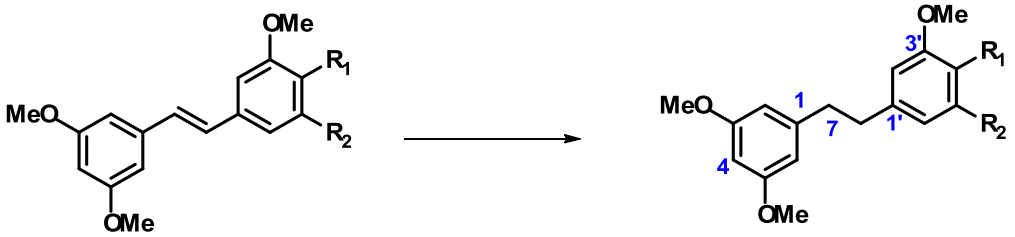

15 R_1 = OMe, R_2 = H
82 R_1 = H, R_2 OMe

150 R_1 = OMe, R_2 = H
151 R_1 = H, R_2 OMe

Scheme 18: EtOH, H_2, Pd/C 10% w/w, rt, 24h.

The ^{1}HNMR spectra of compounds **150** and **151** had suggested the occurred reduction of exocyclic double bond. The appearance of a singlet at around 2.8 - 2.7 ppm for methylene protons at C-7 and C-8 and none evidence for olefinic signals in the ^{1}H-NMR spectrum proved the quantitative hydrogenation of *E*-polymethoxystilbenes **15** and **82**. The signals assignment (reported in Experimental section 5.3.3.) fitted with data reported in literature.[162, 163]

In a collaborative work with Prof. R. Purrello (University of Catania) and with Dr. A. M. Santoro (IBB CNR Catania) the two dihydrostilbenoids **150** and **151** were evaluated as potential proteasome inhibitors employing a preliminary spectrofluorimetric assay. Precisely, the inhibitory activity of the two molecules was tested on the chymotripsyn-like activity and both the two compounds showed an IC_{50} value of 3μM. This preliminary result is very interesting if compared with that of the natural lead broussonin B reported as proteasome inhibitor (IC_{50} = 178 μM).[132]

2.7.2. Synthesis of cinnamic acid amides as proteasome inhibitors

The literature data about the proteasome inhibitory activity of the naturally occurring avenanthramide C (**75**) and of other natural compounds with α-β unsatured amide functions lead the evaluation of some cinnamic amides as proteasome inhibitors. In order to evaluate a possible structure activity relationship amides with different functional groups on cinnamic moiety and various substituents on amine aromatic residue have been designed and synthesized.

These compounds were obtained by amidation reaction of the most common cinnamic acids (**6**, **24**, **25** and **26**) with different amines, by previous activation of carboxylic acid as described in Scheme 19 for compound **118**.

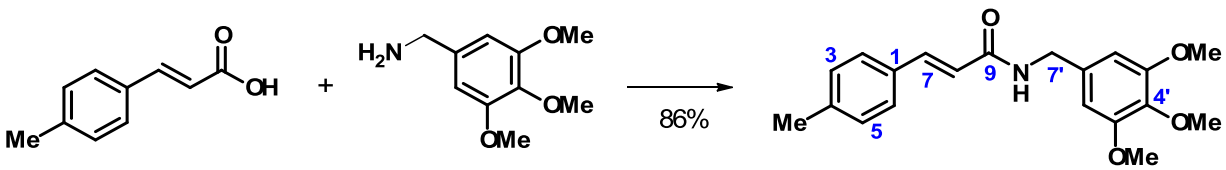

152 **120** **118**

Scheme 19: DMF, TEA, 0 °C, 15 min; BOP solution (CH_2Cl_2) 0 °C, 30 min, rt, 24 h.

Amide **103** was obtained by treating caffeoyl amide **100** (whose synthesis is reported in Scheme 7) with MeI as previously reported in Scheme 8; in this case the permethylated product **103** was obtained together with the partial methyl derivative **102**. After purification, the new compounds **103** and **118** were subjected to full spectroscopic characterization; the ESI MS, ^{1}H and ^{13}C NMR spectra are reported as Supporting Material (Appendix B), while in Table 18 their spectroscopic data are listed.

Table 18: ^{1}H and ^{13}C NMR spectroscopic data of **103** and **118**[a]

position	103[b]		118[c]	
	δ_C	δ_H (mult, *J* Hz)	δ_C	δ_H (mult, *J* Hz)
1	135.4		131.9	
2	110.0	7.16-7.12 (m)	127.6	7.38 (d, 7.9)
3	149.3		129.4	7.15 (d, 7.9)
4	150.8		134.1	
5	111.3	6.96 (d, 8.5)	129.4	7.15 (d, 7.9)
6	111.3	7.16-7.12 (m)	127.6	7.38 (d, 7.9)
7	140.5	7.50 (d, 15.0)	139.8	7.64 (d, 15.9)
8	118.1	6.52 (d, 15.0)	119.5	6.41 (d, 15.9)
9	167.4		166.0	
1′	136.6		136.9	
2′/6′	127.2	7.16-7.12 (m)	104.8	6.51 (s)
3′/5′	128.7	7.21 (d, 8.0)	153.2	
4′	127.9		140.9	
7′	42.6	4.44 (s)	43.9	4.47 (d, 5.5)
4-Me			21.3	2.35 (s)
4′-Me	19.6	2.31 (s)		
3-OMe	55.06	3.86 (s)		
4-OMe	55.01	3.85 (s)		
3′/5′-OMe			55.9	3.81 (s)
C-4′-OMe			60.6	3.81 (s)
NH				6.17 (bt)

[a] 300 MHz for ^{1}H NMR and 75 MHz for ^{13}C NMR. [b] Recorded in CD_3OD. [c] Recorded in $CDCl_3$.

Seven cinnamoyl derivatives, namely compounds **100**, **101**, **103**, **116**, **126**, **127** (whose synthesis is reported in previous paragraphs) together with amide **118** were submitted to an *in vitro* inhibition assay in order to evaluate the chymotrypsin-like activitiy related to one of the catalytic sites of proteasome 20S. The free-cell assay indicated that compounds **101**, **116**, **126** and **127**, with free phenolic function at C-4 position of cinnamic moiety, are the most promising inhibitors ($IC_{50} \sim 3$ μM). Conversely, other compounds such as **103** and **118** in which the phenolic function in C-4 is methylated showed $IC_{50} \geq 10$ μM. Noteworthy the caffeoyl derivative **100** bearing a catechol group, namely two free phenolic groups (in *ortho* position) resulted moderate active (10 μM).

The promising inhibitory activity of compounds **101 126** and **127** lead the evaluation of the other two catalytic activities of proteasome 20S, namely the caspase and trypsin activity. The assay revealed that the coumaroyl amide with the trimethoxybenzyl residue **127** ($IC_{50} = 3$ μM on trypsin site and 2 μM on caspase site) is the most promising proteasome inhibitors.

3. CONCLUSIONS

The aim of this project was the synthesis of new natural-derived polyphenol analogues with potential antitumor activity. The research activity has been developed on different topics, as detailed below:

1. Synthesis and biological evaluation of resveratrol-related polymethoxystilbene glycoconjugates;
2. Synthesis and pharmacokinetic study of two bioactive dimethoxystilbenes;
3. Synthesis of phenolic cinnamic amides as potential *m*PGES-1 inhibitors;
4. Biomimetic synthesis of dihydrobenzofuran neolignanamides, evaluation of their antirpoliferative activity and chiral resolution of racemic mixtures;
5. Synthesis of polydeuterated enterolactone;
6. Synthesis of natural-derived polyphenols as potential proteasome inhibitors.

1. Polymethoxystilbene glycosides **85** – **90** were synthesized and, together with the related 2-hydroxypolymethoxystilbenes **12**, **83** and **84**, were subjected to an antiproliferative activity bioassay, in the laboratory of Prof. D. Condorelli (University of Catania), towards Caco-2 (human colon) and SH-SY5Y (neuroblastoma) cancer cells. Compounds **12** and **83** proved highly active on both cells; **83** showed a GI_{50} value of 3 μM (Caco-2 cells), a value comparable to that of 5-FU. Compound **84** was inactive although its glucoside **87** and more the galactoside **90** showed a weak growth inhibition of Caco-2 and SH-SY5Y cells. Collectively, the data shows that minimal differences in the structure of both stilbenoids and conjugates may substantially affect their antiproliferative activity. The possible hydrolytic release of the aglycones **12**, **83** and **84** by β-glucosidase or β-galactosidase was also evaluated; only **85** and **86** were significantly hydrolysed by β-glucosidase. An evaluation of the β-glucosidase or β-galactosidase activity in the presence of compounds **85** – **90** revealed that all are moderate inhibitors at least towards one of these enzymes. Finally, compounds **86** and **89** showed a promising α-glucosidase inhibition. Thus, these resveratrol-related

conjugates may be considered as lead compounds for future development of antidiabetic or anti-obesity agents.

2. The dimethoxystilbenes **95** and **96**, previously reported for promising biological activities, were synthesized in the frame of a collaborative work with Prof. Lin (Singapore University), aimed to study their pharmacokinetic profile. A validated HPLC method revealed low and erratic plasma exposure, fast clearance and poor oral bioavailability for both compounds.
3. A library of cinnamic amides (**97 - 118**) was evaluated in a virtual screening for *m*PGES-1 inhibition in collaboration with Prof. G. Bifulco (University of Salerno). Six hits (**100**, **102**, **108**, **113**, **114** and **117**), selected on the basis of their binding energy values and specific interactions observed with the catalytic site of enzyme, were prepared and evaluated for *m*PGES-1 inhibition with *in vitro* assayat the laboratory of Prof. O. Werz (University of Jena). Only compound **100**, derived from caffeic acid, resulted a promising *m*PGES-1 inhibitor (30% of inhibition at 10 μM). The structure of compound **100** was optimized and four new caffeoyl amides (**122** – **125**) showing better binding energy values for the catalytic site than the previous amides, were synthesized for further evaluation.
4. A biomimetic oxidative coupling reaction mediated by *Trametes versicolor* Laccase was employed to obtain a small library of racemic dihydrobenzofuran neolignans derived from phenolic cinnamic amides, namely compounds (±)-**57**, (±)-**128** – (±)-**135.** These neolignanamides were evaluated at the laboratory of Prof. D. Condorelli (University of Catania) for their antiproliferative activity (MTT assay) towards three human tumor cell lines, namely Caco-2 (colon cancer), MCF-7 (mammary adenocarcinoma) and PC-3 (prostate carcinoma). A promising antiproliferative activity was observed for some of the racemates; in particular, compound (±)-**130** (GI_{50} of 3.5 and 3.7 μM on Caco-2 and PC-3 respectively) proved to be active as the anticancer drug 5-fluorouracil (**5-FU**) and compound (±)-**135** was even more active than **5-FU** with low-micromolar and sub-micromolar GI_{50} values (GI_{50} of 0.7, 2.0 and 1.9 μM on Caco-2, MCF-7 and PC-3 respectively). The lipophilicity of compounds (±)-**57**, (±)-**128** – (±)-**135** was determined and pointed out that the neolignanamides with the higher antiproliferative activity are also the more lipophilic. The most promising racemic mixtures were resolved by chiral-HPLC and the absolute configuration of pure enantiomers were determined by comparison of their CD-spectra

data and [α] values with previously reported data. Finally the MTT assay on the same cell lines, revealed an higher antiproliferative activity for enantiomer (2*R*,3*R*)-**130** (2.1, 1.7 and 2.4 μM on Caco-2, CF-7 and PC-3 respectively) with respect to activity of both racemate and (2*S*,3*S*)-**130**, suggesting that the antiproliferative activity is related with the stereochemistry of dihydrobenzofuran ring. Conversely, both the enantiomers of (±)-**135** proved to be less active than the racemate on all cell lines, suggesting a possible synergic effect of the two enantiomers, for instance through interaction with different targets.

5. During a stage at Helsinki University, the mono-deuterated enterolactone **146** was prepared applying a new method which allows the deuteration on aliphatic portion. To date only polydeuterated enterolignans at aromatic portion have been obtained. Compound **146** is a versatile synton for future synthesis of enterolactone with higher level of deuteration and polydeuterated enterolignans in general.

6. Part of my research activity was referred to the last topic, namely to the synthesis of natural-derived polyphenols as proteasome inhibitors. In collaboration with Prof. A. Casapullo (Univeristy of Salerno) a chemical proteomic study (CCCP) identified the proteasome 20S as new target for some benzo[*k,l*]xanthene lignans. A new benzoxanthene (**137**) *ad hoc* functionalized with butanediol chains for CCCP study and three previously reported benzoxanthenes (**67**, **138** and **139**) were evaluated as proteasome inhibitors and preliminary *in vitro* and *in vivo* results on HeLa cells showed a promising proteasome inhibition activity for compounds **67** and **139**.

In addition, in a collaborative work with Prof. R. Purrello (University of Catania) and Dr. A. M. Santoro (IBB-CNR, Catania), the dihydropolymethoxystilbenes **150** and **151** (analogues of diaryl propanoid Broussonin B) and seven cinnamic amides (**100**, **101**, **103**, **116**, **118**, **126** and **127**; avenanthramide C analogues) were evaluate for their interaction with Proteasome 20S catalytic sites. Preliminary studies suggest that both the two classes of natural-derived compounds are worthy of further investigation. In particular, among the amides, compounds with free phenolic function at C-4 position of cinnamic moiety resulted the most promising inhibitors.

5. EXPERIMENTAL

5.1. CHEMICALS

All chemicals were of reagent grade and were used without further purification; they were purchased from Sigma Aldrich; while solvents of different grades were purchased from VWR International. *β*-glucosidase from almonds, β-galactosidase from *Aspergillus oryzae*, α-glucosidase from *Saccharomyces cerevisiae*, *p*-nitrophenyl-β-D-glucopyranoside (*p*NP-β-Glc), *o*-nitrophenyl β-D-galactopyranoside (*o*NP-β-Gal) and *p*-nitrophenyl-α-D-glucopyranoside (*p*NP-α-Glc)*Trametes versicolor* Laccase (TvL, 10.0 U/mg), *Pleurotus ostreatus* Laccase (PoL, 11.8 U/mg), *Agaricus bisphorus* Laccase (AbL, 6.8 U/mg), horseradish peroxidase (HRP, Type I), were purchased from Sigma Aldrich.

5.2. INSTRUMENTAL PROCEDURES

Mass spectra were acquired with three different instruments. An Agilent 6400 Triple Quadrupole (6400 Series) mass spectrometer equipped with a Multimodal Ionization Source operating in MMI-ESI, operating in negative mode, was employed for characterization of most of the obtained products. Samples infused were eluted on a cartridge, (ZORBAX Eclipse XDB-C18; 4.6 x 30 mm, 3.5 µm; Agilent) with MeOH:H_2O:HCOOH (98:2:0.1%). Best source parameters for samples ionization were: gas temperature: 300 °C; vaporizer temperature: 250 °C; gas flow: 10 L/min; nebulizer: 60 psi; fragmentator 135 V; capillary voltage: 3500 V; charging: 2000 V. All the intermediates and products obtained in the synthesis of deuterated enterolactone were run on a Jeol JMS-700 SX 102 mass spectrometer equipped with a double-focusing magnetic sector detector operatin with Electron Impact (EI) ion source. Samples were injected by a direct inlet probe and they were detected using an ionization energy of 70 eV. In other cases, a LCQ-DECA ion trap mass spectrometer with electrospray ion source (Thermo Fischer) was used. Samples were directly infused and electrospray mass spectra were acquired from *m*/*z* 150 to 2000 and in negative using the following electrospray ion source parameters: capillary temperature 220 °C; spray voltage 3.5 kV; gas flow rate 30.

Elemental analysis was performed on a Perkin-Elmer 240B microanalyzer.

NMR spectra were run on a Varian Unity Inova spectrometer operating at 499.86 (^{1}H) and 125.70 MHz (^{13}C) and equipped with gradient-enhanced, reverse-detection probe. Chemical shifts (δ) are indirectly referred to TMS using residual solvent signals. All NMR experiments, including two-dimensional spectra, were performed using software supplied by the manufacturers and acquired at constant temperature (300 K). CD_3OD, $CDCl_3$, $(CD_3)_2CO$, C_5D_5N were used as solvent. The NMR spectra of the intermediates and products related to the synthesis of deuterated enterolactone were acquired on a Varian Mercury spectrometer operating at 300 (^{1}H) and 75 MHz (^{13}C). Chemical shifts (δ) are indirectly referred to TMS using residual solvent signals.

CD spectra were run on Jasco J-810 spectropolarimeter; UV spectra were run on Jasco V-630 spectrometer.

Optical rotation was measured with a Rudolph Research Analytical (Autopol I) polarimeter at 589 nm and at 25 °C for glycoconjugates and at 20 °C for neolignanamides.

High-performance liquid chromatography (HPLC) was carried out using an Agilent 1100 Series with auto-sampler and pump (G1311A), an Agilent UV detector (DAD, 1200 Series, G1315D) set at selected wavelengths of 254, 280, 305 and 325 nm. Samples were injected on analytic reverse phase column (Luna C18 column, 5 μm; 4.6 x 250 mm; Phenomenex) and were eluted in in the proper gradient of HPLC-grade H_2O/H^+ (99:1; eluent A) and CH_3CN/H^+(99:1; eluent B), at 1 mL/min.

Enantiomeric resolution was tentatively carried out on three different analytical chiral columns (250 x 4.6 mm; 5 μm): Chiralpak IA (Chiral Technologies), Lux Cellulose-1 (Phenomenex) and Lux Cellulose-2 (Phenomenex); the details are reported below.

Purifications (PLC) were performed on LiChroprep Si 60 (25 - 40 μm or 63 – 200 μm; Merck), Sephadex LH-20 (Sigma Aldrich) or LiChroprep DIOL (40 – 63 μm; Merck) using different solvent systems, as reported for each compound. Thin layer Chromatography (TLC) were carried out using pre-coated silica gel F254 plates (Merck); cerium sulphate and phosphomolybdic acid were used as chromogenic spray reagents.

5.3. SYNTHESIS OF STILBENOIDS AND RELATED COMPOUNDS

5.3.1. Polymethoxystilbene glycosides

Compounds **12**, **15**, **16** and **82** - **84** were synthesized as previously described by Spatafora *et al*.[35] The stilbenoid **15** was obtained by reacting the diethyl (3,5-dimethoxybenzyl)phosphonate **78** (prepared from 3,5-dimethoxybenzylbromide **76**) with the aldehyde **80**; analogously, **16** was synthesized by reacting the diethyl (4-methoxybenzyl)phosphonate **79** (prepared from 4-methoxybenzylchloride **77**) with the aldehyde **81**; analogously, **82** was obtained by reaction of **78** with **81**. Finally, compounds **15**, **16**, and **82** were subjected to a mild hydroxylation in the presence of *m*-chloroperbenzoic acid to give the 2-hydroxystilbenes **12**, **83**, **84**.

5.3.1.1. Preliminary experiments

Reaction conditions were optimized by subjecting compound **84** to preliminary experiments (below indicated as a – c).

a) Synthesis in homogeneous phase. Compound **84** (0.0160 g, 0.017 mmol) was dissolved in KOH solution (1 mL of 1.25 M) in dry EtOH and stirred for 15 minutes. Tetra-*O*-acetyl-α-D-glucopyranosyl bromide (0.0102 g, 0.024 mmol) was added and the mixture was stirred at room temp. for 3 days. The reaction was monitored by TLC (5% $CH_3OH/CHCl_3$); two further aliquots of tetra-*O*-acetyl-α-D-glucopyranosyl bromide (0.0050 g, 0.012 mmol) were added after 12 h and 36 h.

b) Synthesis in heterogeneous phase at room temperature. Compound **84** (0.0044 g, 0.014 mmol) was dissolved in MeOH:H_2O (55:45, 2 mL) and stirred together with K_2CO_3 (0.0200 g, 0.145 mmol) for 15 min at room temp. A mixture of tetrabutylammonium chloride (TBACl, 0.0042 g, 0.014 mmol) and tetra-*O*-acetyl-α-D-glucopyranosyl bromide (0.0145 g, 0.035 mmol) in $CHCl_3$ (2 mL) were added. The biphasic system was stirred at room temp. for 20 h and the reaction was monitored by TLC (5% $CH_3OH/CHCl_3$).

c) Synthesis in heterogeneous phase under reflux. Compound **84** (0.0057 g, 0.020 mmol) was dissolved in MeOH:H_2O (45:55, 2.2 mL) and the solution was stirred with K_2CO_3 (0.0248 g, 0.179 mmol) at room temp. for 15 min. To the solution, 1 mL of $CHCl_3$, TBACl (0.0055 g, 0.018 mmol) and a chloroformic solution of tetra-*O*-acetyl-α-D-glucopyranosyl bromide (0.0185 g, 0.045 mmol, dissolved in 1.2 mL of $CHCl_3$) were added. The heterogeneous mixture was stirred at 60 °C for 24 h. After 10 h, a solution of tetra-*O*-acetyl-α-D-

glucopyranosyl bromide (0.0098 g, 0.024 mmol/2 mL of $CHCl_3$) was added. The reaction was monitored by TLC (5% $CH_3OH/CHCl_3$).

The procedure **c**) gave a higher yield of compound **87** and was also employed to synthesize compounds **86**, **89** and **90**. Under these conditions **85** and **88** were obtained in low yields; higher yields were obtained carrying out the reaction at room temperature (procedure **b**).

*5.3.1.2. (2R,3S,4S,5S)-2-[2-(4-Methoxystyryl)-4,6-dimethoxyphenoxy] tetrahydro-6-hydroxymethyl-2H-pyran-3,4,5,triol (**85**)*

Compound **12** (0.0184 g, 0.064 mmol) was stirred with K_2CO_3 (0.0880 g, 0.637 mmol) in MeOH:H_2O (45:55, 8.3 mL) for 15 min at room temp. The catalyst TBACl (0.0178 g, 0.064 mmol), 3.6 mL of $CHCl_3$ and a solution of tetra-*O*-acetyl-α-D-glucopyranosyl bromide (0.0396 g, 0.096 mmol in 4 mL of $CHCl_3$) were added. The mixture was stirred at room temp. for 24 h. The reaction was monitored by TLC (5% $CH_3OH/CHCl_3$) and a solution of tetra-*O*-acetyl-α-D-glucopyranosyl bromide (0.0175 g, 0.042 mmol/2 mL of $CHCl_3$) was added after 10 h. The reaction was quenched by phase separation. The organic phase was dried over anhydrous Na_2SO_4, evaporated to dryness and the crude residue was purified by flash chromatography on RP-18 silica gel using a gradient of CH_3CN – H_2O (from 10 to 70%). Powder, (0.0056 g, 33% yield). R_f(TLC) = 0.25 (5% $CH_3OH/CHCl_3$). $[\alpha]_D^{25}$ = + 73 (*c* = 0.1, CH_3OH). UV (CH_3OH) λ_{max} (log ε) 306 (4.32) nm. ESI-MS: calcd. For $C_{23}H_{28}O_9Na$ $[M+Na]^+$ 471.16; found 471.2. Elemental analysis C, 61.60; H, 6.29; calcd. For $C_{23}H_{28}O_9$; found C, 61.24 and H, 6.27. NMR data are listed in Table 1.

*5.3.1.3. (2R,3S,4S,5S)-2-[2-(3,4-Dimethoxystyryl)-4,6-dimethoxyphenoxy] tetrahydro-6-hydroxymethyl-2H-pyran-3,4,5,triol (**86**)*

Compound **83** (0.0212 g, 0.067 mmol) was dissolved in MeOH:H_2O (45:55, 8.5 mL) and the solution was stirred with K_2CO_3 (0.0926 g, 0.670 mmol) at room temp. for 15 min. To the aqueous solution TBACl (0.0182 g, 0.067 mmol) in $CHCl_3$ (4 mL), and subsequently, a solution of tetra-*O*-acetyl-α-D-glucopyranosyl bromide (0.0688 g, 0.168 mmol in 4.5 mL of $CHCl_3$) were added. The heterogeneous mixture was heated at 60 °C for 24 h. The reaction was monitored by TLC (4% $CH_3OH/CHCl_3$) and after 10 hours tetra-*O*-acetyl-α-D-glucopyranosyl bromide in $CHCl_3$ (0.0301 g/2 mL) was added. The aqueous phase was extracted with $CHCl_3$ (3 x 8 mL); the combined organic phases were washed with H_2O (3 x 16 mL), dried over Na_2SO_4, filtered, and evaporated to dryness. The crude extract was purified by column chromatography with RP-18 silica gel with a gradient of CH_3CN in H_2O

(from 10 to 50%) affording **86** (0.0087 g, 43%). Amorphous powder, R_f (TLC) = 0.16 (4% $CH_3OH/CHCl_3$). $[\alpha]_D^{25}$ = 22 (*c* = 0.2, CH_3OH). UV (CH_3OH) λ_{max} (log ε) 320 (3.94) nm. ESI-MS: calcd. For $C_{24}H_{30}O_{10}Na$ $[M+Na]^+$ 501.17; found 501.2. Elemental analysis C, 60.24; H, 6.32; calcd. For $C_{24}H_{30}O_{10}$, found C, 60.25 and H, 6.19. NMR assignments are collected in Table 1.

*5.3.1.4. (2R,3S,4S,5S)-2-[2-(3,5-Dimethoxystyryl)-4,6-dimethoxyphenoxy]-tetrahydro-6-hydroxymethyl-2H-pyran-3,4,5,triol (**87**)*

Compound **84** (0.0162 g, 0.051 mmol) was dissolved in MeOH:H_2O (45:55, 7.5 mL) and the solution was stirred with K_2CO_3 (0.0714 g, 0.517 mmol) at room temp. for 15 min. $CHCl_3$ (4 mL), TBACl (0.0142 g, 0.051 mmol) and the solution of tetra-*O*-acetyl-α-D-glucopyranosyl bromide previously prepared (0.0524 g, 0.127 mmol in 3 mL of $CHCl_3$) were added to the aqueous phase. The reaction mixture was stirred at 60 °C for 24 h, and tetra-*O*-acetyl-α-D-glucopyranosyl bromide (0.025 g) in $CHCl_3$ (1.5 mL) were added after 10 hours. The reaction was monitored by TLC (4% $CH_3OH/CHCl_3$). The aqueous phase was extracted with $CHCl_3$ (3 x 6 mL) and the combined organic phases were washed with H_2O (3 x 15 mL). The $CHCl_3$ phase was dried over Na_2SO_4, filtered, and dried in vacuo. The residue was purified by liquid chromatography using a RP-18 silica gel with a gradient of CH_3CN in H_2O (from 40 to 80%). Product **87** was obtained (0.0063 g, 38%). Amorphous powder. R_f (TLC) = 0.37 (4% $CH_3OH/CHCl_3$); $[\alpha]_D^{25}$ = + 55 (*c* = 0.1, CH_3OH). UV (CH_3OH) λ_{max} (log ε) 303 (4.30) nm. ESI-MS: calcd. For $C_{24}H_{30}O_{10}Na$ $[M+Na]^+$ 501.17; found 501.2. Elemental analysis C, 60.24; H, 6.32 calcd. For $C_{24}H_{30}O_{10}$, found C, 60.30 and H, 6.21. NMR data are collected in Table 1.

*5.3.1.5. (2R,3S,4S,5R)-2-[2-(4-Methoxystyryl)-4,6-dimethoxyphenoxy] tetrahydro-6-hydroxymethyl-2H-pyran-3,4,5,triol (**88**)*

Compound **12** (0.0232 g, 0.081 mmol) was stirred with K_2CO_3 (0.1123 g, 0.813 mmol) in MeOH:H_2O (45:55, 10.2 mL) for 15 min at room temp. To the aqueous solution, $CHCl_3$ (4.3 mL), TBACl (0.0226 g, 0.049 mmol), and a solution containing tetra-*O*-acetyl-α-D-galactopyranosyl bromide (0.0666 g, 0.162 mmol) in $CHCl_3$ (4.8 mL) were added. The heterogeneous mixture was stirred at room temp. for 24 h and the reaction was monitored by TLC (5% $CH_3OH/CHCl_3$). Another addition of sugar was done after 10 hours (0.0293 g/2.0 mL). The reaction was quenched by phase separation. The $CHCl_3$ phase was dried over anhydrous Na_2SO_4, filtered, and evaporated in vacuo. The organic extract was purified by column chromatography with RP-18 silica gel with a gradient of CH_3CN in H_2O (from 10 to

70%). Amorphous powder, (0.0069 g, 30%). R_f (TLC) = 0.23 (5% $CH_3OH/CHCl_3$). UV (CH_3OH) λ_{max} (log ε) = 306 (4.01) nm. ESI-MS: calcd. For $C_{23}H_{28}O_9Na$ $[M+Na]^+$ 471.16; found 471.2. Elemental analysis C, 61.60; H, 6.29 calcd. For $C_{23}H_{28}O_9$, found C, 61.42 and H, 6.23. NMR assignments are listed in Table 2.

*5.3.1.6. (2R,3S,4S,5R)-2-[2-(3,4-Dimethoxystyryl)-4,6-dimethoxyphenoxy] tetrahydro-6-hydroxymethyl-2H-pyran-3,4,5,triol (**89**)*

Compound **83** (0.0190 g, 0.060 mmol) was stirred with K_2CO_3 (0.0838 g, 0.606 mmol) in MeOH:H_2O (45:55, 7.7 mL) at room temp. for 15 min. $CHCl_3$ (4 mL), TBACl (0.0163 g, 0.060 mmol) and an organic solution of tetra-*O*-acetyl-α-D-galactopyranosyl bromide (0.0617 g, 0.150 mmol in 4 mL of $CHCl_3$) were added to the aqueous phase. The mixture was heated at 60 °C for 24 h and the reaction was monitored by TLC. After 10 hours tetra-*O*-acetyl-α- D-galactopyranosyl bromide (0.0301 g) in 2 mL of $CHCl_3$ was added to the reaction mixture.

The aqueous phase was extracted with $CHCl_3$ (3 x 6 mL) and the combined organic phases were washed with H_2O (3 x 15 mL), dried with anhydrous Na_2SO_4, filtered, and evaporated to dryness in vacuo. The crude extract was purified by column with RP-18 silica gel eluting with a gradient of CH_3CN in H_2O (from 10 to 30%). By PLC 0.0115 g of galactoside **89** were recovered (46%). R_f (TLC) = 0.23 (4% $CH_3OH/CHCl_3$). $[\alpha]^{25}_D$ = + 80 (c = 0.2, CH_3OH). UV (CH_3OH) λ_{max} (log ε) 322 (4.28) nm. ESI-MS: calcd. For $C_{24}H_{30}O_{10}Na$ $[M+Na]^+$ 501.17; found 501.2. Elemental analysis C, 60.24; H, 6.32 calcd. For $C_{24}H_{30}O_{10}$, found C, 60.17 and H, 6.31. The NMR data are collected in Table 2.

*5.3.1.7. (2R,3S,4S,5R)-2-[2-(3,5-Dimethoxystyryl)-4,6-dimethoxyphenoxy] tetrahydro-6-hydroxymethyl-2H-pyran-3,4,5,triol (**90**)*

Compound **84** (0.0280 g, 0.088 mmol) was stirred in MeOH:H_2O (45:55, 11.3 mL) with K_2CO_3 (0.1226 g, 0.887 mmol) at room temp. for 15 min. After this time, $CHCl_3$ (5 mL), TBACl (0.0244 g, 0.088 mmol) and a solution of tetra-*O*-acetyl-α-D-galactopyranosyl bromide (0.0904 g, 0.220 mmol) in $CHCl_3$ (6.5 mL) was added to the reaction mixture. The heterogeneous mixture was stirred at 60 °C for 24 h, and at 10 h, 0.0396 g/3mL of sugar in $CHCl_3$ were added. The aqueous phase was extracted with $CHCl_3$ (3 x 10 mL) and the combined $CHCl_3$ phases were washed with H_2O (3 x 20 mL), dried over anhydrous Na_2SO_4, filtered, and evaporated to dryness. The crude extraction was purified by column chromatography with RP-18 silica gel with a gradient of CH_3CN in H_2O (from 40 to 70%). From PLC **90** was recovered (0.0109 g, 40%). R_f (TLC) = 0.38 (4% $CH_3OH/CHCl_3$). $[\alpha]_D^{25}$

= + 70 (*c* = 0.03, CH_3OH). UV (CH_3OH) λ_{max} (log ε) 305 (4.46) nm. ESI-MS: calcd. For $C_{24}H_{30}O_{10}Na$ $[M+Na]^+$ 501.17; found 501.2. Elemental analysis C, 60.24; H, 6.32 calcd. For $C_{24}H_{30}O_{10}$, found C, 60.19 and H, 6.29. NMR data are reported in Table 2.

5.3.1.8. Enzymatic cleavage assay

Compounds **85** – **90** were dissolved in DMSO and diluted with phosphate buffer at pH = 7.2 (Na_2HPO_4/ KH_2PO_4 0.050 M) to a final concentration of 5.0 x 10^{-5} M (the final concentration of DMSO did not exceeded 1.0%). β-Glucosidase from almond (1.2 U/mL) or β-galactosidase from *A. oryzae* (0.7 U/mL) was added and the mixtures were incubated at 37 °C under shaking at 400 rpm. Samples (200 μL) were taken at regular time intervals up to 96 h and the enzymatic hydrolysis was monitored by HPLC on an RP-18 column at 305 nm with the following elution gradient: (A = H_2O:HCOOH 99:1; B = CH_3CN:HCOOH 99:1) $t_{0\ min}$ B = 45%, $t_{7\ min}$ B = 80%, $t_{10\ min}$ B = 90%, $t_{12\ min}$ B = 100%, at 1mL/min.

The activity of the enzymes does not change when the solution contains 1.0% of DMSO. All assays were performed in triplicate. In order to quantify the released aglycone by the cleavage assay, calibration curves were created for compounds **12**, **83** and **84**: four solutions of the aglycones prepared within the concentration range of the test (10^{-5} – 10^{-6} M), were eluted by HPLC on an RP-18 column under the same conditions of the assay.

5.3.1.9. Glycosidases enzyme inhibition assay

A slight modification of the method of Tsujii *et al.*[136] was used to evaluate the inhibition of β-glucosidase from almonds, β-galactosidase from *Aspergillus oryzae*, and α-glucosidase from *Saccharomyces cerevisiae* by compounds **85** – **90.** The enzymatic activity was determined spectrophotometrically at 400 nm by monitoring the release of *p*-nitrophenol and *o*-nitrophenol from the substrates *p*NP-β-Glc or *p*NP-α-Glc (for glucosidases) and *o*NP-β-Gal (for galactosidase), respectively. Each substrate was dissolved in DMSO/phosphate buffer (Na_2HPO_4/KH_2PO_4 0.050 M, pH = 7.2) in order to have a final concentration of 6.5 x 10^{-5} M. In each assay, 3 mL of substrate solution were incubated with 0.1, 0.2, 0.4, 0.6 or 1.0 mL of the stock solution of each glycoside (2.6 – 4.7 x 10^{-4} M, for details see Supporting Information) in the presence of the corresponding enzyme (2.9 U/mL for β-glucosidase, 4.0 U/mL for β-galactosidase. And 2.0 U/mL for α-glucosidase) at 25 °C. The final concentration of DMSO of the solutions did not exceed 1.0%. In each set of experiments, the assay was performed in triplicate with five different concentrations. Preliminary kinetic studies of the three enzymes in the presence of pertinent substrate have provided the following incubation times: 30 min for β-glucosidase and β-galactosidase and 2 h for α-glucosidase.

5.3.2. Dimethoxystilenes

*5.3.2.1. (E)-1,2-dimethoxy-4-styrylbenzene (**95**)*

Benzyl bromide **91** (25.20 mmol, 3 mL) was stirred with triethyl phosphite (7mL) under reflux (130 °C) for 5 h. The mixture was diluted with DMF (37 mL) and it was stirred with MeONa (2.7238 g, 54.5 mmol) in ice bath (0 °C) for 30 minutes. Then 3,4-dimethoxybenzaldehyde (**93**, 4.7054 g, 28.3 mmol) was added to reaction's flask and it was stirred at rt for 1 h, at 100 °C for 1 h and finally it was kept under stirring overnight at rt. Compound **95** was obtained as pure product by crystallization from methanol from the crude precipitate obtained adding a mixture of methanol:water (1:2) to reaction. White powder (3.9796 g, 66 %). ^{1}H-NMR (500 MHz, $CDCl_3$, 298 K): δ 7.51 (d, *J* = 7.8, 2H, H-2′, H-6′), 7.36 (t, *J* = 7.8, *J* = 7.5, 2H, H-3′, H-5′), 7.25 (t, *J* = 7.5, 1H, H-4′, signal partial overlapped with residul $CHCl_3$), 7.07 (m, 3H, H-7, H-2, H-6,overlapped signals), 6.98 (d, *J* = 16.5, 1H, H-8), 6.87 (d, *J* = 7.5, 1H, H-5), 3.96 (s, 3H, 3-OCH_3), 3.91 (s, 3H, 4-OCH_3).^{13}C-NMR (125 MHz, $CDCl_3$, 298 K): δ = 149.1 (3-C), 148.9 (C-4), 137.5 (C-1′), 130.5 (C-1), 128.6 (C-3′, C-5′), 128.4 (C-4′), 127.2 (C-7), 126.8 (C-8), 126.2 (C-2′, C-6′), 119.9 (C-6), 111.2 (C-5), 108.8 (C-2), 55.9 (3-OCH_3), 55.8 (4-OCH_3).

*5.3.2.2. (E)-1,2-dimethoxy-3-styrylbenzene (**96**)*

Benzyl bromide (**91**, 3 mL, 25.20 mmol) was dissolved in triethyl phosphite (7 mL) and stirred under reflux at 130 °C for 5 h. The mixture of reaction was diluted with DMF (35 mL) and the solution was stirred with MeONa (2.7540 g, 55.1 mmol) at 0 °C for about 30 minutes. After this time, 2,3-dimethoxybenzaldehyde (**94**, 4.7071 g, 28.3 mmol) was added and the mixture was stirred at rt for 1 h, then it was heated to 100 °C for 1 h. After cooling the reaction was kept under stirring at rt overnight. Crude reaction was quenched with weakly acid solution and extracted with CH_2Cl_2 (200 mL x 3). Finally the combined organic layers were washed with water and dried over anhydrous Na_2SO_4. The recovered organic phase, evaporated to dryness, was purified by PLC using silica gel and a gradient of diethyl ether in petroleum ether (from 0 to 2 %). Purification gave 3.8709 g of pure product **96** (yield: 64 %). ^{1}H-NMR (500 MHz, $CDCl_3$, 298 K):δ = 7.64 (d, *J* = 7.5, 2H, H-2′, H-6′), 7.59 (d, *J* = 16.5, 1H, H-7), 7.45 (t, *J* = 7.5, *J* = 8.0, 2H, H-3′, H-5′), 7.35 (m, 2-H, H-4′, H-6,overlapped signals), 7.23 (d, *J* = 16.5, 1H, H-8), 7.14 (t, *J* = 8.0, *J* = 8.5, 1H, H-5), 6.90 (dd, *J* = 8.0, *J* = 1.5, 1H, H-4), 3.96 (s, 3H, 3-OCH_3), 3.93 (s, 3H, 2-OCH_3). ^{13}C-NMR (125 MHz, $CDCl_3$,

298 K): δ = 152.9 (C-3), 146.8 (C-2), 137.5 (C-1′), 131.3 (C-1), 129.7 (C-4′), 128.5 (C-3′, C-5′), 127.5 (C-7), 126.5 (C-2′, C-6′), 123.9 (C-8), 122.8 (C-5), 117.7 (C-6), 111.3 (C-4), 60.8 (2-OCH_3), 55.9 (3-OCH_3).

5.3.3. Dihydrotetramethoxystilbenes

*5.3.3.1. 4-(3,5-dimethoxyphenethyl)-1,2-dimethoxybenzene (**150**)*

Compound **15** (0.0185 g, 0.062 mmol) was dissolved in 2 mL of absolute ethanol and treated with 10 % w/w of palladium on charcoal. After *in vacuo* air removing, reaction's flask was filled with H_2 and the suspension was stirred at rt for 24 h. After reaction the catalyst was removed by filtration on 0.45 μm filter. From the reaction 0.0181 g of compound **150** were obtained (yield: 97%). ^{1}H-NMR (500 MHz, $CHCl_3$, 298 K): δ = 6.79 (d, *J* = 8.3, 1H, H-5′), 6.73 (dd, *J* = 8.3, *J* = 1.8, 1H, H-6′), 6.67 (d, *J* = 1.8, 1H, H-2′), 6.34 (d, *J* = 2.5, 2 H, H-2, H-6), 6.31 (t, *J* = 2.5, 1H, H-4), 3.86 (s, 3H, 3′-OCH_3), 3.84 (s, 3H, 4′-OCH_3), 3.76 (s, 6H, 3-OCH_3, 5-OCH_3), 2.85 (overlapped quintuplets, 4H, H-7, H-8).

*5.3.3.2. 1,2-bis(3,5-dimethoxyphenyl)ethane (**151**)*

Tetramethoxystilbene **82** (0.0235 g, 0.078 mmol) was dissolved in in 2 mL of absolute ethanol together with 10% (w/w) of carbon supported Palladium catalyst and air was removed from reaction's flask *in vacuo*. The system was filled with H_2 and was stirred at rt for 24 h. At the end of reaction the catalyst was removed by filtration on 0.45 μm filter and **151** was recovered (0.0231 g; 98%). ^{1}H-NMR (500 MHz, $CDCl_3$): δ = 6.24 (d, *J* = 2.0, 4H, H-2, H-6, H-2′, H-6′), 6.20 (t, *J* = 2.0, 2H, H-4, H-4′), 3.65 (s, 12H, 3-OCH_3, 5-OCH_3, 3′-OCH_3, 5′-OCH_3), 2.73 (s, 4 H,H-7, H-8).

5.4. SYNTHESIS OF PHENOLIC CINNAMIC ACID DERIVATIVES

5.4.1. (*E*)-*N*-(4-methylbenzyl)-3-(3,4-dihydroxyphenyl)acrylamide (100)

Caffeic acid (**6**, 358.7 mg, 1.98 mmol) was dissolved in dry DMF (20.1mL) and the solution was stirred with freshly distilled TEA (0.28 mL,1.99 mmol) at 0 °C. After 10 min, 4-methylbenzylamine (**119**, 0.25 mL, 1.98 mmol) and BOP solution (876.9 mg, 1.98 mmol, in 33.0 mL of CH_2Cl_2) were drop wise added to the mixture. The reaction was stirred at 0 °C for 30 min and at rt overnight. The CH_2Cl_2 was removed by evaporation and the residue was extracted with EtOAc (60 mL). The organic phase was extracted with 1 N HCl solution (2 x

30 mL) and to follow with $NaHCO_3$ saturated solution (2 x 30 mL). The combined organic layer was washed with water (40 mL), dried over anhydrous Na_2SO_4 and evaporated until dry. The crude mixture was purified on silica gel column in a gradient of EtOAc in PE (from 40 to 70 %) and 364.7 mg of amide **100** were obtained (yield: 65 %) as yellow powder. R_f (TLC) = 0.50 (30:70 PE:EtOAc). ESI-MS: m/z = 282.1 $[M-H]^-$ $C_{17}H_{16}NO_3$. The NMR data are collected in Table 6.

5.4.2. (*E*)-*N*-(4-methylbenzyl)-3-(4-hydroxy-3-methoxyphenyl)acrylamide (101)

Ferulic acid (**25**, 230.2 mg, 1.16 mmol) were dissolved in 12 mL of DMF and kept under stirring with TEA (0.17 mL, 1.16 mmol) in ice bath for 10 minutes. An excess of the amine **119** (0.20 mL, 1.59 mmol) and gradually a solution of BOP in CH_2Cl_2 (553.5 mg, in 20 mL) were added. The mixture was stirred at 0 °C for 30 minutes and at room temperature overnight. CH_2Cl_2 was removed and the residue was diluted with 40 mL of EtOAc and extracted with 1 N HCl solution (2 x 20 mL) and with a $NaHCO_3$ saturated solution (2 x 20 mL). The combined organic phase was washed with water, dried on anhydrous Na_2SO_4 and evaporated under vacuum. The residue was purified on Silica gel column in a gradient of MeOH (from 0 to 2 %) in CH_2Cl_2 giving 287.2 mg of pure product **101** (yield: 83 %) as yellow oil. R_f (TLC) = 0.37 (2%MeOH-CH_2Cl_2). ESI-MS: m/z = 296.2 $[M-H]^-$, $C_{18}H_{18}NO_3$. NMR data are collected in Table 10.

5.4.3. (*E*)-3-(3-hydroxy-4-methoxyphenyl)-*N*-(4-methylbenzyl)-acrylamide (102) and (*E*)-3-(3,4-dimethoxyphenyl)-*N*-(*p*-tolyl)acrylamide (103)

Amide **100** (67.9 mg, 0.22 mmol) was dissolved in dry acetone (15.2 mL) together with anhydrous K_2CO_3 (87.9 mg; 0.64 mmol); the mixture was stirred for 10 min and MeI (0.015 mL; 0.22 mmol) was added. The reaction was heated at reflux for 20 h. K_2CO_3 was removed by filtration and the crude mixture was purified by flash chromatography on Sephadex LH-20, eluting with $CHCl_3$. PLC gave 48.2 mg of **115** (yield 70%). R_f (TLC): 0.43 (97:3 $CHCl_3$: MeOH). NMR data are listed in Table 6. The same reaction gave the permathylated product **103** after purification on Sephadex LH-20 with 37% yield. R_f (TLC): 0.83 (97:3 $CHCl_3$: MeOH). NMR data are listed in Table 18.

5.4.4. (*E*)-*N*-(4-hydroxyphenetyl)-3-(3,4-dihydroxyphenyl)acrylamide (105)

Caffeic acid (**6**, 310.2 mg, 1.72 mmol) was stirred with TEA (0.24 mL, 1.73 mmol) in 18 mL of DMF in an ice bath for 10 minutes. After this time, tyramine (**121**, 306.3 mg, 2.23

mmol) and gradually the BOP solution (760.2 mg,1.72 mmol in 25 mL of CH_2Cl_2) were added. The mixture was stirred at 0 °C for 30 minutes and then at room temperature overnight. The reaction was quenched by extraction with EtOAc (50 mL) after evaporation of dichloromethane. The organic phase was treated with 1 N HCl solution (2 x 25 mL), then with $NaHCO_3$ saturated solution (2 x 25 mL) and finally washed with water. The dried organic phase was evaporated *in vacuo* and purified on silica gel in a gradient of MeOH (from 2 to 15 %) in $CHCl_3$. Pure amide (396.1 mg, yield: 77 %) was obtained after crystallization in CH_2Cl_2/ MeOH. Yellow powder. R_f (TLC) = 0.37 (92:8 $CHCl_3$:MeOH). ESI-MS: *m*/*z* = 298.2 $[M-H]^-$, $C_{17}H_{16}NO_4$. The acquired NMR data are in agreement with those previously reported.[146]

5.4.5. *(E)*-*N*-(4-hydroxyphenetyl)-3-(4-hydroxy-3-methoxyphenyl)-acrylamide (106)

Ferulic acid (**25**, 201.3 mg, 0.64 mmol) was stirred with TEA (0.10 mL, 0.64mmol) in 10.7 mL of DMF at 0 °C (in ice bath) for 10 minutes. An excess of amine **121** (186.7 mg, 1.36 mmol) was added and to follow, a solution of BOP in CH_2Cl_2 (459.4 mg, 1.36 mmol in 18 mL) was gradually poured in the reaction flask. The mixture was stirred at 0 °C for 30 minutes and the at rt overnight. The reaction mixture was evaporated *in vacuo* to remove CH_2Cl_2 and the residue was diluted with EtOAc (40 mL). The organic layer was extracted with a 1 N HCl solution (2 x 25 mL) and to follow with $NaHCO_3$ saturated solution (2 x 30 mL). Finally the organic phase was washed with water, dried over anhydrous Na_2SO_4, filtered and evaporated to dry. The organic residue was purified on silica gel in a gradient of EtOAc in PE (from 45 to 70 %) and 237.6 mg of pure amide **106** were recovered (yield: 73 %). White powder. R_f (TLC) = 0.35 (97:3 CH_2Cl_2:MeOH). ESI-MS: *m*/*z* = 312.1 $[M-H]^-$, $C_{18}H_{18}NO_4$. NMR data are in agreement with that reported in literature.[148]

5.4.6. (*E*)-*N*-(4-hydroxyphenetyl)-3-(4-hydroxyphenyl)acrylamide (107)

Coumaric acid (**24**, 478.5 mg, 2.91 mmol) was dissolved in 25.0 mL of DMF and the solution was stirred with TEA (0.40 mL, 2.90 mmol) at 0 °C for 10 minutes. The 4-hydroxyphenethylamine (**121**; 558.3 mg, 3.78 mmol) was added to the mixture of reaction and to follow a solution of BOP (1286.2 mg, 2.91 mmol, in 50 mL of CH_2Cl_2) was gradually added. The mixture was stirred at 0 °C for 30 minutes and at room temperature overnight. The CH_2Cl_2 was removed by evaporation and the residue was extracted with EtOAc (80 mL). The

organic phase was extracted with 1 N HCl solution (2 x 40 mL) and to follow with $NaHCO_3$ saturated solution (2 x 40 mL). Finally the organic layer was washed with water, dried on Na_2SO_4 and evaporated to dryness. The crude mixture was purified on silica gel column in a gradient of MeOH (from 2 to 20 %) in $CHCl_3$ and 616.8 mg of amide **107** were obtained (yield: 75 %). White amorphous powder. R_f (TLC) = 0.36 (8:92 MeOH:$CHCl_3$). ESI-MS: *m/z* = 282.2 $[M-H]^-$ $C_{17}H_{16}NO_3$. ^1H NMR e ^{13}C NMR data were in agreement with that reported in literature.[146]

5.4.7. (*E*)-3-(3,4-dimethoxyphenyl)-*N*-(4-methoxyphenethyl)-acrylamide (108)

Amide **105** (80.2 mg, 0.27 mmol) was dissolved in dry acetone (27.0 mL) and K_2CO_3 (149.2 mg; 1.08 mmol) was added to the solution. The suspension was stirred for 15 min at rt an the MeI (0.04 mL, 0.81 mmol) was added. The reaction was refluxed at 60 °C and after 20 h MeI (0.02 mL, 0.4 mmol) was added again. The reaction was stopped at 40 h and K_2CO_3 was removed by filtration. The crude mixture was pufied by flash chromatography using Silica gel and eluting with a gradient of MeOH in $CHCl_3$ (from 0 to 5%). Compound **108** was recovered with 45% yield (41.4 mg). R_f (TLC): 0.53 (97:3 $CHCl_3$: MeOH). NMR data are listed in Table 7.

5.4.8. (*E*)-*N*-(3,4,5-trimethoxybenzyl)-3-(3,4-dihydroxyphenyl)acrylamide(112)

Caffeic acid (**6**, 302.4 mg, 1.68 mmol) and TEA (0.24 mL, 1.69 mmol) were stirred in dry DMF (15.4 mL) at 0 °C for 15 min. After that, 3,4,5-trimethoxybenzyl amine (**120**, 0.35 mL, 2.21 mmol) and BOP solution (752.4 mg; 1.68 mmol; in 30.5 ml of CH_2Cl_2) were gradually poured in the mixture. The reaction was stirred at 0 °C for 30 min and at rt for 24 h. The CH_2Cl_2 was evaporated and the residue was diluted with 80 mL of EtOAc. The solution was extracted with 1 N HCl solution (2 x 40 mL) and to follow with a saturated solution of $NaHCO_3$ (2 x 40 mL). The EtOAc layer was washed with water, dried over anhydrous Na_2SO_4 and evaporated to dryness. The crude residue was purified on silica gel column with a gradient of MeOH in $CHCl_3$ (from 1 to 10 %) and 385.9 mg of amide **112** were recovered (Yield: 64 %) as yellow powder. R_f (TLC) = 0.22 (93:7 $CHCl_3$:MeOH). ESI-MS: *m/z* = 358.1 $[M-H]^-$, $C_{19}H_{20}NO_6$. The NMR assignments are reported in Table 6.

5.4.9. (*E*)-*N*-(3,4,5-trimethoxybenzyl)-3-(4-hydroxy-3-methoxyphenyl)-acrylamide (113)

Ferulic acid (**25**; 224.6 mg, 1.16 mmol) was dissolved in dry DMF (10.4 mL) and TEA (0.40 mL) was added; the mixture was kept under stirring in ice bath for 15 min. A dichloromethane solution of BOP (513.2 mg, 1.16 mmol, in 20.8 mL of CH_2Cl_2) and 3,4,5-trimethoxybenzylamine (**120**, 0.18 mL, 1.30 mmol) were added drop wise to cooled reaction. The mixture was stirred at 0 °C for 30 min and at rt for 24 h. The crude mixture was diluted with CH_2Cl_2 (30 mL) extracted with 1 N HCl solution (3 x 20 mL). The organic layer was extracted with $NaHCO_3$ saturated solution (3 x 20 mL) and finally it was washed with water (30 mL), dried on anhydrous Na_2SO_4 and concentrated *in vacuo*. The crude extract was purified on Silica gel using a gradient of MeOH in CH_2Cl_2 (from 1 to 10%) and amide **113** was recovered (305.4 mg, yield: 57 %) as yellow oil. R_f (TLC): 0.44 (20:80 PE: EtOAc). ESI-MS: m/z = 392 $[M - H]^-$; $C_{20}H_{22}NO_6$. ^1H and ^{13}C resonances assignment is reported in Table 7.

5.4.10. (*E*)-3-(3-hydroxy-4-methoxyphenyl)-*N*-(3,4,5-trimethoxybenzyl)-acrylamide (114)

Amide **112** (71.2 mg, 0.20mmol) was dissolved in dry acetone (15.0 mL), K_2CO_3 (55.2 mg, 0.40 mmol) was added to this solution and the mixture was stirred for 10 min at rt. KI (0.02 mL, 0.40 mmol) was added and the suspension was heated at reflux for 24 h. After filtration, the crude mixture was purified on Sephadex column with $CHCl_3$ and amide **114** (17.9 mg) was recovered with 24% yield. R_f (TLC) = 0.32 (97:3 $CHCl_3$:MeOH). Spectral data are reported in Table 7.

5.4.11. (*E*)-3-(4-hydroxy-3,5-dimethoxyphenyl)-*N*-(3,4,5-trimethoxybenzyl)-acrylamide (116)

Sinapic acid (**26**, 180.0 mg, 0.80 mmol) was stirred with TEA (0.12 mL 0.85 mmol) in dry DMF (10 mL) at 0 °C for 10 min. After this time 3,4,5-trimethoxybenxylamine (**120**, 0.12 mL, 0.94 mmol) and gradually BOP solution (375.7 mg; 0.85 mmol in 10 mL of CH_2Cl_2) were added to the reaction. The mixture was stirred at 0 °C for 30 min and at rt overnight. The reaction was extracted with EtOAc (50 mL) after evaporation of dichloromethane. The organic phase was treated with 1 N HCl solution (2 x 25 mL), then with $NaHCO_3$ saturated solution (2 x 25 mL). The organic layer was washed with wather, dried over Na_2SO_4 and

concentrated under vacuum. Pure amide **116** (275.1 mg) was obtained by crystallization (50 :50 EtOAc: MeOH) with 80% yield. White powder. R_f (TLC) = 0.28 (95:5 $CHCl_3$:MeOH). ESI-MS: m/z = 426.2 $[M+Na]^+$, $C_{21}H_{25}NO_7Na$. The NMR data are collected in Table 7.

5.4.12. (*E*)-*N*-(3,4,5-trimethoxybenzyl)-3-(3,4,5-trimethoxyphenyl) acrylamide (117)

Amide **116** (62.4 mg, 0.15 mmol) and K_2CO_3 (20.7 mg, 0.15 mmol) were stirred in dry acetone (13.4 mL) at rt for 10 min. MeI (0.015 mL, 0.30 mmol) was added to the mixture and the suspension was refluxed at 60 °C for 20 h. K_2CO_3 was removed by filtration and the crude mixture was concentrated *in vacuo*. The reaction furnished pure amide **117** (57.5 mg) without further purification with 92% yield. R_f (TLC): 0.69 (95:5 $CHCl_3$. MeOH). NMR data are reported in Table 7.

5.4.13. *(E)*-*N*-(3,4,5-trimethoxybenzyl)-3-*p*-tolylacrylamide (118)

The 4-methylcinnamic acid (**152**, 321.7 mg, 1.98 mmol) was stirred with 0.25 mL of TEA (1.96 mmol) in 16.0 mL of DMF at 0 °C (in ice bath) for 10 minutes. After this time, an excess of amine **120** (0.35 mL, 2.57 mmol) was added and to follow, a solution of BOP (875.1 mg, 1.98 mmol in 28 mL of CH_2Cl_2) was gradually poured in the reaction flask. The mixture was stirred at 0 °C for 30 minutes and the at rt overnight. The reaction mixture was evaporated *in vacuo* to remove CH_2Cl_2 and the residue was diluted with EtOAc (40 mL). The organic layer was extracted with 1N HCl solution (2 x 20 mL) and to follow with a saturated solution of $NaHCO_3$ (2 x 20 mL). Finally the organic phase was washed with water, dried with Na_2SO_4 anhydrous, filtered and evaporated to dry. The organic residue was purified on silica gel in a gradient of MeOH in CH_2Cl_2 (from 0 to 15%) and 581.6 mg of pure amide **118** were recovered (yield: 86 %).White amorphous powder. R_f (TLC) = 0.82 (90:10 CH_2Cl_2:MeOH). ESI-MS: m/z = 364.2 $[M+Na]^+$, $C_{20}H_{24}NO_4Na$; N m/z = 342.3 $[M+H]^+$, $C_{20}H_{24}NO_4$. The NMR data are reported in Table 18.

5.4.14. (*E*)-*N*-(4-(1,2,3-thiadiazol-4-yl)benzyl)-3-(3,4-dihydroxyphenyl)-acrylamide (122)

Caffei acid (**6**; 75.3 mg, 0.42 mmol) was solved in dry DMF (3 mL) and in TEA (0.060 mL, 0.43 mmol). The solution was cooled on an ice bath for 15 min. Separately, 4-(1,2,3-thiadiazol-4-yl)phenyl)methanamine (**122a**; 100.0 mg, 0.45 mmol) was dissolved in dry DMF (1 mL) and in TEA (0.065 mL, 0.47 mmol) and it was stirred on an ice bath for 10

min. The solution containing amine **122a** was added to the caffeic acid solution and to follow the solution of BOP (188.2 mg,0.43 mmol, in 7.0 mL of CH_2Cl_2). The mixture was stirred at 0 °C for 30 min and at rt for 24 h. CH_2Cl_2 was removed and the residue was diluted with EtOAc (50 mL) and it was extracted with 1 N HCl solution (20 mL) and with $NaHCO_3$ saturated solution (20 mL). The organic phase was washed with water (2 x 20 mL), dried over anhydrous Na_2SO_4, filtered and evaporated. The crude mixture was purified by flash chromatography on silica gel and with a gradient of MeOH in CH_2Cl_2 (from 2 to 20%). Amide **122** (90.4 mg) was recovered with 61% yield as yellow powder. R_f (TLC): 0.49 (92:8 CH_2Cl_2:MeOH). ESI-MS: m/z = 352.1 $[M-H]^-$, $C_{18}H_{15}N_3O_3S$. NMR data are listed in Table 9.

5.4.15. (*E*)-*N*-(2-(benzo[*d*]thiazol-2-yl)ethyl)-3-(3,4-dihydroxyphenyl)-acrylamide (123)

Caffeic acid (**6**, 90.3 mg, 0.50 mmol) was dissolved in dry DMF (5.0 mL) and in TEA (0.070 mL, 0.50 mmol) and the solution was kept under stirring at 0 °C for 15 min. 2-(benzo[*d*]thiazol-2-yl)ethanamine (**123a**; 98.6 mg, 0.55 mmol) was added, followed by the BOP solution (221.4 mg, 0.50 mmol, in 8 mL of CH_2Cl_2). The reaction was stirred on an ice bath for 30 min and at rt overnight. Dichloromethane was evaporated and the crude mixture was diluted with EtOAc (50 mL). The organic phase was extracted with 1 N HCl solution (20 mL), with a saturated solution of $NaHCO_3$ and finally with water (2 x 20 mL). The organic layer was dried overNa_2SO_4, filtered and evaporated until dry. The crude residue was purified by flash chromatography on Silica gel and with a gradient of MeOH in CH_2Cl_2 (from 2 to 10%) and amide **123** (68.0 mg) was recovered with 40% yield as yellow powder. R_f (TLC): 0.32 (92:8 CH_2Cl_2:MeOH). ESI-MS: m/z = 339.1 $[M-H]^-$, $C_{18}H_{16}N_2O_3S$. NMR data are listed in Table 9.

5.4.16. (*E*)-3-(3,4-dihydroxyphenyl)-*N*-(3-(pyrimidin-2-yl)benzyl)-acrylamide (124)

Caffeic acid (**6**, 23.5 mg, 0.13 mmol) was dissolved in dry DMF (1.7 mL) and the solution was stirred with TEA (0.020 mL, 0.14 mmol) at 0 °C for 15 min. 3-(pyrimidin-2-yl)benzyl amine (**124a**; 25.0 mg, 0.13 mmol) and BOP solution (57.5 mg, 0.13 mmol, in 2.3 mL of CH_2Cl_2) were added to the reaction cooling at 0 °C for 30 min. The mixture was stirred at rt overnight. CH_2Cl_2 was removed under vacuum and the crude was diluted with 40 mL of EtOAc. The organic phase was extracted with 1 N HCl solution (15 mL), with $NaHCO_3$ saturated solution (15 mL) and finally with water (20 mL). The organic layer was dried over

anhydrous Na_2SO_4, filtered and concentrate until dry. The organic residue was purified on Silica gel with a gradient of MeOH in $CHCl_3$ (from 1 to 15%) and 15.6 mg of amide **124** were obtained (Yield: 34%) as yellow oil. R_f (TLC): 0.35 (92:8 $CHCl_3$:MeOH). ESI-MS: *m/z* = 346.2 $[M-H]^-$, $C_{20}H_{17}N_3O_3$. NMR data are listed in Table 9.

5.4.17. (*E*)-3-(3,4-dihydroxyphenyl)-*N*-methyl-*N*-(4-(pyrimidin-2-yl)benzyl)-acrylamide (125)

Caffeic acid (**6**, 8.9 mg, 0.05 mmmol) was dissolved in 0.7 mL of DMF and TEA (0.01 mL; 0.07mmol); the solution was cooled on an ice bath for 15 min. *N*-methyl-1-(4-(pyrimidin-2-yl)phenyl)methanamine (**125a**; 10.0 mg, 0.05 mmol) and BOP solution (21.2 mg, 0.05 mmol, in 1.5 mL of CH_2Cl_2) were added to the mixture. The reaction was stirred at 0 °C for 30 min and at rt overnight. The mixture was diluted with 10 mL of CH_2Cl_2 and it was extracted with 1 N HCl solution (5 mL), with $NaHCO_3$ saturated solution (5 mL) and with water. The organic layer was dried over Na_2SO_4, filtered and evaporated under vacuum. Compound **125** (3.4 mg) was obtained by crystallization ($CHCl_3$:MeOH) with 19% yield. Yiellow powder. R_f (TLC): 0.35 (92:8 $CHCl_3$:MeOH). ESI-MS: *m/z* = 360.2 $[M-H]^-$, $C_{21}H_{21}N_3O_3$.

5.4.18. (*E*)-4-hydroxybutyl 3-(3,4-dihydroxyphenyl)acrylate (136)

Caffeic acid (**6**; 415.8 mg; 2.31 mmol) was solved in butanediol (7.2 mL, 81.26 mmol) and in concentrated H_2SO_4 (0.4 mL). The solution was heated at 50 °C for 24 h. (*E*)-4-hydroxybutyl 3-(3,4-dihydroxyphenyl)acrylate (**136**) was recovered by extraction with EtOAc (100 mL) and $NaHCO_3$ saturated solution (2 x 50 mL). The organic layer was washed with water, dried over Na_2SO_4 and concentrated in vacuo.
Yellow powder (551.8 mg; 95% yield). R_f (TLC): 0.44 (92:8 CH_2Cl_2:MeOH). ESI-MS: *m/z* = 251.2 $[M-H]^-$, $C_{13}H_{16}O_5$. The NMR data are reported in Table 15.

5.5. SYNTHESIS OF LIGNANS AND NEOLIGNANS

5.5.1. Biomimetic synthesis of dihydrobenzofuran neolignanamides

5.5.1.1. Preliminary screenings

Each substrate (compounds **100**, **101**, **105 – 107**, **112**, **113**, **126** and **127**; 2 mg) was dissolved in 1 mL of three different solvents, namely EtOAc, CH_2Cl_2, 2 % DMSO in acetate

buffer (pH = 4.7). The three different solutions of each compound were treated with the following enzymes: TvL, PoL, AbL, HRP (2 mg), in acetate buffer (1 mL, 0.1M, pH = 4.7) for a total of 96 samples. The reactions were stirred at room temperature in vials without caps except for HRP-mediated reactions; in these latter 1 μL of 30 % H_2O_2 (v/v) was added to each mixture and the reactions were carried out in capped vials. Each experiment was reproduced in the same conditions without enzyme as blank.

The course of reaction was monitored at selected times by HPLC with reverse phase column (RP-18) with the following gradient of CH_3CN/H^+ (99:1v/v; B) in H_2O/H^+ (99:1v/v; A) at 1 ml/min: $t_{0\ min}$ B = 20 %, $t_{30\ min}$ B = 80 %. The Diode array detector was set at 254, 280, 305 and 325 nm.

*5.5.1.2. (±)-(E)-2-(4-hydroxy-3-methoxyphenyl)-N-(4-hydroxyphenethyl) 5-(3-((4-hydroxyphenethyl)amino)-3-oxoprop-1-en-1-yl)-7-methoxy-2,3-dihydro-benzofuran-3-carboxamide [(±)-**57**]*

Feruloyl amide **106** (120.3 mg, 0.38 mmol) was solved in 60.0 mL of EtOAc and the organic phase was stirred with an acetate buffer solution containing the enzyme TvL (115.8 mg dissolved in 48 mL). The reaction was carried out at room temperature and after 4 h it was stopped. The two phases were separated and the aqueous solution was extracted with EtOAc (2 x 30 mL). The combined organic phase was washed with water; dried over anhydrous Na_2SO_4 and the solvent was *in vacuo* evaporated after filtration. The crude mixture was purified on silica gel with a gradient of MeOH in $CHCl_3$ (from 2 to 10%) affording 19.3 mg of dihydrobenzofuran (±)-**57** (Yield: 32%) as yellow oil. R_f (TLC) = 0.29 (90:10 $CHCl_3$:MeOH). The spectral data were in agreement with the previous reported in literature.[146b]

*5.5.1.3. (±)-5-((E)-2-(3,4,5-trimethoxybenzylcarbamoyl)vinyl)-N-(3,4,5-trimethoxybenzyl)-2,3-dihydro-2-(4-hydroxyphenyl)benzofuran-3-carboxamide [(±)-**128**]*

Coumaroyl amide **127** (117.6 mg, 0.34 mmol) was dissolved in 0.5 mL of DMSO and diluted to 55 mL with EtOAc. The organic phase was stirred with the enzyme solution (108.2 mg of TvL in 55 mL of acetate buffer) at room temperature for 24 h. The aqueous solution, after separation from the organic phase, was extracted with EtOAc (2 x 25 mL) and the total organic phase was finally washed with water. The dried EtOAc solution was filtered and evaporated until dry. By silica gel column on the crude mixture, eluting in a gradient of

acetone in CH_2Cl_2 (from 4 to 20%) the neolignanamide (±)-**128** was recovered (39.4 mg, yield: 34 %). White powder. R_f (TLC) = 0.35 (84:16 CH_2Cl_2:acetone). ESI-MS: *m*/*z* = 683.4 $[M-H]^-$, $C_{38}H_{39}N_2O_{10}$. NMR data are collected in Table 11.

*5.5.1.4. (±)-5-((E)-2-(4-hydroxyphenethylcarbamoyl)vinyl)-N-(4-hydroxyphenethyl)-2,3-dihydro-2-(4-hydroxyphenyl)benzofuran-3-carboxamide [(±)-**129**]*

Amide **107** (105 mg, 0.37 mmol) was dissolved in 0.50 mL of DMSO and diluted with 49.5 mL of EtOAc. The organic phase was stirred with a solution of TvL (102 mg in 50 mL of acetate buffer) at room temperature for 24 h. Atfer the two phases separation, the enzyme solution was removed by extraction with EtOAc (2 X 25 mL) and the recovered organic phase was finally washed with water (30 mL), dried and evaporated until dryness. The organic residue was purified on silica gel column in a gradient of MeOH in CH_2Cl_2 (from 2 to 10 %) and 16.8 mg of pure dihydrobenzofuran (±)-**129** were recovered (Yield: 16 %) as white solid. R_f (TLC) = 0.35 (92:8 CH_2Cl_2:MeOH). ESI-MS: *m*/*z* = 563.3 $[M-H]^-$, $C_{34}H_{31}N_2O_6$. NMR data are reported in Table 11.

*5.5.1.5. (±)-5-((E)-2-(4-methylbenzylcarbamoyl)vinyl)-N-(4-methylbenzyl)-2,3-dihydro-2-(4-hydroxyphenyl)benzofuran-3-carboxamide [(±) -**130**]*

Amide **126** (130.8 mg, 0.49 mmol) was dissolved in 0.70 mL of DMSO and 59.3 mL of EtOAc. The organic phase was stirred with 115.2 mg of TvL previously dissolved in 60 mL of acetate buffer at room temperature for 24 h. After separation of the two phases, the aqueous phase was extracted with EtOAc (2 x 30 mL) and the total organic phase was washed with water (50 mL), dried on Na_2SO_4, filtrated and evaporated *in vacuo*. The crude mixture was purified on silica gel column in a gradient of MeoH in CH_2Cl_2 (from 0 to 5 %) and the dihydrobenzofuran amide (±)-**130** was recovered. By further crystallization (acetone) 38.3 mg of pure compound were obtained (Yield: 29 %) as white solid. R_f (TLC) = 0.25 (96:4 CH_2Cl_2:MeOH). ESI-MS: *m*/*z* = 531.3 $[M-H]^-$, $C_{34}H_{31}N_2O_4$. NMR data are summarized in Table 11.

*5.5.1.6. (±)-5-((E)-2-(3,4,5-trimethoxybenzylcarbamoyl)vinyl)-N-(3,4,5-trimethoxy-benzyl)-2,3-dihydro-7-hydroxy-2-(3,4-dihydroxyphenyl)benzofuran-3-carboxamide [(±)-**131**]*

The caffeic amide **112** (105.8 mg, 0.29 mmol) was dissolved in 50 mL of CH_2Cl_2; the organic phase was stirred with 104.2 mg of TvL previously dissolved in 50 mL of acetate buffer at room temperature for 2 h. After separation of the two phases, the aqueous phase was

extracted with EtOAc (2 x 25 mL) and the total organic phase was washed with water (50 mL), dried on Na_2SO_4, filtrated and evaporated *in vacuo*. The crude mixture was purified on silica gel column in a gradient of MeoH in $CHCl_3$ (from 0 to 10 %) and the dihydrobenzofuran amide **(±)-131** was recovered (24.8 mg, Yield: 24 %) as yellow oil.
R_f (TLC) = 0.55 (92:8 $CHCl_3$:MeOH). ESI-MS: *m/z* = 715.2 $[M-H]^-$, $C_{38}H_{39}N_2O_{12}$. NMR data are reported in Table 11.

*5.5.1.7. (±)-(E)-2-(3,4-dihydroxyphenyl)-7-hydroxy-N-(4-hydroxyphenethyl)-5-(3-((4-hydroxyphenethyl)amino)-3-oxoprop-1-en-1-yl)-2,3-dihydrobenzofuran-3-carboxamide [(±)-**132**]*

Amide **105** (118.2 mg, 0.40 mmol) was dissolved in 60.2 mL of CH_2Cl_2 ; the organic phase was stirred with a solution of TvL (108.6 mg in 51.0 mL of 0.1 M acetate buffer, pH = 4.7) at room temperature for 2 h. The reaction was quenched by phases separation and the aqueous solution was extracted with CH_2Cl_2 (2 x 25 mL).The combined organic phases were washed with water (50 mL) and finally dried on anhydrous Na_2SO_4 and took to dry. The organic residue was purified on silica gel in a gradient of MeOH in $CHCl_3$ (from 3 to 15%) and 7.6 mg of pure neolignanamides (±)-**132** were recovered (Yield:13%) as yellow oil. R_f (TLC) = 0.41 (88:12 $CHCl_3$:MeOH). ESI-MS: *m/z* = 595.1 $[M-H]^-$, $C_{34}H_{32}N_2O_8$; NMR data are collected in Table 12.

*5.5.1.8. (±)-5-((E)-2-(4-methylbenzylcarbamoyl)vinyl)-N-(4-methylbenzyl)-2,3-dihydro-7-hydroxy-2-(3,4-dihydroxyphenyl)benzofuran-3-carboxamide [(±)-**133**]*

Amide **100** (131.2 mg, 0.46 mmol) was dissolved in 65 mL of CH_2Cl_2 and to this solution 128.4 mg of TvL in acetate buffer (65 mL) were added. The biphasic system was stirred at room temperature for 2 h. After the two phases separation, the aqueous phase was extracted with CH_2Cl_2 (2 X 25 mL) and finally the total organic phase was washed with water (50 mL), dried and evaporated to dryness. The crude organic residue was purified on silica gel column in a gradient of MeOH in CH_2Cl_2 (from 2 to 5 %) and 21.2 mg of pure dihydrobenofuran amide (±)-**133** were obtained (Yield: 16 %) as yellow oil. R_f (TLC) = 0.56 (92:8 CH_2Cl_2:MeOH). ESI-MS: *m/z* = 563.2 $[M-H]^-$, $C_{34}H_{31}N_2O_6$. NMR data are collected in Table 12 .

*5.5.1.9. (±)-5-((E)-2-(3,4,5-trimethoxybenzylcarbamoyl)vinyl)-N-(3,4,5-trimethoxybenzyl)-2,3-dihydro-2-(4-hydroxy-3-methoxyphenyl)-7-methoxybenzofuran-3-carboxamide [(±)-**134**]*

Compound **113** (0.0736 g; 0.20 mmol) was dissolved in 10 mL of EtOAc. A buffer solution of TvL (10 U/mg) previously prepared (0.0085 g in 5 mL of acetate buffer 0.1 M, pH = 7.4) was added to organic solution and the biphasic system was stirred at rt for 4 h. The crude mixture was quenched by phase separation and the dried organic phase was purified by chromatography on Sephadex LH-20 eluting with $CHCl_3$. Neolignan (±)-**134** was obtained as yellow oil (0.0125 g, 17 %). ESI-MS: *m/z* = 743 $[M-H]^-$, $C_{40}H_{43}N_2O_{12}$. NMR data are collected in Table 12.

*5.5.1.10. (±)5-((E)-2-((4-methylbenzylcarbamoyl)vinyl)-N-(4-methylbenzyl)-2,3-dihydro-7-methoxy-2-(4-hydroxy-3-methoxyphenyl)benzofuran-3-carboxamide [(±)-**135**]*

Amide **101** (122.6 mg, 0.41 mmol) was dissolved in 60 mL of EtOAc. The organic phase was stirred with the enzyme solution (118.2 mg of TvL in 60 mL of acetate buffer) at room temperature for 4 h. The aqueous solution, after separation from the organic phase, was extracted with EtOAc (2 X 25 mL) and the total organic phase was finally washed with water. The dried EtOAc solution was filtrated and evaporated under vaccum. By silica gel column on the crude mixture, eluting in a gradient of EtOAc in EP (from 35 to 75%) the neolignanamide (±)-**135** was recovered (19.3 mg, yield: 16 %) as yellow amorphous powder. R_f (TLC) = 0.46 (93:7 CH_2Cl_2:MeOH). ESI-MS: *m/z* = 591.3 $[M-H]^-$, $C_{36}H_{35}N_2O_6$. NMR data are collected in Table 12.

5.5.1.11. Measurements of the capacity factor (K)

The measurements of the capacity factor were performed using Luna-C18 column (5 µm; 4.6 × 250 mm; Phenomenex) and a gradient of H_2O/H^+ (99/1; A) – CH_3CN/H^+ (99/1; B) at 1 mL/min with the following elutin profile: $t_{0\ min}$ B = 20 %, $t_{30\ min}$ B = 80 %. The capacity factor K was calculated using the following expression:

$$K = (t_R - t_0)/t_0$$

where t_R is the retention time of the tested substance, and t_0 is retention time of ascorbic acid (**AA**) used as standard.

Calculated log P values were obtained with ACD/labs log P program version 11.

*5.5.1.12. Chiral resolution of racemic mixtures (±)-**130** and (±)-**135***

Enantiomeric resolution was tentatively carried out on three different analytical chiral columns (250 x 4.6 mm; 5 μm) and with many solvent systems in order to find the best resolution conditions (Rs >1).

- The Chiralpack IA column was eluted with: *n*-hexane: IPA 70:30, *n*-hexane: IPA 75:25, CH_3CN: EtOH 80:20, CH_3CN: EtOH 90:10;
- Lux Cellulose-1 column was eluted with: *n*-hexane: IPA 80: 20, *n*-hexane: IPA $t_{0\ min \rightarrow 7\ min}$ 80:20, $t_{7\ min \rightarrow 15\ min}$ 75:25, CH_3CN: IPA 90:10, CH_3CN: IPA 80: 20, CH_3CN: IPA 70: 30, *n*-hexane: EtOH 55:45;
- Lux Cellulose-2 column was eluted with: CH_3CN:EtOH 80:20, CH_3CN:EtOH 90:10, *n*-hexane:EtOH 45:55, *n*-hexane:EtOH 35:65, *n*-hexane:EtOH 30:70.

All the eluitions were run at 0.5 mL/min, and the best condition for the elution of both the racemic mixture were obtained on Lux Cellulose-2 employing *n*-hexane:EtOH as eluent.

130-A = (**2*S***,**3*S***)-**130**: t_R = 8.09 min (Lux Cellulose-2, *n*-hexane:EtOH 35:65, 0.5 mL/min); $[\alpha]_D^{20}$ = +108.3 (*c* = 0.11, CH_3OH); CD (*c* = 3.6 x 10^{-5} M, MeOH) nm (Δε): 276 (+5.25).

130-B = (**2*R***,**3*R***)-**130**: t_R = 11.42 min (Lux Cellulose-2, *n*-hexane:EtOH 35:65, 0.5 mL/min); $[\alpha]_D^{20}$ = -105.0 (*c* = 0.12, CH_3OH); CD (*c* = 3.6 x 10^{-5} M, MeOH) nm (Δε): 276 (-5.88).

135-A = (**2*S***,**3*S***)-**135**: t_R = 11.59 min (Lux Cellulose-2, *n*-hexane:EtOH 30:70, 0.5 mL/min); $[\alpha]_D^{20}$ = + 117.8 (*c* = 0.10, CH_3OH); CD (*c* = 2.2 x 10^{-5} M, MeOH) nm (Δε): 250 (+2.36), 310 (+2.32).

135-B = (**2*R***,**3*R***)-**135**: t_R = 13.63 min (Lux Cellulose-2, *n*-hexane:EtOH 30:70, 0.5 mL/min); $[\alpha]_D^{20}$ = - 114.6 (*c* = 0.12, CH_3OH); CD (*c* = 2.2 x 10^{-5} M, MeOH) nm (Δε): 250 (-3.69), 310 (-2.96).

5.5.2. Synthesis of benzo[*k,l*]xanthene lignans

*5.5.2.1.diphenethyl 6,9,10-trihydroxybenzo[k,l]xanthene-1,2-dicarboxylate (**67**)*

CAPE (**7**; 157.3 mg, 0.55 mmol) was added to a suspension of $Mn(OAc)_3$ (442.2 mg, 1.65 mmol, in 48 mL of CH_2Cl_2). The mixture was stirred at room temperature for 6 h and then it was treated with ascorbic acid saturated solution (in MeOH). The crude organic residue was purified on silica Diol with a gradient of MeOH in CH_2Cl_2 (from 0 to 5%) furnishing 117.5 mg of **67** (yield: 76%). NMR and MS data were in agreement with those previously reported.[100]

*5.5.2.2. bis(4-hydroxybutyl)6,9,10-trihydroxybenzo[k,l]xanthene-1,2-dicarboxylate (**137**)*

The oxidant agent $Mn(OAc)_3$ (2.4665 g, 9.2 mmol) was suspended in CH_2Cl_2 (260 mL) and it was stirred. A solution of **136** (518.3 mg, 2.06 mmol) was added to the suspension and the mixture was heated at reflux for 3 h. The reaction was quenched by addition of ascorbic acid saturated solution (100 mL) and it was extracted with CH_2Cl_2 (6 x 50 mL). The combined organic layer was dried over Na_2SO_4, filtered and took to dry. The crude mixture was purified by flash chromatography on Silica Diol with a gradient of EtOH in CH_2Cl_2 (from 5 to 15%). Compound **137** (235.8 mg) was recovered with 46% yield as yellow oil: R_f (TLC): 0.57 (82:18 CH_2Cl_2:EtOH). ESI-MS: m/z = 497.3 $[M-H]^-$, $C_{26}H_{26}O_{10}$. The NMR data are reported in Table 16.

*5.5.2.3. diethyl 6,9,10-trihydroxybenzo[k,l]xanthene-1,2-dicarboxylate (**138**)*

Ethyl caffeate (**138a**, 175.2 mg, 0.84 mmol) was added to a suspension of $Mn(OAc)_3$ (223.8 mg, 0.84 mmol in 74 mL of $CHCl_3$) and the mixture was stirred at rt for 10 h. The mixture was treated with a saturated solution of ascorbic acid in methanol and after filtration, the solvent was removed *in vacuo*. The organic residue was purified by PLC on silica Diol with a gradient of MeOH in CH_2Cl_2 (from 0 to 5%) and 249 mg of pure benzo[*k,l*]xanthene **138** were recovered (yield: 54%). The acquired NMR and MS data are in agreement with those reported in literature.[103]

*5.5.2.4. dibutyl 6,9,10-trihydroxybenzo[k,l]xanthene-1,2-dicarboxylate (**139**)*

To a stirred suspension of $Mn(OAc)_3$ (229.3 mg, 0.86 mmol in 75.8 mL of $CHCl_3$) butyl caffeate (**139a**, 203.5 mg, 0.86 mmol) was added. The mixture was stirred at room temperature for 7 h and the was treated with a saturated solution of ascorbic acid in MeOH. After filtration, the solvent was removed under reduced pressure and the crude residue was purified by flash chromatography on silica Diol with a gradient of MeOH in CH_2Cl_2 (from 0 to 6%) and benzo[*k,l*]xanthene **139** (100.2 mg) was recovered with 50% yield. NMR and MS data were in agreement with those reported in literature.[103]

5.5.3. Synthesis of deuterated enterolactone

*5.5.3.1. 3-(benzyloxy)benzaldehyde (**141**)*

The aldehyde **140** (2.0051 g; 16.4 mmol) was dissolved in 28 mL of absolute EtOH and the solution was stirred with anhydrous K_2CO_3 (3.2998 g; 23.0 mmol) and with KI

(3.6409 g; 23.9 mmol) for 15 min. Benzyl alcohol (2.7 mL; 21.9 mmol) was added and the mixture was refluxed. The course of the reaction was followed by TLC (85:15 PE:EtOAC) and at 4 h the crude mixture was filtered out to remove the K_2CO_3 and the KI and the filtrate was evaporated until dry. The crude mixture was solved with CH_2Cl_2 (70 mL) and this organic phase was washed with water (2 x 35 mL); the organic layer was dried over anhydrous Na_2SO_4 and evaporated to dry (crude mixture 4.4962 g). The mixture was purified by flash chromatography on Silica gel with a gradient of EtOAc in PE (from 1 to 15 %) and 2.9883 g of pure compound were obtained (yield: 87 %).
White powder. R_f (TLC): 0.62 (85:15 PE:EtOAc). The ^1H and ^{13}C NMR spectra signals were in agreement with that reported in literature.[164]

*5.5.3.2. (E)-dimethyl 2-(3-benzyloxybenzylidene) succinate (**143**)*

Succinic acid dimethyl ester **142** (1.0 mL, 7.6 mmol) and the intermediate **141**(1.6219 g, 7.6 mmol) were added to a solution of EtONa (4.5 mL of 21% w in EtOH solution; 15.2 mmol) in dry EtOH (11.2 mL). After heating under reflux for 4 h, ethanol was removed. The residue was cooled and acidified with 1 N HCl solution (40 mL). The mixture was extracted with EtOAc (3 x 30 mL). The combined organic layer was then washed with a saturated solution of $NaHCO_3$ (2 x 20 mL) and to follow with water (30 mL).The EtOAc layer was dried over anhydrous Na_2SO_4 and concentrated *in vacuo*. This residue was dilute with MeOH (18.4 mL), concentrated H_2SO_4 (0.3 mL) was added and the mixture was heated at reflux for 12 h. The reaction mixture was concentrated *in vacuo* and extracted with EtOAc (50 mL) and with a saturated solution of $NaHCO_3$ (2 x 30 mL). Finally the organic phase was washed with water (40 mL) and it was dried over Na_2SO_4 and took to dry. Flash column chromatography of the residue afforded compound **143** (1.8605 g, 72%). Yellow oil. EI-MS: m/z = 340 $[M]^{+\bullet}$, $C_{20}H_{20}O_5$; NMR data are collected in Table 18.

*5.5.3.3. [7-^{2}H]-3-(benzyloxy)benzyl alcohol (**144**)*

Protected aldehyde **141** (217.3 mg, 1.02 mmol) was dissolved in dry Et_2O (4.2 mL) and $LiAlD_4$ (61.5 mg, 1.46 mmol) was added portion wise cooling the mixture with an ice bath. The reaction was stirred at room temperature for 20 min and the course of reaction was monitored by TLC (80:20 PE: EtOAc). The mixture was diluted with 20 mL of Et_2O and it was extracted with 1 N HCl solution (3 x 20 mL). The combined organic layer was washed with water (30 mL), dried over anhydrous Na_2SO_4 and evaporated until dry. After work-up 208.6 mg of **144** were obtained (yield: 96 %). White powder R_f (TLC): 0.20 (80: 20 PE:

EtOAc). EI-MS: *m/z* = 215 $[M]^{+\bullet}$, HR-MS: *m/z* = 215.1050 (100%); $C_{14}H_{13}{}^{2}HO_2$. ^{1}H NMR (300 MHz, $CDCl_3$) δ: 7.44 – 7.20 (7 H; H-2′/6′, H-3′/5′, H-4′ of benzyloxy and H-5), 7.00 (m; 1 H; H-2), 6.94 (d; *J* = 7.6 Hz; 1 H; H-4), 6.90 (dd; *J* = 8.2, 2.6 Hz; 1 H; H-6), 5.06 (s; 2 H; H-7′), 4.62 (bs; 1 H; H-7) ppm. ^{13}C NMR (75 MHz, $CDCl_3$) δ: 159.1 (C-3), 142.7 (C-1), 137.1 (C-1′), 129.6 (C-4′), 128.6 (C-3′, C-5′), 128.0 (C-5), 127.6 (C-2′, C-6′), 119.5 (C-6), 114.1 (C-4), 113.3 (C-2), 70.0 (C-7′), 64.6 (t, C-7) ppm.

*5.5.3.4. [7-^{2}H]-3-(benzyloxy)benzyl bromide (**145**)*

The alcohol **144** (195.3 mg, 0.71 mmol) was dissolved in 2.5 mL of dry benzene under Ar atmosphere. The PBr_3 (0.3 mL, 2.84 mmol) was infused in the flask and the mixture was stirred at room temperature under Ar atmosphere. The reaction was followed by TLC (75:25 PE:EtOAc) and at 2 h it was stopped. The crude mixture was carefully diluted in a with a saturated solution of Na_2CO_3 (15 mL) and then it was extracted with EtOAc (3 x 30 mL). The combined organic layer was washed with water (40 mL), dried over anhydrous Na_2SO_4 and evaporated until dry. White solid: 157.4mg (yield: 80 %). R_f: (TLC): 0.78 (75:25 PE:EtOAc). EI-MS: *m/z* = 277, 279 $[M]^{+\bullet}$, HR-MS: *m/z* = 277.0212 (50.2%) $C_{14}H_{12}{}^{2}H^{79}BrO$, 279.0199 *m/z* (49.8%) $C_{14}H_{12}{}^{2}H^{81}BrO$. H^{1} NMR (300 MHz, $CDCl_3$) δ: 7.45 – 7.23 (7 H; H-2′/6′, H-3′/5′, H-4′ of benzyloxy and H-5), 7.02 (m; 1 H; H-2), 6.99 (d; *J* = 7.9 Hz; 1 H; H-4), 6.91 (dd; *J* = 8.2, 2.5 Hz; 1 H; H-6), 5.07 (s; 2 H; H-7′), 4.45 (bs; 1 H; H-7) ppm. ^{13}H NMR (75 MHz, $CDCl_3$) δ: 159.2 (C-3), 139.3 (C-1), 137.0 (C-1′), 130.0 (C-4′), 128.8 (C-3′, C-5′), 128.3 (C-5), 127.8 (C-2′, C-6′), 121.8 (C-6), 115.7 (C-4), 115.2 (C-2), 70.3 (C-7′), 33.4 (t, C-7) ppm.

*5.5.3.5. (E)-Dimethyl2-(3',benzyloxybenzylidene)-3-([7''-2H]-3''benzyloxybenzyl) succinate (**146**)*

Lithium diisopropyl amide (LDA) was prepared *in situ* as follow. Freshly distilled diisopropylamine (0.06 mL, 0.42 mmol) was diluted in dry DMF (0.9 mL). The solution was cooled at – 78 °C and *n*-Butyl lithium solution (1.38 M in *n*-hexane; 0.29 mL) was added drop wise. The mixture was stirred for 15 minutes at – 78 °C.

A solution of compound **143** (110.9 mg, 0.35 mmol, in 0.5 mL of dry THF) was added and the mixture was stirred for 20 minutes. Finally a solution of **145** (98.0 mg, 0.35 mmol, 0.3 mL of dry THF) was added. The reaction was monitored on TLC (90:10 PE: EtOAc) and at 24 h it was quenched with NH_4Cl saturated solution (40 mL). The crude mixture was extracted with EtOAc (3 x 30 mL) and the combined organic phase was washed with water until

neutrality, dried over anhydrous Na_2SO_4, and concentrated *in vacuo*. Flash chromatography on Silica gel, eluted in a gradient of EtOAc in PE (from 7 to 20 %) gave 65.8 mg of **146** (Yield: 35 %). Colorless oil. R_f (TLC): 0.22 (90:10 PE: EtOAc). EI-MS: m/z = 537 $[M]^{+\bullet}$, 506, 446, 354. NMR data are reported in Table 18.

LIST OF PUBLICATIONS

Shermain Yali Ng, Nunzio Cardullo, Samuel Chao Ming Yeo, Carmela Spatafora, Corrado Tringali, Pei-Shi Ong, Hai-Shu Lin. Quantification of resveratrol analogs trans-2,3-dimethoxystilbene and trans-3,4-dimethoxystilbene in rat plasma: application to pre-clinical pharmacokinetic study. *Molecules 19*, 9577-9590, (**2014**).

Rosa Chillemi, Nunzio Cardullo, Valentina Greco, Giuseppe Malfa, Barbara Tomasello, Sebastiano Sciuto. Synthesis of amphiphilic resveratrol lipoconjugates and evaluation of their anticancer activity towards neuroblastoma SH-SY5Y cell line. *European Journal of Medicinal Chemistry 96*, 467 – 481, (**2015**).

Nunzio Cardullo, Carmela Spatafora, Nicolò musso, Vincenza Barresi, Daniele Condorelli, Corrado Tringali. Resveratrol-Related Polymethoxystilbene Glycosides: Synthesis, Antiproliferative Activity and Glycosidase Inhibition.. *Journal of Natural Products 78*(11), 2675 - 2683, (**2015**).

LIST OF COMUNICATIONS

Nunzio Cardullo, Valentina Greco, Cristina Satriano, Sebastiano Sciuto, Corrado Tringali. "Synthesis and biological properties of phosphatidyl conjugates of *trans*-resveratrol". VIII Convegno Congiunto delle Sezioni Calabria e Sicilia, Arcavacata di Rende, December 6-7th 2012. Oral.
Nunzio Cardullo, Carmela Spatafora, Nicolò Musso, Vincenza Barresi, Daniele Condorelli, Corrado Tringali. "Synthesis and antiproliferative activity of glycoconjugates of resveratrol-related stilbenoid". Convegno Congiunto delle Sezioni Calabria e Sicilia, Catania, December 2-3th 2013. Oral.
Nunzio Cardullo, Luana Pulvirenti, Carmela Spatafora, Corrado Tringali. "Lignans and neolignans of ferulic acid amides : enzymes mediated biomimetic synthesis". Convegno Congiunto delle Sezioni Calabria e Sicilia, Catania, December 2-3th 2013. Poster.
Nunzio Cardullo, Carmela Spatafora, Nicolò Musso, Vincenza Barresi, Daniele Condorelli, Corrado Tringali. "Glicoconiugati di analoghi del resveratrolo: sintesi, attività antiproliferativa e inibizione di glicosidasi". XXV Convegno Nazionale della Società Chimica Italiana, Arcavacata di Rende, September 5-12th 2014. Poster.
Nunzio Cardullo, Luana Pulvirenti, Carmela Spatafora, Corrado Tringali. "Sintesi biomimetica di neolignanammidi mediata da laccasi". XXV Convegno Nazionale della Società Chimica Italiana, Arcavacata di Rende, September 5-12th 2014. Poster.
Nunzio Cardullo, Luana Pulvirenti, Nicolò Musso, Carmela Spatafora, Vincenza Barresi, Daniele Condorelli, Corrado Tringali. "Biomimetic synthesis and biological evaluation of new natural-related neolignanamides". International Summer School on Natural Products "Luigi Minale" and "Ernesto Fattorusso". Naples, Italy, July 6 – 10th 2015. Oral.
Nunzio Cardullo, **Luana Pulvirenti**, Simone Di Micco, Carmela Spatafora, Corrado Tringali, Oliver Werz, Raffaele Riccio, Giuseppe Bifulco. "Nature-derived phenolic amides as potential inhibitors of mPGES-1". International Summer School on Natural Products "Luigi Minale" and "Ernesto Fattorusso". Naples, Italy, July 6 – 10th 2015. Poster.
Nunzio Cardullo, **Vera Muccilli**, Carmela Spatafora, Vincenzo Cunsolo, Corrado Tringali. "Extraction, fractionation and HPLC-MS-MS analysis of the main antioxidative constituents from an oak wood (Quercus robur) commercial tannin". XXXVI Convegno Nazionale della Divisione di Chimica Organica, Bologna, September 13 – 17th 2015. Poster.
Nunzio Cardullo, Luana Pulvirenti, Nicolò Musso, Carmela Spatafora, Vincenza barresi, Daniele Condorelli, Corrado Tringali. "Bioinspired neolignans: chemo-enzymatic synthesis and antiproliferative activity". Convegno Nazionale della Divisione di Chimica dei Sistemi Biologici, Siracusa, September 24 – 25th 2015. Oral.
N.Cardullo, **A. Cunsolo**, A. M. Santoro, A. D'Urso, M. Stefanelli, M. Gobbo, R. Paolesse, T.Torres, D.A. Cristaldi, C Spatafora, C Tringali, R. Purrello, D. Milardi. "Porphyrinoids and polyphenols: pluripotent scaffolds for the design of novel proteasome inhibitors". Convegno Nazionale della Divisione di Chimica dei Sistemi Biologici, Bologna, September 24 – 25th 2015. Poster.

6. REFERENCES

[1] Tringali, C. (**2001**) From *Bioactive Compounds from Natural Sources*. First Edition: C. Tringali Ed., Taylor & Francis, London and New York.

[2] Newman, D. J. (**2008**) Natural Products as Leads to Potential Drugs: An Old Process or the New Hope for Drug Discovery? *Journal of Medicinal Chemistry 51*, 2589 – 2599.

[3] Haslam, E. (**1998**). *Practical Polyphenolics: From Structure to Molecular Recognition and Fisiological Action*. Cambridge.

[4] Ayers D. C. and J. D. Loike. (**1990**). *Lignans. Chemical, biological and clinical properties*. Cambridge

[5] Walle, T. (**2007**). Methoxylated flavones, a superior cancer chemopreventive flavonoid subclass? *Seminars in Cancer Biology 17*, 354 – 362.

[6] Ramos, S. (**2008**). Cancer chemoprevention and chemotherapy: Dietary polyphenols and signalling pathways. *Molecular Nutrition & Food Research 52*, 507 – 526.

[7] Boudet, A.-M. (**2007**). Evolution and current status of research in phenolic compounds. *Phytochemistry 68*, 2722 – 2735.

[8] Quideau, S.; Deffieux, D.; Douat-Casassus, C.; Pouységu, L. (**2011**). Plant polyphenols: chemical properties, biological activities, and synthesis. *Angewandte Chemie International Edition*, *50*, 586 – 621.

[9] Surh, Y. J. (**2003**). Cancer chemoprevention with dietary phytochemicals. *Nature Reviews Cancer 3*, 768 – 780.

[10] Nichenametla, S. N.; Taruscio, T. G.; Barney D. L.; Exon J. H. (**2006**). A review of the effects and mechanisms of polyphenolics in cancer. *Critical Reviews in Food Science and Nutrition 46*, 161 – 183.

[11] Aggarwal, B. B.; Shishodia, S. (**2006**). Molecular targets of dietary agents for prevention and therapy of cancer. *Biochemical Pharmacol*ogy *71*, 1397 – 1421.

[12] Le Marchand, L. Murphy, S. P. ; Hankin, J. H. ; Wilkens, L. R.; Kolonel, L. N. (**2000**). Intake of flavonoids and lung cancer. *Journal of the National Cancer Institute 92*, 154 – 160.

[13] Thomasset, S. C.; Berry, D. P.; Garcea, G.; Marczylo, T.; Steward, W. P.; Gescher. A. J. (**2006**). Dietary polyphenolic phytochemicals - promising cancer chemopreventive agents in humans? A review of their clinical properties. *International Journal of Cancer 120*, 451 – 458.

[14] Pezzuto, J.M. (**2008**), Resveratrol as an Inhibitor of Carcinogenesis. *Pharmaceutical Biology 46*, 443 – 573.

[15] Renaud, S.C.; De Lorgeril, M. (**1992**). Wine, alcohol, platelets, and the French paradox for coronary heart disease. *Lancet*, *339*, 1523 – 1526.

[16] Shanafelt, T. D.; Lee, Y. K.; Call, T. G. (**2006**). Clinical effects of oral green tea extracts in four patients with low grade B cell malignancies. *Leukemia Research 30*, 707 – 712

[17] Chen L.; Zhang H. Y. (**2007**). Cancer Preventive Mechanisms of the Green Tea Polyphenol (-)-Epigallocatechin-3-gallate. *Molecules 12*, 946-957

[18] Maheshwari, R. K.; Singh, A. K.; Gaddipati, J.; Srimal, R. C. (**2006**). Multiple biological activities of curcumin: A short review. *Life Sciences 78*, 2081–2087.

[19] Murtaza, G.; Karim, S.; Akram, M. R.; Khan, S. A.; Azhar, S.; Mumtaz, A.; Asad, M. H. H. B. (**2014**). Caffeic acid phenethyl ester and therapeutic potentials. *Biomed Research International 2014*.

[20] Walle T. (**2011**). *Bioavailability of resveratrol. Annals of the New York Academy of Science* 1215, 9 – 15.

[21] Yang, C.S.; Sang, S.; Lambert, J.D.; Lee, M.J. (**2008**). Bioavailability issues in studying the health effects of plant polyphenolic compounds. *Molecular Nutrition & Food Research* 52, S139 – S151.

[22] Chillemi, R.; Sciuto, S.; Spatafora, C.; Tringali, C. (**2007**). Anti-tumor properties of stilbene-based resveratrol analogues: recent results. *Natural Product Communications 2*, 499 – 513.

[23] Spatafora, C.; Tringali, C. (**2012**) From Natural Polyphenols to Synthetic Antitumor Agents in: *Bioactive Compounds from Natural Sources*, Natural Products as Lead Compounds in Drug Discovery, 299 – 338. Second Edition: C. Tringali Ed., CRC Press-Taylor & Francis, Boca Raton

[24] Spatafora, C.; Tringali, C. (**2012**) Natural-derived Polyphenols as Potential Anticancer Agents. *Anti-Cancer Agents in Medicinal Chemistry 12*, 902 – 918.

[25] Pettit, G. R.; Singh, S. B.; Hamel, E.; Lin, C. M.; Alberts, D. S.; Garcia, K. D. (**1989**). *Experientia 45*, 209 – 211.

[26] Tron, G. C.; Pirali, T.; Sorba, G.; Pagliai, F.; Busacca, S.; Genazzani, A. A. (**2006**). Medicinal chemistry of combretastatin A4: Present and future directions. *Journa of Medicinal Chemistry 49*, 3033 – 3044.

[27] Kingston D. G. I. (**2009**). Tubulin interactive natural products as anticancer agents. *Journal of Natural Products 72*, 507 – 515.

[28] Tozer, G. M.; Kanthou, C.; Parkins, C. M.; Hill S. A. (***2002)***. The biology of combretastatins as tumour vascular targeting agents. *International Journal of Experimental Pathology 83*, 21 – 38.

[29] Cai, Y.-C.; Zou, Y.; Ye, Y-L.; Sun, H.-Y.; Su, Q.-G.; Wang Z.-X.; Zeng Z.-L.; Xian L.-J. (**2011**). Anti-tumor activity and mechanisms of a novel vascular disrupting agent, (*Z*)-3,4′,5-trimethoxylstilbene-3′-*O*-phosphate disodium (M410). *Investigational New Drugs 29*, 300 – 311.

[30] Mazué, F.; Colin, D.; Gobbo, J.; Wegner, M.; Rescifina, A.; Spatafora, C., Fasseur, D.; Delmas, D.; Meunier, P.; Tringali, C.; Latruffe, N. (**2010**). Structural determinants of resveratrol for cell proliferation inhibition potency: experimental and docking studies of new analogs. *European Journal of Medicinal Chemistry 45*, 2972 – 2980.

[31] Senger, D. R.; Davis, G. E. *(***2011**). Angiogenesis*. Cold Spring Harbor Perspectives in* Biology *3*(8)*,* a005090.

[32] Albini A.; Tosetti, F.; Li, V. W.; Noonan, D. M.; Li, W. W. *(***2012**). Cancer prevention by targeting angiogenesis*. Nature Reviews Clinical Oncology 9*, 498 – 509.

[33] Huang, X.-F.; Ruan, B.-F.; Wang, X.-T.; Xu, C.; Ge, H.-M.; Zhu, H.-L.; Tan, V. (**2007**). Synthesis and cytotoxic evaluation of a series of resveratrol derivatives modified in C2 position. *European Journal of Medicinal Chemistry 42*, 263 – 267.

[34] Basini, G.; Tringali, C.; Baioni, L.; Bussolati, S.; Spatafora, C.; Grasselli, F. (**2010**). Biological effects on granulosa cells of hydroxylated and methylated resveratrol analogues. *Molecular Nutrition & Food Research 54*, 236 – 243

[35] Spatafora C.; Basini G.; Baioni L.; Grasselli F.; Sofia A.; Tringali, C. (**2009**). ‚Antiangiogenic resveratrol analogues by mild *m*-CPBA aromatic hydroxylation of 3,5-dimethoxystilbenes. *Natural Product Communications 4*, 239 – 246.

[36] Sale, S.; Verschoyle, R. D.; Boocock, D.; Jones, D. J.; Wilsher, N.; Ruparelia K. C.; Potter G. A.; Farmer, P. B.; Steward, W. P.; Gescher, A. J. (**2004**). Pharmacokinetics in mice and growth-inhibitory properties of the putative cancer chemopreventive agent resveratrol and the synthetic analogue *trans*-3,4,5,4′-tetramethoxystilbene. *British Journal Cancer 90*, 736 – 744.

[37] Saiko, P.; Pemberger, M.; Horvath, Z.; Savinc, I.; Grusch, M.; Handler, N.; Erker, T.; Jaeger, W.; Fritzer-Szekeres, M.; Szekeres, T. (**2008**). Novel resveratrol analogs induce apoptosis and cause cell cycle arrestin HT29 human colon cancer cells: inhibition of ribonucleotide reductase activity. *Oncology Reports 19*, 1621 – 1626.

[38] Ferreira, M.-J. U.; Duarte, N.; Gyémánt, N.; Radics, R.; Cherepnev, G.; Varga, A.; Molnar, J. (**2006**). Interaction between doxorubicin and the resistance modifier stilbene on multidrug resistant mouse lymphoma and human breast cancer cells. *Anticancer Research 26*, 3541 – 3546.

[39] Valdameri, G.; Pereira, L. R.; Spatafora, C.; Guitton, J.; Gauthier, C.; Arnaud, O.; Pereira, Ferreira, A.; Falson, P.; Winnischofer, S. M. B.; Rocha, M. E. M.; Tringali, C.; Di Pietro, A. (**2012**) Methoxy stilbenes as potent, specific, untransported, and noncytotoxic inhibitors of breast cancer resistance protein. *ACS Chemical Biology 7*, 322 – 330

[40] Lin, H. S.; Ho, P. C. (**2009**). A rapid HPLC method for the quantification of 3,5,4′-trimethoxy-*trans*-stilbene (TMS) in rat plasma and its application in pharmacokinetic study. *Journal of Pharmaceutical and Biomedical Analysis 49*, 387 – 392.

[41] Lin, H.-S.; Tringali, C.; Spatafora, C.; Choo, Q.-Y.; Ho, P.C. (**2010**). LC determination of *trans*-3,5,3′,4′,5′-pentamethoxystilbene in rat plasma. *Chromatographia 72,* 827 – 832.

[42] Weng C. J.; Yang, Y.T.; Ho, C.T.; Yen, G.C. (**2009**) Mechanisms of apoptotic effects induced by resveratrol, dibenzoylmethane, and their analogues on human lung carcinoma cells. *Journal of Agricultural and Food Chemistry 57*, 5235 – 5243.

[43] Pan, M.-H.; Lin, C.-L.; Tsai, J.-H.; Ho, C.-T.; Chen, W.-J. (**2010**). 3,5,3′,4′,5′-Pentamethoxystilbene (MR-5), a synthetically methoxylated analogue of resveratrol, inhibits growth and induces G1 cell cycle arrest of human breast carcinoma MCF-7 cells. *Journal of Agricultural and Food Chemistry 58*, 226 – 234.

[44] Li, H.; Wu, W. K. K.; Zheng, Z.; Che, C. T.; Yu, L.; Li, Z. J.; Wu, Y. C.; Cheng, K.-W.; Yu, J.; Cho, C. H.; Wang, M. (**2009**). 2,3′,4,4′,5′-Pentamethoxy-*trans*-stilbene, a resveratrol derivative, is a potent inducer of apoptosis in colon cancer cells via targeting microtubules. *Biochemical Pharmacology 78*, 1224 – 1232.

[45] Li, H.; Wu, W.K. K.; Li, Z. J.; Chan, K. M.; Wong, C. C. M.; Ye, C. G.; Yu, L.; Sung, J.J. Y.; Cho, C. H.; Wang, M. (**2010**). 2,3′,4,4′,5′-Pentamethoxy-*trans*-stilbene, a resveratrol derivative, inhibits colitis-associated colorectal carcinogenesis in mice. *British Journal of Pharmacology 160*, 1352 – 1361.

[46] Lee, J.; Kim, S. J.; Choi, H.; Kim, Y. H.; Lim, I. T.; Yang, H.-M.;. Lee, C. S.; Kang, H. R.; Ahn, S. K.; Moon, S. K.; Kim, D.-H.;. Lee, S, Choi, N. S.; Lee, K. J. (**2010**). Identification of CKD-516: A Potent Tubulin Polymerization Inhibitor with Marked Antitumor Activity against Murine and Human Solid Tumors. *Journal of Medicinal. Chemistry* 53, 6337 – 6354.

[47] Wu, J.; Lu, Y.; Lee, A.; Pan, X.; Yang, X.; Zhao, X.; Lee, R. J. (**2007**). Reversal of multidrug resistance by transferrin-conjugated liposomes co-encapsulating doxorubicin and verapamil. *Journal of Pharmacy & Pharmaceutical Sciences 10*, 350 – 357.

[48] Calvaresi, E. C.; Hergenrother, P. J. (**2013**). Glucose conjugation for the specific targeting and treatment of cancer. *Chemical Science 4*, 2319 – 2333.

[49] Carvalho, K. C.; Cunha, I. W.; Rocha,R. M.; Ayala, F. R.; Cajaìba, M. M.; Begnami, M. D.; Vilela, R. S.; Paiva, G. R.; Andrade,R. G.; Soares, F. A. (**2011**). GLUT1 expression in malignant tumors and its use as an immunodiagnostic marker. *Clinical Science 66*, 965 – 972.

[50] Rabinovich, G. A. (**2005**). Galectin-1 as a potential cancer target. *British Journal of Cancer 92*, 1188 – 1192.

[51] Young, C.D.; Anderson, S. M. (**2008**) Sugar and fat-that's where it's at: metabolic changes in tumors. *Breast Cancer Research* 10, 202 – 210.

[52] Ganapathy-Kanniappan, S.; Geschwind, J. F. H. (**2013**). Tumor glycolysis as a target for cancer therapy: progress and prospects. *Molecular Cancer 12*, 152 – 163.

[53] Aggarwal, B. B.; Sundaram, C.; Malani, N.; Ichikawa, H. (**2007**). *Curcumin: the Indian solid gold*. *Advances* in *Experimental Medicine* and *Biology 595*, 1 – 75.

[54] Arafa, H. M. M. (**2010**) Possible contribution of β-glycosidases and caspases in the cytotoxicity of novel glycoconjugates in colon cancer cells. *Invest New Drugs 28*, 306 – 317.

[55] Dembitsky, V. M. (**2005**). Astonishing Diversity of Natural Surfactants: 5. Biologically Active Glycosides of Aromatic Metabolites. *Lipids 40*, 869 – 900.

[56] Kimura, Y.; Okuda, H. (**2000**). Effects of Naturally Occurring Stilbene Glucosides from Medicinal Plants and Wine, on Tumor Growth and Lung Metastasis in Lewis Lung Carcinoma- Bearing Mice. *Journal of Pharmacy and Pharmacology 52*, 1287 – 1295.

[57] Sharma, P. (**2011***).* Cinnamic acid derivatives: A new chapter of various pharmacological activities. *Journal of Chemical and Pharmaceutical Research 3,* 403 –423.

[58] Nam, N. H.; You, Y. J.; Kim, Y. D.; Hong, H.; Kim, H. M.; Ann, Y. Z. (**2001**). Syntheses of certain 3-aryl-2-propenoates and evaluation of their cytotoxicity. *Bioorganic Medicinal Chemistry Letters* 11, 1173-1176.

[59] Mori, H.; Kawabata, K.; Matsunaga, K.; Ushida, J.; Fujii, K.; Hara, A.; Tanaka, T.; Murai, H. (**2000**). Chemopreventive effects of coffee bean and rice constituents on colorectal carcinogenesis. *Biofactors 12*, 101 – 105.

[60] Jin, U. H.; Lee, J. Y.; Kang, S. K.; Kim, J. K.; Park, W. H.; Kim, J. G.; Moon, S. K.; Kim, C. H. (**2005**). A phenolic compound, 5-caffeoylquinic acid (chlorogenic acid), is a new type and strong matrix metalloproteinase-9 inhibitor: isolation and identification from methanol extract of *Euonymus alatus*. *Life Science 77*, 2760 – 2769.

[61] Lee, Y. L.; Liao, P. H.; Chen, W. K.; Yang, C. C. (**2000**). Preferential cytotoxicity of caffeic acid phenethyl ester analogues on oral cancer cells. *Cancer Letters 153*, 51 – 56.

[62] Cellia, N.; Mariani, B.; Dragani, L. K.; Murzilli, S.; Rossi, C.; Rotili, D.; (**2004**). Development and validation of a liquid chromatographic – tandem mass spectrometric method for the determination of caffeic acid phenethyl ester in rat plasma and urine; *Journal of Chromatography B 810*, 129 – 136.

[63] Hellberg, M. R.; Graff, G.; Gamache, D. A.; Nixon, J. C.; Garner, W. H. (**1998**). Esters and amides of non-steroidal anti-inflammatory carboxylic acids which may be used as anti-oxidants, 5-lipoxygenase inhibitors and non-steroidal anti-inflammatory products. US5811438 A.

[64] Chochkova, M.; Stoykova, B.; Ivanova, G.; Ranz, A.; Guo, X.; Lankmayr, E.; Milkova, T. (**2013**). *N*-Hydroxycinnamoyl amides of fluorinated amino acids: Synthesis, anti-tyrosinase and DPPH scavenging activities. *Journal of Fluorine Chemistry 156*, 203 – 208.

[65] a) Nie, W.; Luo, J.-G.; Wang, X.-B.; Yin, H.; Sun, H.-B.; Yao, H.-Q.; Kong, L.-Y. (**2011**). Synthesis of New a-Glucosidase Inhibitors Based on Oleanolic Acid Incorporating Cinnamic Amides. *Chemical Pharmaceutical Bullettin 59*, 1051—1056. b) Niwa, T.; Doi U.; Osawa, T. (**2003**). Inhibitory Activity of Corn-Derived Bisamide Compounds against α –Glucosidase. *Journal of Agriculture and Food Chemistry 51,* 90 – 94.

[66] Rajan, P.; Vedernikova, I.; Cos, P.; Van den Berghe D.; Augustynsa, K.; Haemersa, A. (**2001**). Synthesis and Evaluation of Caffeic Acid Amides as Antioxidants. *Bioorganic & Medicinal Chemistry Letters 11*, 215 – 217.

[67] Roh, J. S.; Han, J. Y.; Kim, J. H.; Hwang, J. K. (**2004**). Inhibitory Effects of Active Compounds Isolated from Safflower (*Carthamus tinctorius L.*) Seeds for Melanogenesis. *Biological & Pharmaceutical Bulletin 27*, 1976 – 1978.

[68] Cho, S. J., Roh, J. S.; Sun, W. S.; Kim, S. H.; Par,k K. D. (**2006**). *N*-Benzylbenzamides: A new class of potent tyrosinase inhibitors. *Bioorganic & Medicinal Chemistry Letters 16*, 2682 – 2684.

[69] Logan, A.; Weatherhead B. (**1980**) Post-tyrosinase inhibition of melanogenesis by melatonin in hair follicles *in vitro*. *The Journal of Investigative Dermatology 74*, 47 – 50.

[70] Xie, Y.; Huang, B.; Yu, K.; Sh,i F.; Liu, T.; Xu, W. (**2013**). Caffeic acid derivatives: A new type of influenza neuraminidase inhibitors. *Bioorganic & Medicinal Chemistry Letters 23* 3556 – 3560.

[71] Yang, X-H.; Wen, Q.; Zhao, T.-T.; Sun, J.; Li, X.; Xing, M.; Lu, X.; Zhu, H.-L. (**2012**). Synthesis, biological evaluation, and molecular docking studies of cinnamic acyl 1,3,4-thiadiazole amide derivatives as novel antitubulin agents. *Bioorganic & Medicinal Chemistry 20*, 1181 – 1187.

[72] Shi, Z. H.; Li, N. G.; Shi, Q. P.; Tang, H.; Tang, Y. P.; Li, W.; Yin, L.; Yang, J. P.; Duan, J. A. (**2013**). Synthesis and structure–activity relationship analysis of caffeic acid amides as selective matrix metalloproteinase inhibitors; *Bioorganic & Medicinal Chemistry Letters 23*, 1206 – 1211

[73] Ganesh, T.; Jiang, J.; Yang, M.-S.; Dingledine, R. (**2014**). Lead Optimization Studies of Cinnamic Amide EP2 Antagonists. *Journal of Medicinal Chemistry 57*, 4173 – 4184.

[74] Friesen, R. W.; Mancini, J. A. (**2008**). Microsomal Prostaglandin E2 Synthase-1 (mPGES-1): A Novel Anti-Inflammatory Therapeutic Target. *Journal of Medicinal Chemistry 51*, 4059 – 4067.

[75] Arhancet, G. B.; Walke,r D. P.; Metz S.; Fobian, Y. M.; Heasley, S. E.; Carter, J. S.; Springer, J. R.; Jones, D. E.; Hayes, M. J.; Shaffer, A. F.; Jerome, G. M.; Baratta, M. T.; Zweifel, B.; Moore ,W. M.; Masferrer, J. L.; Vazquez, M. L. (**2013**). Discovery and SAR of PF-4693627, a potent, selective and orally bioavailable mPGES-1 inhibitor for the potential treatment of inflammation. *Bioorganic & Medicinal Chemistry Letters 23*, 1114 – 1119.

[76] Shiro, T.; Takahashi, H.; Kakiguchi, K.; Inoue, Y.; Masuda, K.; Nagata, H.; Tobe, M. (**2012**). Synthesis and SAR study of imidazoquinolines as a novel structural class of microsomal prostaglandin E2 synthase-1 inhibitors. *Bioorganic & Medicinal Chemistry Letters 22*, 285 – 288.

[77] Park, S. J.; Han, S. G.; Ahsan, H. M.; Lee, K.; Lee, J. Y.; Shin, J. S.; Lee, K. T.; Kang, N. S.; Yu, Y. G. (**2012**). Identification of novel mPGES-1 inhibitors through screening of a chemical library. *Bioorganic & Medicinal Chemistry Letters 22*, 7335 – 7339.

[78] Apers, S.; Paper, D.; Bürgermeister, J.; Baronikova, S.; Van Dyck, S.; Lemière, G.; Vlietinck, A.; Pieters, L. (**2002**). Antiangiogenic activity of synthetic dihydrobenzofuran lignans. *Journal of Natural Products 65*, 718 – 720.

[79] Ghisalberti, E. L. (**1997**). Cardiovascular activity of naturally occurring lignans. *Phytomedicine 4*, 151 – 166.

[80] Charlton, J. L. (**1998**). Antiviral activity of lignans. *Journal of Natural Products 61,* 1447 – 1451.

[81] Van Miert, S.; Van Dyck, S.; Schmidt, T. J.; Brun, R.; Vlietinck, A.; Lemière, G.; Pieters, L. (**2005**). Antileishmanial activity, cytotoxicity and QSAR analysis of synthetic dihydrobenzofuran lignans and related benzofurans. *Bioorganic & Medicinal Chemistry 13*, 661–669.

[82] Harmatha, J.; Nawrot, J. (**2002**). Insect feeding deterrent activity of lignans and related phenylpropanoids with a methylenedioxyphenyl (piperonyl) structure moiety. *Entomologia Experimentalis et Applicata 104*, 51–60.

[83] Spatafora, C.; Tringali, C. (**2007**). Phenolic oxidative coupling in the biomimetic synthesis of heterocyclic lignans, neolignans and related compounds. In *Targets in Heterocyclic Systems. Chemistry and Properties*. Eds.: Attanasi, O., Spinelli, D. *10,* pp. 284 – 312. Società Chimica Italiana, Roma.

[84] Dewick, P. M. (**2001**). *Medicinal Natural Products*. *A Biosynthetic Approach. 2nd* Edition, John Wiley & Sons, Chichester, UK p. 133.

[85] Davin, L. B.; Lewis, N. G. (**2004**). An historical perspective on lignan biosynthesis: monolignol, allylphenol and hydroxycinnamic acid coupling and downstream metabolism. *Phytochemistry Reviews 2*, 257 − 288.

[86] Davin, L. B.; Wang, H.-B.; Crowell, A. L.; Bedgar, D. L.; Martin, D. M.; Sarkanen, S.; Lewis, N. G. (**1997**). Stereoselective Bimolecular Phenoxy Radical Coupling by an Auxiliary (Dirigent) Protein Without an Active Center. *Science 275*, 362 − 366.

[87] Pickel, B; Schaller, A. (**2013**). Dirigent proteins: molecular characteristics and potential biotechnological applications. *Applied Microbiology and Biotechnology 97*, 8427–8438.

[88] Moss, G. P. (**2000**). Nomenclature of lignans and neolignans (IUPAC Recommendations 2000). *Pure and Applied Chemistry*, *72* , 1493 – 1523.

[89] http://www.chem.qmul.ac.uk/iupac/lignan/

[90] Pieters, L.; De Bruyne, T.; Claeys, M.; Vlietinck, A.; Calomme, M.; Vanden Berghe, D. (**1993**). Isolation of a Dihydrobenzofuran Lignan from South American Dragon's Blood (*Croton* spp.) as an Inhibitor of Cell Proliferation. *Journal of Natural Products 56*, 899 – 906.

[91] Pieters, L.; Van Dyck, S.; Gao, M.; Bai, R.; Hamel, E.; Vlietinck, A.; Lemière, G. (**1999**). Synthesis and Biological Evaluation of Dihydrobenzofuran Lignans and Related Compounds as Potential Antitumor Agents that Inhibit Tubulin Polymerization. *Journal of Medicinal Chemistry 42*, 5475 – 5481.

[92] Bose, J. S.; Gangan, V.; Prakash, R.; Jain, S. K.; Manna, S. K. (**2009**). A Dihydrobenzofuran Lignan Induces Cell Death by Modulating Mitochondrial Pathway and G2/M Cell Cycle Arrest. *Journal of Medicinal Chemistry 52,* 3184 – 3190.

[93] Manna, S. K.; Bose, J. S.; Gangan, V.; Raviprakash, N.; Navaneetha, T.; Raghavendra, P. B.; Babajan,; B., Kuma,r C. S.; Jain, S. K. (**2010**). Novel Derivative of Benzofuran Induces Cell Death Mostly by G2/M Cell Cycle Arrest through p53-dependent Pathway but Partially by Inhibition of NF-κB. *The Journal of Biological Chemistry 285*, 22318 – 22327.

[94] Bose, J. S.; Gangan, V.; (**2008**). Cinnamic acid, vanillic acid and benzofuran compounds as chemotherapeutic agents against inflammation and cancer PTC Int. App. WO 2008062466 A2 20080529

[95] Moujir, L.; Seca, A. M. L.; Silva, A. M. S.; López, M. R.; Padilla, N.; Cavaleiro, J. A. S.; Neto, C. P. (**2007**). Cytotoxic activity of lignans from *Hibiscus cannabinus*. *Fitoterapia 78*, 385 – 387.

[96] Ma, C-Y.; Liu, W. K.; Che, C-T. (**2002**). Lignanamides and Nonalkaloidal Components of *Hyoscyamus niger* Seeds. *Journal of Natural Products 65,* 206-209.

[97] Li, J. X.; Shi, Q.; Xiong, Q. B.; Prasain, J. K.; Tezuka, Y.; Hareyama, T.; Wang, Z. T.; Tanaka, K.; Namba, I.; Kadota, S. (**1998**). Tribulusamide A and B, New Hepatoprotective Lignanamides from the Fruits of Tribulus terrestris: Indicators of Cytoprotective Activity in Murine Hepatocyte Culture. *Planta Medica 64*, 628-631.

[98] Qu, Z-Y.; Zhang, Y-W.; Yao, C-L.; Jin, Y-P.; Zheng, P-H.; Sun, C-H.; Liu, J-X.; Wang, Y-S.; Wang, Y-P. (**2015**). Chemical constituents from *Orobanche cernua* Loefling. *Biochemical Systematics and Ecology 60*, 199-203.

[99] a) Maeda, S.; Masuda, H.; Tokoroyama, T. (**1994**). *Chemical and Pharmaceutical Bulletin 42*, 2506–2513; b) Maeda, S.; Masuda, H.; Tokoroyama, T. (**1995**). *Chemical and Pharmaceutical Bulletin 43*, 935–940.

[100] Daquino, C.; Rescifina, A.; Spatafora, C.; Tringali, C. (**2009**). Biomimetic Synthesis of Natural and "Unnatural" Lignans by Oxidative Coupling of Caffeic Esters. *European Journal Organic Chemistry* 6289 – 6300.

[101] Di Micco, S.; Mazue, F.; Daquino, C.; Spatafora, C.; Delmas, D. Latruffe, N.; Tringali, C.; Riccio, R. Bifulco, G. (**2011**).Structural basis for the potential antitumour activity of DNA-interacting benzo[*kl*]xanthene lignans. *Organic Biomolecular Chemistry* 9, 701– 710.|

[102] Basini, G.; Baioni, L.; Bussolati, S.; Grasselli, F.; Daquino C.; Spatafora, C.; Tringali, C. (**2012**). Antiangiogenic properties of an unusual benzo[*k,l*]xanthenes lignan derived from CAPE (Caffeic Acid Phenethyl Ester). *Investigational New Drugs 30*,186–190

[103] Spatafora, C.; Barresi, V.; Bhusainahalli, V. M.; Di Micco, S.; Musso, N.; Riccio, R.; Bifulco, G.; Condorelli, D.; Tringali, C. (**2014**). Bio-inspired benzo[*k,l*]xanthene lignans: synthesis, DNA-interaction and antiproliferative properties. *Organic & Biomolecular Chemistry 12*, 2686-2701.

[104] Stitch, S. R.; Toumba, J. K.; Groen, M. B.; Funke, C. W.; Leemhuis, J.; Vink, J.; Woods, G. F. (**1980**). Excretion, isolation and structure of a new phenolic constituent of female urine. *Nature 287*, 738 – 740.

[105] Setchell, K. D. R.; Lawson, A. M.; Mitchell, F. L.; Adlercreutz, H.; Kirk, D. N.; Axelson, M. (**1980**). Lignans in man and animal species. *Nature 287*, 740 – 742.

[106] Clavel, T.; Lippman, R.; Gavini, F.; Doré, J.; Blaut, M. (**2007**). *Clostridium saccharogumia* sp. nov. and *Lactonifactor longoviformis* gen. nov., sp. nov., two novel human faecal bacteria involved in the conversion of the dietary phytoestrogen secoisolariciresinol diglucoside. *Systematic and Applied Microbiology 30*, 16 – 26.

[107] Landete, J. M. (**2012**). Plant and mammalian lignans: A review of source, intake, metabolism, intestinal bacteria and health. *Food Research International 46*, 410 – 424.

[108] McCann, M. J.; Rowland, I. R.; Roy, N. C. (**2014**). The Anti-Proliferative Effects of Enterolactone in Prostate Cancer Cells: Evidence for the Role of DNA Licencing Genes, mi-R106b Cluster Expression, and PTEN Dosage *Nutrients 6*, 4839 – 4855.

[109] Carreau, C.; Flouriot, G.; Bennetau-Pelissero C.; Potier M. (**2008**). Enterodiol and enterolactone, two major diet-derived polyphenol metabolites have different impact on ER transcriptional activation in human breast cancer cells. *Journal of Steroid Biochemistry & Molecular Biology 110*, 176 – 185

[110] Leppälä, E.; Pohjoispää, M.; Koskimies, J.; Wähälä, K. (**2008**). Synthesis of new deuterium-labelled lignanolactones. *Labelled Compounds Radiopharmaceuticals 51*, 407 – 412.

[111] Syrjänen, K.; Brunow, G. (**2000**). Regioselectivity in lignin biosynthesis. The influence of dimerization and cross-coupling. *Journal of Chemical Soc*iety, *Perkin Transactions 1*, 183–187.

[112] Adelakun, O. E.; Kudanga, T.; Parker, A.; Green, I. R.; le Roes-Hill, M.; Burton, S. G. (**2012**). Laccase-catalyzed dimerization of ferulic acid amplifies antioxidant activity. *Journal of Molecular Catalysis B: Enzymatic 74*, 29 – 35.

[113] Piontek, K.; Antorini, M.; Choinowski, T. (**2002**). Crystal Structure of a Laccase from the Fungus *Trametes versicolor* at 1.90-Å Resolution Containing a Full Complement of Coppers. *Journal of Biological Chemistry 277,* 37663 – 37669.

[114] Guzik, U.; Hupert-Kocurek, K.; Wojcieszyńska, D. (**2014**). Immobilization as a Strategy for Improving Enzyme Properties Application to Oxidoreductases. *Molecules 19*, 8995 – 9018.

[115] Duràn, N.; Rosa, M. A.; D'Annibale, A.; Gianfreda, L. (**2002**). Applications of laccases and tyrosinases (phenoloxidases) immobilized on different supports: a review. *Enzyme and Microbial Technology 31*, 907–931.

[116] Van de Velde, F.; Van Rantwijk, F.; Sheldon, R. A. (**2001**). Improving the catalytic performance of peroxidases in organic synthesis. *Trends in Biotechnology 19*, 73 – 80.

[117] Saliu, F.; Tolppa, E. L.; Zoia, L.; Orlandi, L. (**2011**). Horseradish peroxidase catalyzed oxidative cross-coupling reactions: the synthesis of 'unnatural' dihydrobenzofuran lignans. *Tetrahedron Letters 52*, 3856–3860.

[118] Mogharabia, M.; Faramarzi,M. A. (**2014**). Laccase and Laccase-Mediated Systems in the Synthesis of Organic Compounds. *Advanced Synthesis & Catalysis 356*, 897 – 927.

[119] Tavares, A. P. M.; Cristóvão, R. O.; Loureiro, J. M.; Boaventura, R. A. R.; Macedo, E. A. (**2009**). Application of statistical experimental methodology to optimize reactive dye decolourization by commercial laccase. *Journal of Hazardous Materials 162*, 1255–1260; b) Cristóvão, R. O.; Tavares A. P. M., Ferreira L. A., Loureiro J. M., Boaventura R. A., Macedo, E. A. (**2009**). Modeling the discoloration of a mixture of reactive textile dyes by commercial laccase. *Bioresource. Technolology 100*, 1094– 1099.

[120] a) Osma, J. F.; Toca-Herrera, J. L.; Rodriguez-Couto, S. (**2010**). Uses of Laccases in the Food Industry. *Enzyme Research,* 1-10. b) Mayer, A. M.; Staples, R. C. (**2002**), Laccase: new functions for an old enzyme. *Phytochemistry 60*, 551 – 565.

[121] Tsukamoto, S.; Yokosawa, H. (**2010**) Inhibition of the ubiquitin-proteasome system by natural products for cancer therapy. *Planta Medica 76*, 1064 – 1074.

[122] a) Ishii, Y.; Waxman, S.; Germain, D. (**2007**). Targeting the ubiquitin-proteasome pathway in cancer therapy. *Anti-Cancer Agents in Medicinal Chemistry* 7, 359 – 365. b) Landis-Piwowar, K. R.; Milacic, V.; Chen, D.; Yang, H.; Zhao, Y.; Chan, T. H.; Yan, B.; Dou, Q. P. (**2006**). The proteasome as a potential target for novel anticancer drugs and chemosensitizers. *Drug Resistance Updates 9*, 263 – 273.

[123] Adams, J. (**2004**). Targeting the ubiquitin-proteasome pathway in cancer therapy. *Cancer Cells 5*, 417 – 421.

[124] Piel, J.; Hui, D.; Wen, G.; Butzke, D.; Platzer, M.; Fusetani, N.; Matsunaga, S. (**2004**). Antitumor polyketide biosynthesis by an uncultivated bacterial symbiont of the marine sponge *Theonella swinhoei*. *Proceedings of the National Academy Science 101*, 16222 – 16227.

[125] Gulder, T. A. M.; Moore, B. S. (**2010**). Salinosporamide natural products: potent 20S proteasome inhibitors as promising cancer chemotherapeutics. *Angewandte Chemie International Edition 49*, 9346 – 9367.

[126] Raja, S. M.; Chen, S.; Yue, P.; Acker, T. M.; Lefkove, B.; Arbiser, J. L.; Khuri, F. R.; Sun, S.-Y. (**2008**). The Natural Product Honokiol Preferentially Inhibits c-FLIP and Augments Death Receptor-induced Apoptosis. *Molecular Cancer Therapeutics 7*, 2212 – 2223.

[127] a) Archer, C. R.; Koomoa, D.- L. T.; Mitsunaga, E. M.; Clerc, J.; Shimizu, M.; Kaiser, M.; Schellenberg, B.; Dudler, R.; Bachmann, A. S. (**2010**). Syrbactin class proteasome inhibitor-induced apoptosis and autophagy occurs in association with p53 accumulation and Akt/PKB activation in neuroblastoma. *Biochemical Pharmacology 80*, 170 – 178. b) Groll, M; Schellenberg, B.; Bachmann, A. S.; Archer, C. R.; Huber, R., Powell, T. K.; Lindow, S.; Kaiser, M.; Dudler, R. (**2008**). A plant pathogen virulence factor inhibits the eukaryotic proteasome by a novel mechanism. *Nature 452*, 755-758.

[128] Nam, S.; Smith, D. M.; Dou, Q. P. (**2001**). Ester Bond-containing Tea Polyphenols Potently Inhibit Proteasome Activity *in Vitro* and *in Vivo. The Journal of Biological Chemistry 276*, 13322 – 13330.

[129] Wan, S. B.; Landis-Piwowar, K. R.; Kuhn, D. J.; Chen, D.; Dou, Q. P.; Chan, T. H. (**2005**). Structure-activity study of epi-gallocatechin gallate (EGCG) analogs as proteasome inhibitors. *Bioorgorganic & Medicinal Chemistry 13*, 2177 – 2185.

[130] Landis-Piwowar, K. R.; Huo, C.; Chen, D.; Milacic, V.; Shi, G.; Chan, T. H.; Dou, Q. P. (**2007**). A Novel Prodrug of the Green Tea Polyphenol (–)-Epigallocatechin- 3-Gallate as a Potential Anticancer Agent. *Cancer Research 67*, 4303 – 4310.

[131] Wyke, S. M.; Russell, S. T.; Tisdale, M. J. (**2004**). Induction of proteasome expression in skeletal muscle is attenuated by inhibitors of NF-kB activation. *British Journal of Cancer 91*, 1742 – 1750.

[132] Tsukamoto, S.; Wakana, T.; Koimaru, K.; Yoshida, T.; Sato, M.; Ohta, T. (**2005**). 7-hydroxy-3-(4-hydroxybenzyl)chroman and broussonin b: neurotrophic compounds, isolated from *Anemarrhena asphodeloides* BUNGE, function as proteasome inhibitors. *Biological & Pharmaceutical Bulletin 28*, 1798 – 1800.

[133] Guo, W.; Wise, M. L.; Collins, F. W.; Meydani, M. (**2008**). Avenanthramides, polyphenols from oats, inhibit IL-1β-induced NF-κB activation in endothelial cells. *Free Radical Biology & Medicine 44*, 415 – 429.

[134] Cardullo, N.; Spatafora, C.; Musso, N.; Barresi, V.; Condorelli, D.; Tringali, C. (**2015**). Resveratrol-Related Polymethoxystilbene Glycosides: Synthesis, Antiproliferative Activity and Glycosidase Inhibition. *Journal of Natural Products 78*, 2675-2683.

[135] Jacobsson M., Malmberg J., Ellervik U., (**2006**). Aromatic O-glycosylation. *Carbohydrate Research 341*, 1266-1281.

[136] Tsujii, E.; Muroi, M.; Shiragami, M.; Takatsuki, A. (**1996**). Nectrisine Is a Potent Inhibitor of α-Glucosidases, Demonstrating Activities Similarly at Enzyme and Cellular Levels. *Biochememical and Biophysical Research Communications 220*, 459 - 466.

[137] de Melo, E.B.; Gomes, A.D.; Carvalho, I. (**2006**). Alpha- and beta-Glucosidase inhibitors: chemical structure and biological activity. *Tetrahedron* 62, 10277-10302

[138] Scheen, A.J. (**1998**). Clinical efficacy of acarbose in diabetes mellitus: A critical review of controlled trials. *Diabetes & Metabolism 24*, 311 - 320.

[139] Du, Z.Y.; Liu, R.R.; Shao, W.Y.; Mao, X.P.; Ma, L.; Gu, L.Q.; Huang, Z.S.; Chan, A.S.C. (**2006**). Alpha-glucosidase inhibition of natural curcuminoids and curcumin analogs. *European Journal of Medicinal Chemistry 41*, 213 - 218.

[140] Lam, S.H.; Chen, J.M.; Kang, C.J.; Chen, C.H.; Lee, S.S. (**2008**). Alpha-Glucosidase inhibitors from the seeds of *Syagrus romanzoffiana*, *Phytochemistry 69*, 1173 - 1178.

[141] Kerem, Z.; Bilkis, I.; Flaishman, M.A.; Sivan, U. (**2006**). Antioxidant activity and inhibition of alpha-glucosidase by trans-resveratrol, piceid, and a novel trans-stilbene from the roots of Israeli *Rumex bucephalophorus* L. *Journal of Agriicultural Food and Chemistry 54*, 1243 - 1247.

[142] Kim, S.; Jin, Y.; Choi, Y.; Park, T. (**2011**). Resveratrol exerts anti-obesity effects via mechanisms involving down-regulation of adipogenic and inflammatory processes in mice, *Biochemical Pharmacology 81*, 1343 - 1351

[143] Babu, K.S.; Tiwari, A.K.; Srinivas, P.V.; All, A.Z.; Raju, B.C.; Rao, J.M. (**2004**). Yeast and mammalian alpha-glucosidase inhibitory constituents from Himalayan rhubarb *Rheum emodi Wall*.ex Meisson. *Bioorganic & Medicinal Chemistry Letters 14*, 3841 - 3845.

[144] Zhang, L.; Jing, H.; Cui, L.; Li, H.; Zhou, B.; Zhou, G.; Dai, F. (**2013**). 3,4-Dimethoxystilbene, a resveratrol derivative with anti-angiogenic effect, induces both macroautophagy and apoptosis in endothelial cells. *Journal of Cellular Biochemistry 114*, 697–707.

[145] Ng, S. Y.; Cardullo, N.; Yeo, S. C. M.; Spatafora, C.; Tringali, C.; Ong, P-S.; Lin, H-S. (**2014**). Quantification of the Resveratrol Analogs *trans*-2,3-Dimethoxystilbene and *trans*-3,4-Dimethoxystilbene in Rat Plasma: Application to Pre-Clinical Pharmacokinetic Studies. *Molecules 19*, 9577-9590.

[146] a) Kim, D. K.; Lim, J. P.; Kim, J. W.; Park, H. W.; Eun, J. S. (**2005**). Antitumor and Antiinflammatory Costituents from *Celtis sinensis. Archives of Pharmacal Research 28*, 39 – 43. b) Santos, L. P.; Boaventura, M. A. D.; De Oliveira, A. B.; Cassady, J. M. (**1996**). Grossamide and *N-trans*-caffeoyltyramine from *Annona crassiflora seeds. Planta Medica 62*, 77 – 78.

[147] Koeberle, A.; Zettl, H.; Greiner, C.; Wurglics, M.; Schubert-Zsilavecz, M.; Werz, O. (**2008**). Pirinixic acid derivatives as novel dual inhibitors of microsomal prostaglandin E2 synthase-1 and 5-lipoxygenase, *Journal of Medicinal Chemistry 51*, 8068 - 8076.

[148] Yoshihara,T.; Takamatsu, S.; Sakamura, S. (**1978**). Three New Phenolic Amides from the Roots of Eggplant (*Solanum melongena L.*). *Agricultural and Biological Chemistry 42*, 623 – 627.

[149] Mosmann, T. (**1983**) Rapid colorimetric assay for cellular growth and survival: application to proliferation and cytotoxicity assays. *Journal of Immunological Methods 65*, 55 - 63.

[150] a) Henchoz, Y.; Guillarme, D.; Rudaz, S.; Veuthey, J. L.; Carrupt, P. A. (**2008**). High-throughput log P determination by ultraperformance liquid chromatography: a convenient tool for medicinal chemists. *Journal of Medicinal Chemistry 51*, 396 – 399; b) Giaginis, C.; Tsantili-Kakoulidou, A. (**2008**). Current State of the Art in HPLC Methodology for Lipophilicity Assessment of Basic Drugs. A Review. *Journal of Liquid Chromatography & Related Technologies 31*, 79 – 96.

[151] a) Calvani, M.; Critelli, L.; Gallo, G.; Giorgi, F.; Gramiccioli, G.; Santaniello, M.; Scafetta, N.; Tinti, M. O.; De Angelis, F. (**1998**). L-carnitine esters as "soft", broad-spectrum antimicrobial amphiphiles. *Journal of Medicinal Chemistry 41*, 2227 – 2233; b) Drews, A.; Bovens, S.; Roebrock, K.; Sunderkotter, C.; Reinhardt, D.; Schafers, A. van der Velde, A. S.; Elfringhoff, J.; Lehr. F. M. (**2010**). 1-(5-Carboxyindol-1-yl)propan-2-one Inhibitors of Human Cytosolic Phospholipase $A_2\alpha$ with Reduced Lipophilicity: Synthesis, Biological Activity, Metabolic Stability, Solubility, Bioavailability, And Topical in Vivo Activity. *Journal of Medicinal Chemistry 53*, 5165 – 5178.

[152] N., Berova; G., Ellestad; K., Nakanishi; N., Harada. (**2012**). Recent Advances in the Application of Electronic Circular Dichroism for Studies of Bioactive Natural Products in: *Bioactive Compounds from Natural Sources*, Natural Products as Lead Compounds in Drug Discovery, 133–166. Second Edition: C. Tringali Ed., ISBN: 978-1-4398-2229-6, CRC Press-Taylor & Francis, Boca Raton.

[153] Lemière, G.; Gao, M.; De Groot, A.; Dommisse, R.; Lepoivre, J.; Pieters, L.; Buss, V. (**1995**). 3′,4-di-*O*-methylcedrusin: synthesis, resolution and absolute configuration. *Journal of the Chemical Society, Perkin Transactions 1*, 1775-1779.

[154] Kurosawa, W.; Kobayashi, H.; Kan, T.; Fukuyama, T. (**2004**). Total synthesis of (K)-ephedradine A: an efficient construction of optically active dihydrobenzofuran-ring via C–H insertion reaction. *Tetrahedron 60*, 9615–9628

[155] Wakimoto, T.; Nitta, M.; Kasahara, K.; Chiba, T.; Yiping, Y.; Tsuji, K.; Kan, T.; Nukaya, H.; Ishiguro, M.; Koike, M.; Yokoo, Y., Suwa, Y. (**2009**). Structure-Activity Relationship Study on α_1 Adrenergic Receptor Antagonists from Beer. *Bioorganic & Medicina Chemistry Letters 19*, 5905 - 5908.

[156] Liu, Y.; Guo, M. (**2014**). Chemical proteomic strategies for the discovery and development of anticancer drugs. *Proteomics 14*, 399–411.

[157] Rix, U.; Superti-Furga, G. (**2009**). Target profiling of small molecules by chemical proteomics. *Nature chemical biology 5*, 616-624.

[158] Leppälä, E.; Pohjoispää, M.; Koskimies, J.; Wähälä K. (**2008**). Synthesis of new deuterium-labelled lignanolactones. *Journal of Labelled Compaunds and Radiopharmaceutcals 51*, 407–412

[159] Pohjoispää, M.; Mera-Adasme, R.; Sundholm, D.; Heikkinen, S.; Hase, T.; Wähälä, K. (**2014**). Capricious Selectivity in Electrophilic Deuteration of Methylenedioxy Substituted Aromatic Compounds. *The Journal of Organic Chemistry 79*, 10636−10640.

[160] Wang, Q.; Yang, Y.; Li, Y.; Yu, W.; Hou, Z. J. (**2006**). An efficient method for the synthesis of lignans. *Tetrahedron 62,* 6107-6112.

[161] Hart, R. J.; Heller, H. G. (**1972**). Overcrowded molecules. Part VII. Thermal and photochemical reactions of photochromic (*E*)- and (*Z*)-benzylidene(diphenylmethylene)-succinic anhydrides and imides. *Journal of Chemical Society, Perkin Transactions 1*, 1321-1324.

[162] Alonso, E.; Ramón, D. J.; Yus M. (**1997**). Simple synthesis of 5-resorcinols: a revisited family of interesting bioactive molecule. *Journal of Organic Chemistry 62*, 417 – 421.

[163] Blangetti, M.; Fleming, P.; O'Shea, D. F. (**2012**). Homo- and hetero- oxidative coupling of benzyl aninons. *Journal of Organic Chemistry 77*, 2870 – 2877.

[164] Chang, C.Y.; Kuo, S.C.; Lin, Y.L.; Wang, J.; Huang L.J. (**2001**). Benzyloxybenzaldehyde Analogues as Novel Adenylyl Cyclase Activators. *Bioorganic & Medicinal Chemistry Letters 11*, 1971 - 1974.

7. SUPPORTING MATERIAL

7.1. APPENDIX A

In this section the MS and NMR spectra of polymethoxystilbene glycosides (**85** – **90**) are reported.

Compound 85

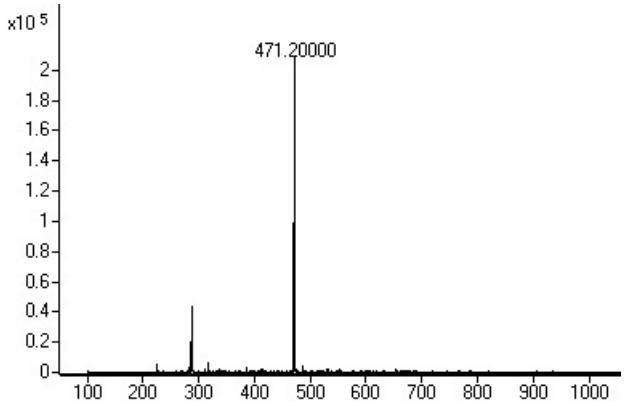

Figure 1S: ESI MS spectrum of **85**

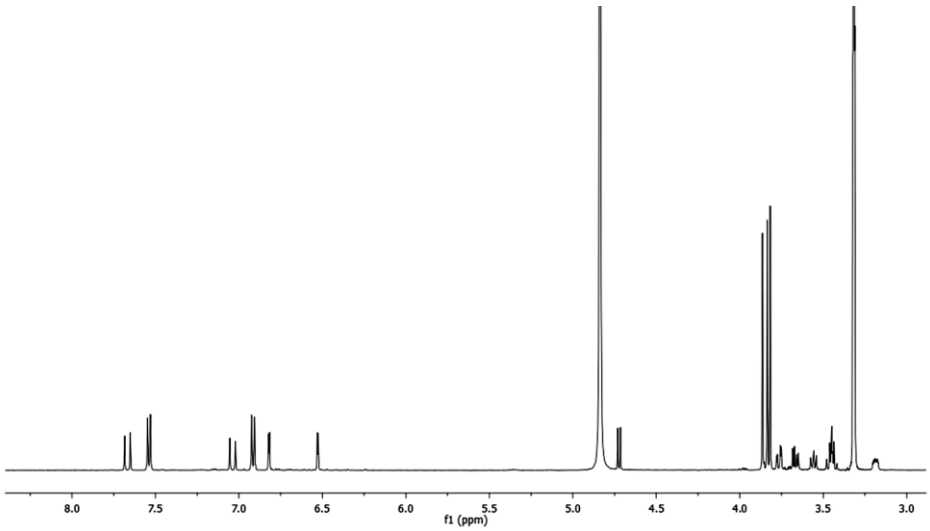

Figure 2S: ^{1}H-NMR spectrum (CD_3OD, 500 MHz) of **85**

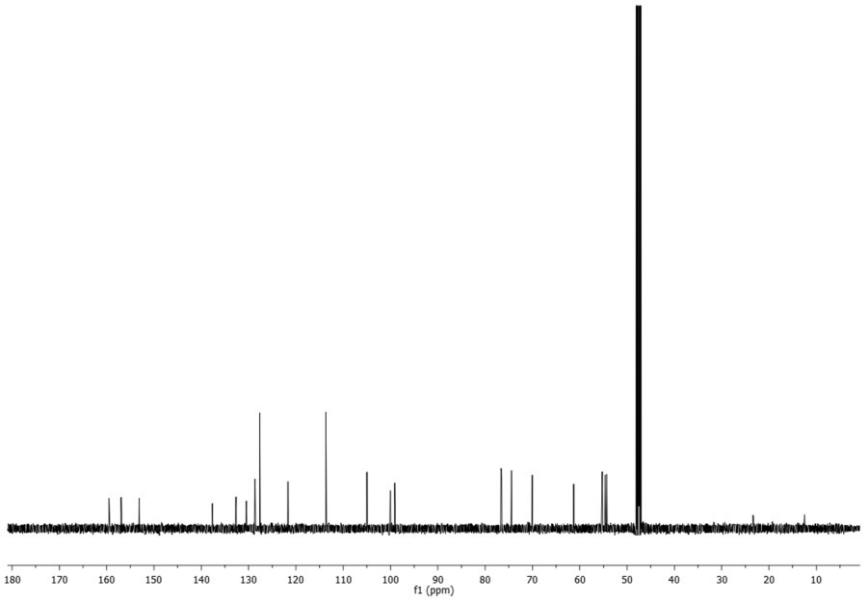

Figure 3S: ^{13}C-NMR spectrum (CD_3OD, 125 MHz) of **85**

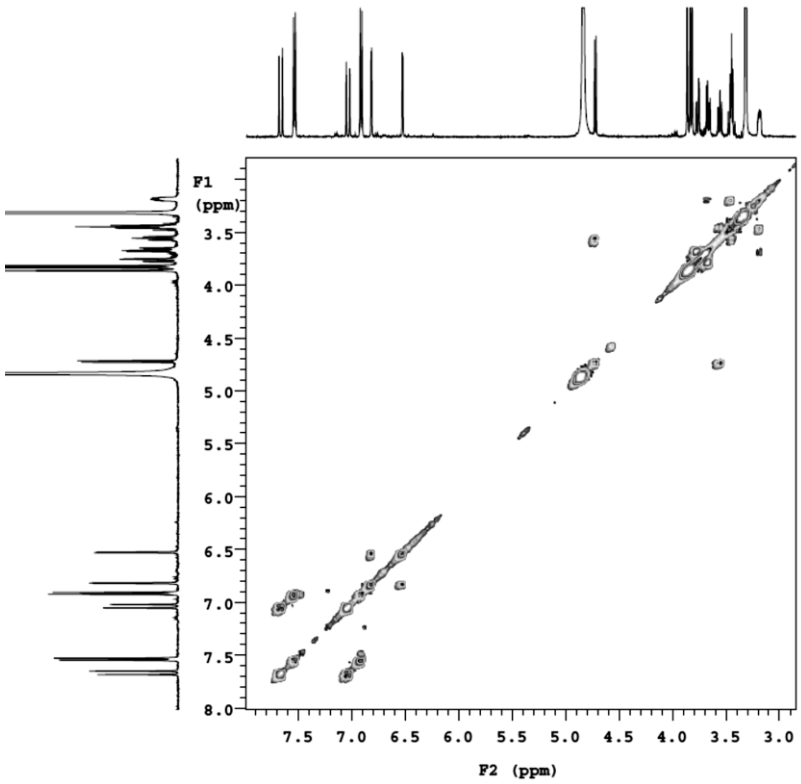

Figure 4S: g-COSY spectrum of **85**

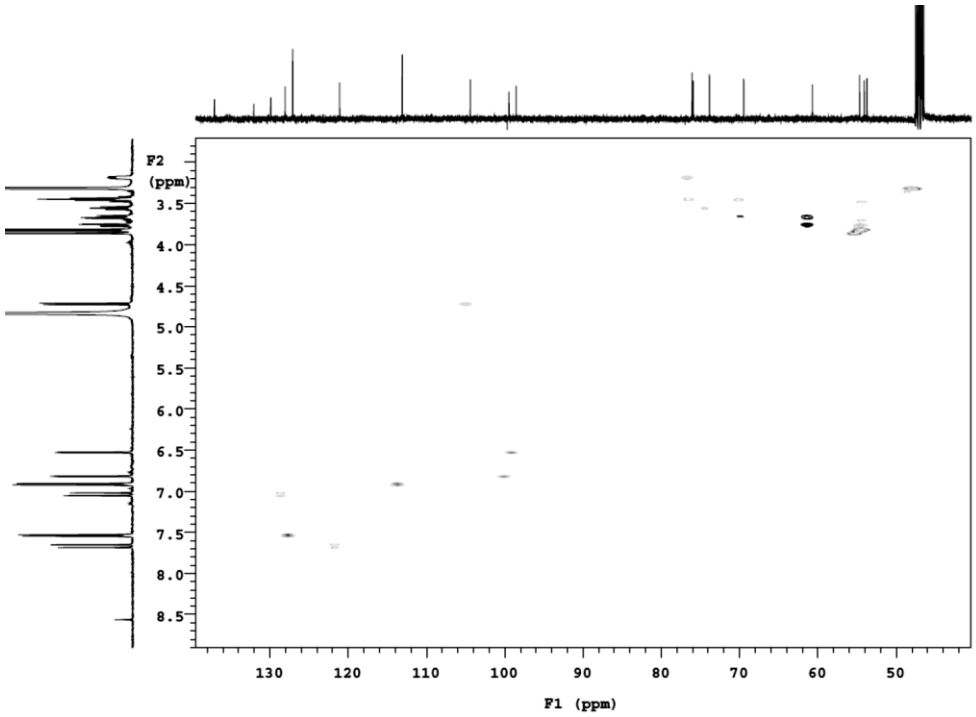

Figure 5S: g-HSQCAD spectrum of **85**

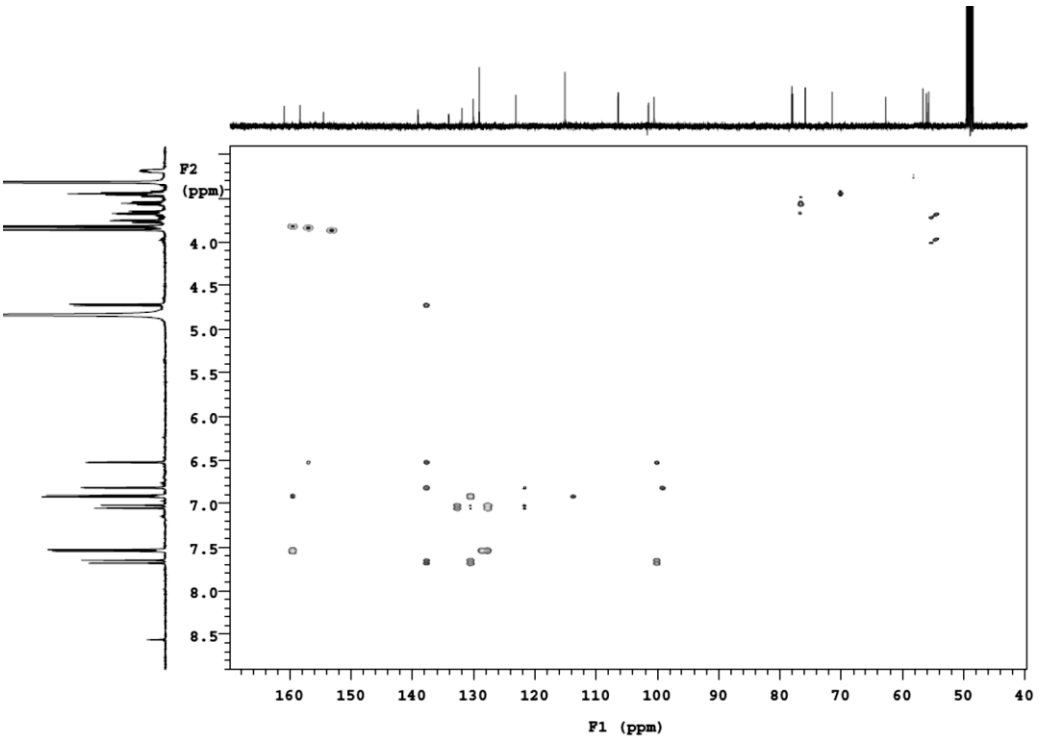

Figure 6s: g-HMBCAD spectrum of **85**

Compound 86

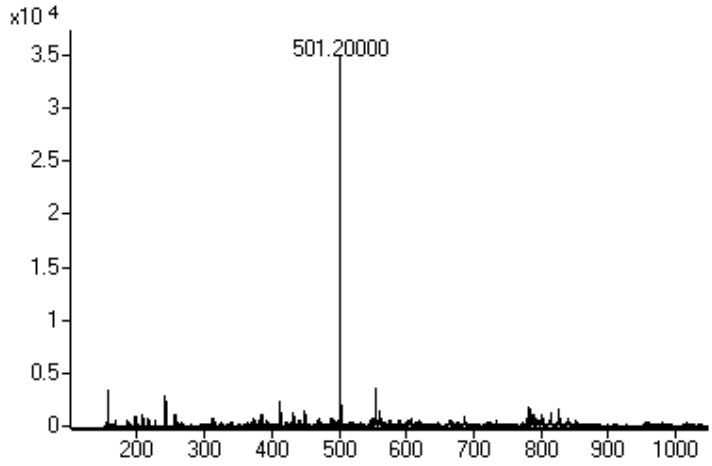

Figure 7S: ESI Mass spectrum of **86**

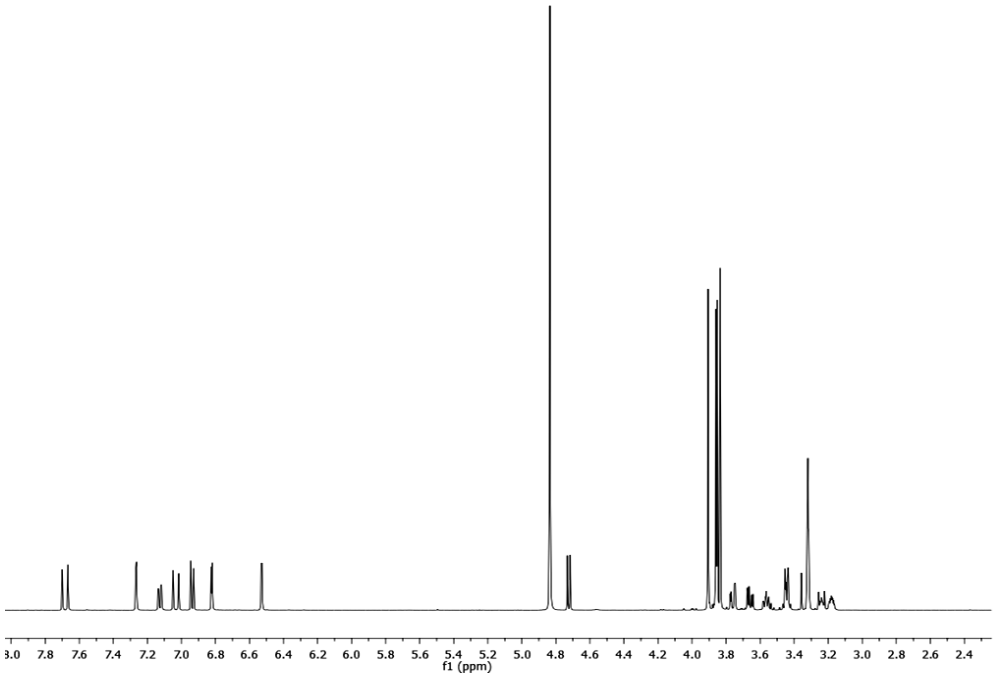

Figure 8S: ^{1}H NMR spectrum (CD_3OD, 500 MHz) of **86**

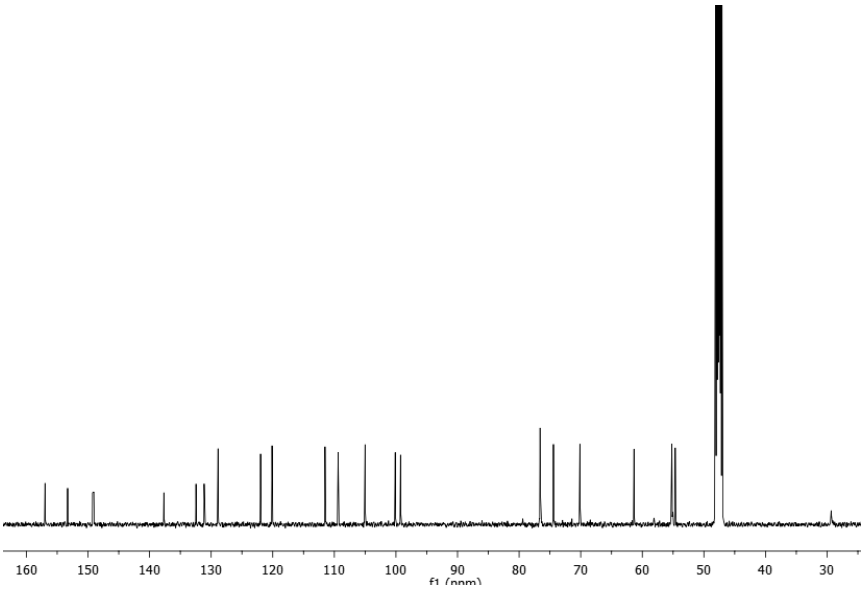

Figure 9S: ^{13}C NMR spectrum (CD_3OD, 125 MHz) of **86**

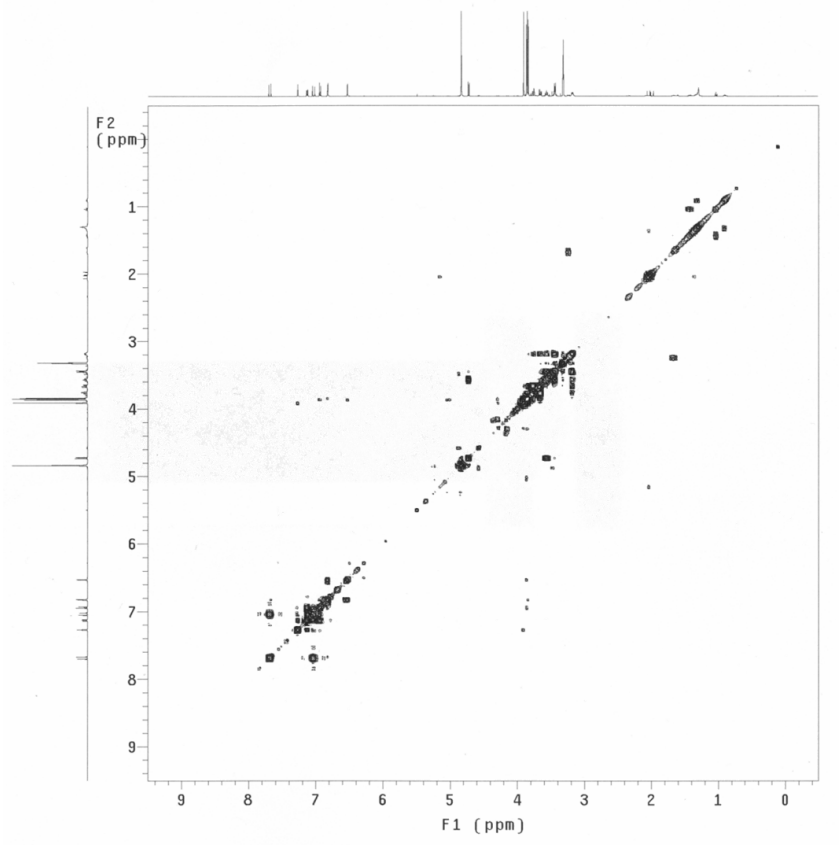

Figure 10S: COSY spectrum of **86**

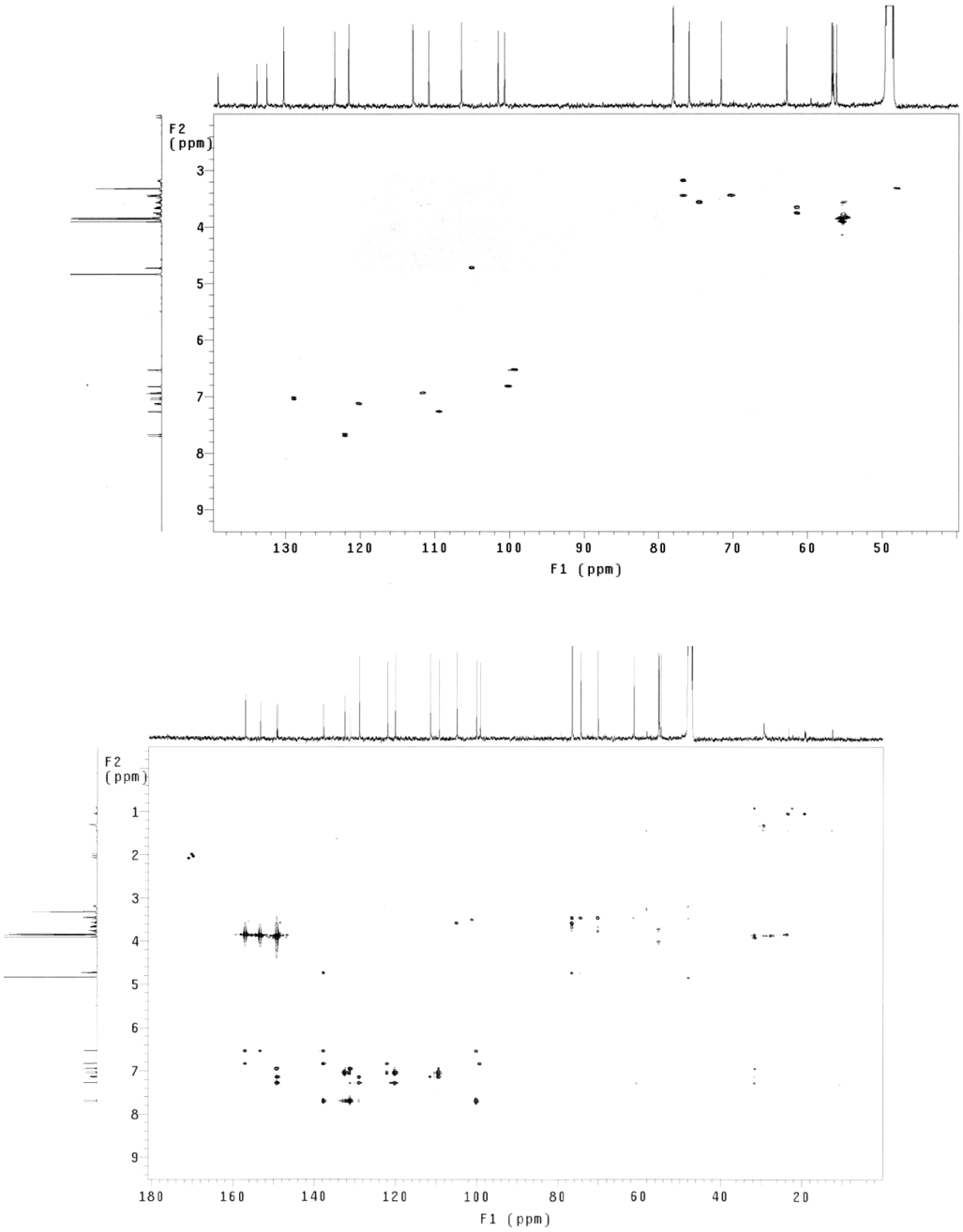

Figure 12S: HMBC spectrum of **86**

Compound 87

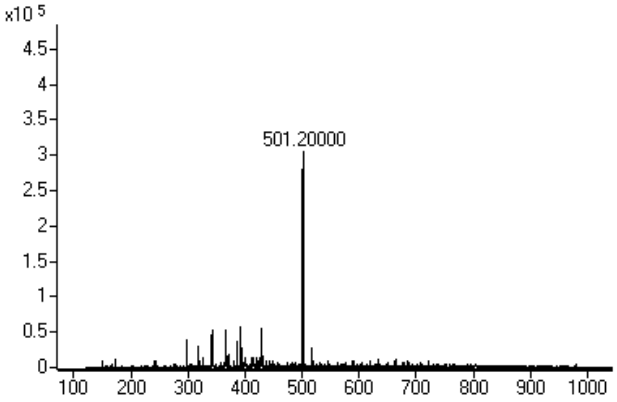

Figure 13S: ESI Mass spectrum of **87**

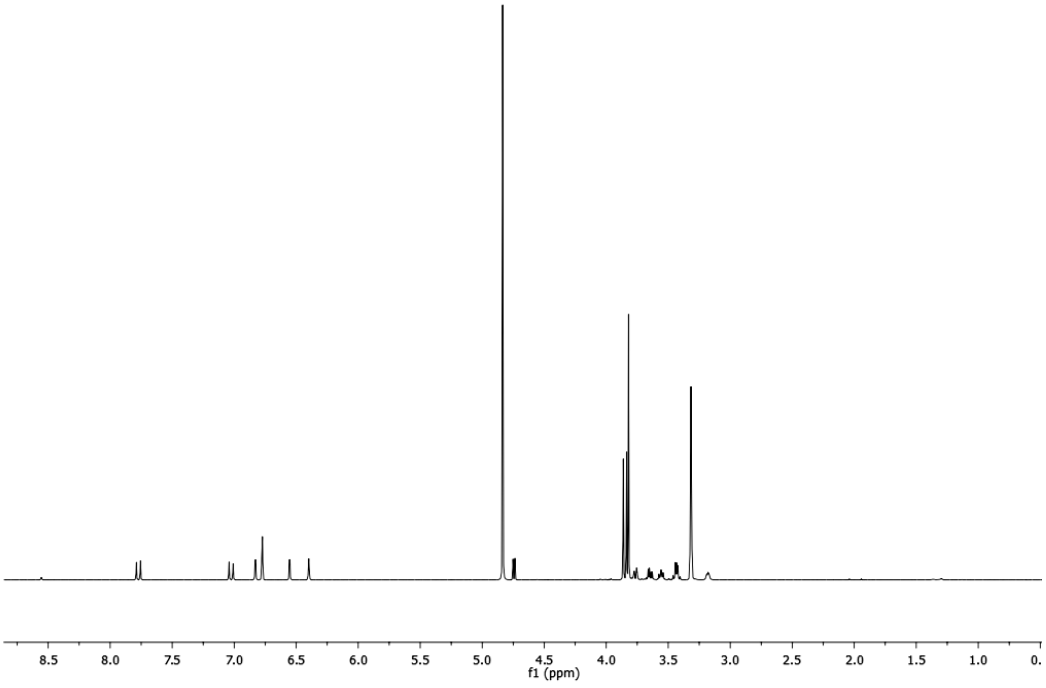

Figure 14S: ^{1}H NMR spectrum (CD_3OD, 500 MHz) of **87**

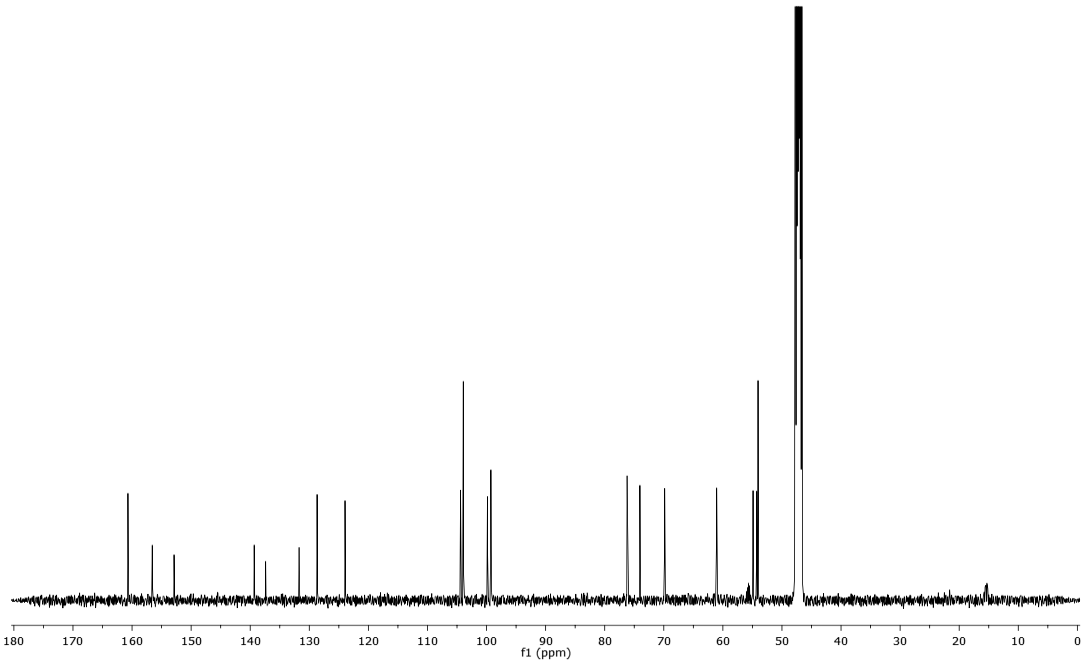

Figure 15S: ^{13}C NMR spectrum (CD_3OD, 125 MHz) of **87**

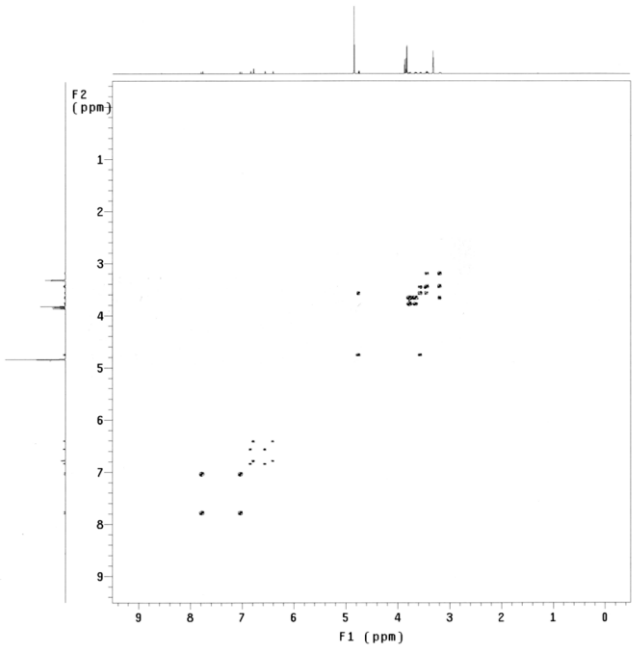

Figure 16S: COSY spectrum of **87**

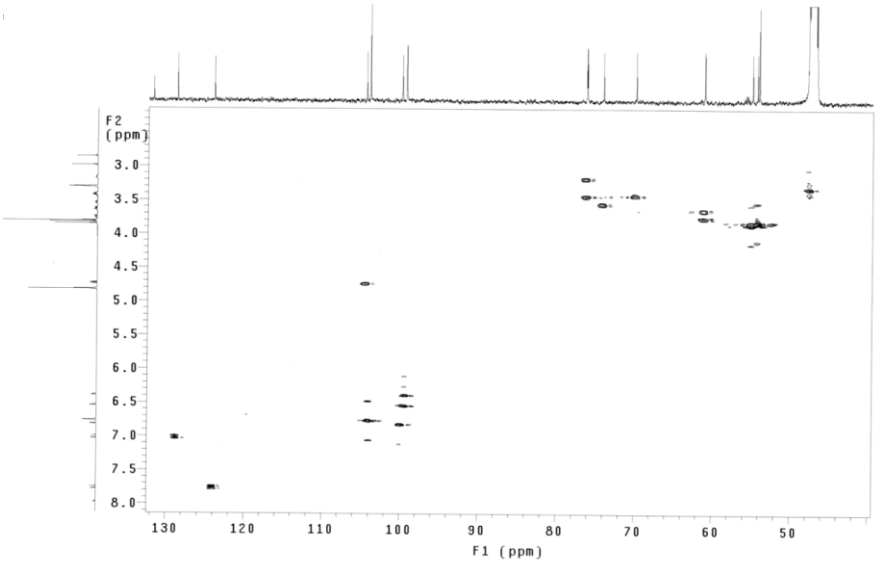

Figure 17S: HSQC spectrum of **87**

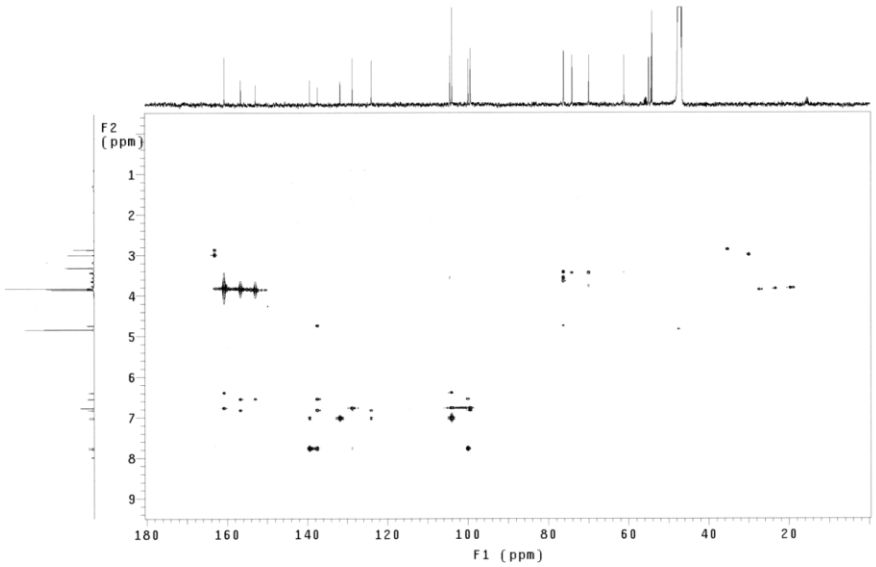

Figure 18S: HMBC spectrum of **87**

Compound 88

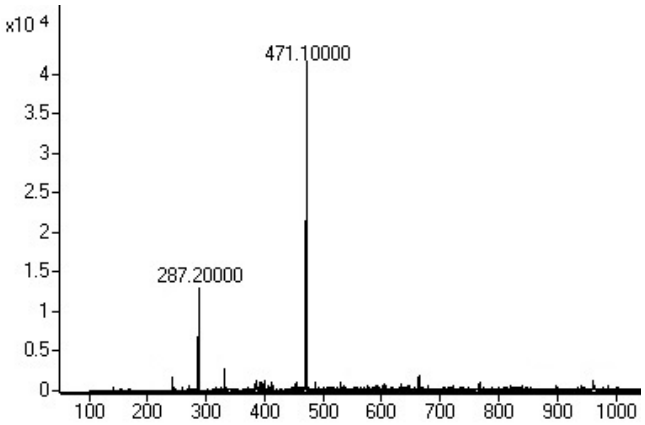

Figure 19S: ESI MS spectrum of **88**

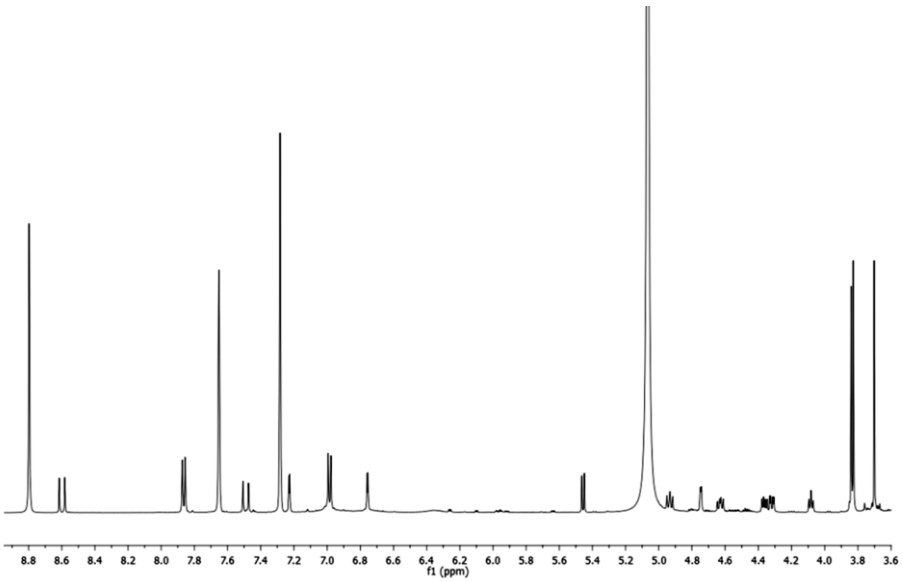

Figure 20S: ^{1}H-NMR spectrum (C_5D_5N, 500 MHz) of **88**

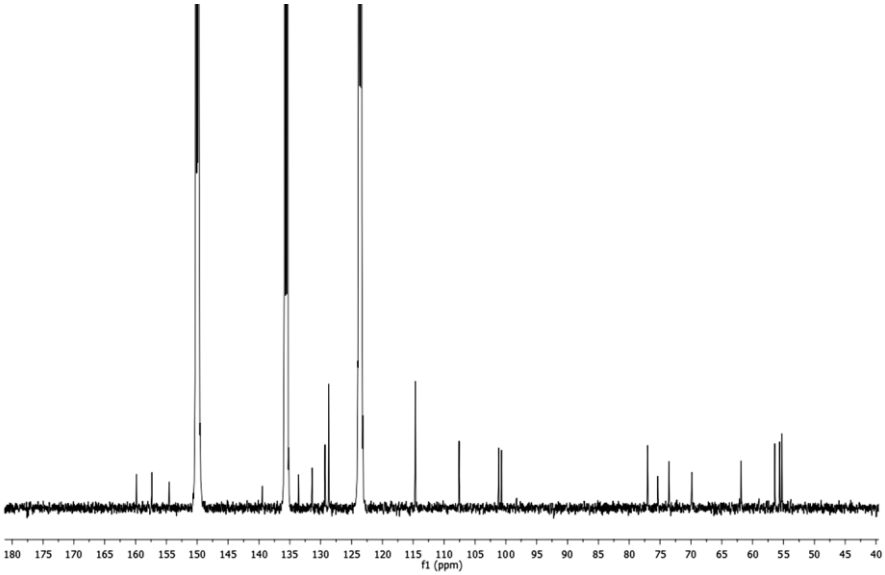

Figure 21S: ^{13}C-NMR spectrum (C_5D_5N, 125 MHz) of **88**

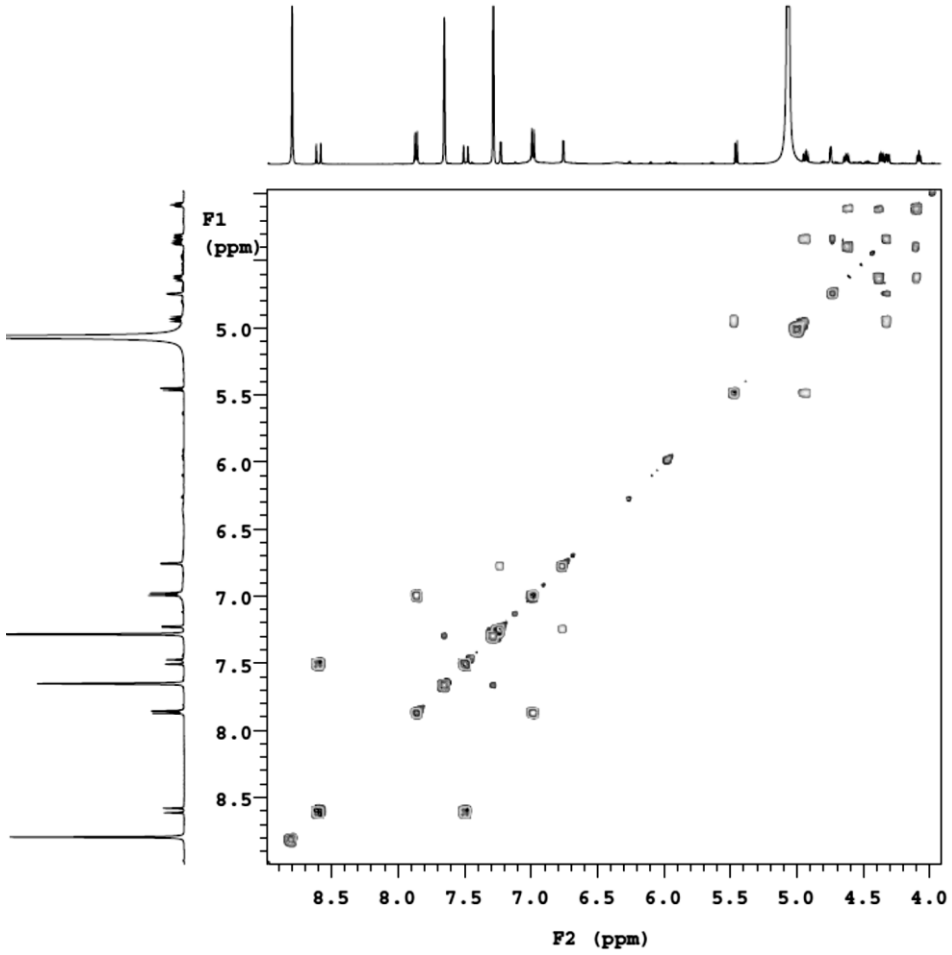

Figure 22S: g-COSY spectrum of **88**

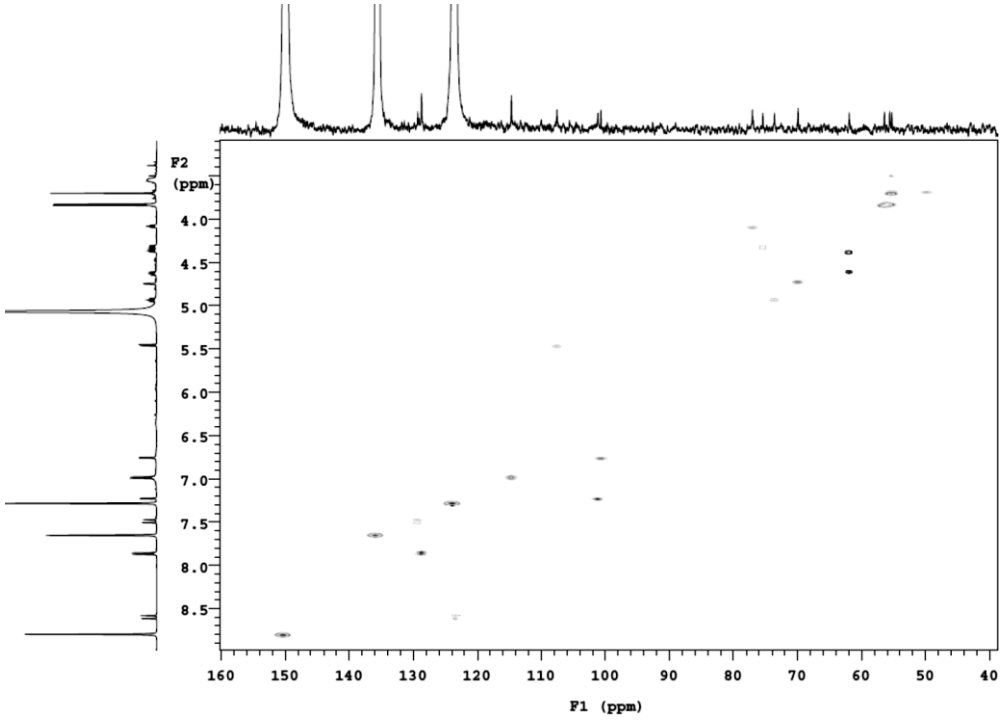

Figure 23S: g-HSQCAD spectrum of **88**

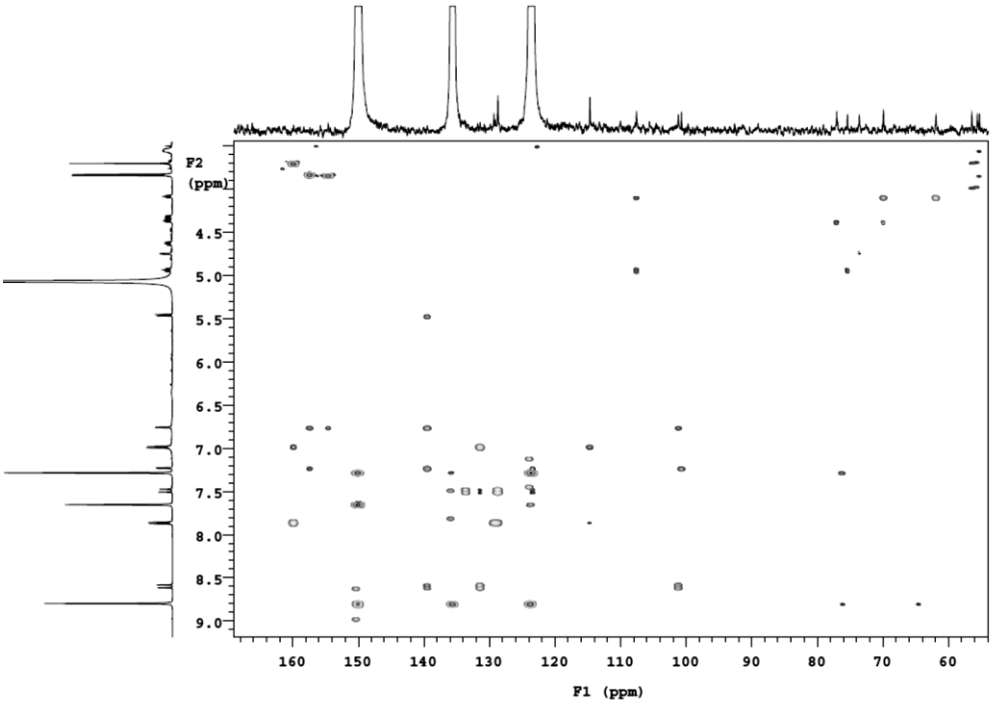

Figure 24S: g-HMBCAD spectrum of **88**

Compound 89

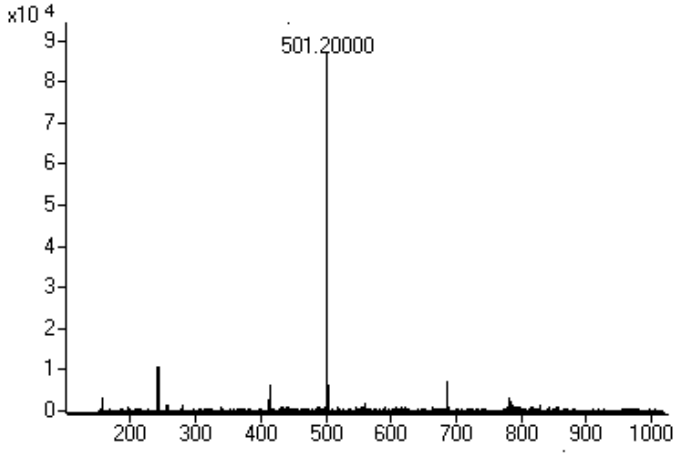

Figure 25S: ESI Mass spectrum of **89**

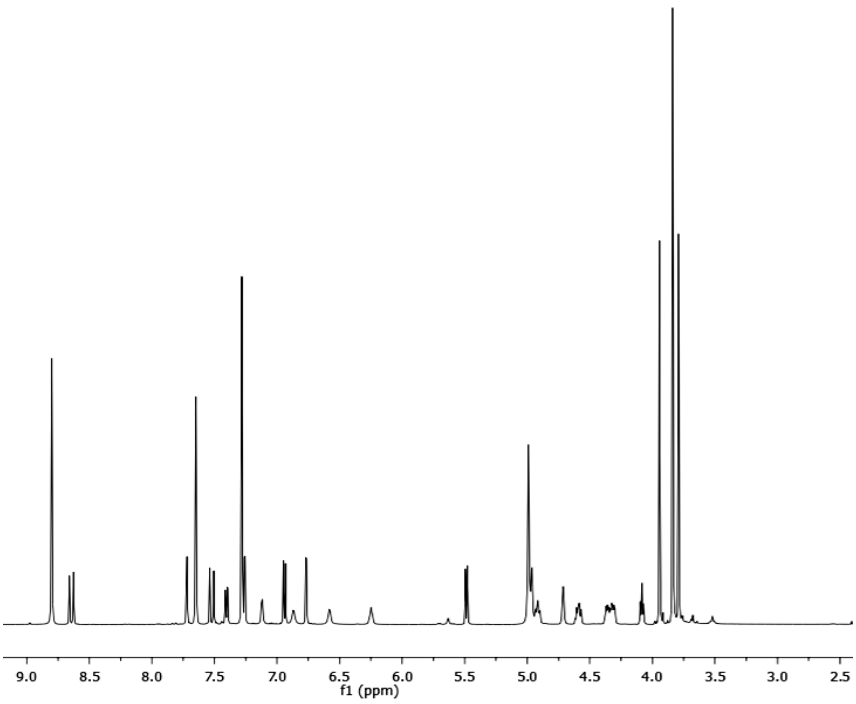

Figure 26S: ^{1}H NMR (C_5D_5N, 500 MHz) of **89**

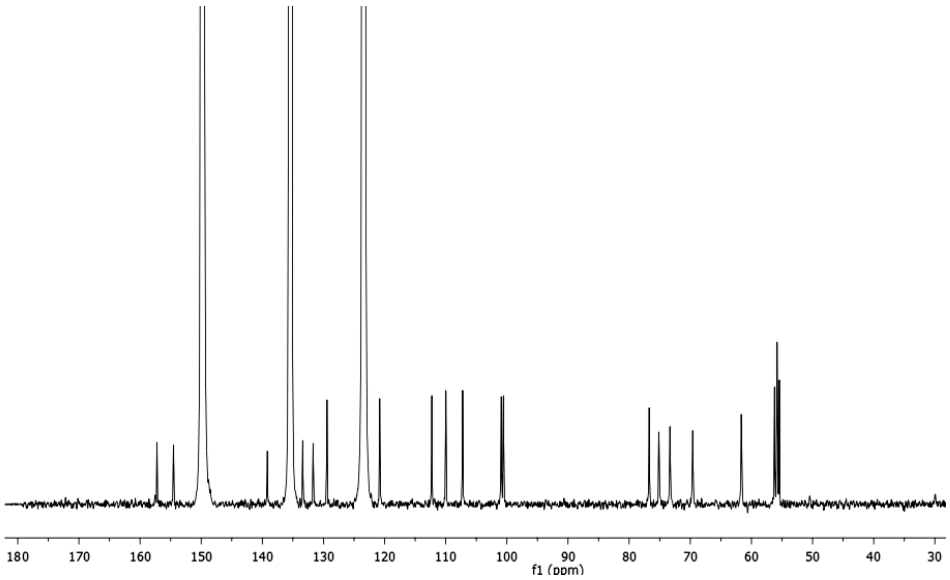

Figure 27S: ^{13}C NMR (C_5D_5N, 125 MHz) of **89**

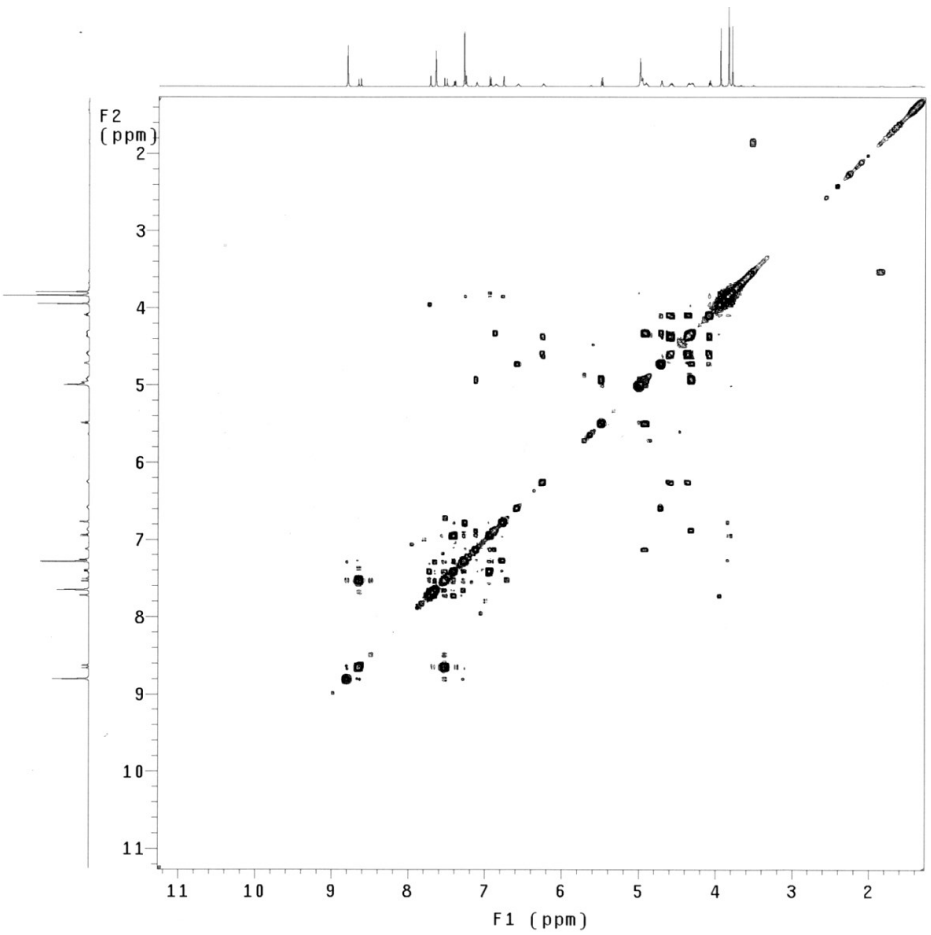

Figure 28S: COSY spectrum of **89**

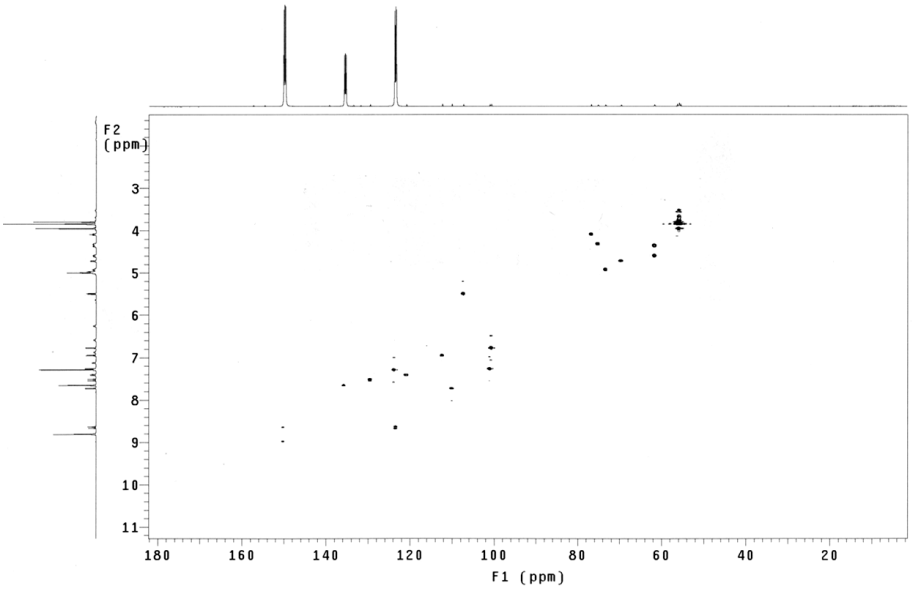

Figure 29S: HSQC spectrum of **89**

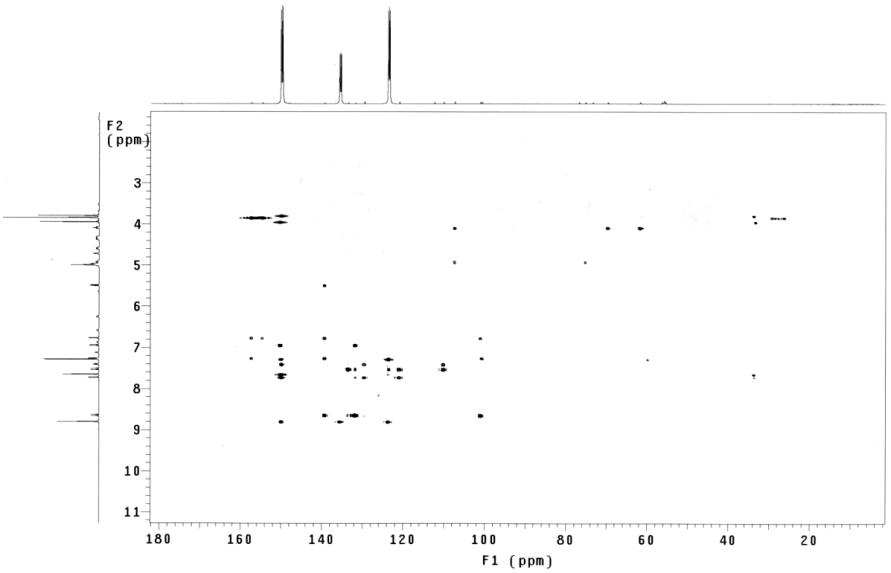

Figure 30S: HMBC spectrum of **89**

Compound 90

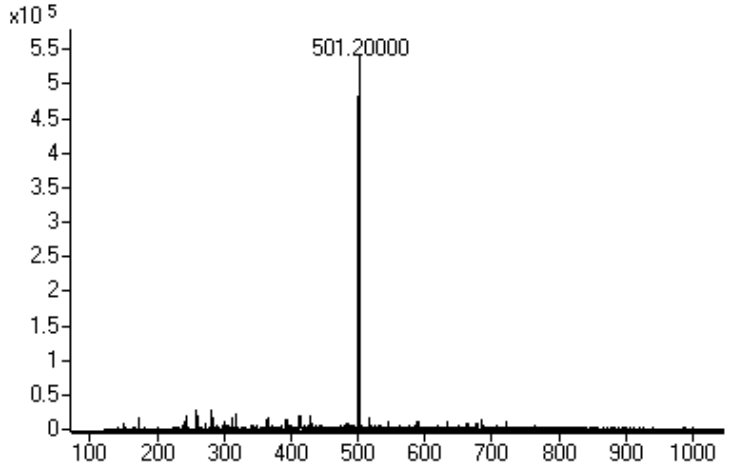

Figure 31S: Mass spectrum of **90**

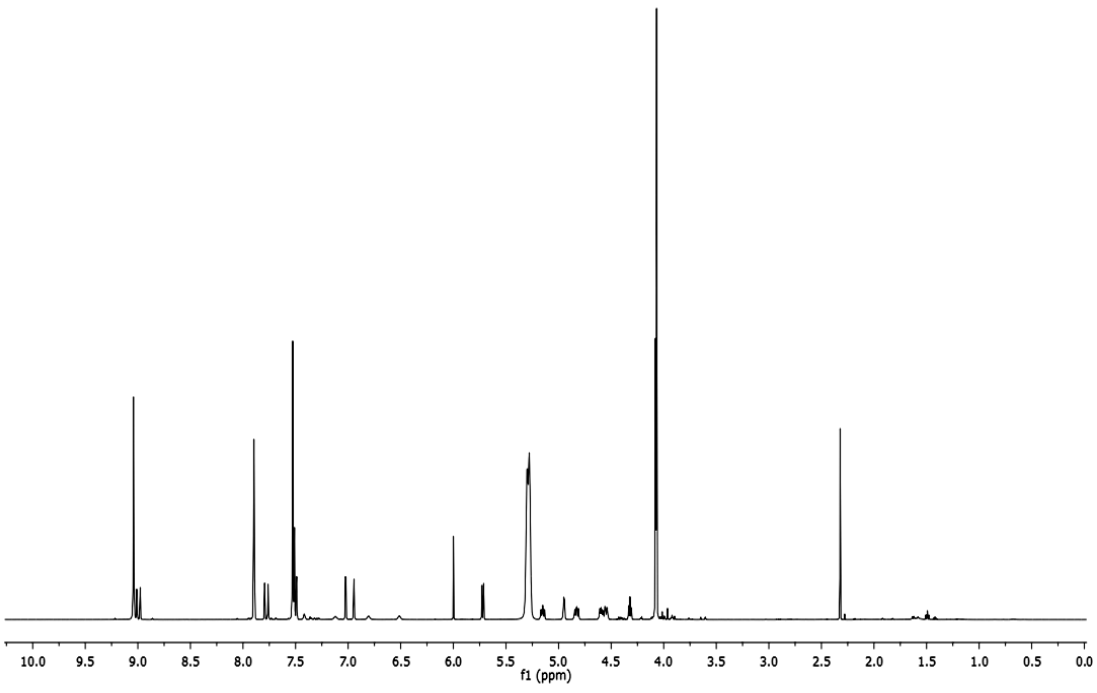

Figure 32S: ^{1}H NMR (500 MHz, C_5D_5N) of **90**

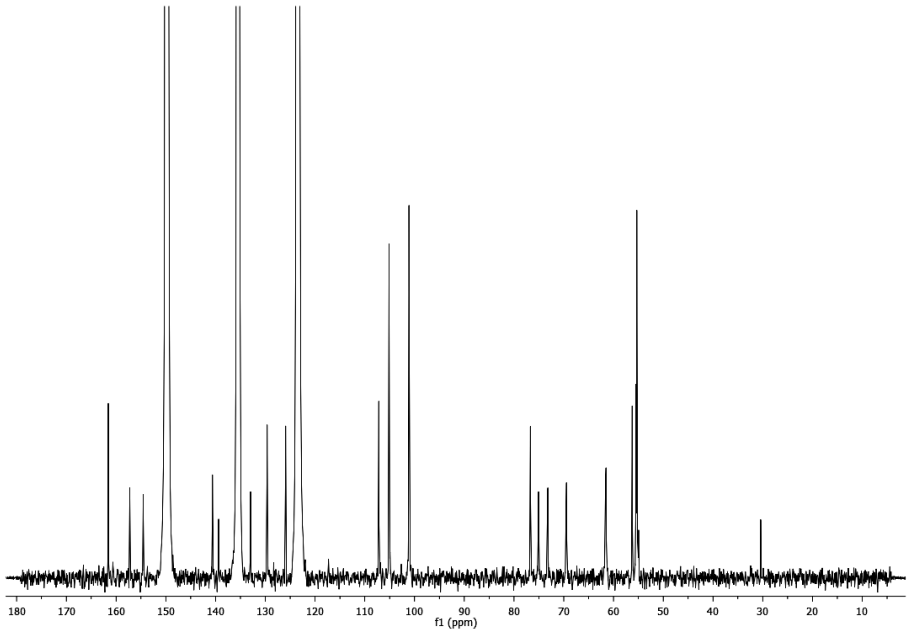

Figure 33S: ^{13}C NMR (125 MHz, C_5D_5N) of **90**

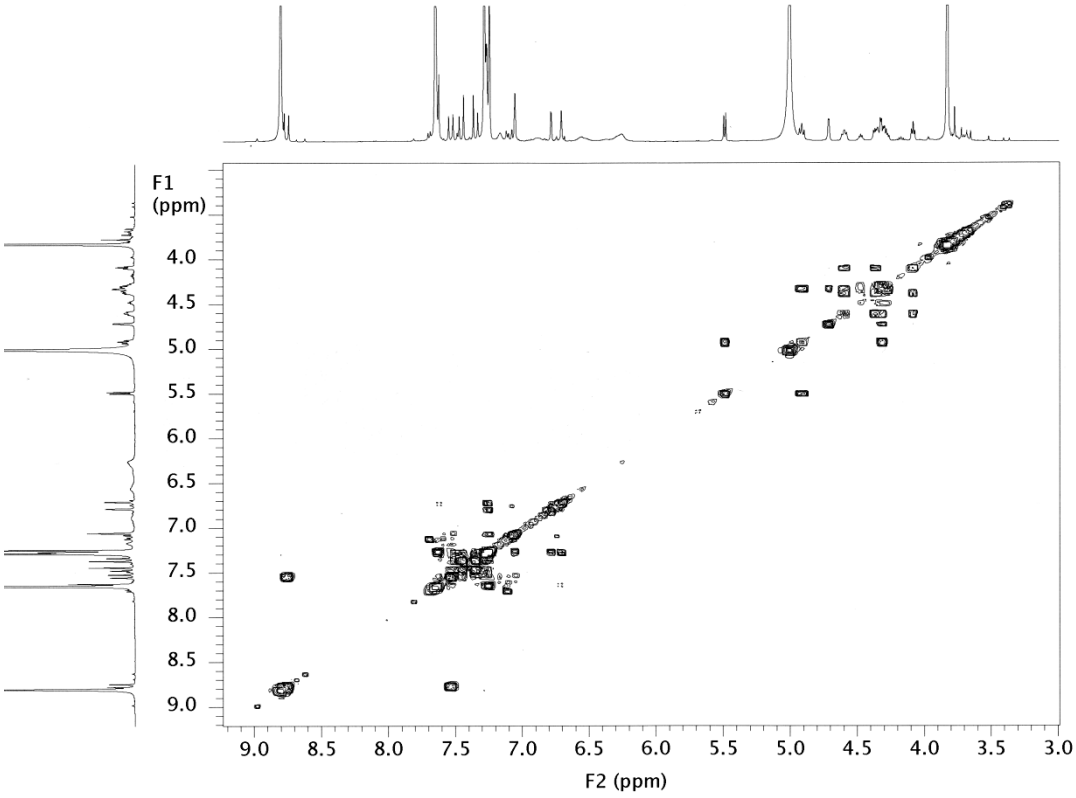

Figure 34S: COSY spectrum of **90**

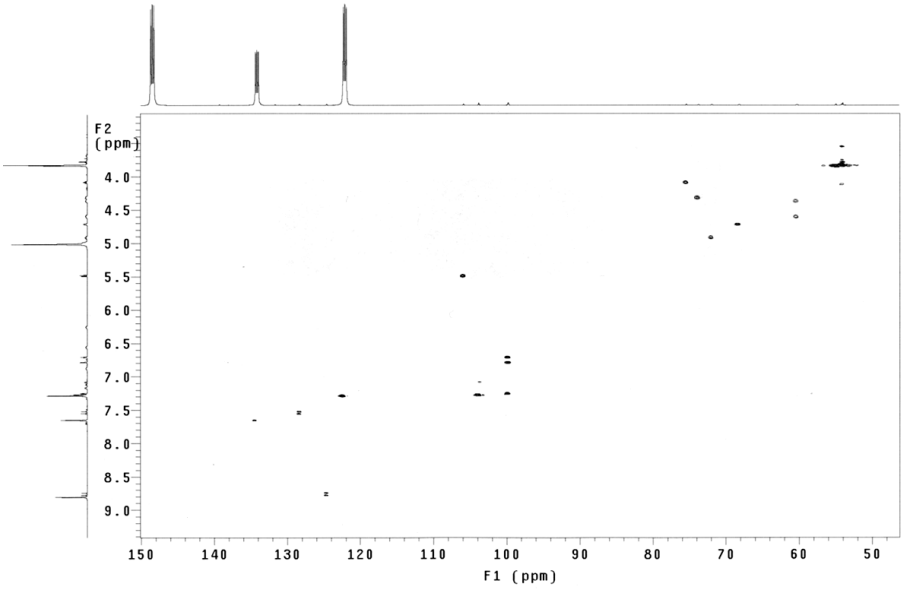

Figure 35S: HSQC spectrum of **90**

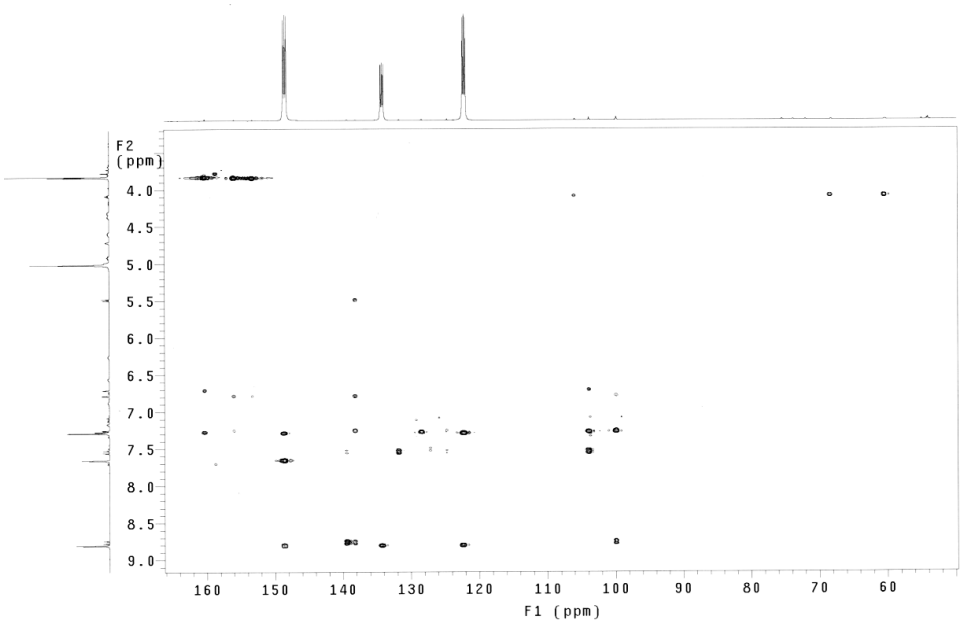

Figure 36S: HMBC spectrum of **90**

7.2. APPENDIX B

In this section the MS and NMR spectra of phenolic cinnamic acid derivatives (**100** – **103**, **105** – **108**, **112** – **114**, **116** -**118**, **122** – **127** and **136**) are reported.

Amide 100

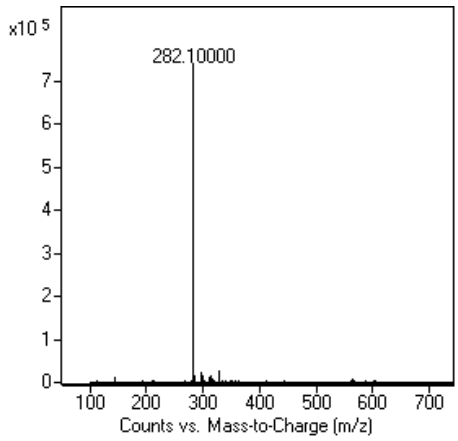

Figure 37S: ESI MS spectrum of **100**

Amide 101

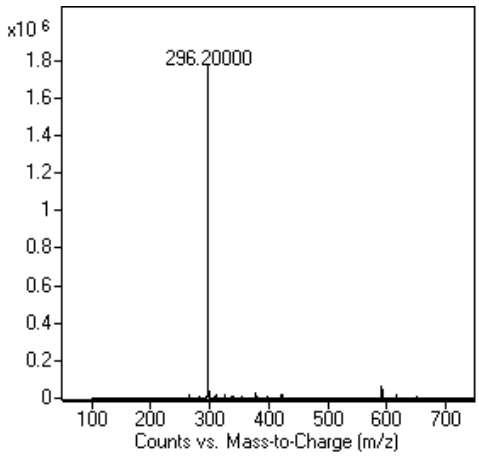

Figure 38S: ESI MS spectrum of **101**

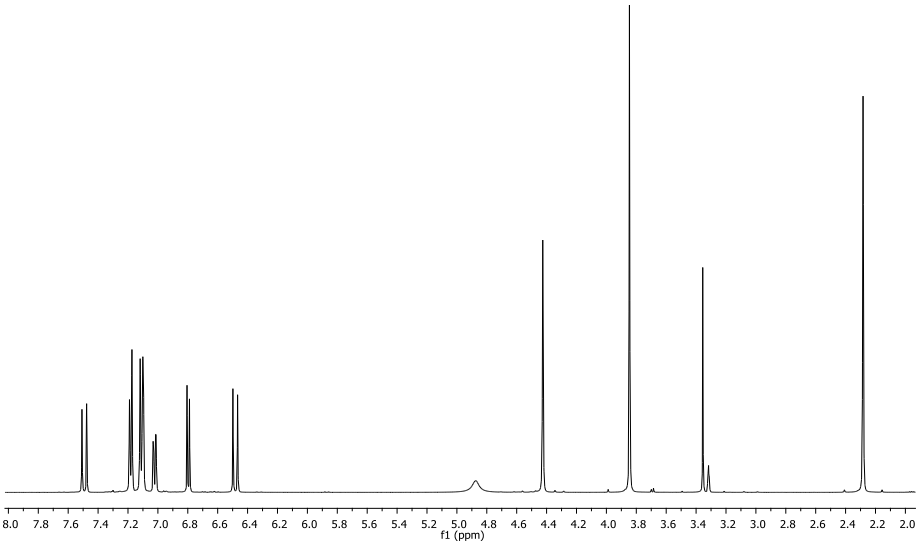

Figure 39S:[1]H NMR spectrum (CD_3OD, 500 MHz) of **101**

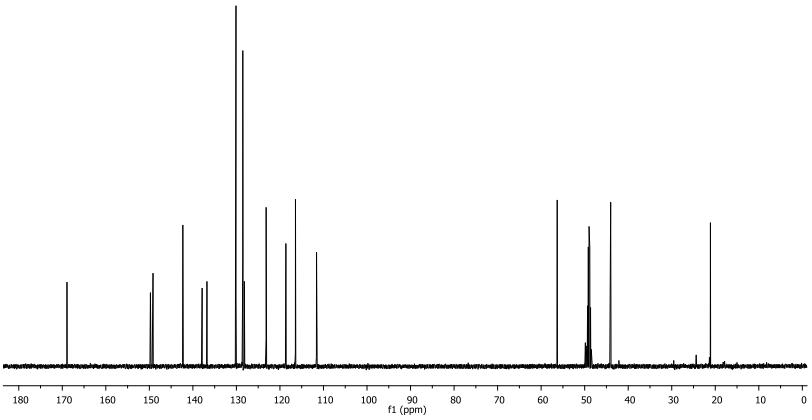

Figure 40S: [13]C NMR (CD_3OD, 125 MHz) of **101**

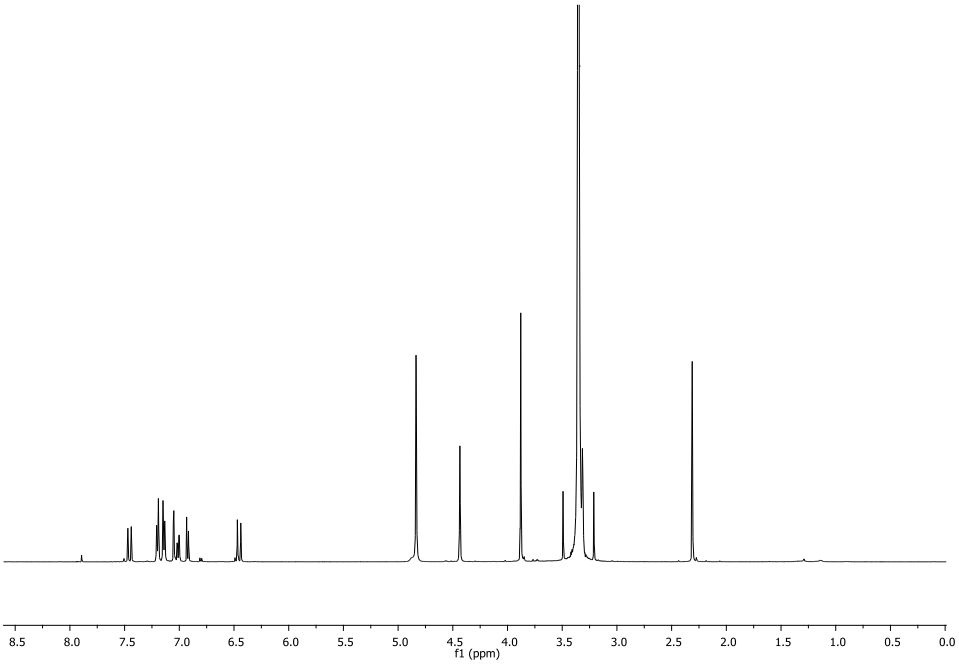

Figure 41S: ^{1}H NMR spectrum (CD_3OD, 500 MHz) of **102**

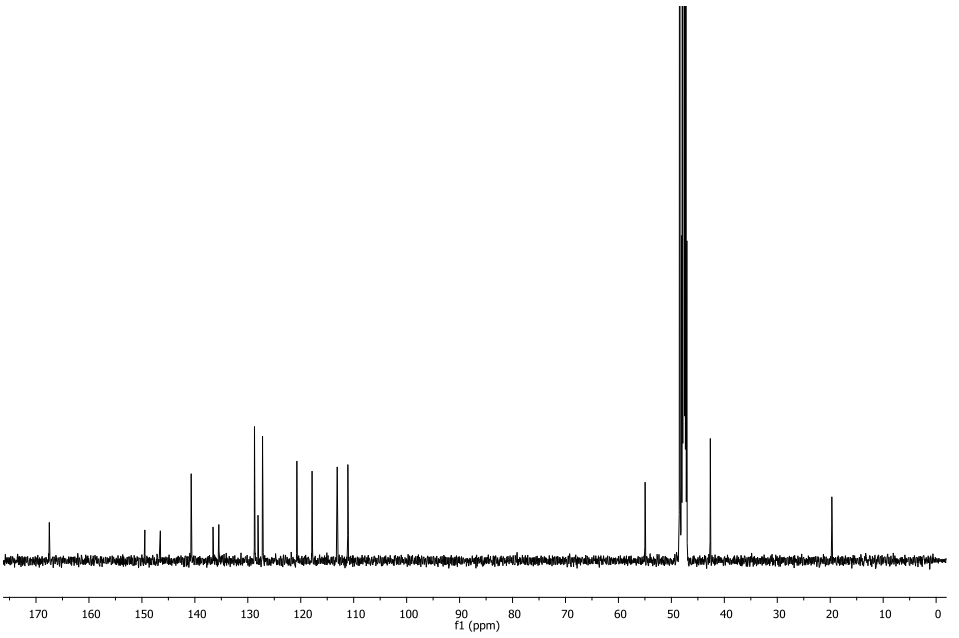

Figure 42S: ^{13}C NMR spectrum (CD_3OD, 125 MHz) of **102**

Amide 103

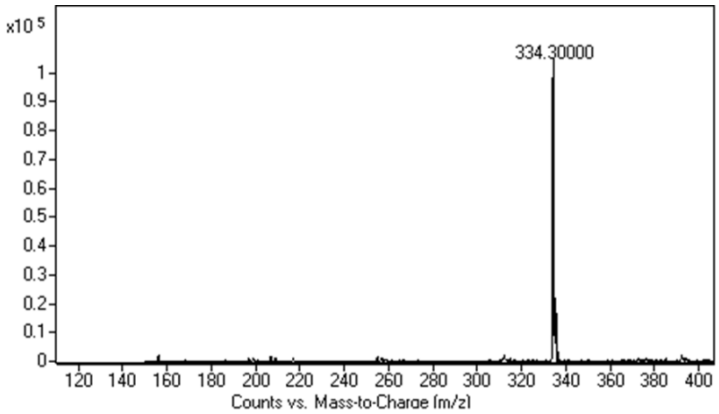

Figure 43S: ESI MS spectrum of **103**

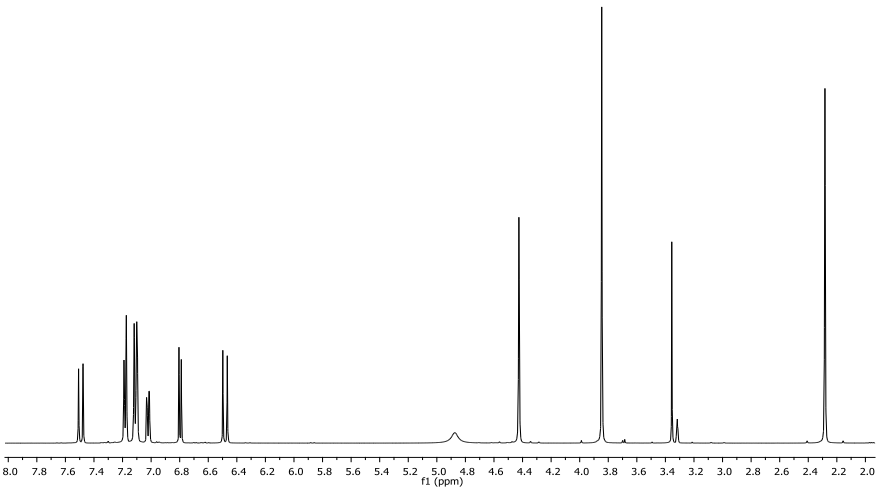

Figure 44s: ^{1}H NMR spectrum (CD_3OD, 500 MHz) of **103**

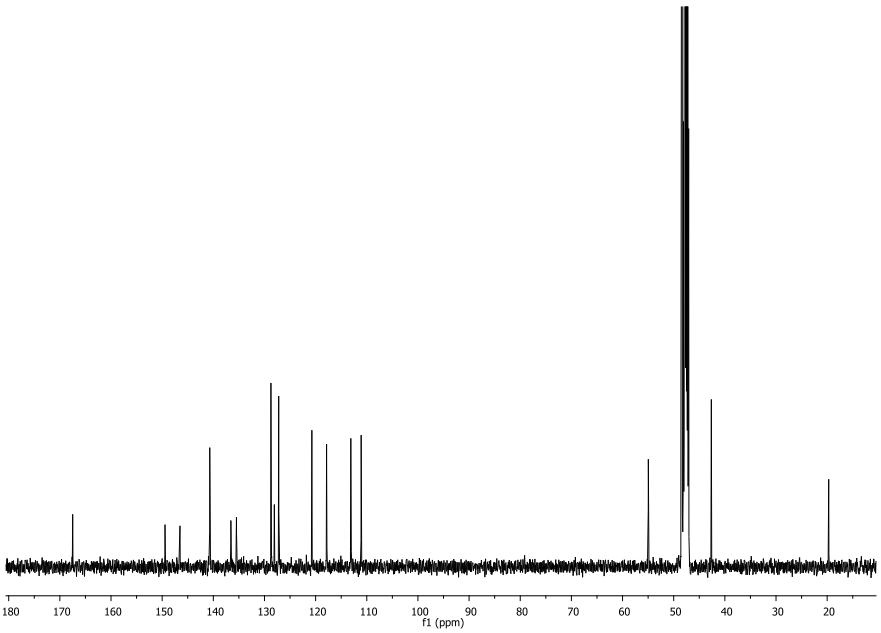

Figure 45S: ^{13}C NMR spectrum (CD_3OD, 125 MHz) of **103**

Amide 105

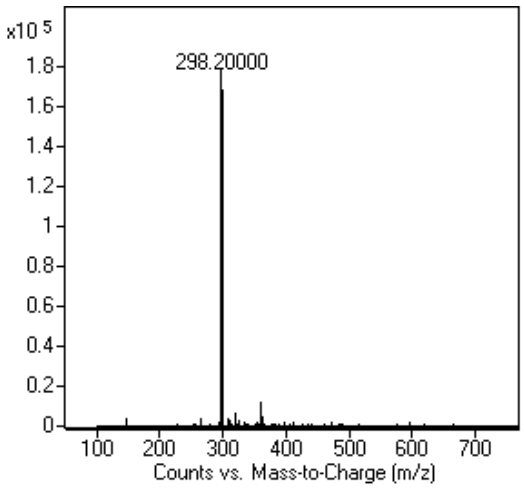

Figure 46S: ESI MS spectrum of **105**

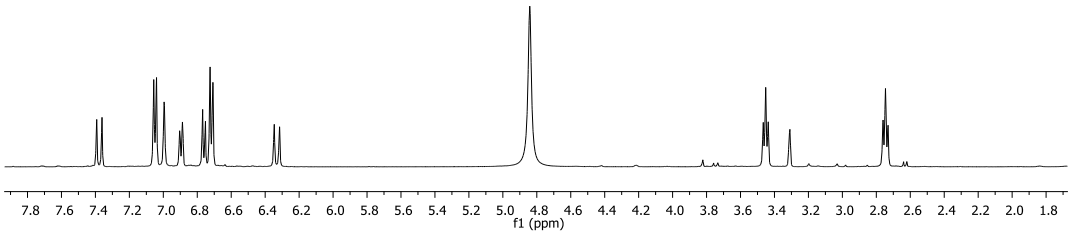

Figure 47S: ^{1}H NMR spectrum (CD_3OD, 500 MHz) of **105**

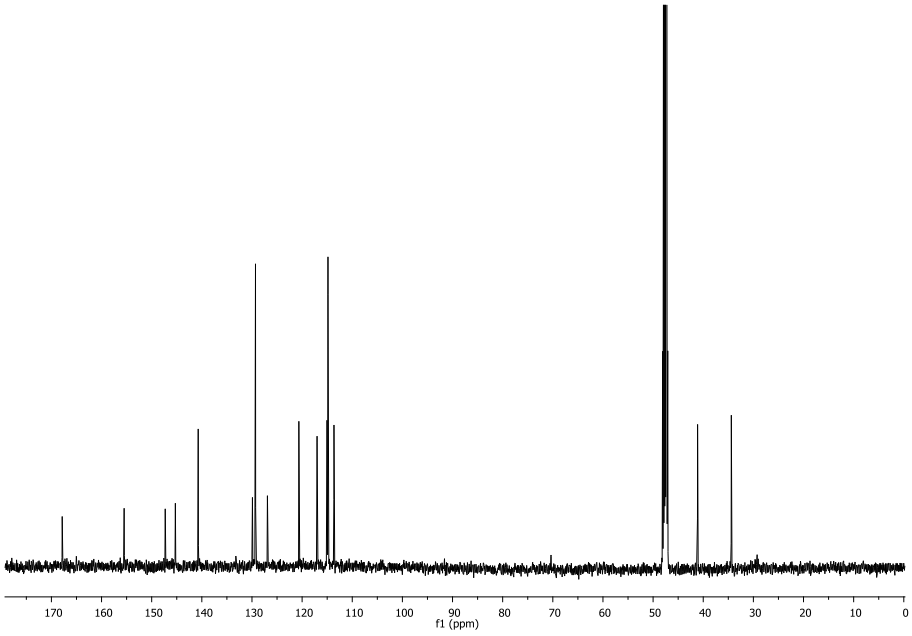

Figure 48S: ^{13}C NMR spectrum of (CD_3OD, 125 MHz) of **105**

Amide 106

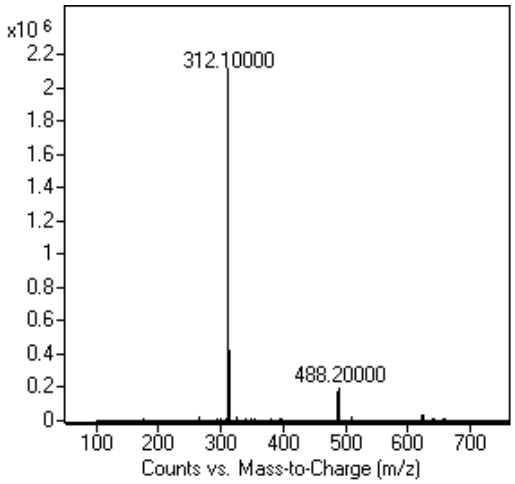

Figure 49S: ESI MS spectrum of **106**

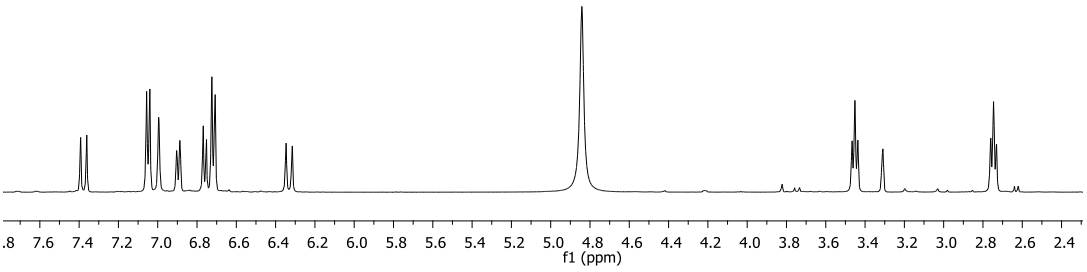

Figure 50S: ^{1}H NMR spectrum (CD_3OD, 500 MHz) of **106**

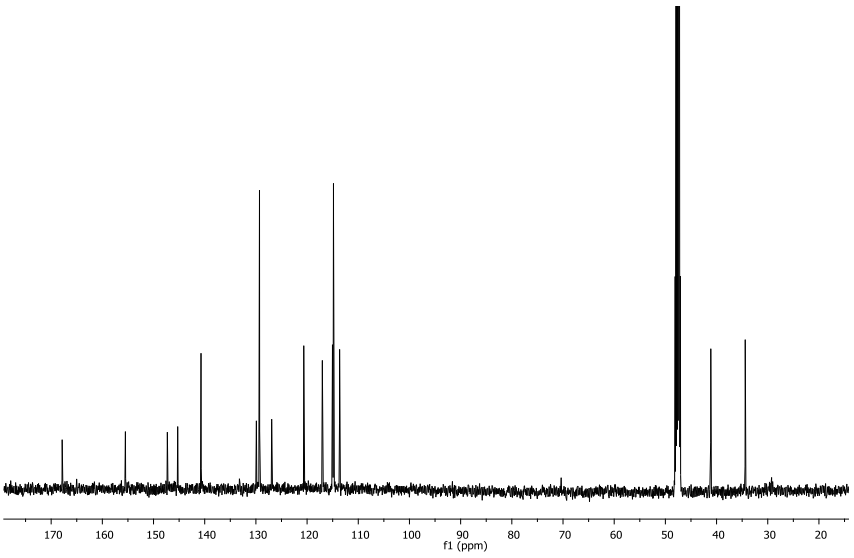

Figure 51S: ^{13}C NMR spectrum (CD_3OD, 125 MHz) of **106**

Amide 107

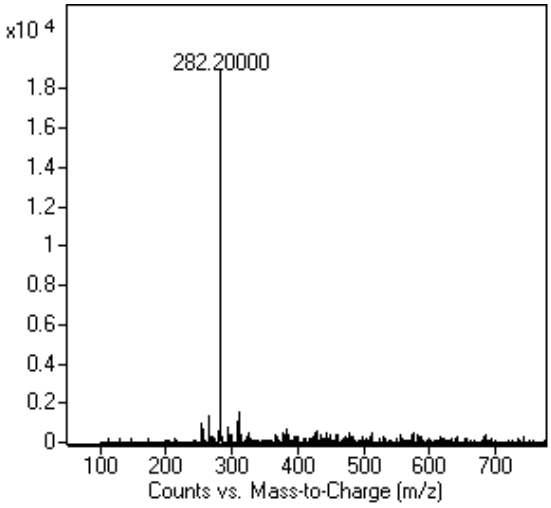

Figure 52S: ESI MS spectrum of **107**

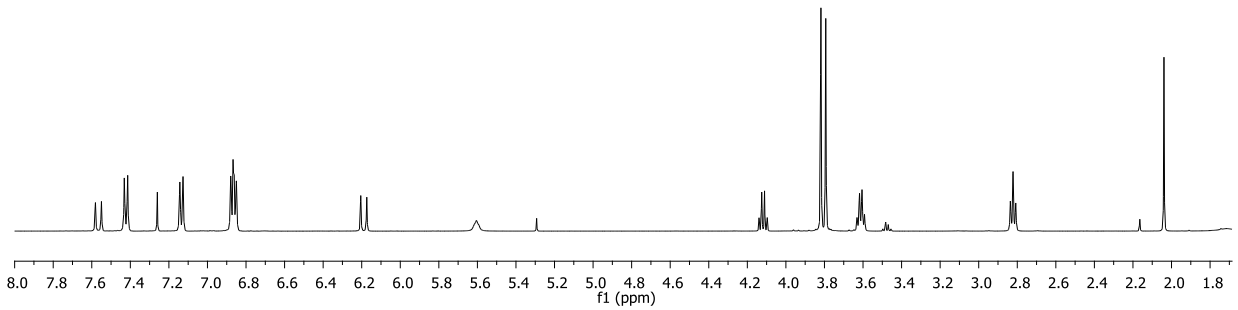

Figure 53S: ^{1}H NMR spectrum (CD_3OD, 500 MHz) of **107**

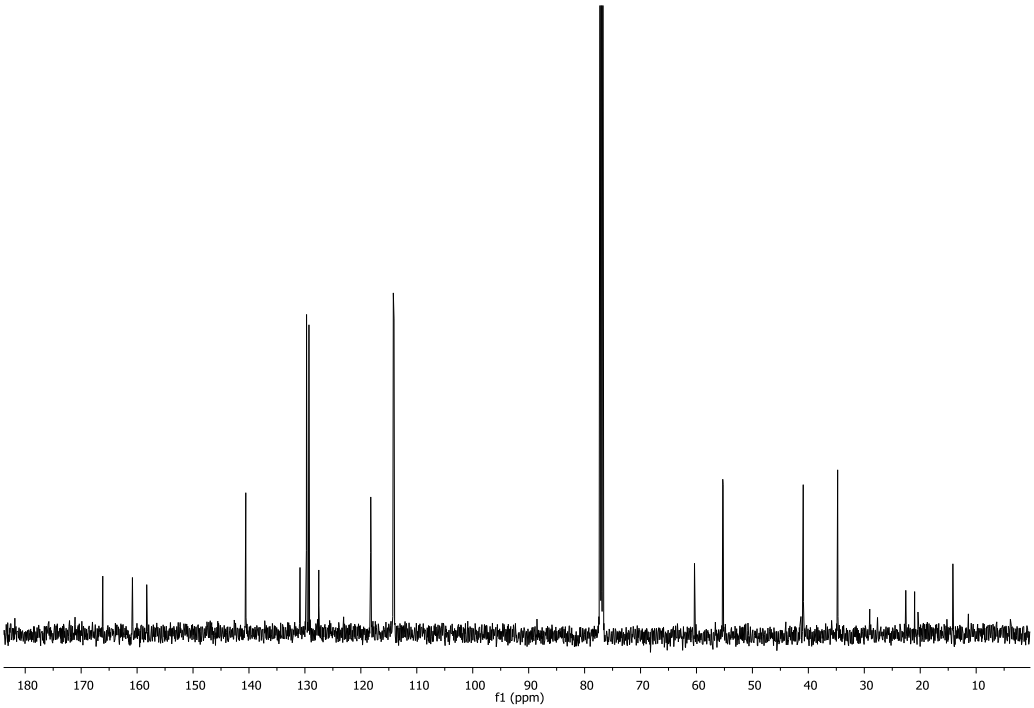

Figure 54S: ^{13}C NMR spectrum (CD_3OD, 125 MHz) of **107**

Amide 108

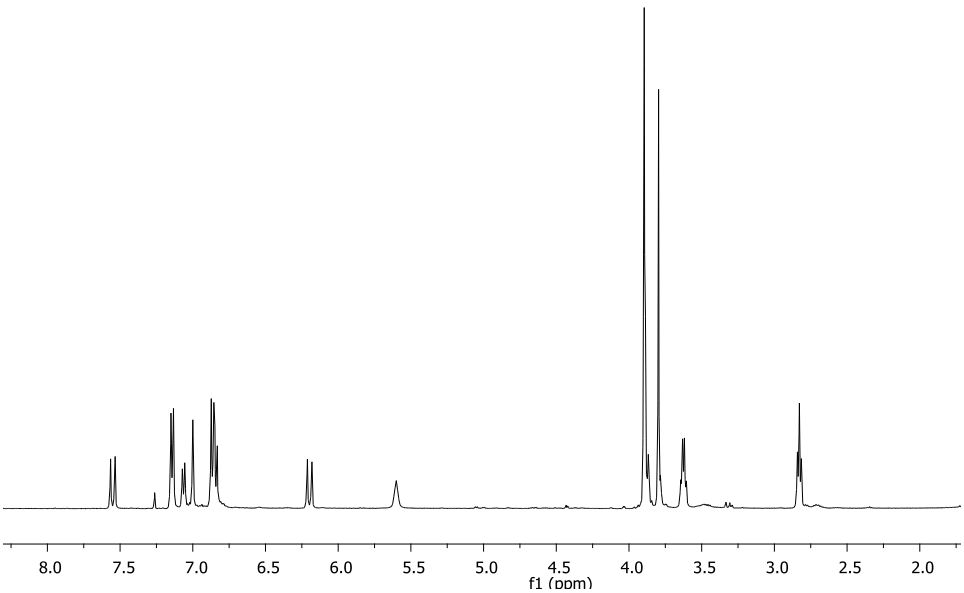

Figure 55S: ^{1}H NMR spectrum ($CDCl_3$, 500 MHz) of **108**

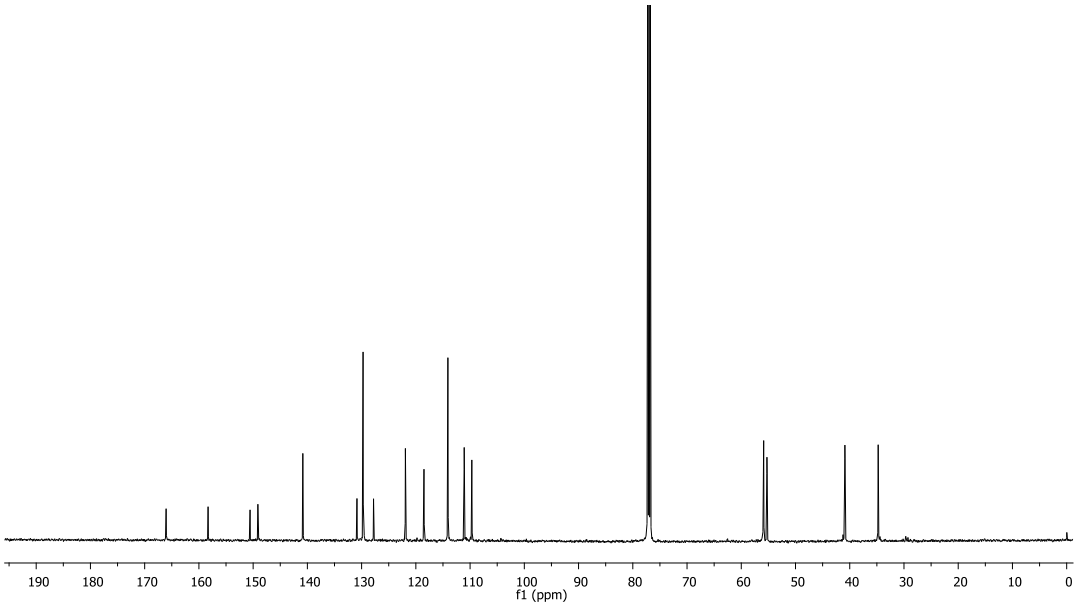

Figure 56S: ^{13}C NMR spectrum ($CDCl_3$, 125 MHz) of **108**

Amide 112

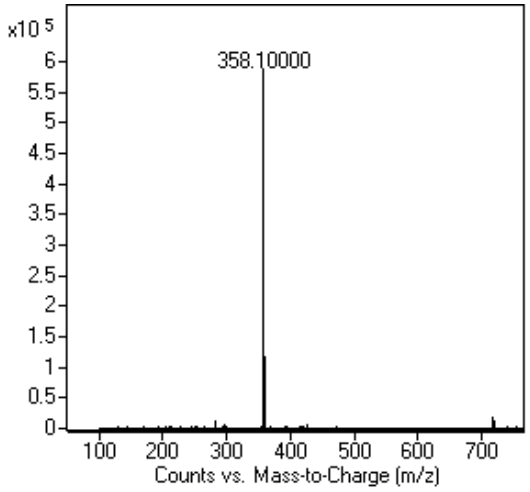

Figure 57S: ESI MS spectrum of **112**

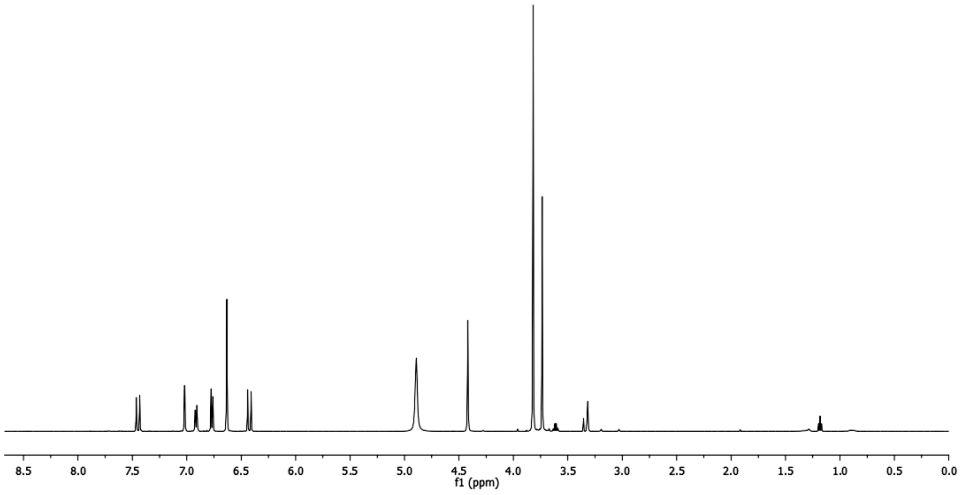

Figure 58S: ^{1}H NMR spectrum (CD_3OD, 500 MHz) of **112**

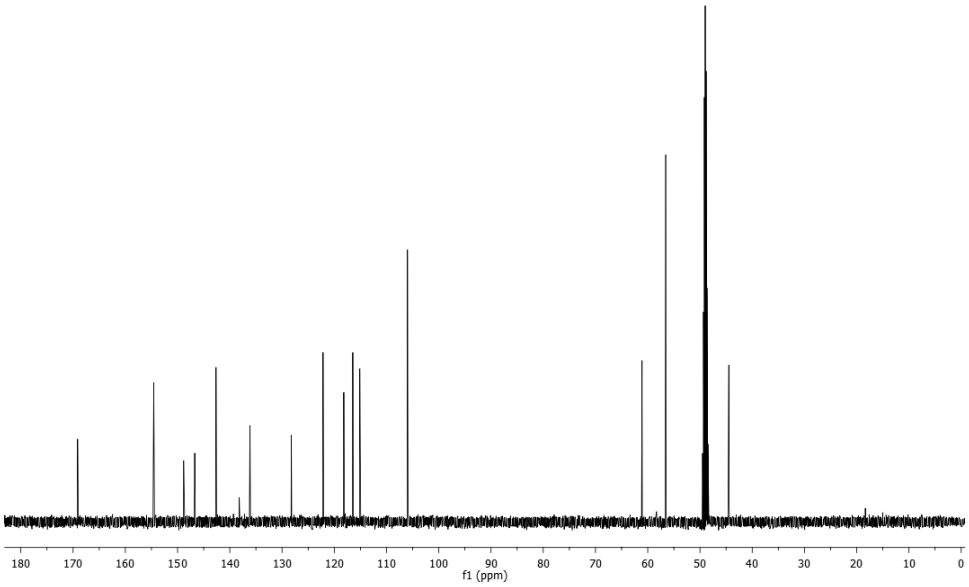

Figure 59S: ^{13}C NMR spectrum (CD_3OD, 125 MHz) of **112**

Amide 113

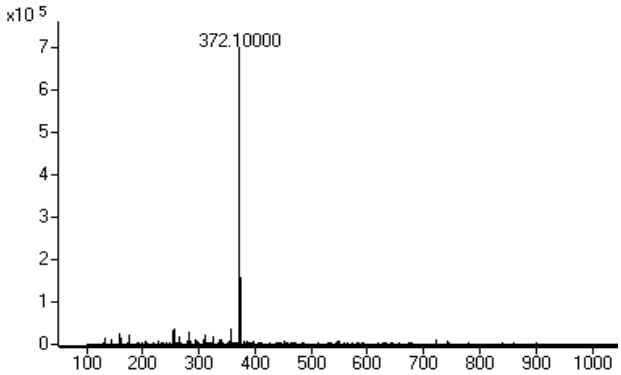

Figure 60S: ESI Mass spectrum of **113**

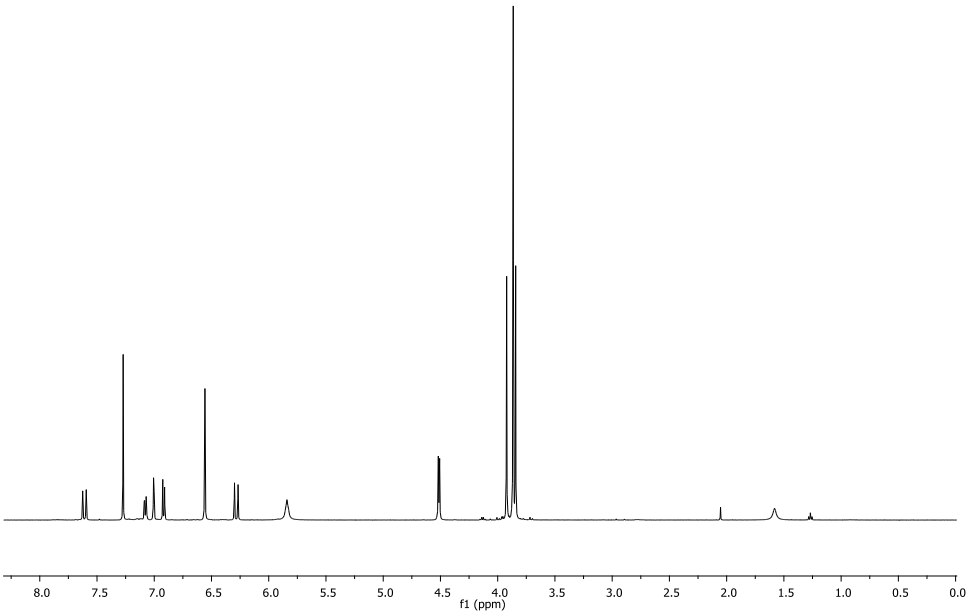

Figure 61S: ^{1}H-NMR (500 MHz, $CDCl_3$) spectrum of **113**

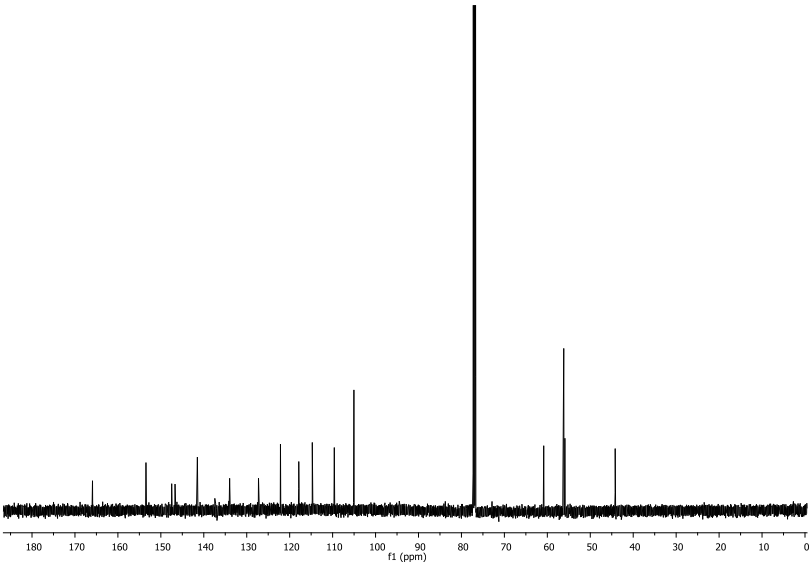

Figure 62S: ^{13}C-NMR (125 MHz, $CDCl_3$) spectrum of **113**

Amide 114

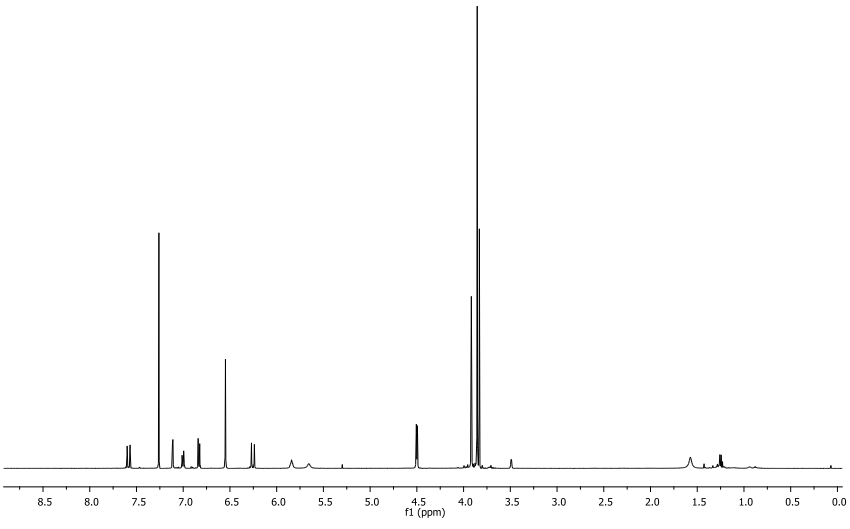

Figure 63S: ^{1}H NMR spectrum ($CDCl_3$, 500 MHz) of **114**

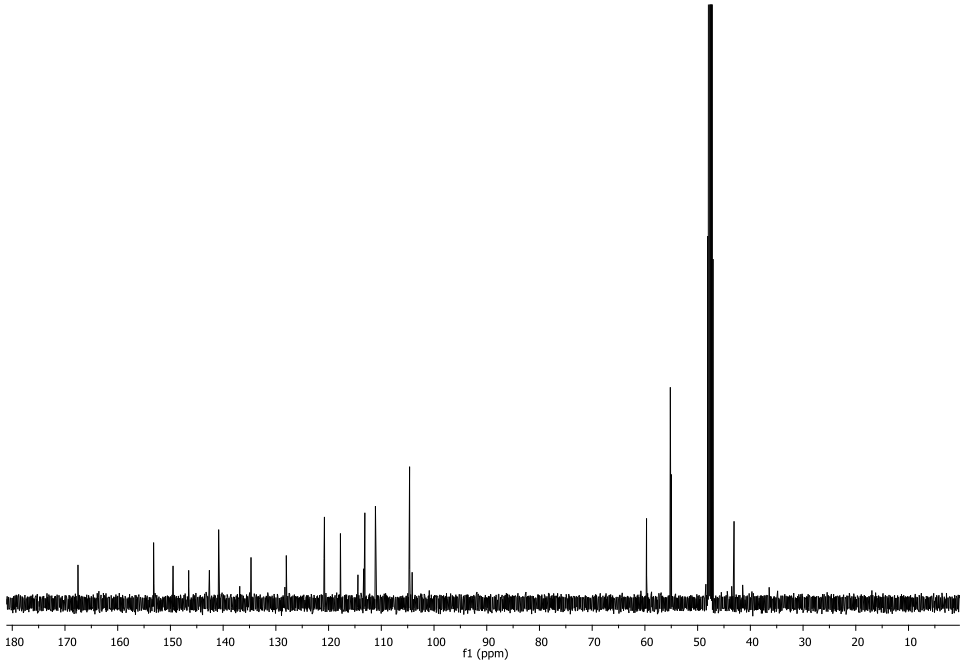

Figure 64S: ^{13}C NMR spectrum ($CDCl_3$, 125 MHz) of **114**

Amide 116

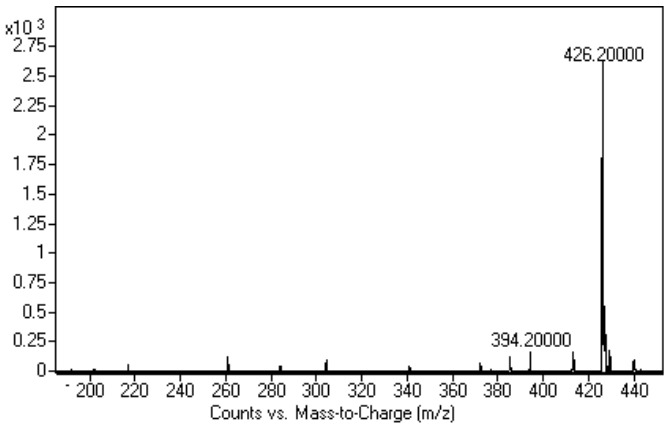

Figure 65S: ES MS spectrum of **116**

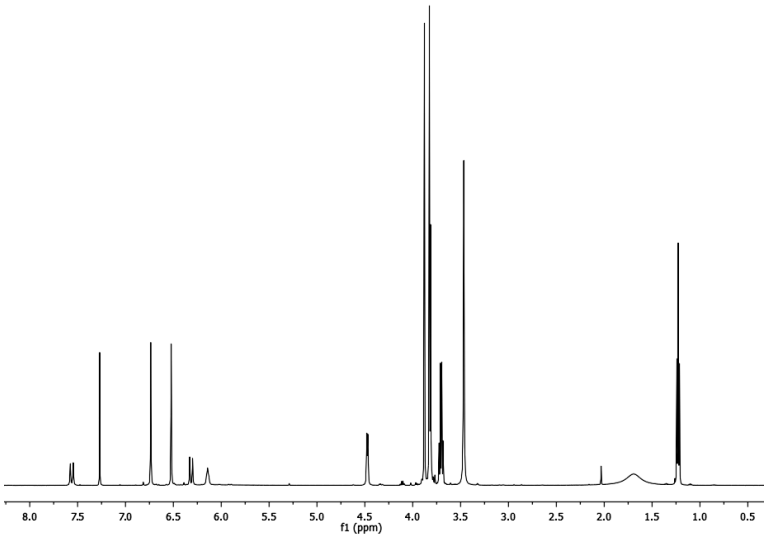

Figure 66S: ^{1}H NMR spectrum($CDCl_3$, 500 MHz) of **116**

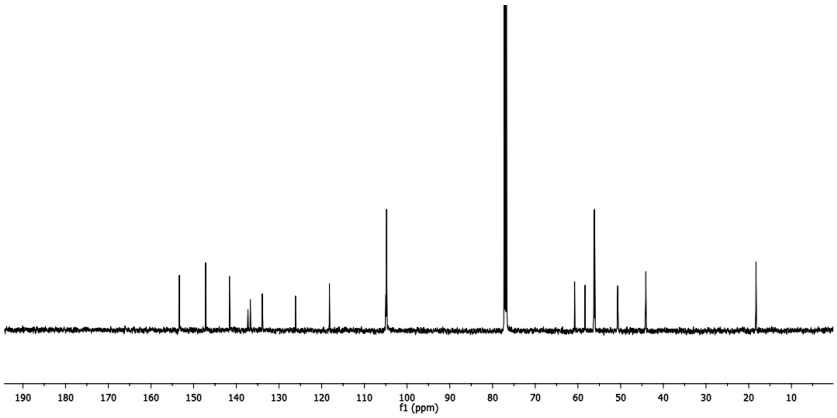

Figure 67S: ^{13}C-NMR spectrum($CDCl_3$, 125 MHz) of **116**

Amide 117

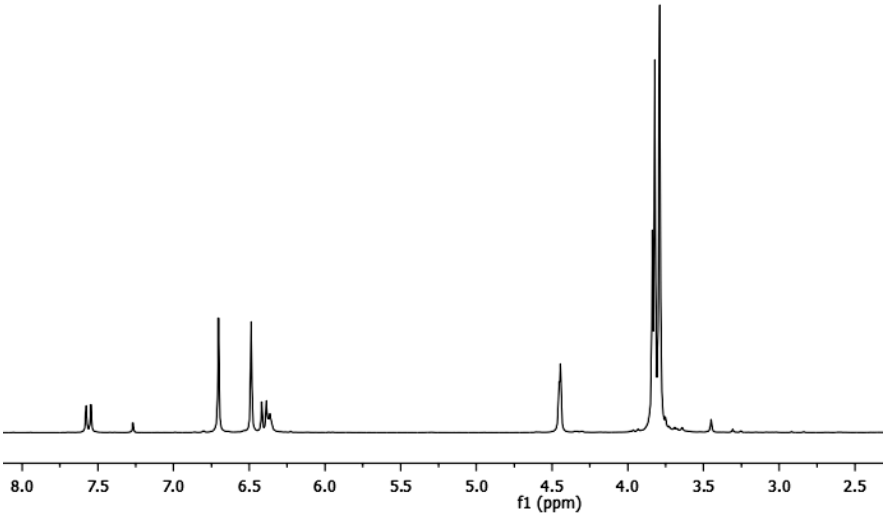

Figure 68S: ^{1}H NMR spectrum ($CDCl_3$, 500 MHz) of **117**

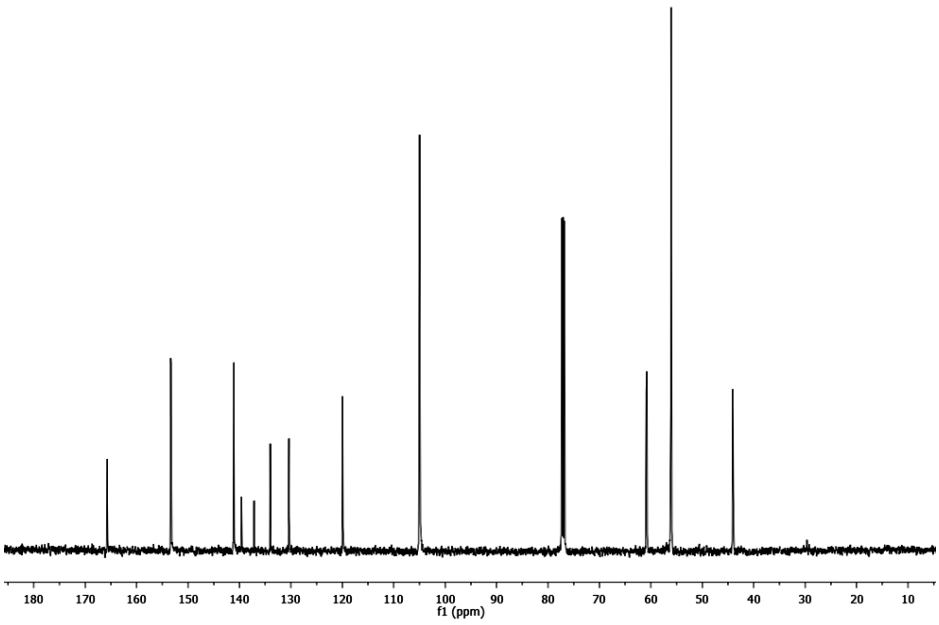

Figure 69S: ^{13}C NMR spectrum ($CDCl_3$, 125 MHz) of **117**

Amide 118

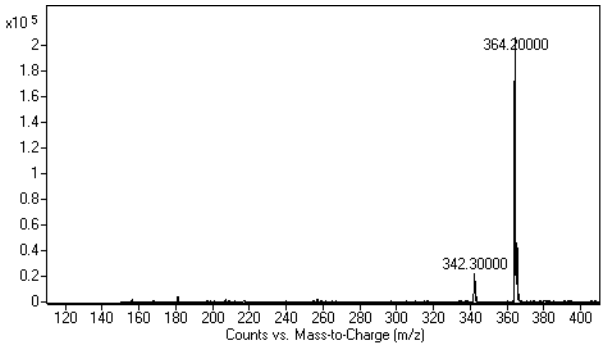

Figure 70S: ESI MS spectrum of **118**

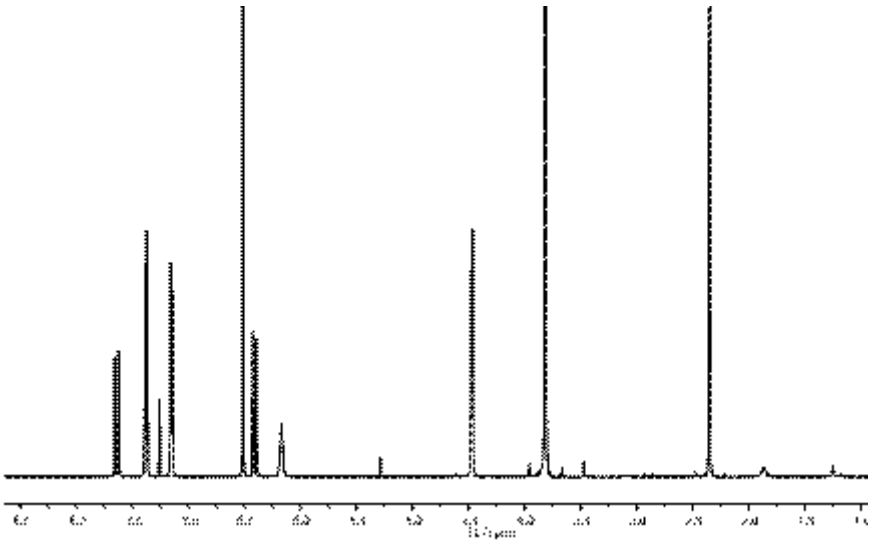

Figure 71S: ^{1}H NMR spectrum ($CDCl_3$, 500 MHz) of **118**

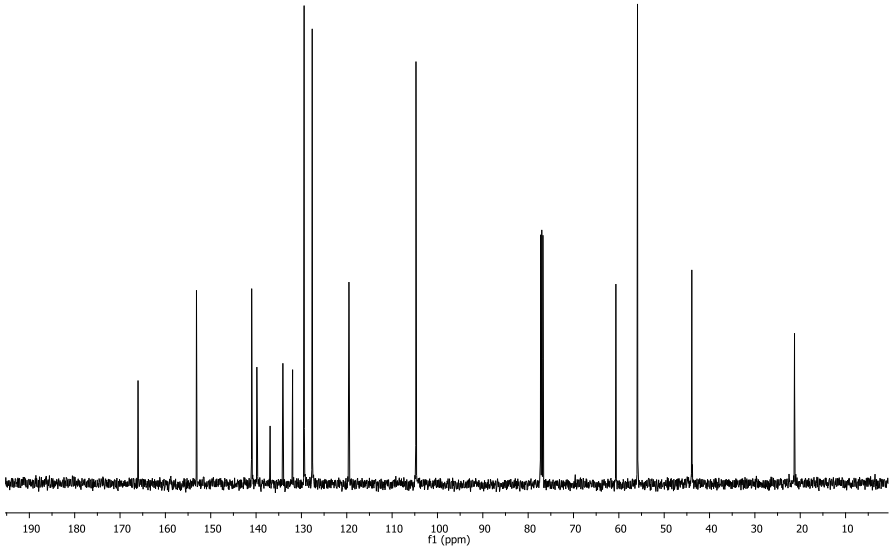

Figure 72S: ^{13}C NMR spectrum ($CDCl_3$, 125 MHz) of **118**

Amide 122

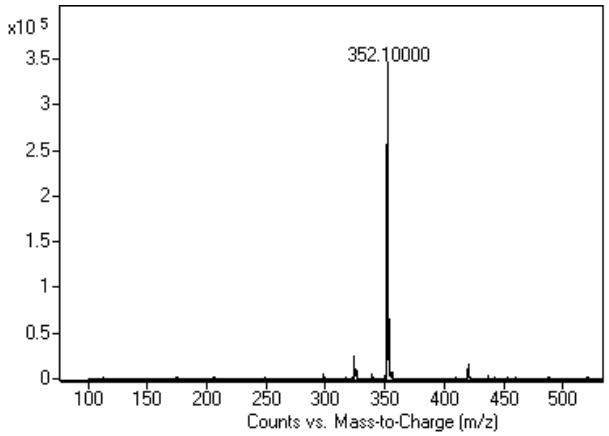

Figure 73S: ESI MS spectrum of **122**

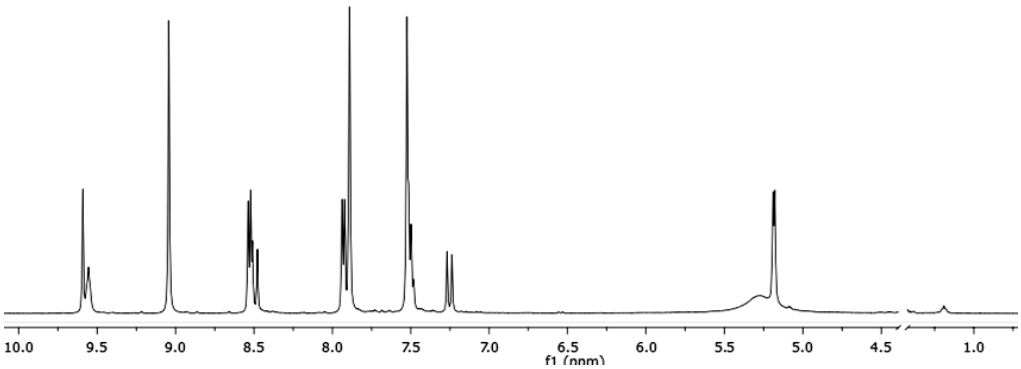

Figure 74S: ^{1}H NMR spectrum (500 MHz, pyridine-d_5) of **122**

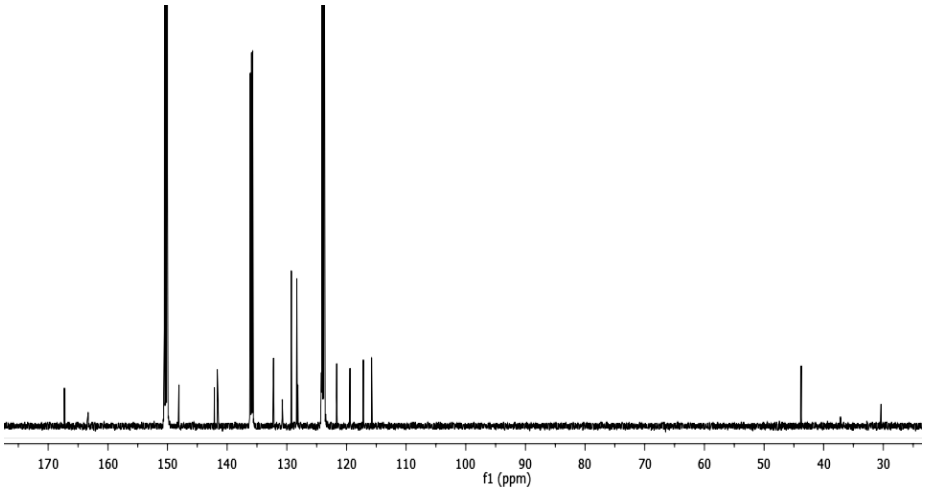

Figure 75S: ^{13}C NMR spectrum (125 MHz, pyridine-d_5) of **122**

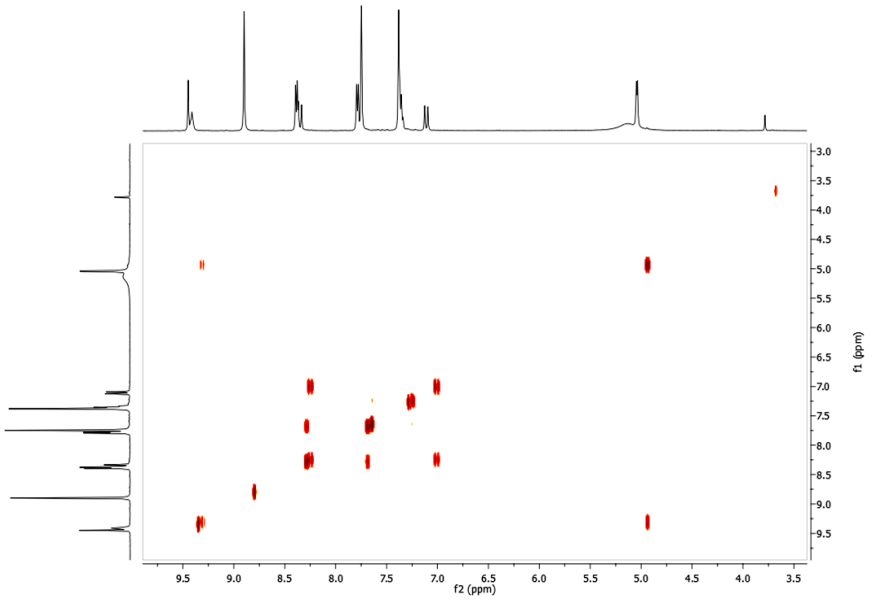

Figure 76S:gCOSY spectrum of **122**

Amide 123

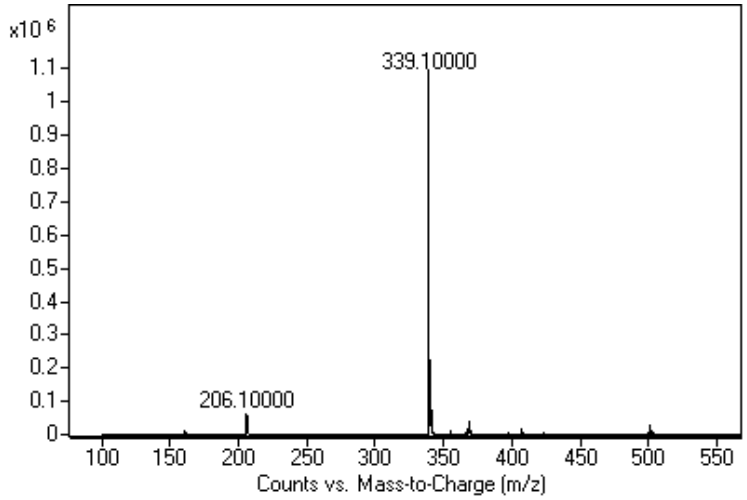

Figure 77S: ESI MS spectrum of **123**

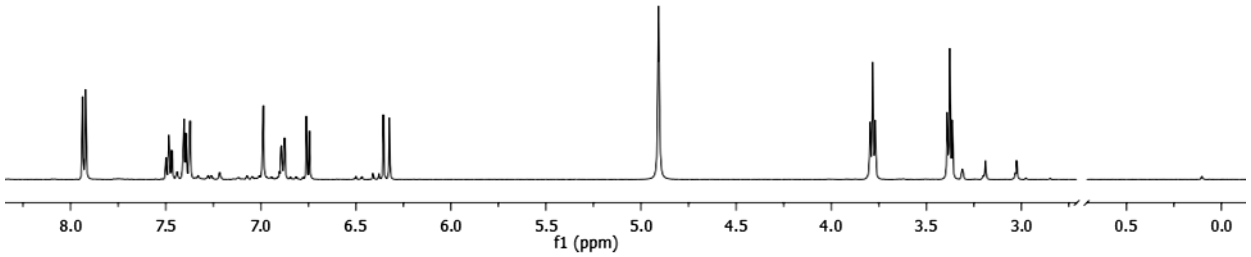

Figure 78S: ^{1}H NMR spectrum (CD_3OD, 500 MHz) of **123**

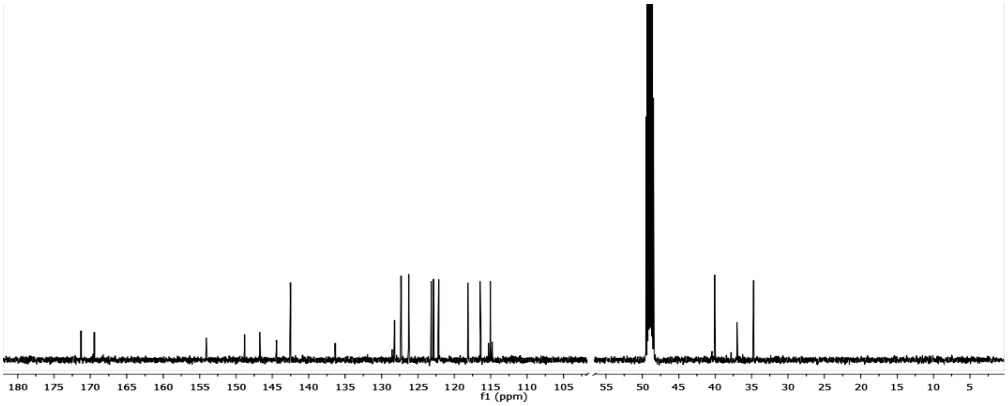

Figure 79S: ^{13}C NMR spectrum (CD_3OD, 125 MHz) of **123**

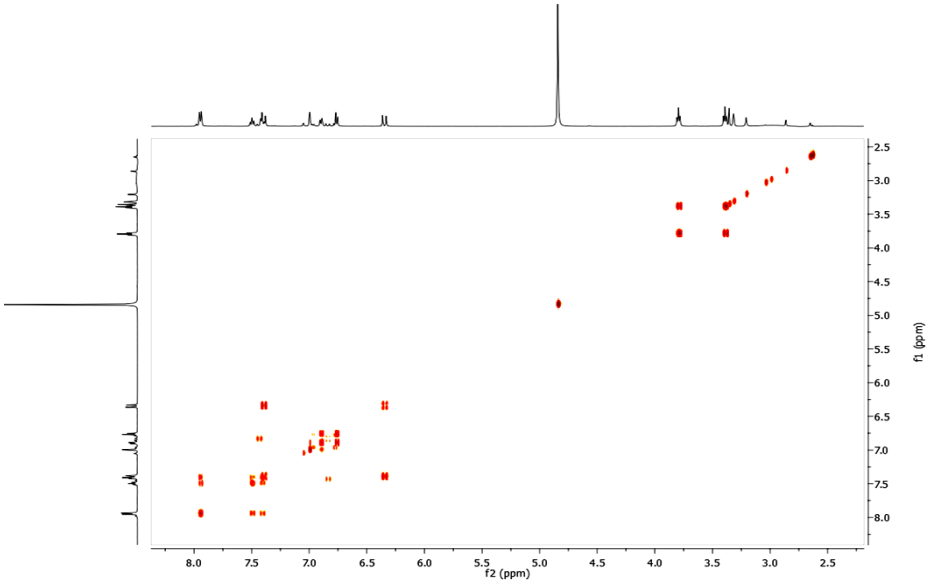

Figure 80S: gCOSY spectrum of **123**

Amide 124

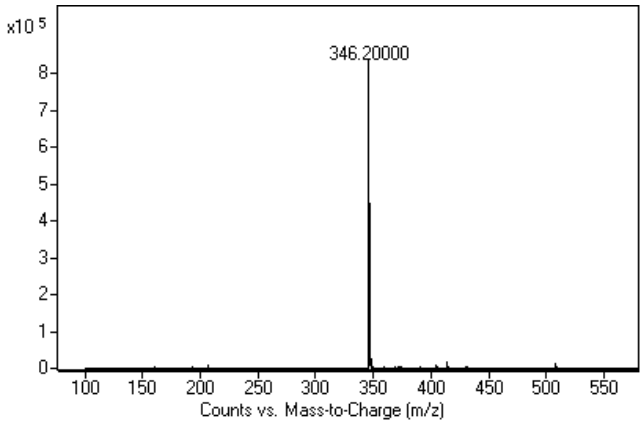

Figure 81S: ESI MS spectrum of **124**

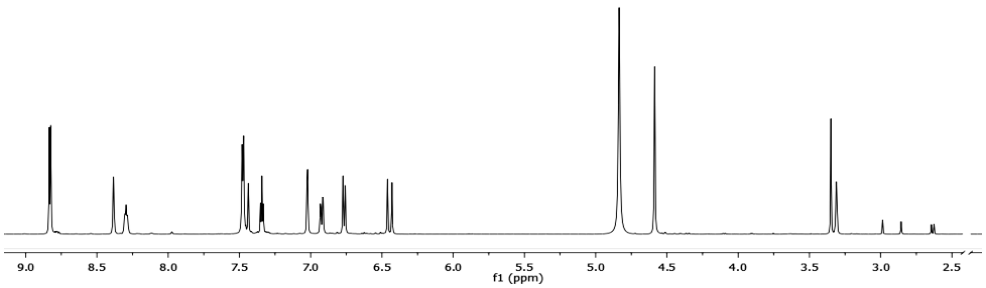

Figure 82S: ^{1}H NMR spectrum (500 MHz, CD_3OD) of **124**

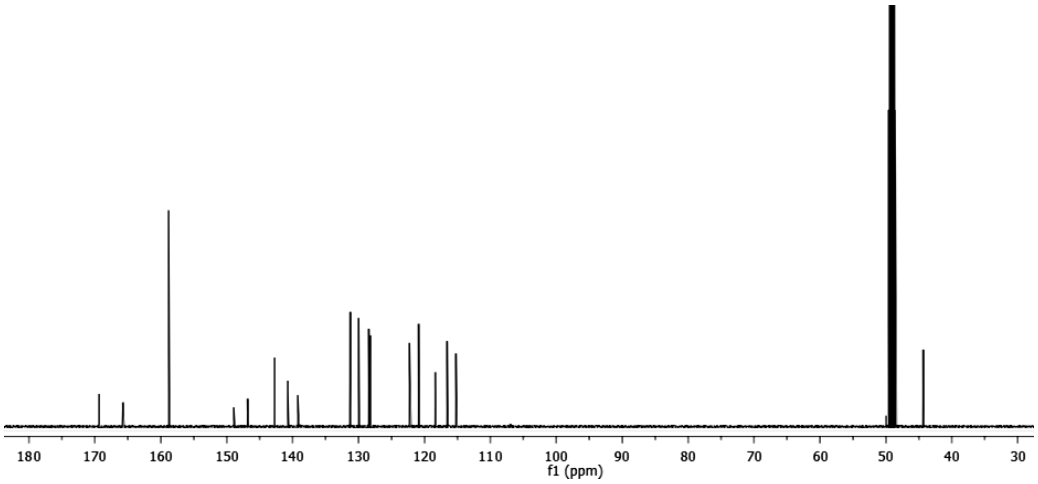

Figure 83S: ^{13}C NMR spectrum (125 MHz, CD_3OD) of **124**

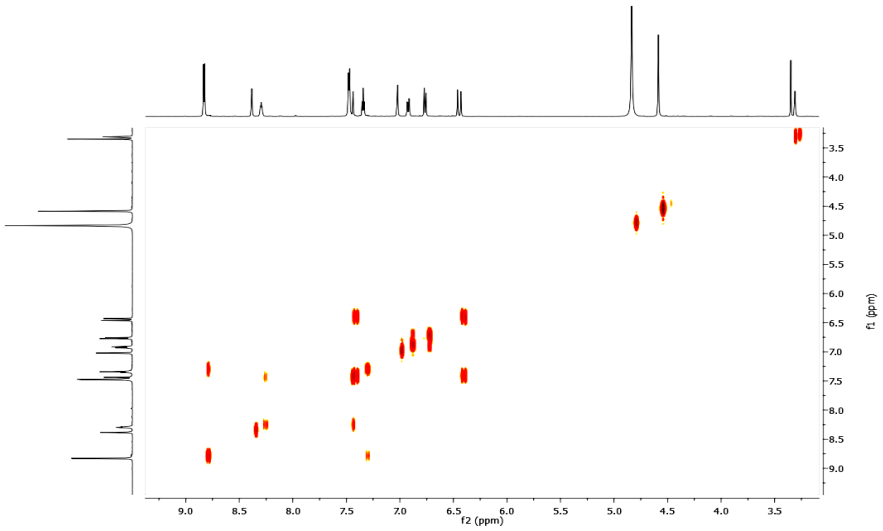

Figure 84S: gCOSY spectrum of **124**

Amide 125

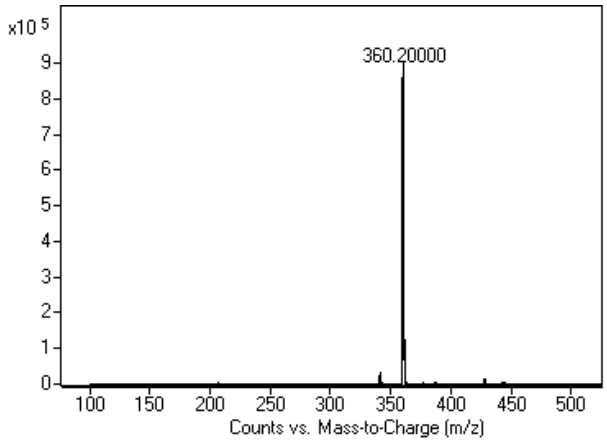

Figure 85S: ESI-MS spectrum of **125**

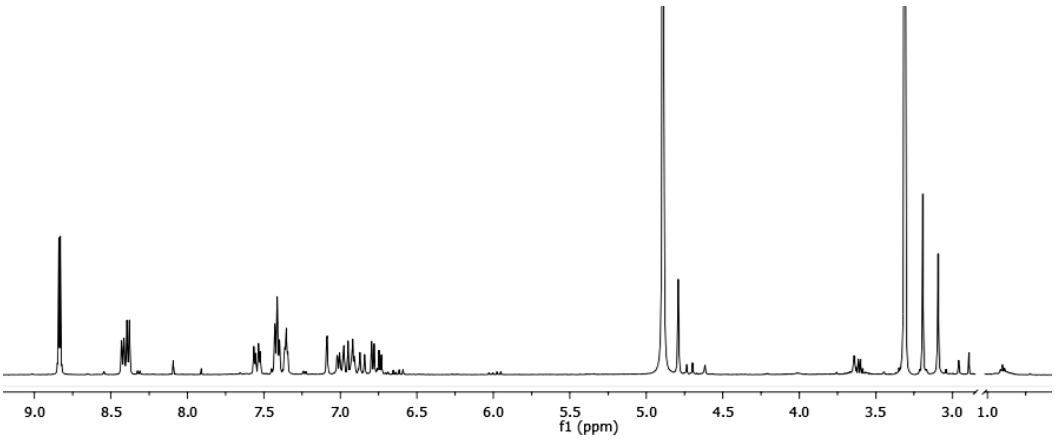

Figure 86S: ^{1}H NMR spectrum (500 MHz, CD3OD) of **125**

Amide 126

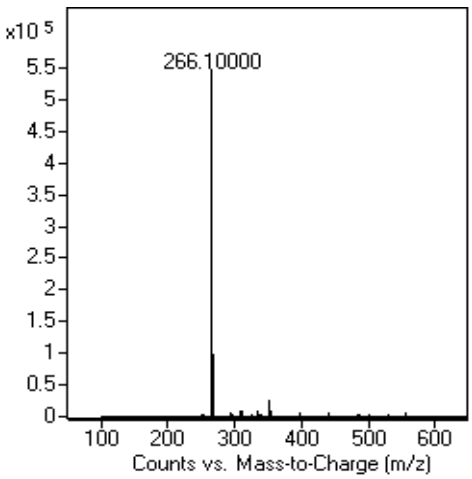

Figure 87S: ESI MS spectrum of **126**

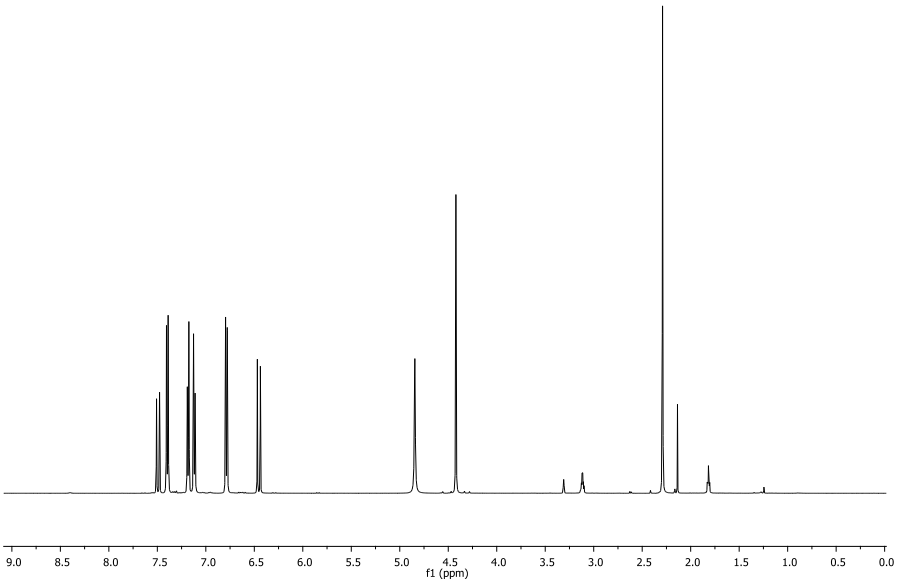

Figure 88S: ^{1}H NMR spectrum (CD_3OD, 500 MHz) of **126**

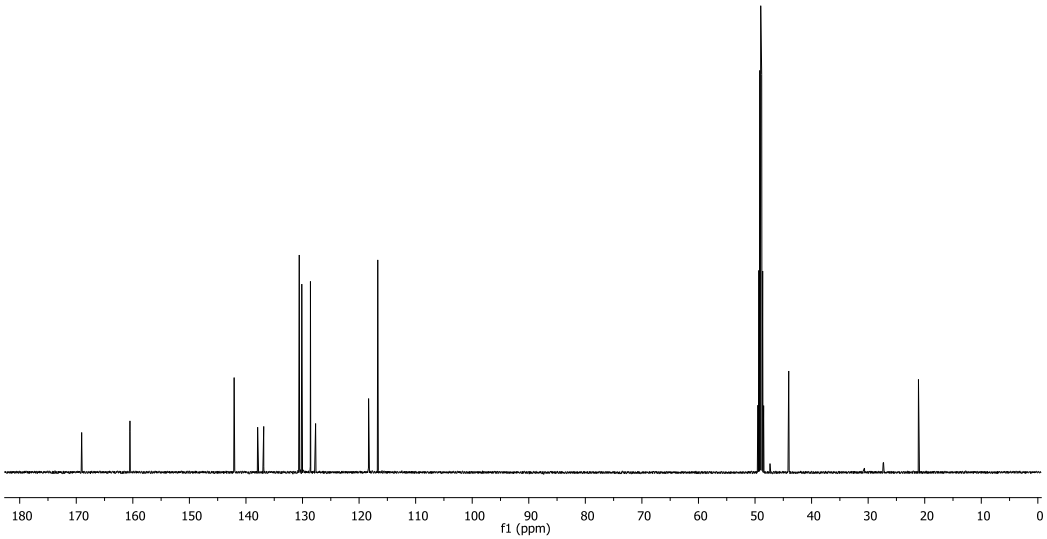

Figure 89S: ^{13}C NMR spectrum (CD_3OD, 125 MHz) of **126**

Amide 127

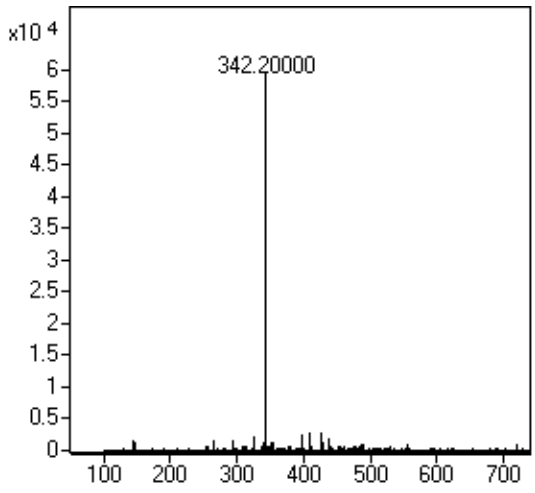

Figure 90S: ESI MS spectrum of **127**

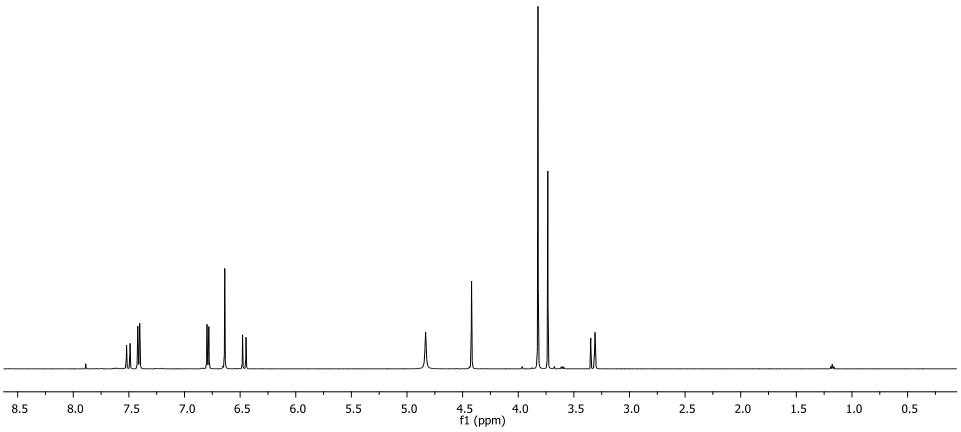

Figure 91S: ^{1}H NMR spectrum (CD_3OD, 500 MHz) of **127**

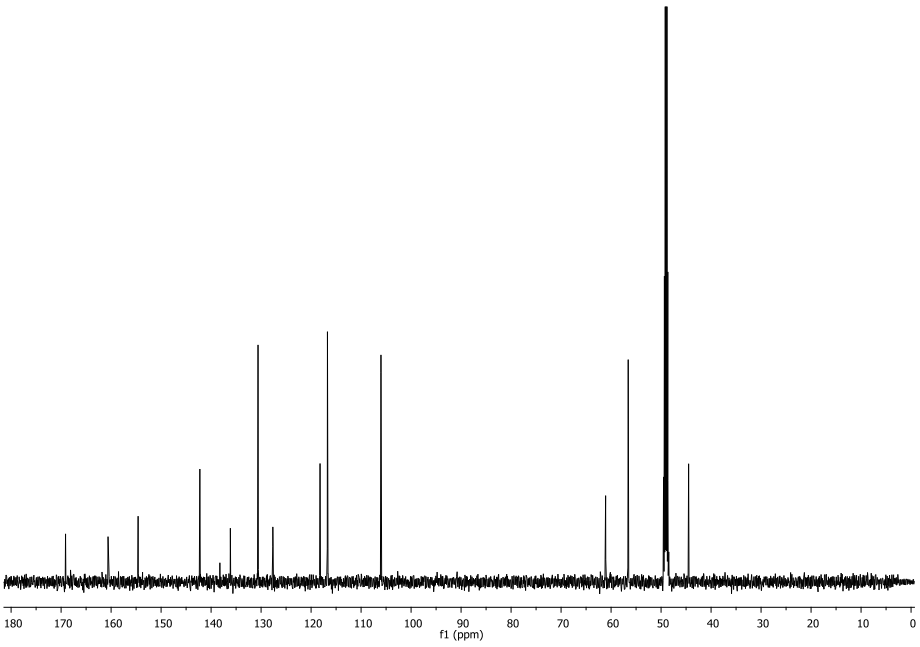

Figure 92S: ^{13}C NMR spectrum (CD_3OD, 125 MHz) of **127**

Amide 136

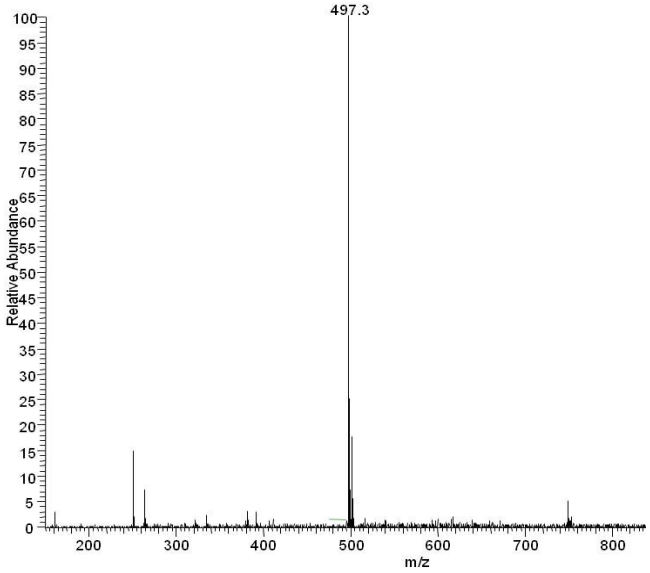

Figure 93S: ESI-MS spectrum of **132**

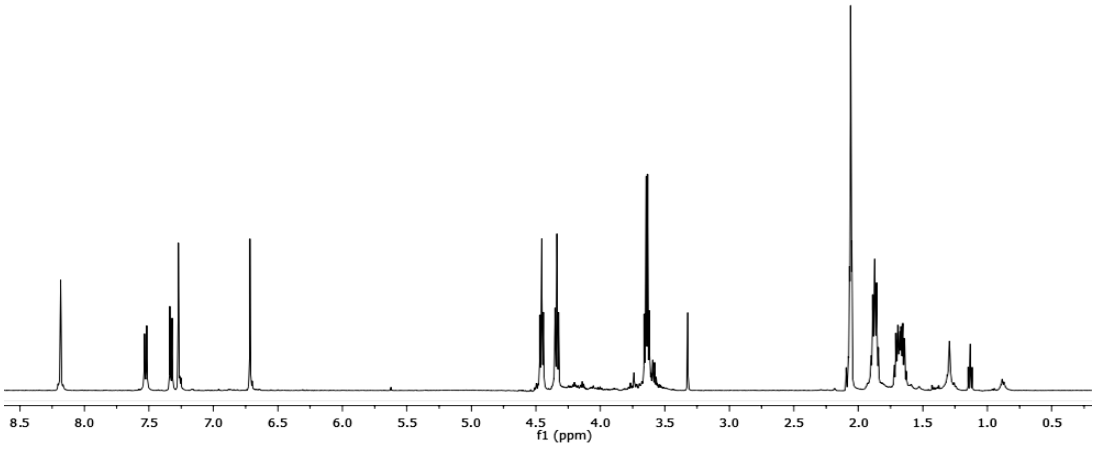

Figure 94S: ^{1}H NMR spectrum (500 MHz, acetone-d_6) of **132**

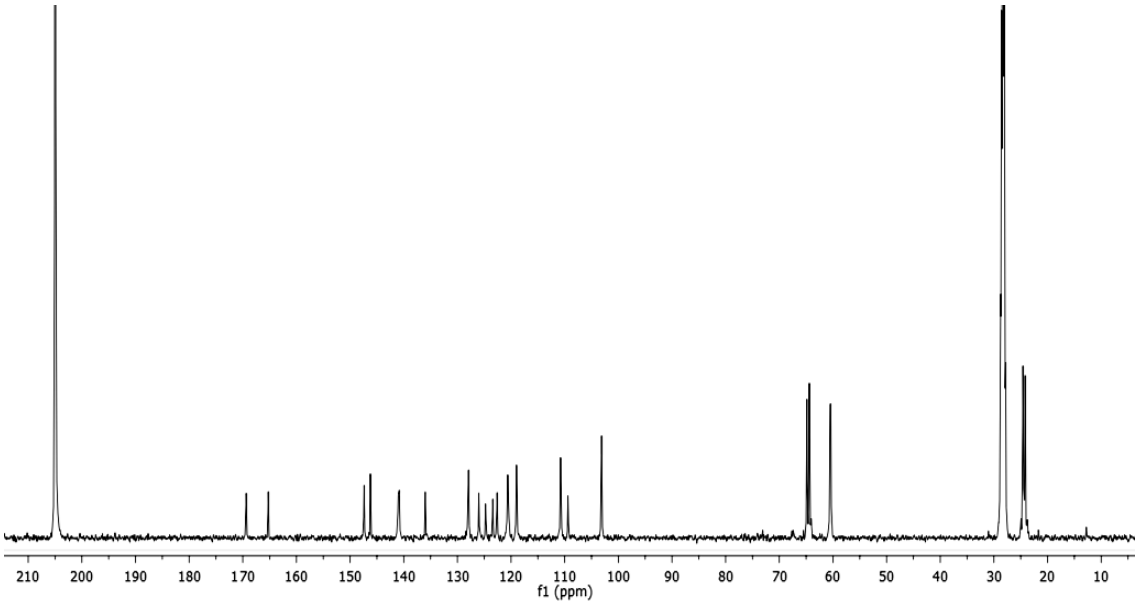

Figure 95S: ^{13}C NMR spectrum (125 MHz, acetone-d_6) of **132**

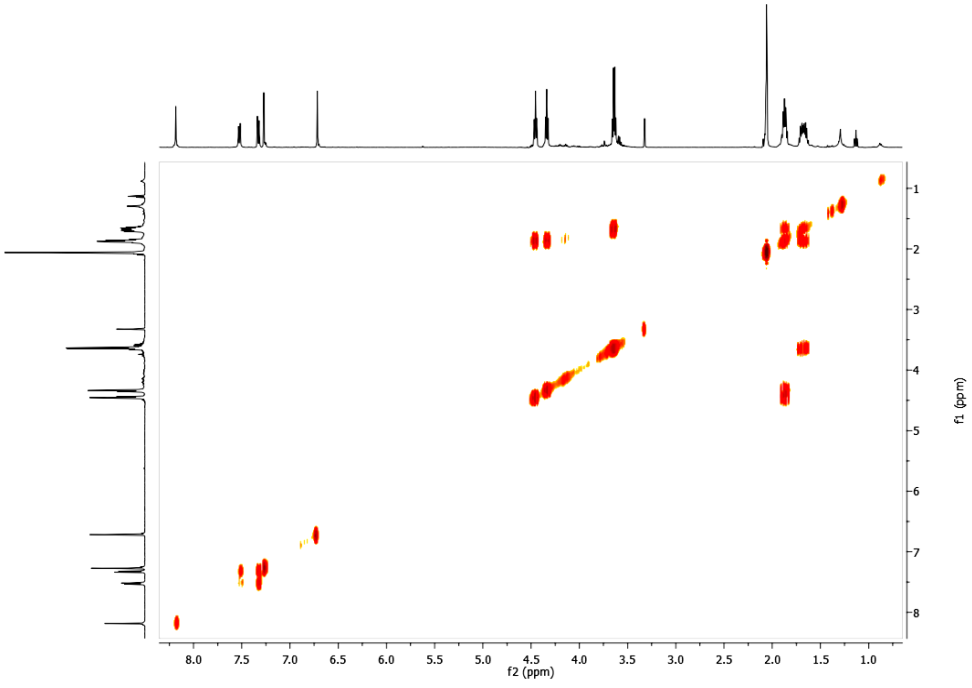

Figure 96S: gCOSY spectrum of **132**

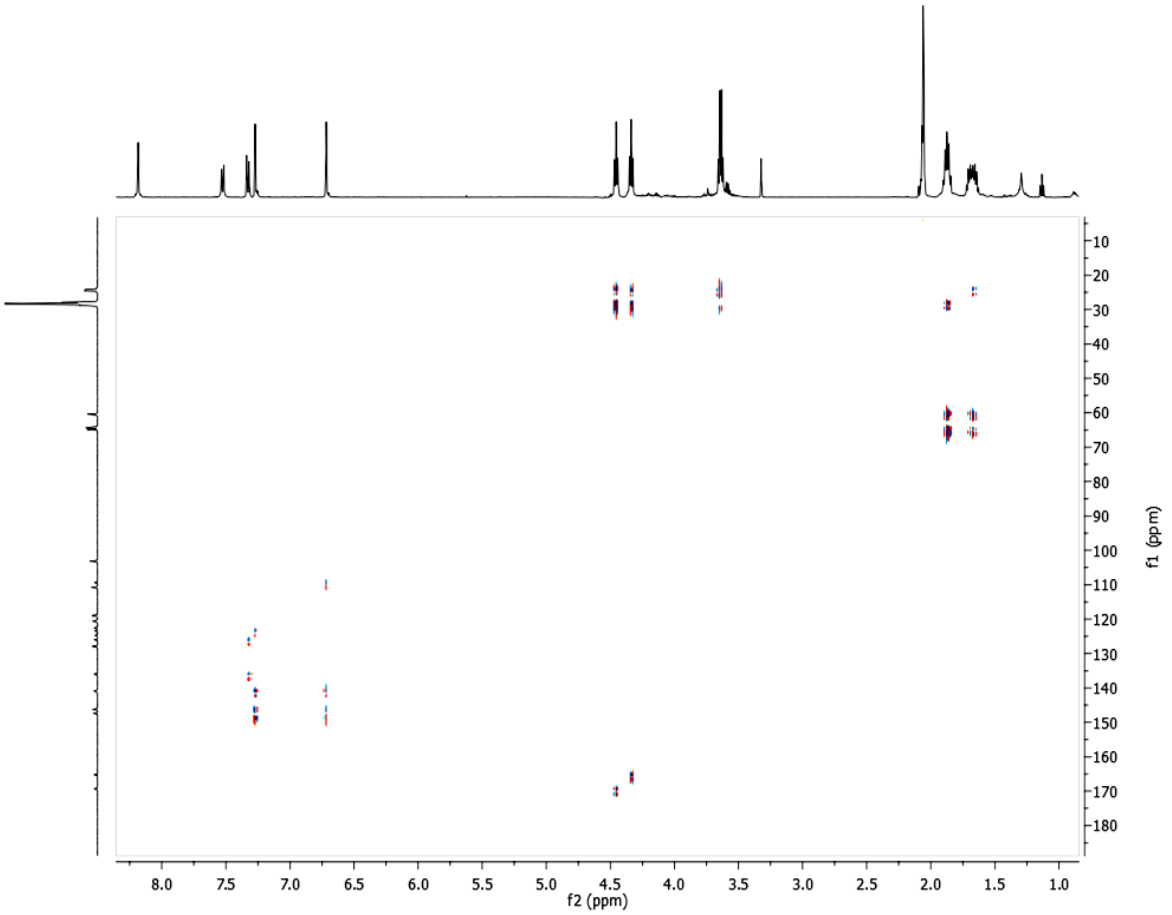

Figure 97S: gHMBCAD spectrum of **132**

7.3. APPENDIX C

In this section the MS and NMR spectra of neolignanamdes (±)-**59**, (±)-**128** – (±)-**135** and of the benzoxanthene lignan **137** are reported.

Trans-grossamide (±)-59

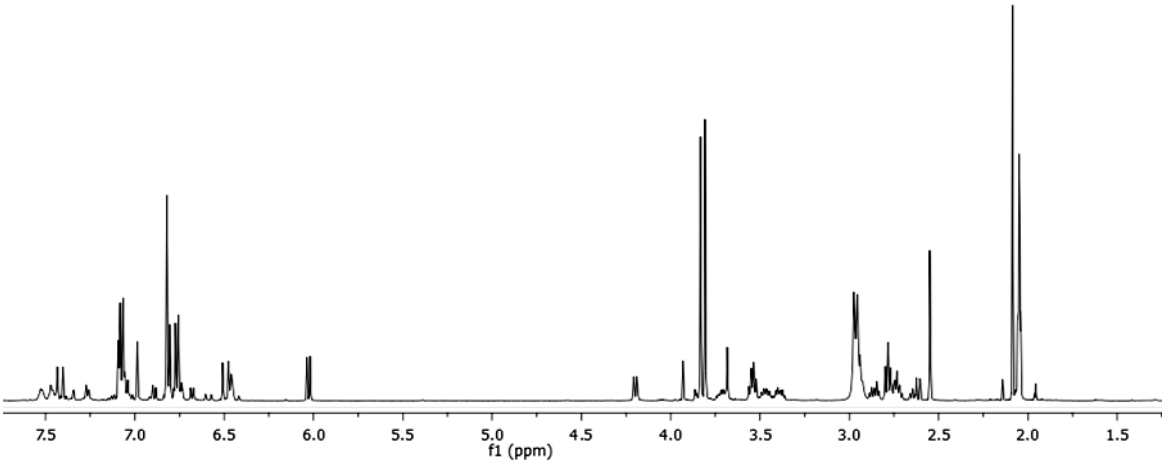

Figure 98S: ^{1}H NMR spectrum [$(CD_3)_2CO$, 500 MHz] of (±)-**59**

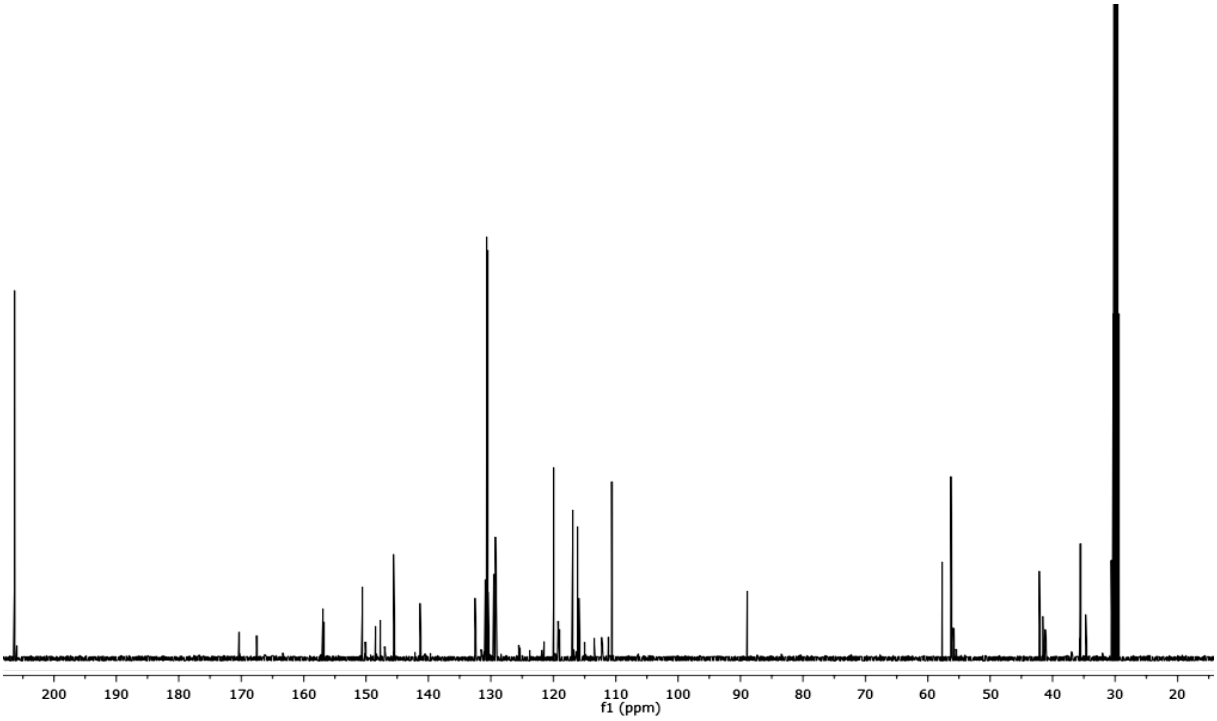

Figure 99S: ^{13}C NMR spectrum [$(CD_3)_2CO$, 125 MHz] of (±)-**59**

Neolignanamide (±)-128

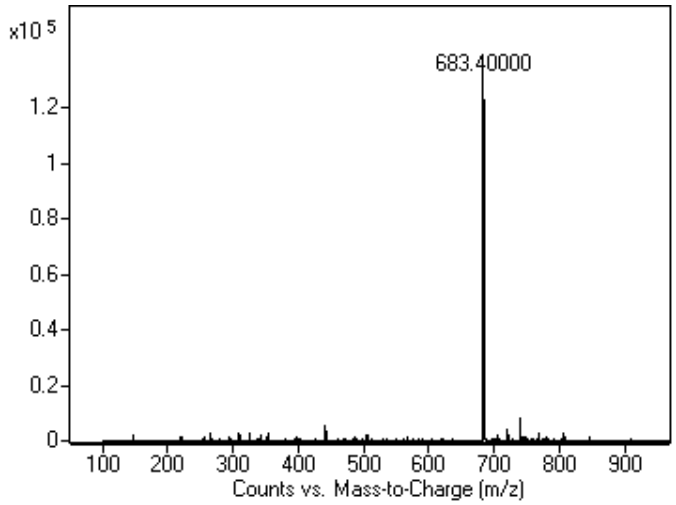

Figure 100S: ESI MS spectrum of **(±)-128**

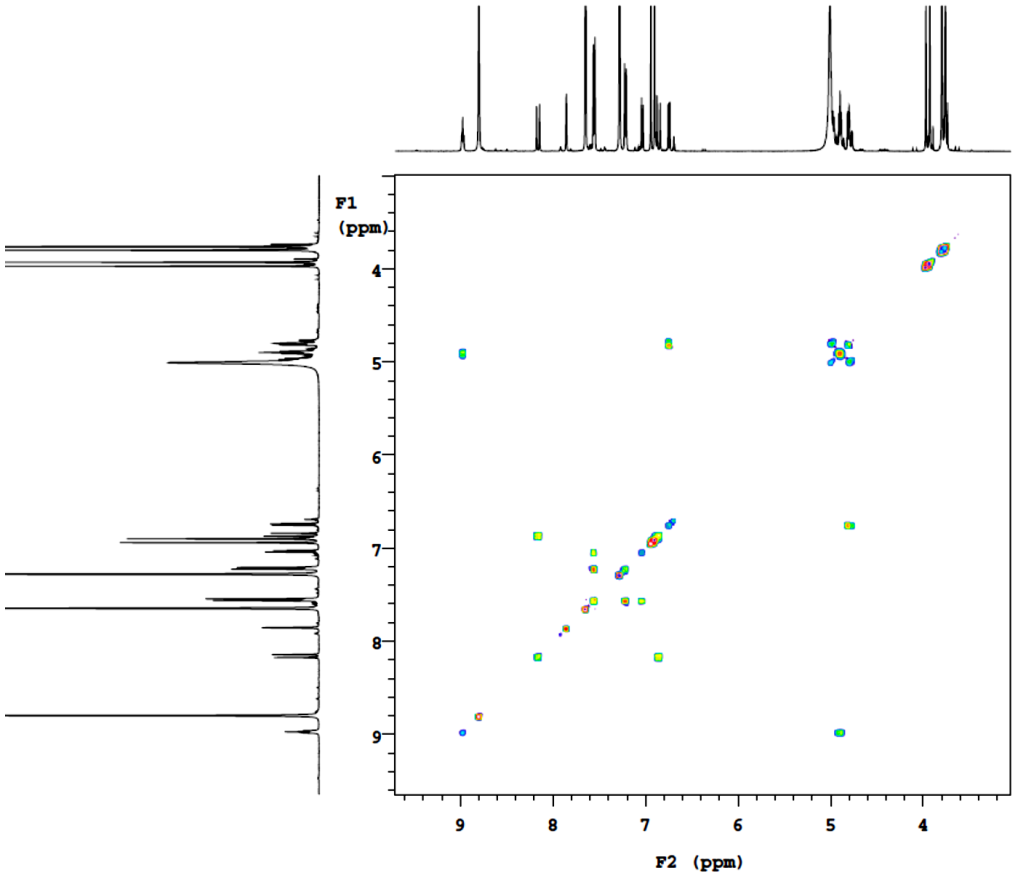

Figure 101S: g-COSY spectrum of **(±)-128**

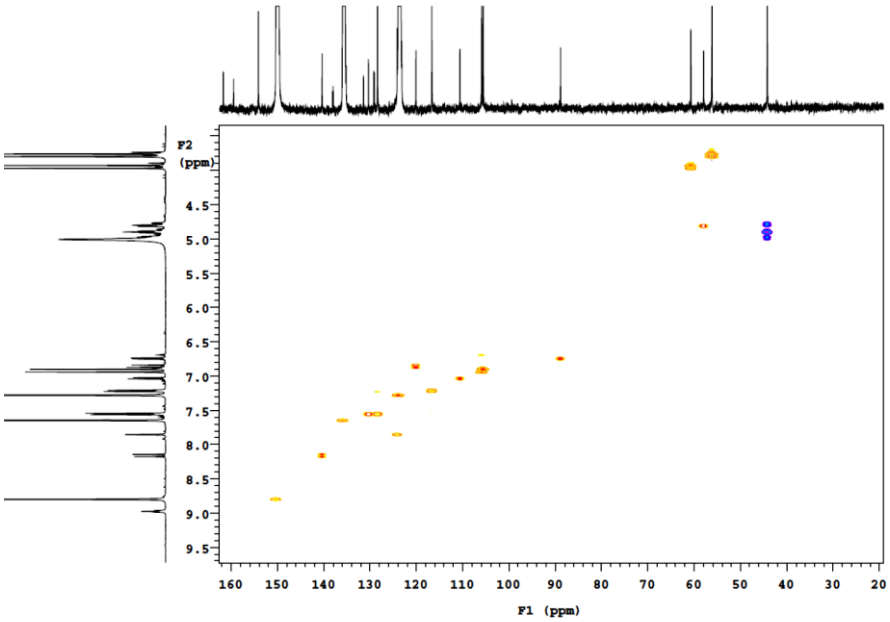

Figure 102S: g-HSQCAD spectrum of **(±)-128**

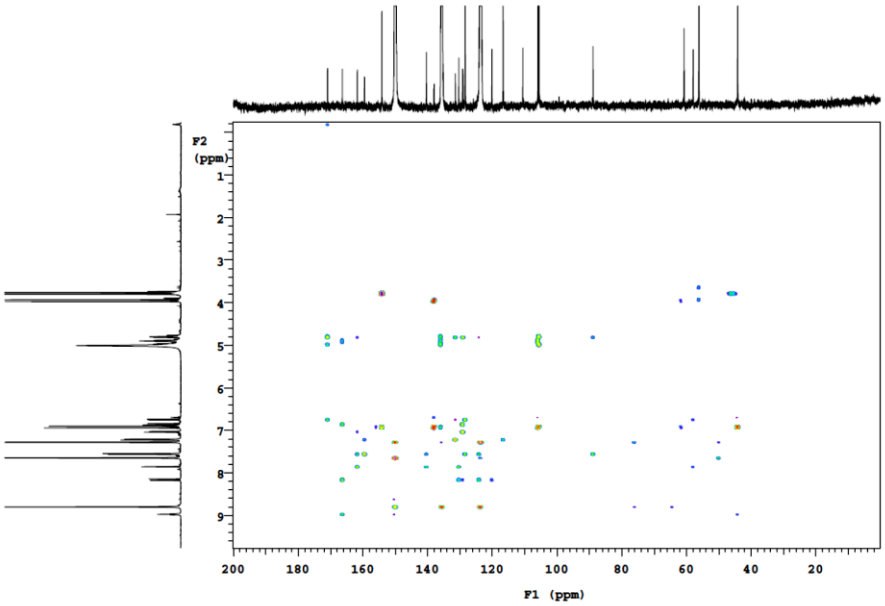

Figure 103S: g-HMBCAD spectrum of **(±)-128**

Neolignanamide (±)-129

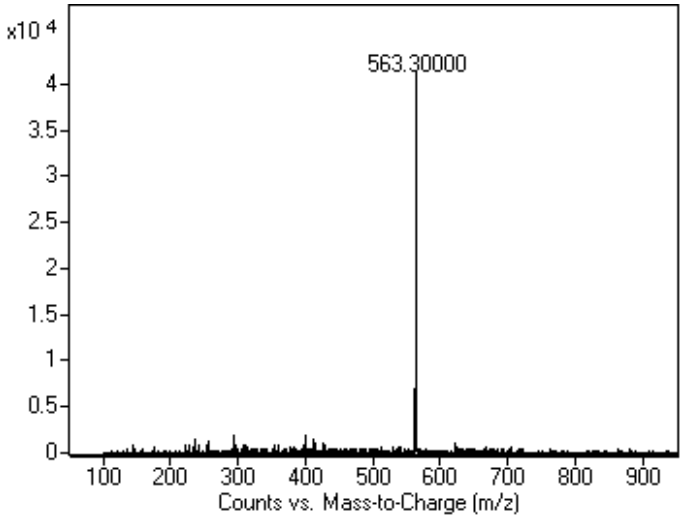

Figure 104S: ESI MS spectrum of **(±)-129**

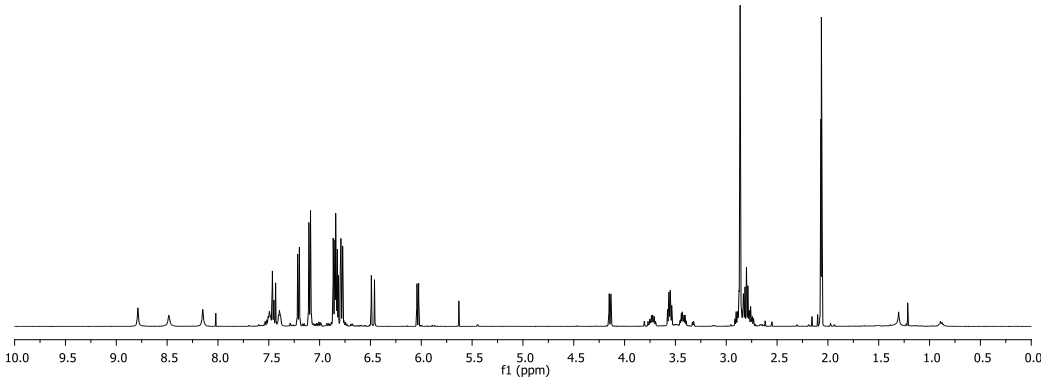

Figure 105S: ^{1}H NMR spectrum (CD_3COCD_3, 500 MHz) of **(±)-129**

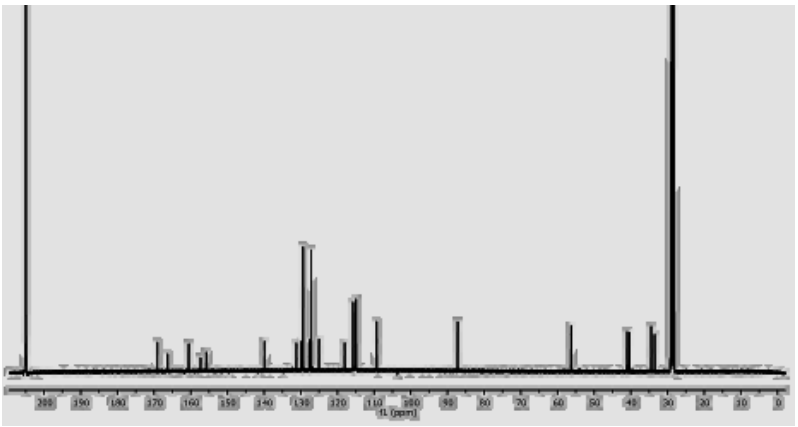

Figure 106S: ^{13}C NMR spectrum (CD_3COCD_3, 125 MHz) of **(±)-129**

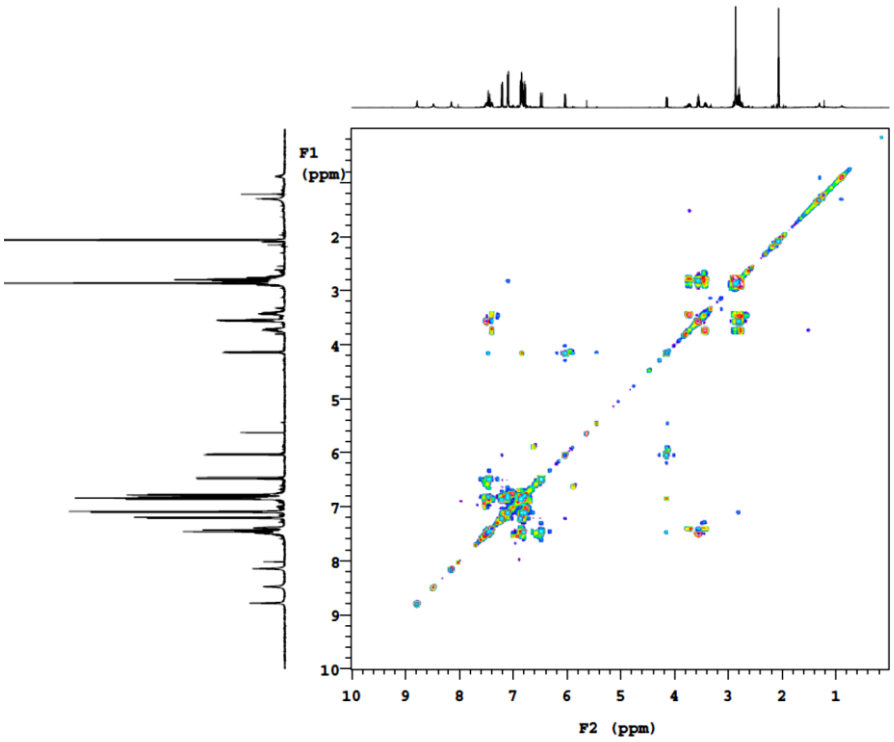

Figure 107S: g-COSY spectrum of **(±)-129**

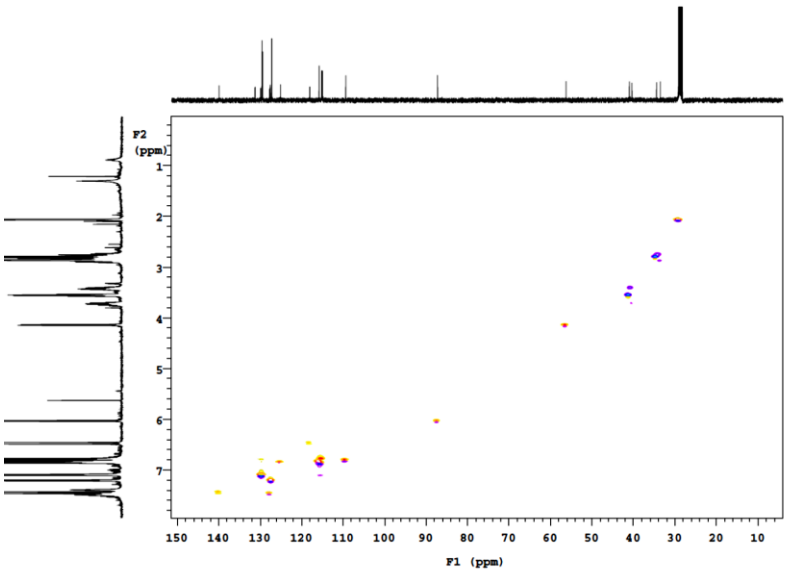

Figure 108S: g-HSQCAD spectrum of (±)-**129**

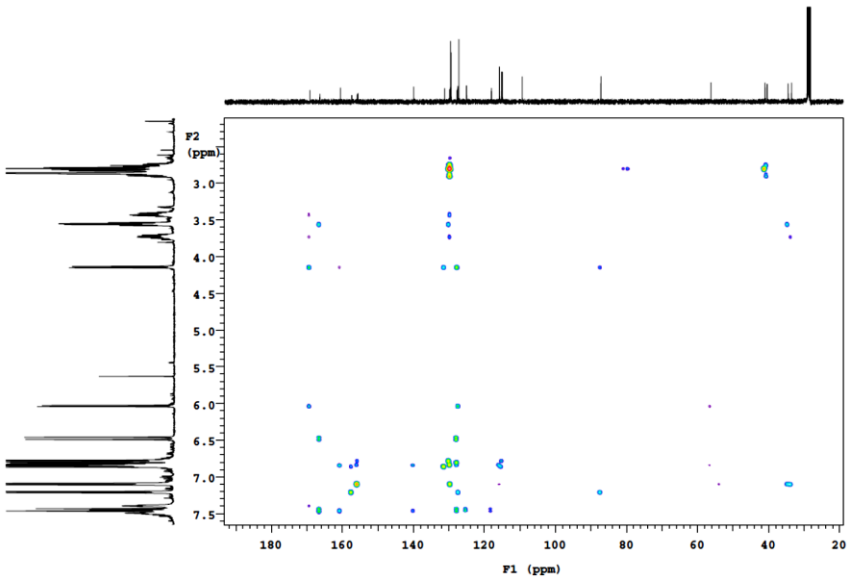

Figure 109S: g-HMBCAD spectrum of **(±)-129**

Neolignanamide (±)-130

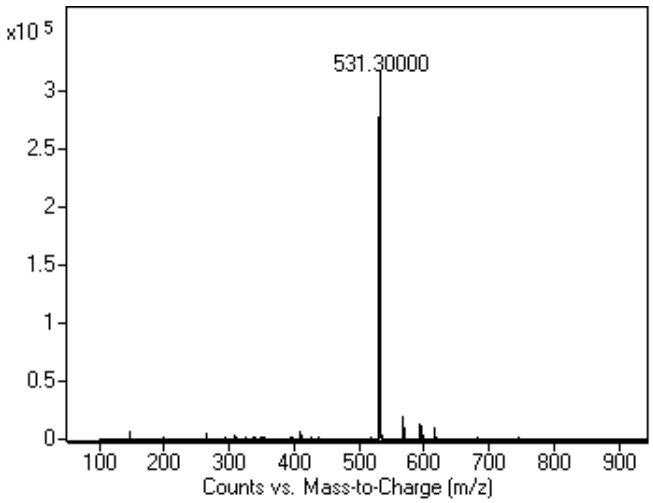

Figure 110S: ESI MS spectrum of **(±)-130**

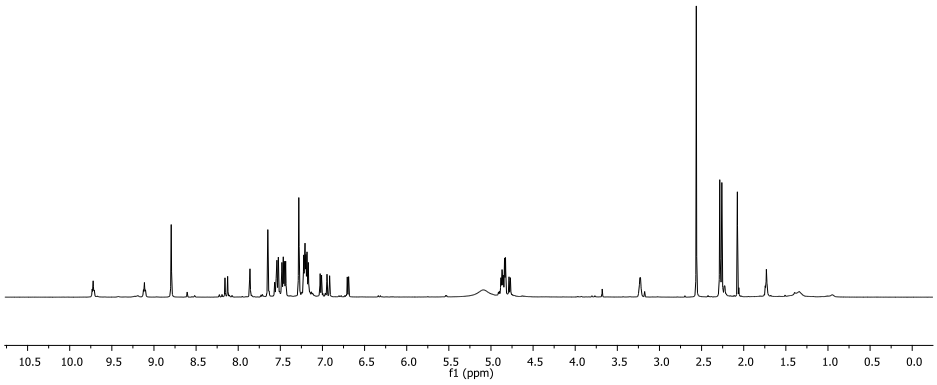

Figure 111S: ^{1}H NMR spectrum (C_5D_5N, 500 MHz) of **(±)-130**

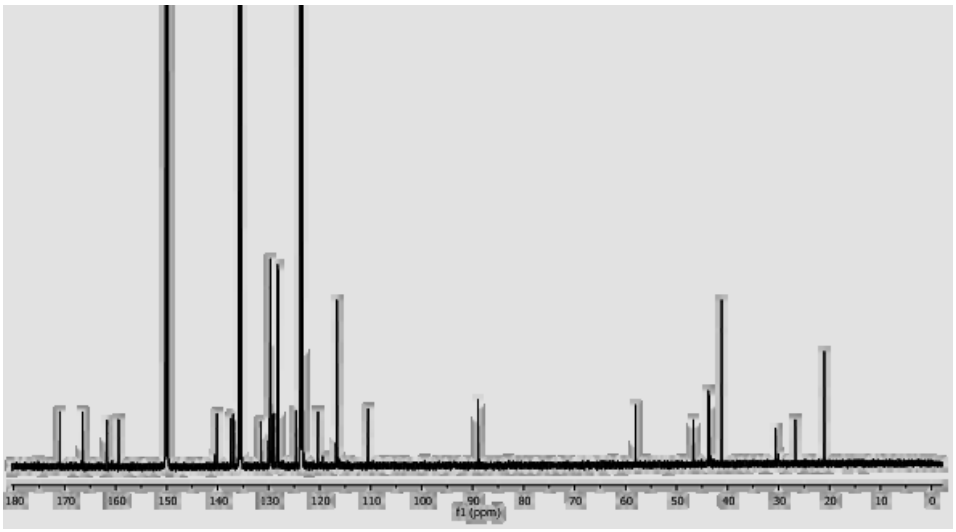

Figure 112S: ^{13}C NMR spectrum (C_5D_5N, 125 MHz) of **(±)-130**

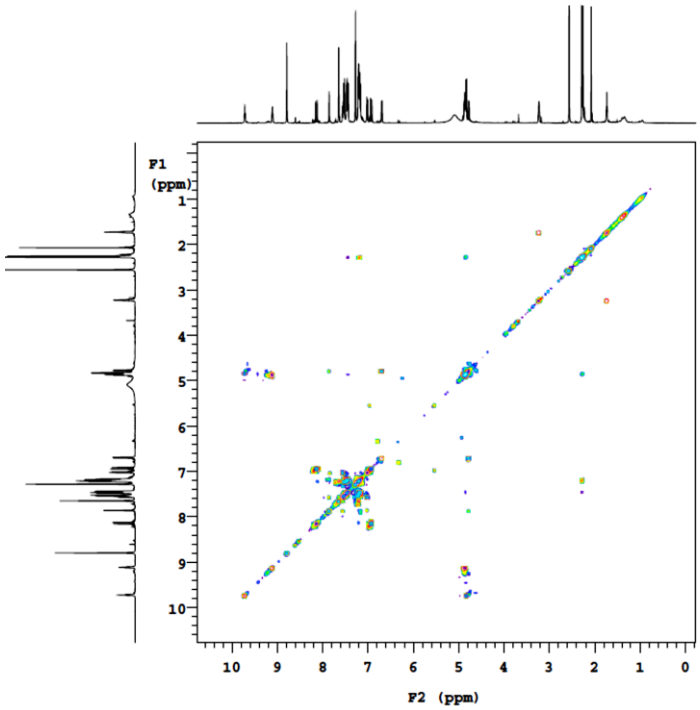

Figure 113S: g-COSY of **(±)-130**

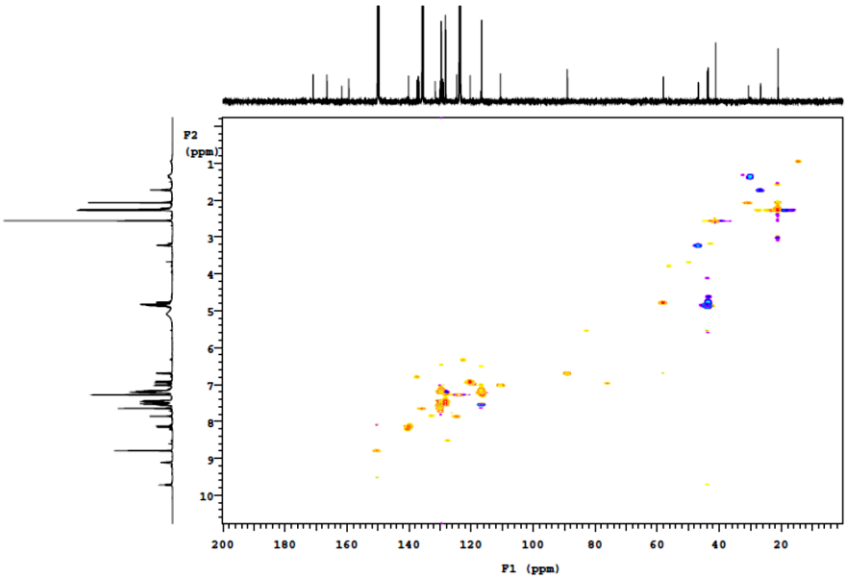

Figure 131S: g-HSQCAD of **(±)-130**

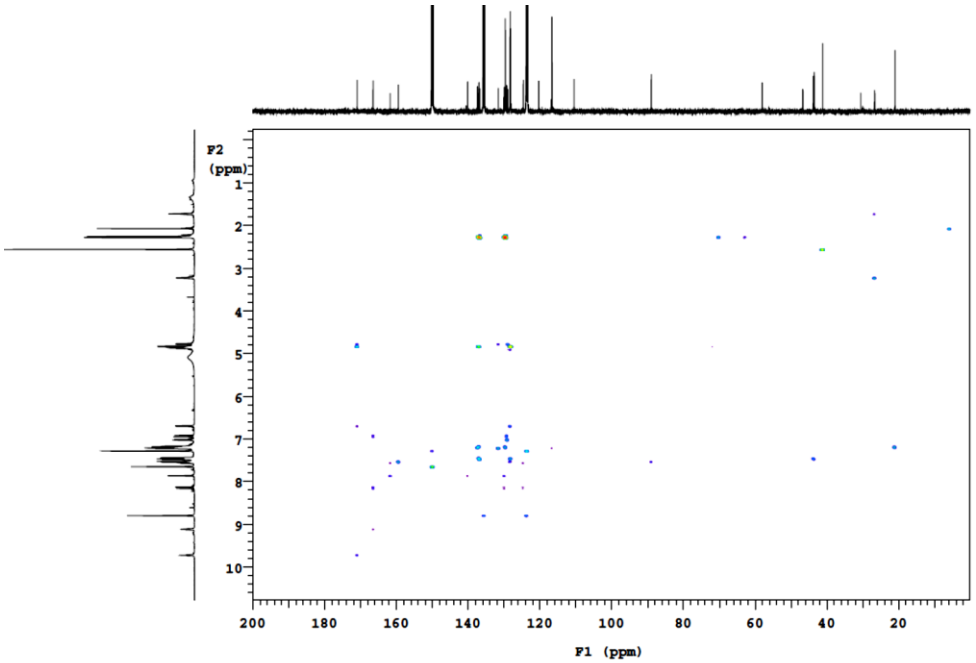

Figure 132S: g-HMBCAD of **(±)-130**

Neolignanamide (±)-131

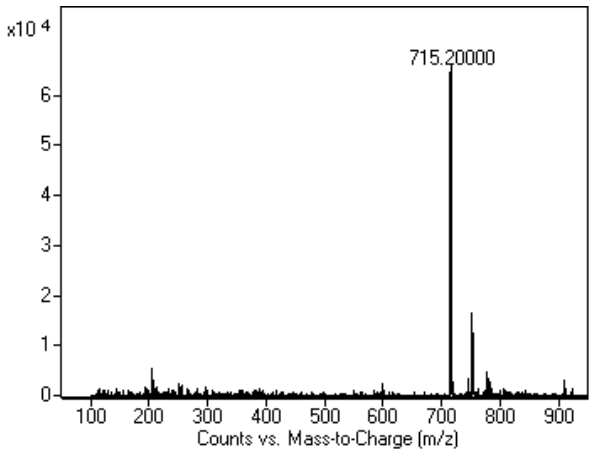

Figure 133S: ESI MS spectrum of **(±)-131**

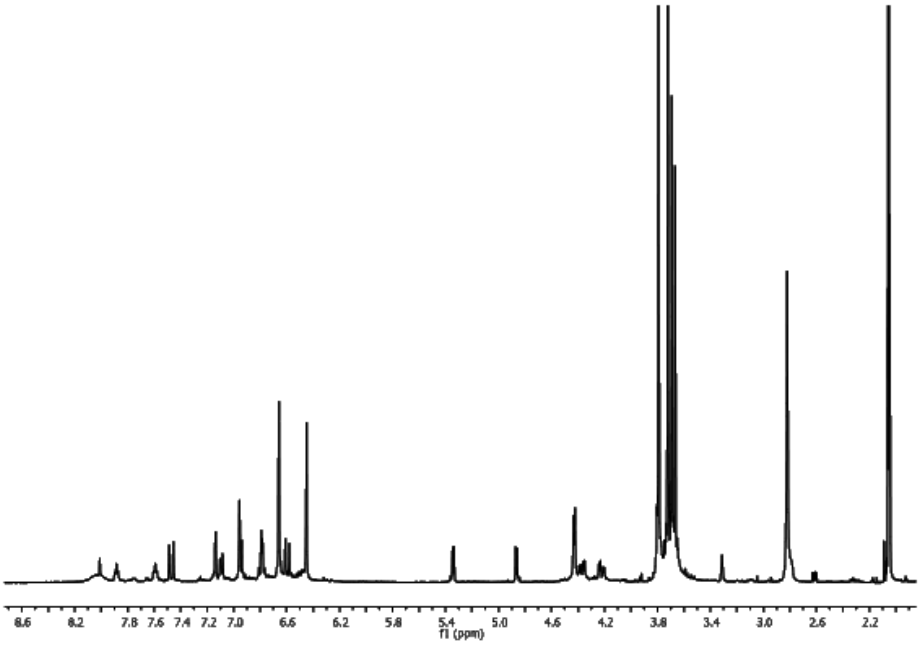

Figure 134S: ^{1}H NMR spectrum (CD_3COCD_3, 500 MHz) of **(±)-131**

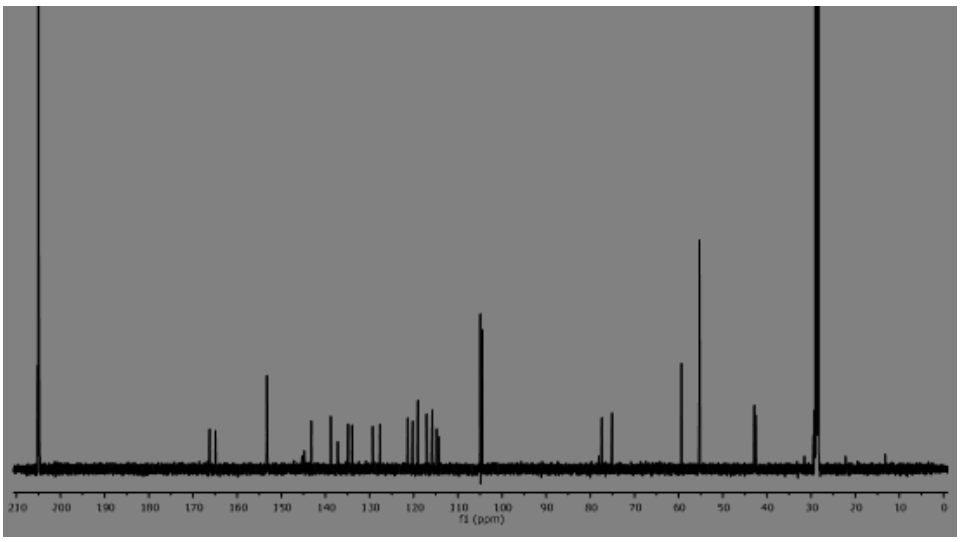

Figure 135S: ^{13}C NMR spectrum (CD_3COCD_3, 125 MHz) of **(±)-131**

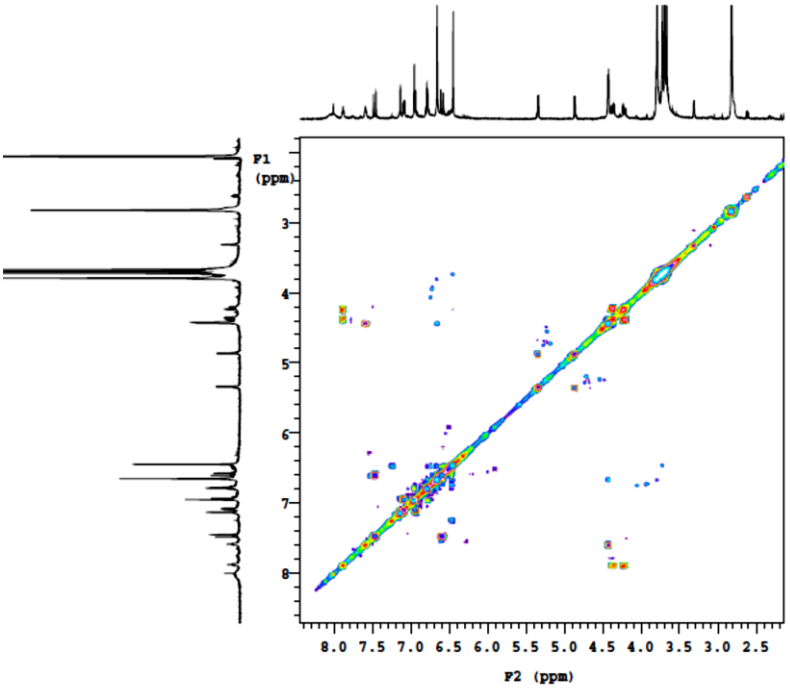

Figure 136S: g-COSY spectrum of **(±)-131**

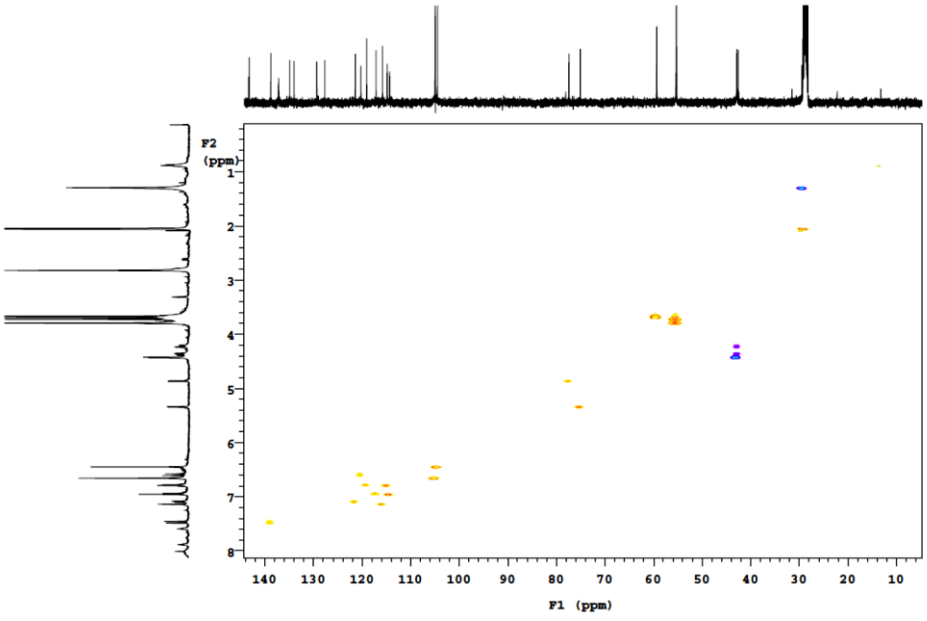

Figure 137S: g-HSQCAD spectrum of **(±)-131**

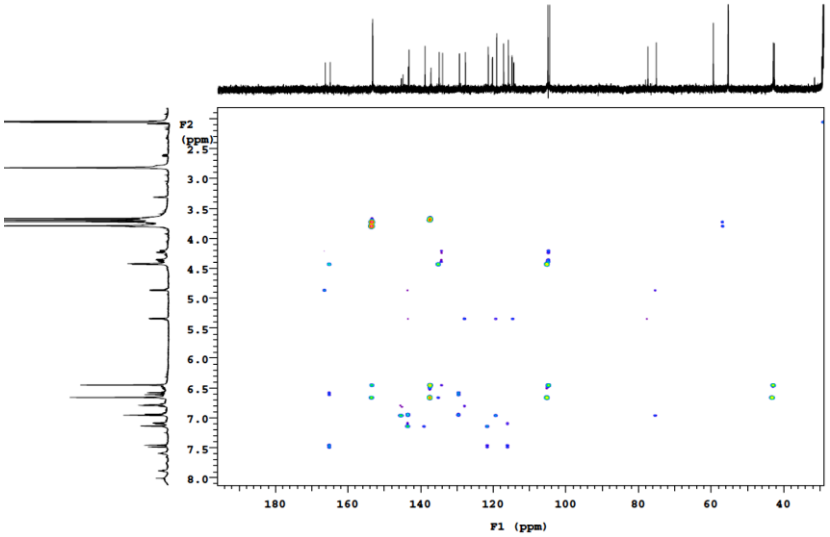

Figure 138S: g-HMBCAD spectrum of **(±)-131**

Neolignanamide (±)-132

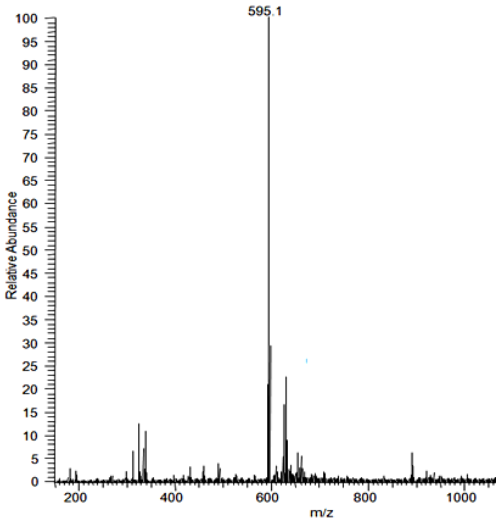

Figure 139S: ESI MS spectrum of (±)-**132**

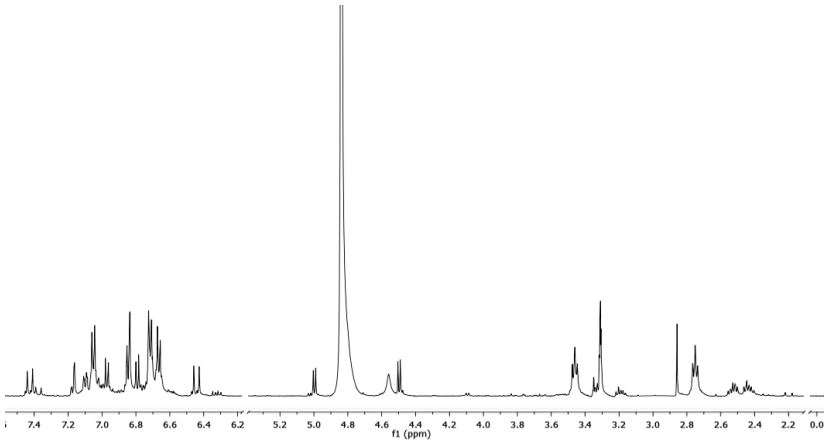

Figure 140S: ^{1}HNMR spectrum (500 MHz, CD_3OD) of (±)-**132**

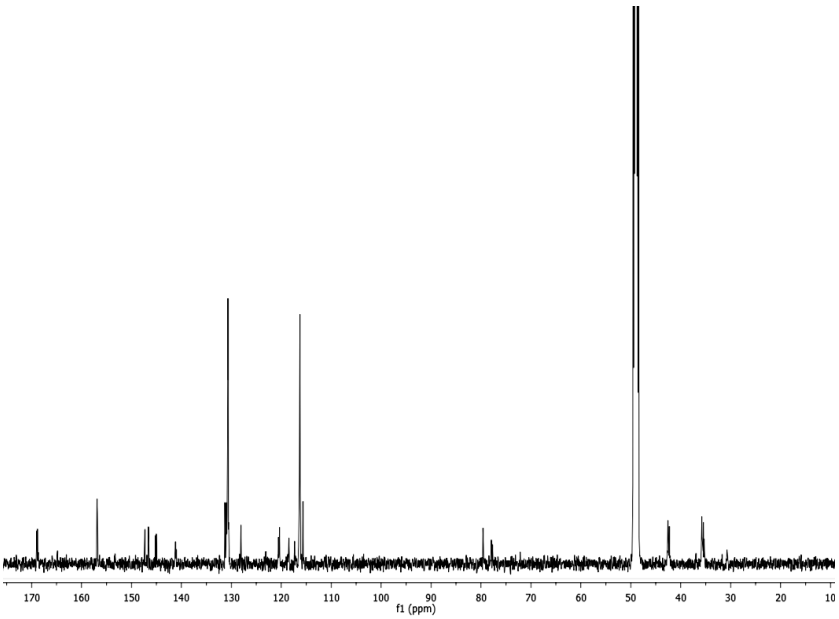

Figure 141S: ^{1}HNMR spectrum (125 MHz, CD_3OD) of (±)-**132**

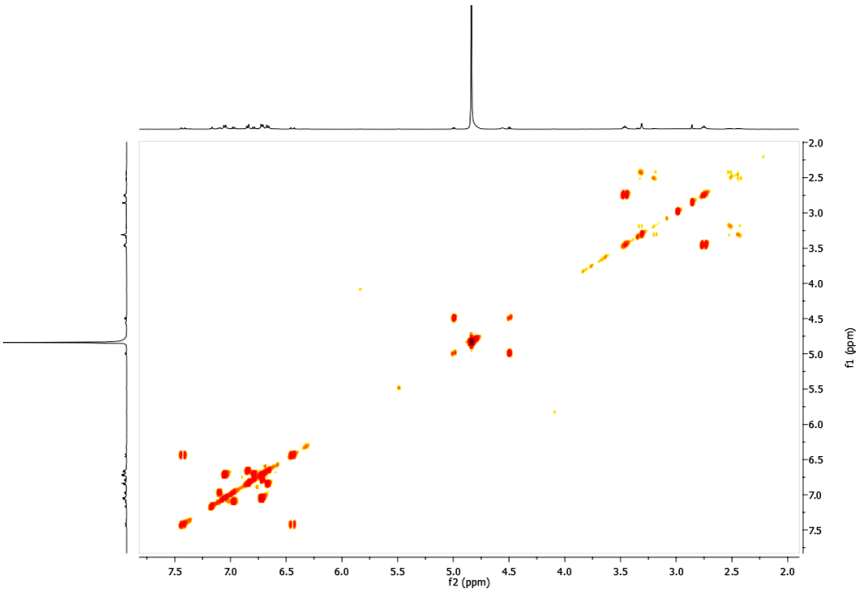

Figure 142S: gCOSY spectrum of (±)-**132**

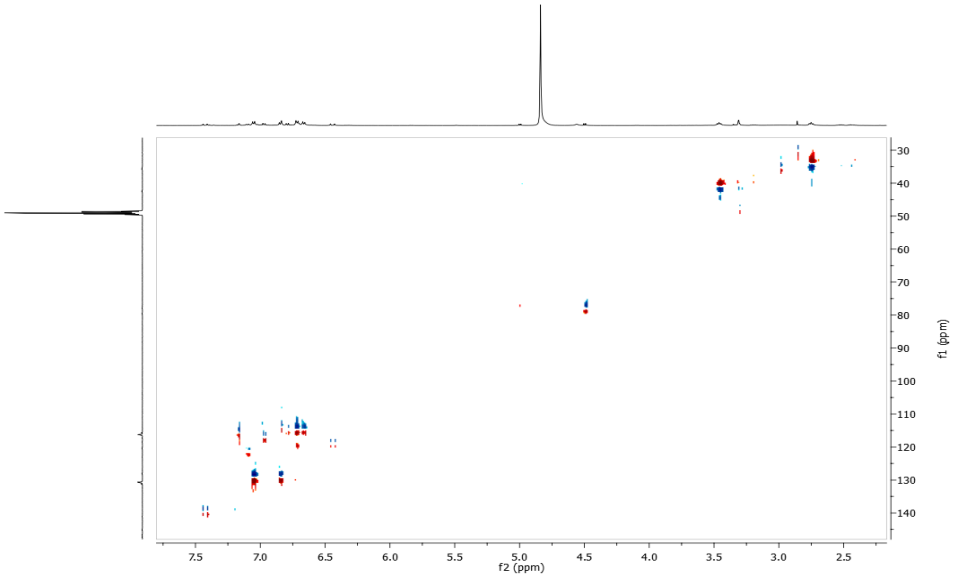

Figure 143S: gHSQCAD spectrum of (±)-**132**

Neolignanamide (±)-133

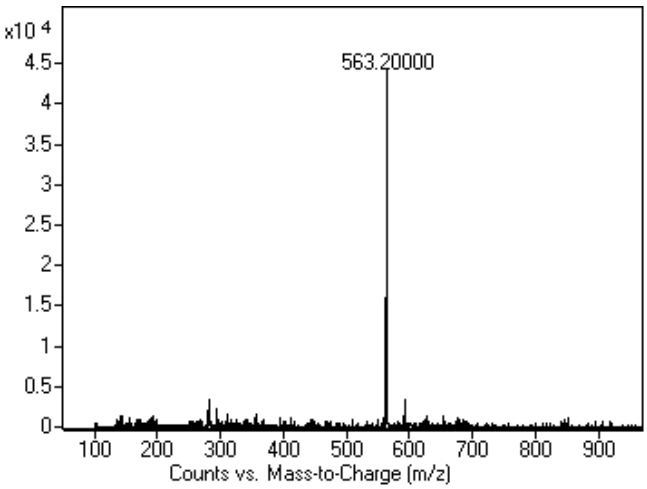

Figure 144S: ESI MS spectrum of **(±)-133**

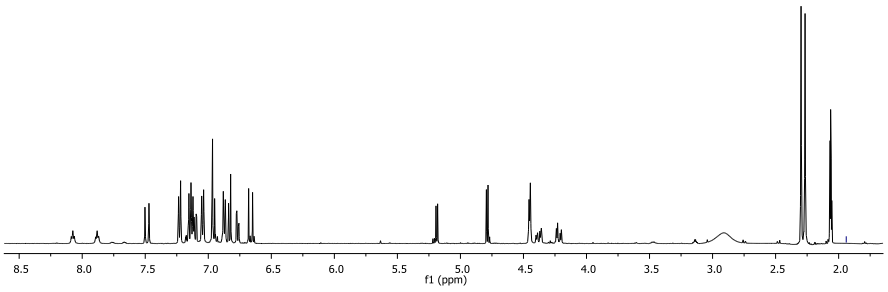

Figure 145S: ^{1}H NMR spectrum (CD_3COCD_3, 500 MHz) of **(±)-133**

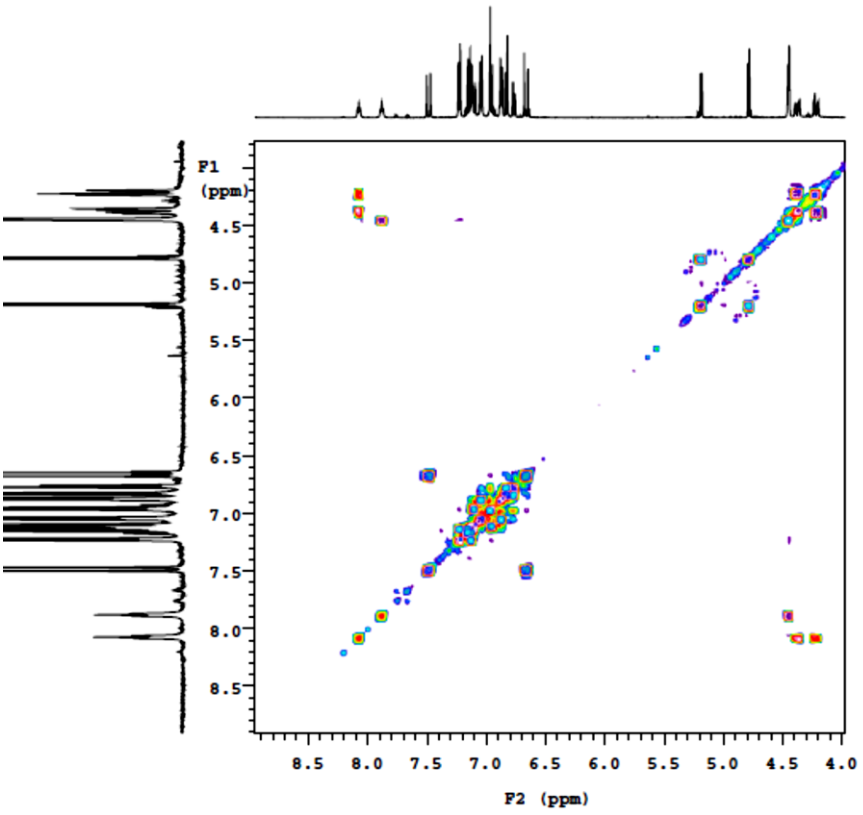

Figure 146S: g-COSY spectrum of **(±)-133**

Neolignanamide (±)-134

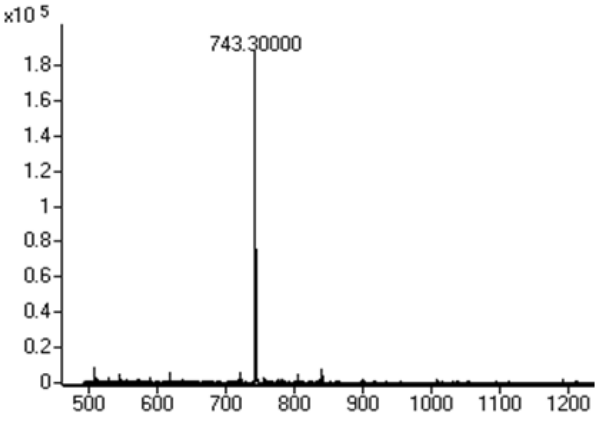

Figure 147S: ESI Mass spectrum of **134**

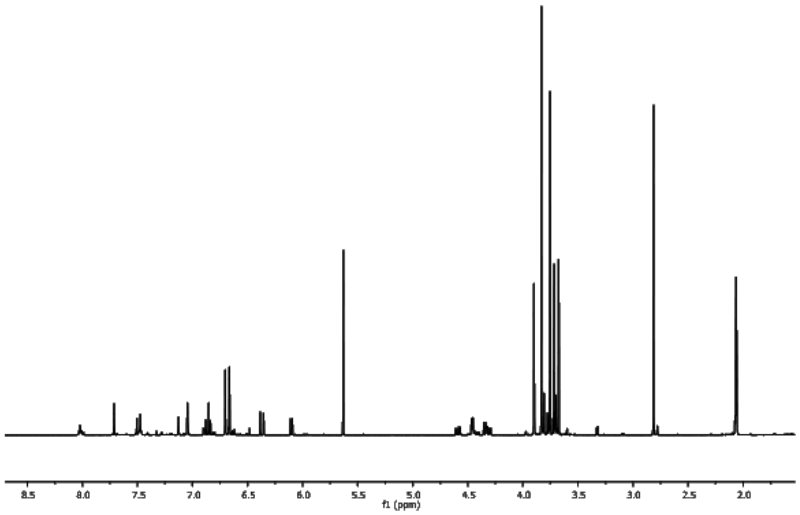

Figure 148S: ^{1}H NMR (500 MHz, $(CD_3)_2CO$) spectrum of **134**

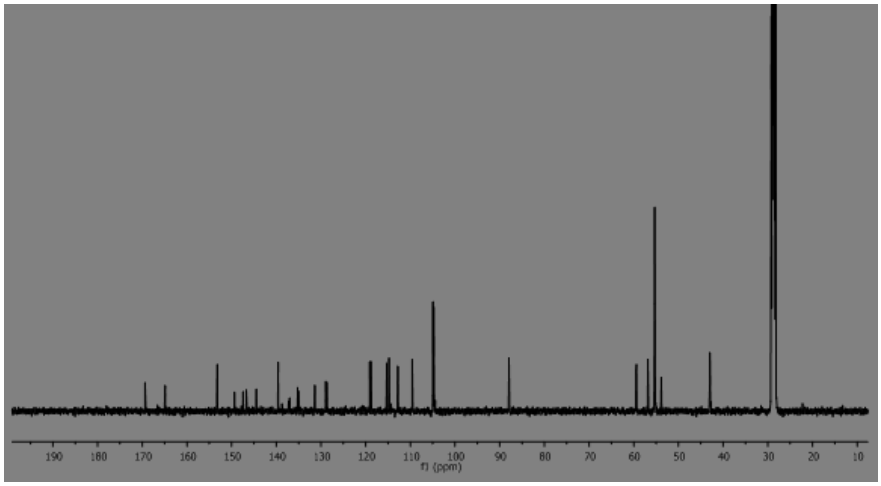

Figure 149S: ^{13}C NMR (125 MHz, $(CD_3)_2CO$) spectrum of **134**

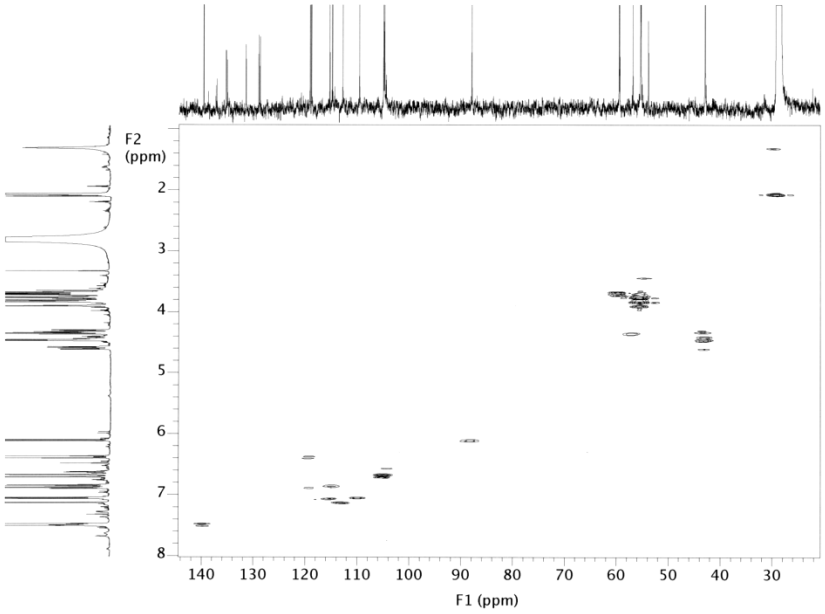

Figure 150S: HSQC spectrum of **134**

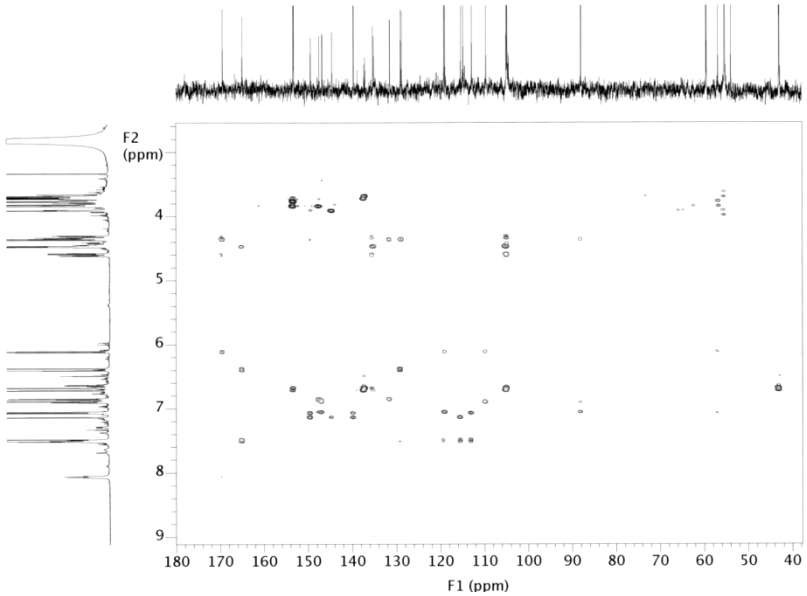

Figure 151S: HMBC spectrum of **134**

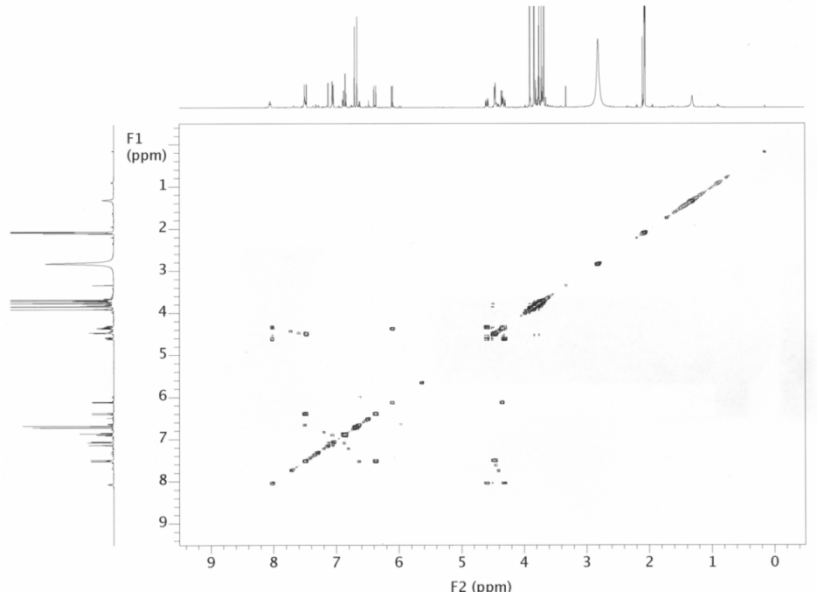

Figure 152S: COSY spectrum of **134**

Neolignanamide (±)-135

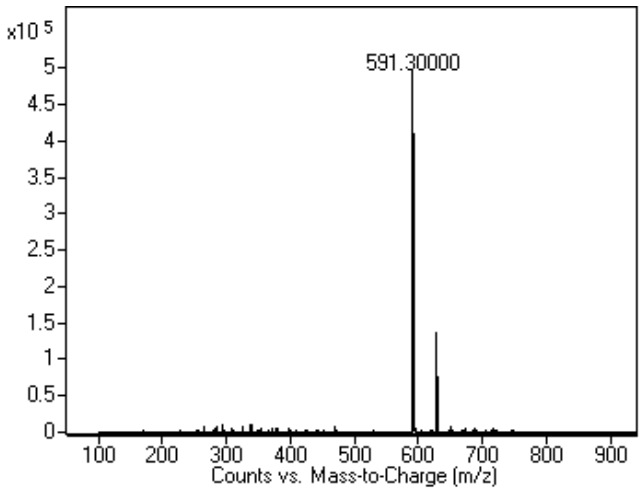

Figure 153S: ESI MS spectrum of **(±)-135**

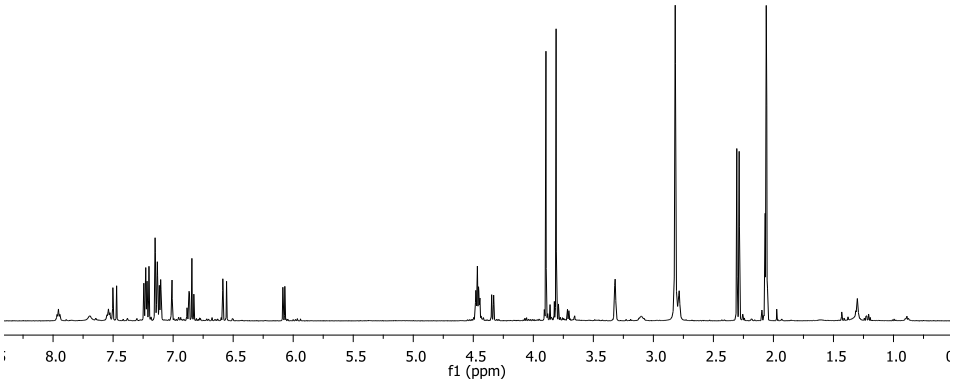

Figure 154S: ^{1}H NMR spectrum (CD_3COCD_3, 500 MHz) of **(±)-135**

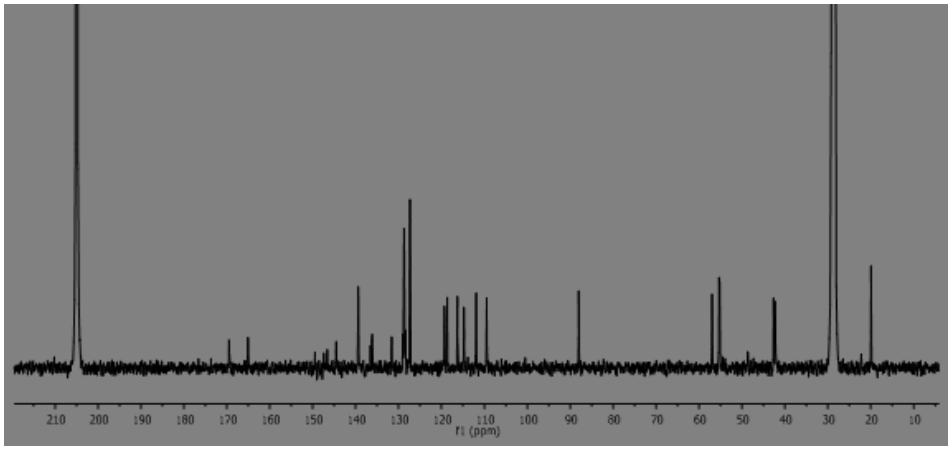

Figure 155S: ^{13}C NMR spectrum (CD_3COCD_3, 125 MHz) of **(±)-135**

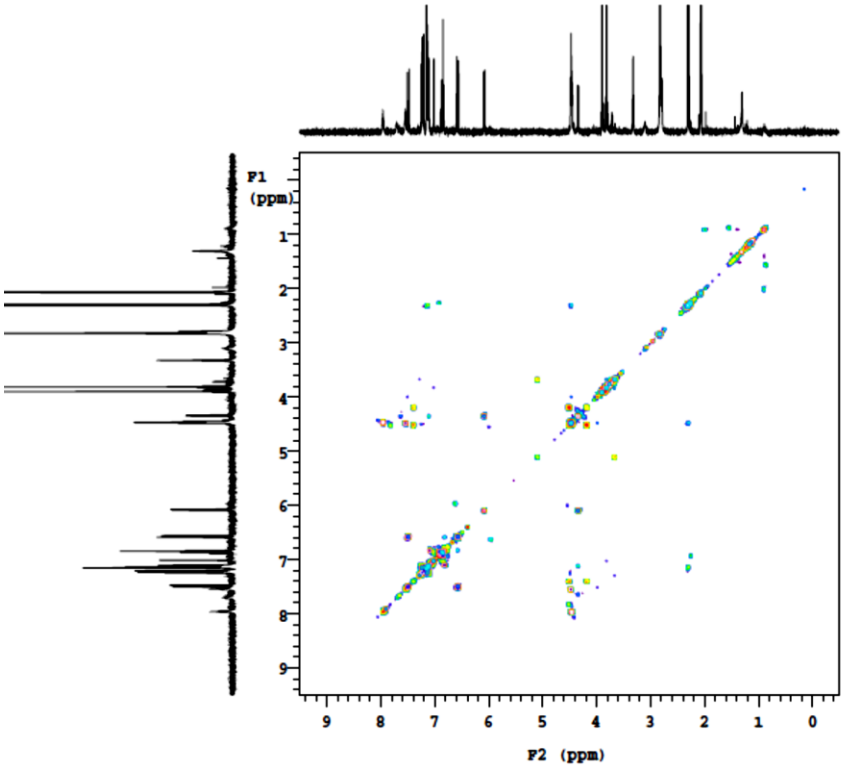

Figure 156S: g-COSY spectrum of **(±)-135**

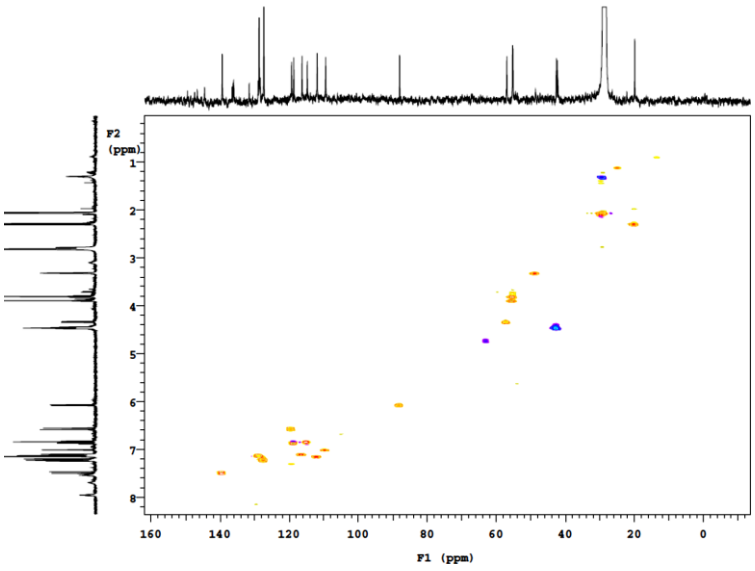

Figure 157S: g-HSQCAD spectrum of **(±)-135**

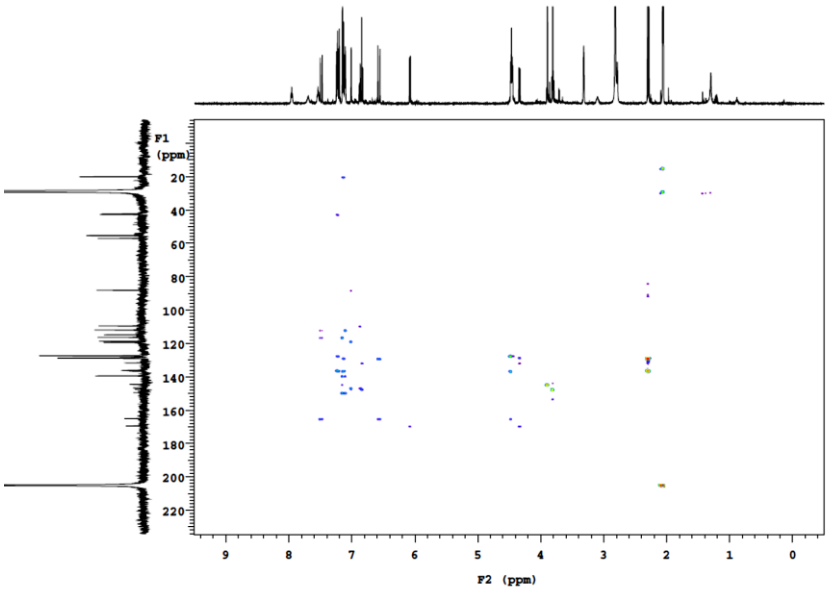

Figure 158S: g-HMBCAD spectrum of **(±)-135**

Benzoxanthene 137

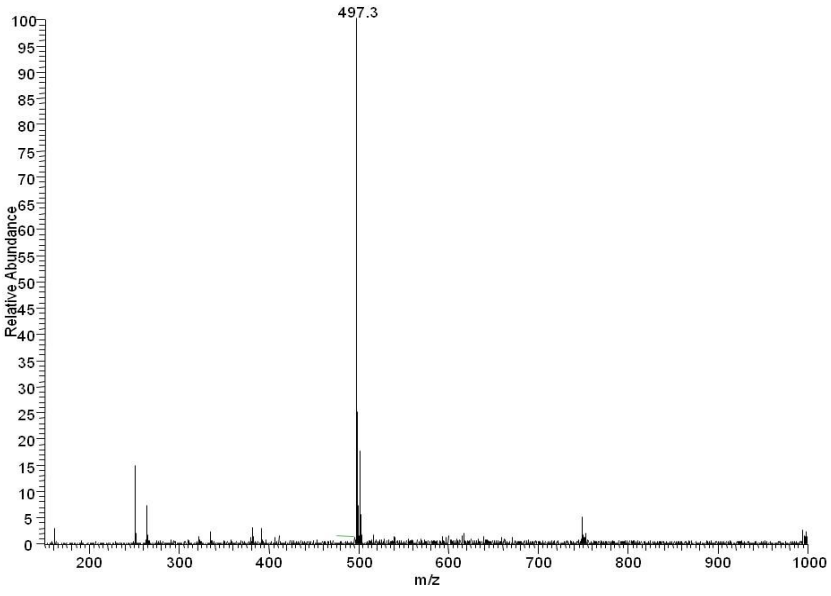

Figure 159S: ESI MS spectrum of **137**

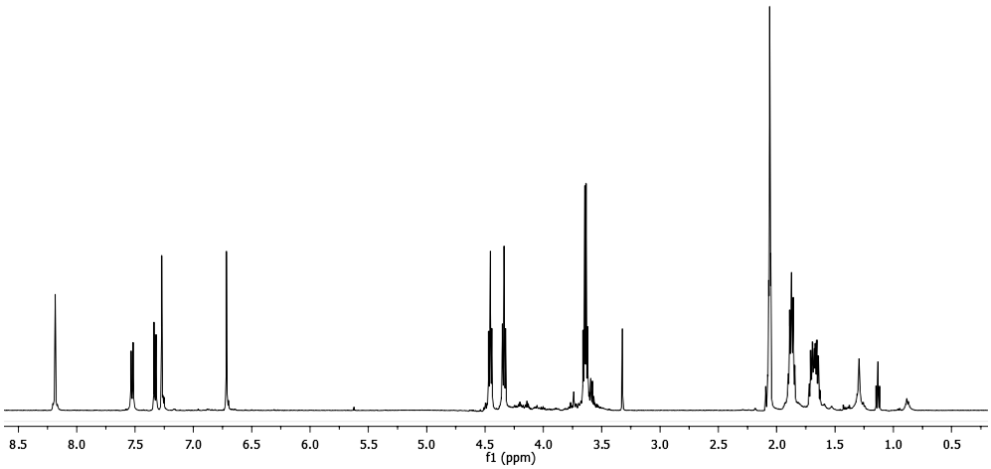

Figure 160S: ^{1}H NMR spectrum (500 MHz, acetone-d_6) of **137**

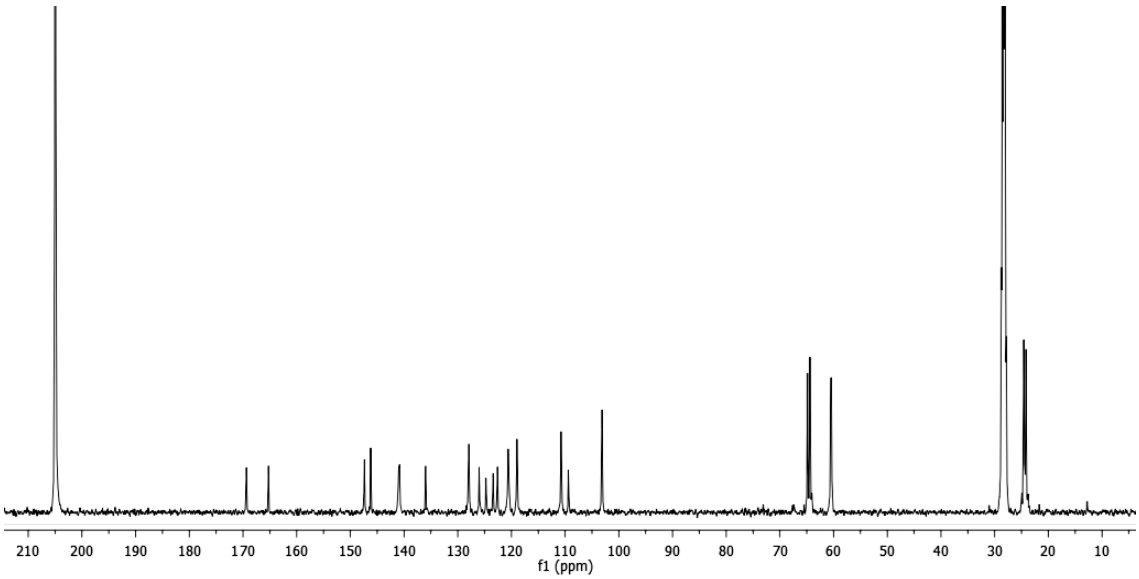

Figure 161S: ^{13}C NMR spectrum (125 MHz, acetone-d_6) of **137**

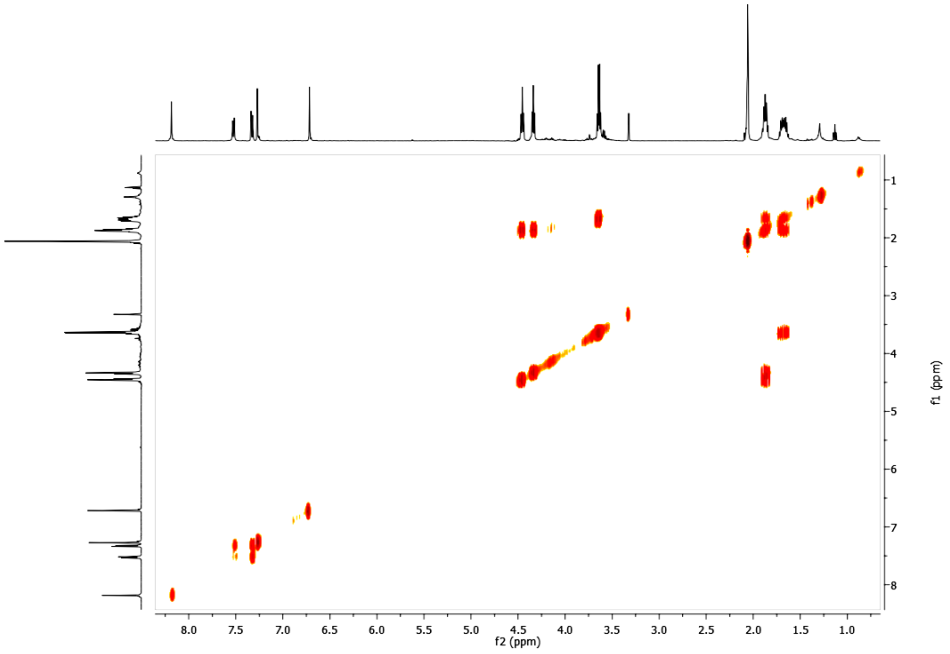

Figure 161S: gCOSY spectrum of **137**

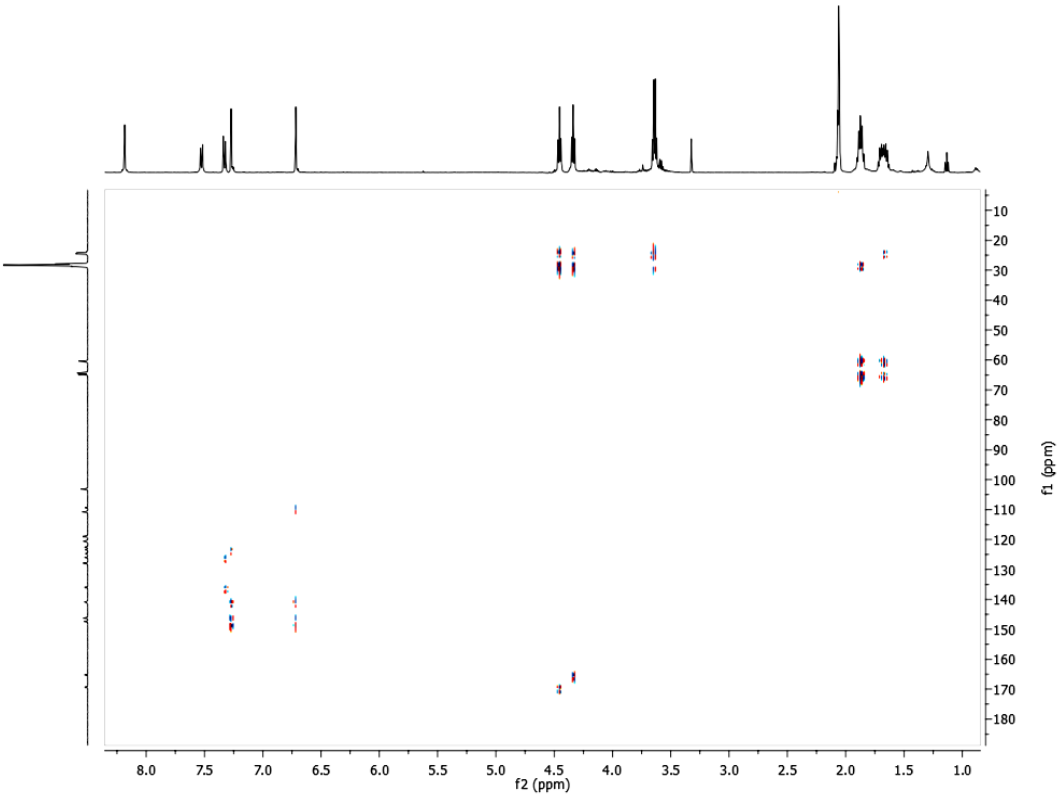

Figure 162S: gHMBCAD spectrum of **137**

7.4. APPENDIX D

In this section the MS and NMR spectra of intermediates and product obtained in the synthesis of monodeuterated enterolactone **146** are reported.

Compound 143

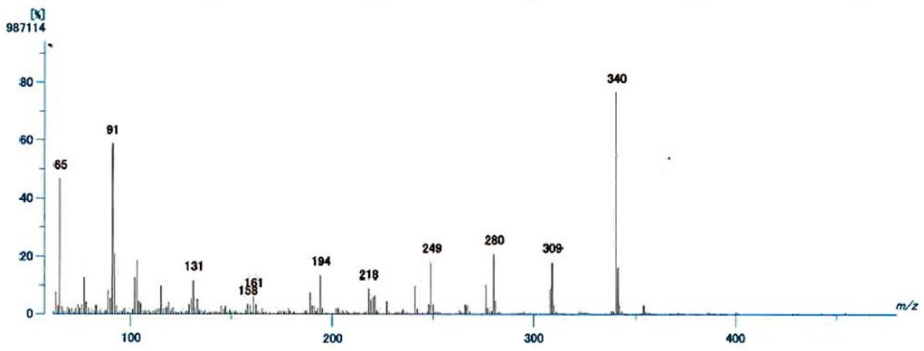

Figure 163S: EI MS spectrum of **143**.

Compound 144

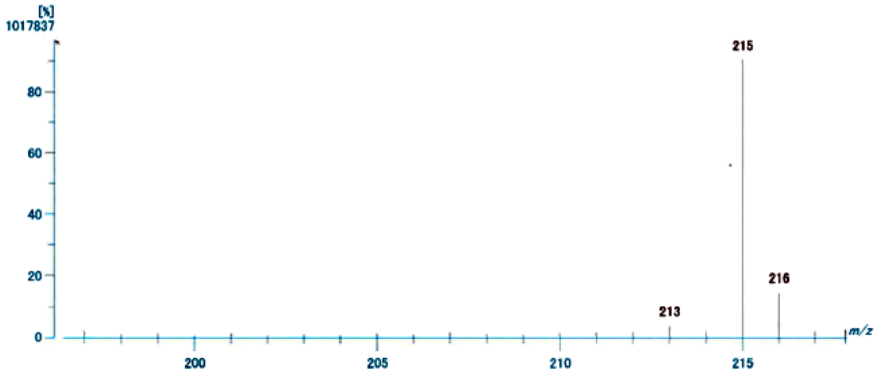

Figure 164S: EI MS spectrum of **144**

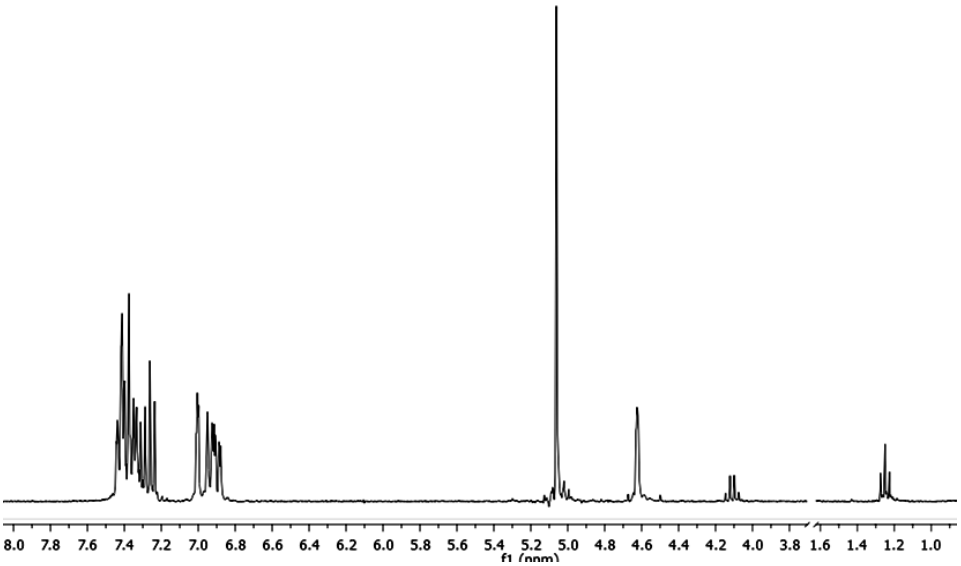

Figure 165S: ^{1}H NMR sperctrum ($CDCl_3$, 300 MHz) of **144**

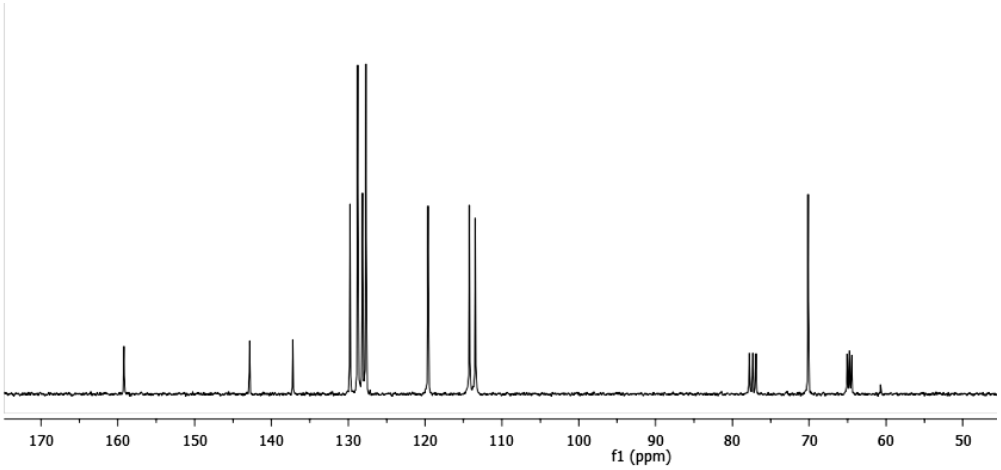

Figure 166S: ^{13}C NMR sperctrum ($CDCl_3$, 75 MHz) of **144**

Compound 145

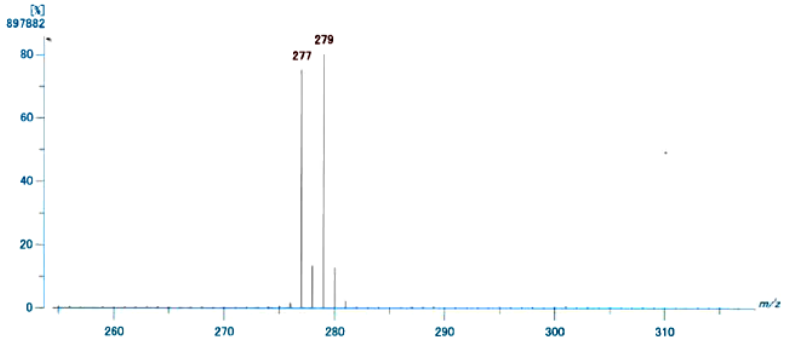

Figure 167S: EI MS spectrum of **145**

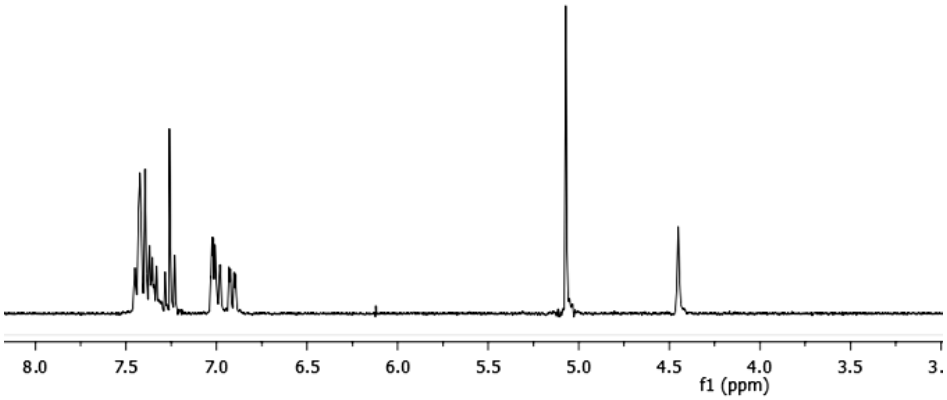

Figure 169S: ^{1}H NMR spectrum ($CDCl_3$, 300 MHz) of **145**

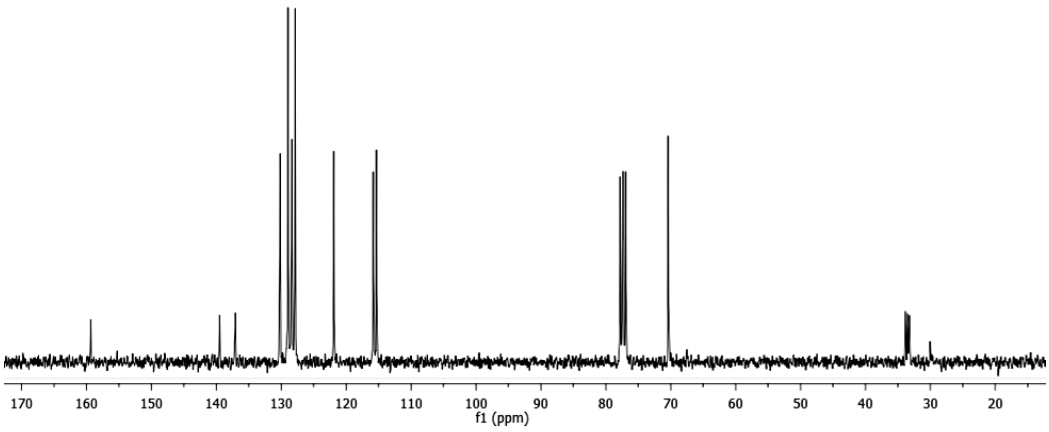

Figure 170S: ^{13}C NMR spectrum ($CDCl_3$, 75 MHz) of **145**

Compound 146

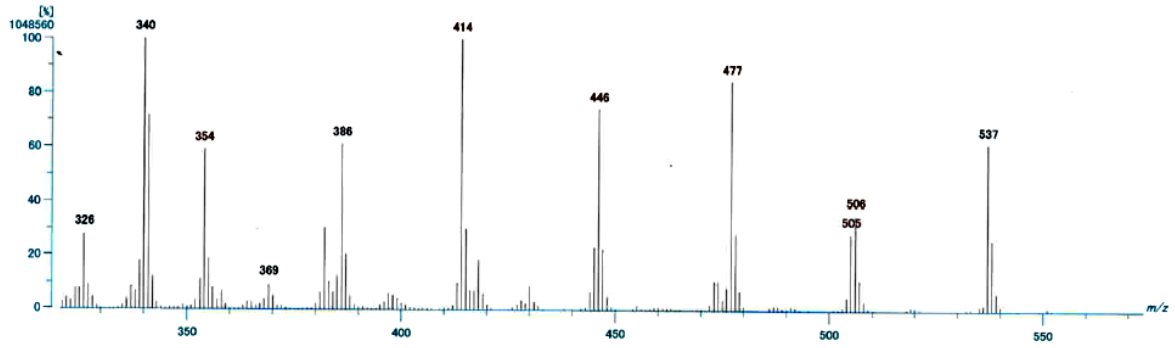

Figure 171S: EI MS spectrum of **146**